

https://dspace.org/

A multi-scale approach to assessing the influence of gas phase combustion mechanisms on the prediction of pulverised coal flames

Naidoo, Reshendren

2022

https://hdl.handle.net/10539/34161

Downloaded from a DSpace repository. https://dspace.org/



A Multi-Scale Approach to Assessing the Influence of Gas Phase Combustion Mechanisms on the Prediction of Pulverised Coal Flames

Reshendren Naidoo

(Student number: 9802700F)

School of Mechanical, Industrial and Aeronautical Engineering,

University of the Witwatersrand

Johannesburg, South Africa.

Supervisors:

Supervisor: Prof. Walter Schmitz (Wits)

Co-Supervisor: Prof Norbert Modliński (WUST)

A research dissertation submitted to the Faculty of Engineering and the Built Environment, University of the Witwatersrand, in fulfilment of the requirements for the degree of Master of Science in Engineering.

SCHOOL OF MECHANICAL, INDUSTRIAL & AERONAUTICAL ENGINEERING

PLAGIARISM DECLARATION TO BE SIGNED BY ALL HIGHER DEGREE STUDENTS

I, **Reshendren Naidoo** (Student number: **9802700F**) am a student registered for the degree of **Master of Science in Engineering by Research Mechanical, Industrial and Aeronautical** in the academic year **2**

I hereby declare the following:

- I am aware that plagiarism (the use of someone else's work without their permission and/or without acknowledging the original source) is wrong.
- I confirm that the work submitted for assessment for the above degree is my own unaided work except where I have explicitly indicated otherwise.
- I have followed the required conventions in referencing the thoughts and ideas of others.
- I understand that the University of the Witwatersrand may take disciplinary action against me if there is a belief that this is not my own unaided work or that I have failed to acknowledge the source of the ideas or words in my writing.

Signature:_____ Date: 2nd February 2022

Abstract

Computational fluid dynamics simulations were conducted to assess the effect of using different gas phase combustion mechanisms (one, two and five-step) in predicting the flame structure and combustion species distribution during the pulverised coal combustion process. The simulations were conducted at several scales i.e., Laboratory, Pilot Scale and Full Scale. To enable this a comprehensive model of the Eskom Research, drop tube furnace and pilot scale combustion test facility was developed. The full-scale assessment was done on a 200 MWe pulverised coal boiler operating in the South African power generation industry. It was shown that it is essential to develop detailed characterisations of the devolatilisation and char combustion characteristics of the reference coal using advanced techniques. The predictive capability using an iterative approach using ANSYS Fluent® and PC-Coal Lab® was extended from previous work and demonstrated that the reference coal exhibits an atypically slow burn out characteristic. This behaviour was modelled successfully by introducing modifications to the mass diffusion coefficient in the char combustion model. These sub-models were applied to the pilot scale simulations, and it was demonstrated that the choice of gas phase combustion mechanism has a profound effect on the predicted structure of the pulverised coal flame. The use of the more advanced five-step mechanism improved the temperature predictions within the pilot scale combustion test facility's furnace. The latter part of the study considered the application of the techniques developed at the lower scales, to a full-scale boiler. Hence, a comprehensive model of a full-scale boiler was developed, which included a faithful representation of the boiler geometry and particularly the behaviour of the burners. A simplified burner was developed for use in the full-scale model and its behaviour was verified against the results predicted by a detailed model of the installed low NOx burner. The simplified burner demonstrated that it could mimic the flow structure emanating from the detailed model, with specific emphasis on the velocity and turbulence profiles. The full-scale model simulations further emphasised the role of the gas phase combustion mechanisms on the prediction of pulverised coal flames. This was made starkly evident as the five-step mechanism provided better correlation with the measured data and moreover predicted a fundamentally different combustion flow and temperature field, that was considered realistic as it confirmed the observed flame behaviour. The five-step mechanism demonstrated an extended ability over the one and two-step mechanisms, to address the strong coupling between localised flame aerodynamics, thermodynamics, chemistry, and

particle dynamics. This whilst also showing a sensitivity to the char burn out characteristics. The five-step mechanism provided the best prediction of temperature, O_2, and importantly CO at the furnace exit. Furthermore, it also demonstrated good correlations with measured NOx values when used in conjunction with the standard NOx post-processing algorithm. It was concluded that the one and two step mechanisms were appropriate for predicting bulk quantities such as furnace and boiler exit temperature (to an extent) but provided erroneous predictions in the near burner and overall burner belt region. The five-step model also showed that adverse phenomena such as particle roping and its effect on ignition can be predicted. The research study also showed that the particle burnout characteristics were consistent across all scales, and this gives credence to the established testing and evaluation criteria used to specify a coal for large scale adoption in the production environment. However, a subtlety was noted in terms of the size basis for the drop tube tests and recommendations for improvement were proposed. In summary, the research work also confirmed that the choice of gas phase combustion model, and its underlying assumptions has a profound effect on the prediction of the structure of a pulverised coal flame. An ancillary observation also played a key role i.e., that the peculiarities of South African coals must be assessed using advanced CFD and phenomenological models for char and devolatilisation. This is to effectively model a realistic combustion characteristic. The work demonstrates that the appropriate use of the tools developed could be used to assess the performance of existing coal fired furnaces using South African coals and could provide key insight in optimising their thermal performance and reducing their emissions footprint as the global energy landscape changes to a more environmentally friendly future.

Acknowledgements

This work has been the culmination of several years of effort and I would not have completed it without the continued motivation and inspiration of my wife, Swarna. She always kept me honest and kept me going in the right direction. The latest addition to my life, my son, Shaurya added complications but moreover gave me purpose and belief that there is bigger reason to keep trying.

I would like to thank my supervisor Professor Walter Schmitz for his supervision and guidance and importantly his perspective to keep the research industrially and scientifically relevant. And I would also like to thank my co-supervisor, Prof. Norbert Modliński for his invaluable insight and technical guidance with the little details that made the difference.

I would also like to extend my gratitude to the Eskom Power Plant Engineering Institute and the Combustion Engineering Specialisation Centre within the School of Mechanical, Industrial and Aeronautical Engineering, for funding this research and the infinite patience they have shown in allowing me to complete it.

Finally, I would like to thank Dr Renier Dreyer at the CrunchYard high performance computing company for his advice and support in running large, parallel simulations. I would also like to acknowledge the Centre for High Performance Computing for allowing me access to their extensive number crunching capability.

Table of Contents

List of Figures iii

List of Tables ix

Nomenclature xi

Acronyms xii

Definitions xiv

1 Introduction 15

1.1 Background 19

1.2 Gaps Identified 22

1.3 Research Questions 23

2 Literature Review 24

2.1 State of the Art in Coal Combustion Modelling 24

2.2 Combustion Modelling Framework in CFD 27

2.3 Sub Models for Chemical Kinetics of Coal Combustion 28

2.3.1 Devolatilisation of Coal Particles 29

2.3.2 Modelling Techniques for Coal Particle Devolatilisation 33

2.3.2.1. Arrhenius Models for Devolatilisation 35

2.3.2.2. Phenomenological Models for Devolatilisation 37

2.3.2.3. Flashchain® 39

2.3.3 Modelling Techniques for Coal Particle Char Combustion 40

2.3.3.1. Global Models for Char Combustion 43

2.3.3.2. Intrinsic Model of Char Combustion and Other Advanced Models 46

2.3.4 Gas Phase Combustion Mechanisms 47

2.3.5 In-Furnace Radiation 52

2.4 The Principle of Operation of a Low NOx Burner 55

2.5 The Characteristics of Coal – A South African Perspective 59

3 Hypothesis....62
4 Research Objectives....62
5 Research Method and Results....64
5.1 Research Tools....64
5.2 Drop Tube Furnace Simulations....65
5.2.1 Background....65
5.2.2 DTF Rig Layout and Operation....65
5.2.3 CFD Model of the Drop Tube Furnace....69
5.2.4 Devolatilisation Results....73
5.2.5 Char Combustion Results....80
5.2.6 Discussion of Drop Tube Simulation Results....91
5.3 Gas Phase Combustion Modelling....92
5.3.1 One-Step Combustion Mechanism....92
5.3.2 Two-Step Combustion Mechanism....95
5.3.3 Five Step Combustion Mechanism....98
5.4 Pilot Scale Combustion Test Facility Simulations....108
5.4.1 Background....108
5.4.2 PSCTF Rig Layout and Operation....108
5.4.3 PSCTF CFD Model....110
5.4.4 PSCTF Simulation Results....117
5.4.5 Discussion of PSCTF Results....127
5.5 Full Scale Simulation of a 200 MWe Pulverised Coal Fired Boiler....129
5.5.1 Background....129
5.5.2 Modelling Objectives....129
5.5.3 Modelling Requirements....130
5.5.4 Pulverised Coal Fired Boiler Geometry....132
5.5.5 Process Conditions....137

5.5.6 Burner Flow Characterisation 139
5.5.7 Boiler Heat Exchanger Characterisation 146
5.5.8 Full Boiler Simulation Results 151
5.5.9 Discussion of Full-Scale Boiler Results 174
6 Conclusions 176
7 Recommendations for Future Research 178
8 References 180
Appendix A : Devolatilisation Wall Temperature Profile UDF 186
Appendix B : Char Combustion Wall Temperature Profile UDF 187
Appendix C : One and Two Step Reaction Chemistry Calculation 188
Appendix D : Five Step Reaction Chemistry Calculation 193
Appendix E : Heat Exchanger Pressure Loss Calculation 223
Appendix F : Additional PSCTF Postprocessing 226
Appendix G : PSCTF Experimental Temperature Profiles 227
Appendix H : Additional Full Scale Boiler Post Processing 228

List of Figures

Figure 1-1: Historical Coal Consumption of Selected Countries [1] 15
Figure 1-2: Annual CO_2 Emission from Coal for Selected Countries [2] 16
Figure 1-3: Energy Intensity for Selected Countries [3] 17
Figure 1-4: Typical Processes in a Pulverised Coal Fired Boiler [5] 19
Figure 2-1: Essential Elements of a Coal Fired Furnace Simulation (adapted from [9]) 25
Figure 2-2: Combustion Process for a Single Coal Particle [10] 26

Figure 2-3: Chemical Kinetics Sub Models (adapted from [9]) 28

Figure 2-4: Volatile Release from Coal Particles for Typical North American Coals [8] 29

Figure 2-5: Ignition and Burning Characteristics of Pulverised Coal [12].....30

Figure 2-6: Flame Propagation Model [12] 30

Figure 2-7: Ignition Characteristic of U.S. Coal in Transparent Wall Reactor [13].....32

Figure 2-8: Ignition Characteristic of South African Coal in Transparent Wall Reactor [13] 32

Figure 2-9: Schematic of the DTF (a) and Typical Wall Temperature Variation in the Test Section (b).....34

Figure 2-10: Chemical Structural Model of Bituminous Coal [22].....38

Figure 2-11: Primary and Secondary Pyrolysis Processes [30].....39

Figure 2-12: Validation of PC-Coal Lab® Devolatilisation Capability [22].....40

Figure 2-13 : Scanning electron microscope images of a coal particle at different phases of the combustion process (Adapted from [31]) 41

Figure 2-14: Coal Particle Radiation Mechanism [44].....53

Figure 2-15: Principle of Operation of a Low NOx burner [52].....56

Figure 2-16: NOx formation and Reduction Pathways [53].....57

Figure 2-17: 550 MW Coal Fired Boiler CFD Simulation [54] 58

Figure 2-18: Low NOx Burner Temperature and Flow Field [54].....58

Figure 2-19: Energy Content and ASTM Rank of Various Coals [51] 59

Figure 4-1: Research Objectives: Complexity vs Scale.....63

Figure 5-1: Layout of the Eskom Drop Tube Furnace [13].....65

Figure 5-2: Reference Coal Experimental Devolatilisation Characteristic [13].....68

Figure 5-3: CFD Model of Eskom DTF 70

Figure 5-4: Implementation of Measured Furnace Wall Temperature (Devolatilisation) 72

Figure 5-5: DTF Velocity Profiles During Devolatilisation 73

Figure 5-6: DTF Temperature Profiles During Devolatilisation 74

Figure 5-7: Volatile Gas Species Evolution During Devolatilisation 75

Figure 5-8: Iterative Algorithm for Optimisation of Coal Devolatilisation Kinetics 76

Figure 5-9: Devolatilisation Characteristic for the Reference Coal 78

Figure 5-10: Particle Temperature History for Flashchain and CFD DTF Simulations During Devolatilisation 79

Figure 5-11: Gas Temperature Profiles for CFD DTF Simulations During Devolatilisation .. 79

Figure 5-12: Implementation of Measured Furnace Wall Temperature (Char Combustion) .. 82

Figure 5-13: DTF Velocity Profiles During Char Combustion 82

Figure 5-14: DTF Temperature Profiles During Char Combustion 83

Figure 5-15: Oxygen Concentration and Char Consumption during Char Combustion 84

Figure 5-16: Iterative Algorithm for Optimisation of Coal Char Combustion Kinetics 85

Figure 5-17: Effect of Varying Char Oxidation Reactivity on Particle Burnout 88

Figure 5-18: Char Combustion Characteristic for the Reference Coal 89

Figure 5-19: Particle Burnout for Reference Coal for Different Char Combustion Kinetics .. 90

Figure 5-20: Oxygen Consumption Profiles for Different Char Combustion Kinetics 90

Figure 5-21: Mass fractions of Char, Tar and Gas as predicted by PC Coal Lab® 100

Figure 5-22: Mass fractions of the Non-Condensable Gases as predicted by PC Coal Lab® 100

Figure 5-23: Mass fractions of the Hydrocarbon Gases as predicted by PC Coal Lab® 101

Figure 5-24: Elemental Composition of Tar as predicted by PC Coal Lab® 101

Figure 5-25: Elemental Composition of Tar as predicted by PC Coal Lab® 102

Figure 5-26: Schematic of the PSCTF [60] 110

Figure 5-27: CFD model of the Pilot Scale Combustion Test Facility.....111

Figure 5-28: PSCTF Computational Mesh Details.....112

Figure 5-29: Secondary and Tertiary Swirler Configuration.....113

Figure 5-30: (a) Swirler Block Orientation for 45° and radial flow settings. (b) Fluid regions for 45°, radial and mid-positions as implemented in CFD model 113

Figure 5-31: Reference Viewing Directions for the PSCTF CFD Model 117

Figure 5-32: Temperature Contours on Mid-Section Planes for Three Different Gas Phase Combustion Mechanisms.....118

Figure 5-33: Temperature Measurements at Selected Points for Three Different Gas Phase Combustion Mechanisms.....118

Figure 5-34: Normalised Heat Release for Three Different Gas Phase Mechanisms.....120

Figure 5-35: Particle Tracks Coloured by Char Mass Fraction for Three Gas Phase Combustion Mechanisms.....121

Figure 5-36: Particle Concentration for Three Different Gas Phase Mechanisms 122

Figure 5-37: Volatile Species Distribution for Three Different Gas Phase Mechanisms.....123

Figure 5-38: Distribution of Initial Volatiles, Light Hydrocarbons and Heavy Hydrocarbons for the Five-Step Gas Phase Combustion Mechanism.....124

Figure 5-39: Required Focus Areas to Develop a Comprehensive PF Boiler Model.....130

Figure 5-40: Boiler CFD Model Layout 132

Figure 5-41: Front Wall Burner Details 133

Figure 5-42: Rear Wall Burner Details 133

Figure 5-43: Burner Swirl Implementation 134

Figure 5-44: Boiler CFD Model Volume Decomposition 135

Figure 5-45: Boiler CFD Model Computational Mesh 135

Figure 5-46: Velocity Magnitude Contours for Detailed Burner Model 140

Figure 5-47: Tertiary and Secondary Air Split 140

Figure 5-48: Simplified Burner Layout 141

Figure 5-49: Secondary and Tertiary Swirl Visualised with Streamlines 142

Figure 5-50: Comparison of Burner Flow Fields between Detailed and Simplified Models 143

Figure 5-51: Data Extraction Location in the Burner Flow Field 143

Figure 5-52: Comparison of Velocity Profiles for Detailed and Simplified Models. (a) Centreline Velocity, (b) Radial Velocity at 0m (c) Radial Velocity at 0.5m (d) Radial Velocity at 1m 144

Figure 5-53: Comparison of Turbulent Kinetic Energy Profiles for Detailed and Simplified Models. (a) TKE at 0 m, (b) TKE at 0.5 m (c) TKE at 1 m 145

Figure 5-54: Heat Exchanger Tube Bundle Arrangement 147

Figure 5-55: Primary Superheater Pressure Loss Characteristic 149

Figure 5-56: Visualisation Planes for Full Boiler Model 151

Figure 5-57: Velocity Contours on Vertical Section Planes through the Centrelines of the Burner 1 to 4 (Cold Flow) 152

Figure 5-58: Velocity Contours on Horizontal Section Planes through the Centrelines of the Burner Rows (Cold Flow) 152

Figure 5-59: Temperature Contours on Horizontal Section Planes through the Centrelines of the Burner Rows 153

Figure 5-60: Temperature Contours on Vertical Section Planes through the Centrelines of the Burner 1 to 4 154

Figure 5-61: Parameter Study on Boiler Model using Five Step Combustion Mechanism: (a) Baseline result, (b) Default Mass Diffusion Constant, (c) Reduced Swirl - 15°, (d) Reduced Swirl - 5° 156

Figure 5-62: Coal Particle Concentrations on Bottom Burner Row for Three Different Gas Phase Combustion Mechanisms. 158

Figure 5-63: Initial Volatile Mole Fractions on Bottom Burner Row for Three Different Gas Phase Combustion Mechanisms. 159

Figure 5-64: Predicted Initial Volatiles, Light and Heavy Hydrocarbons on the Bottom Burner Row using the Five-Step Combustion Mechanism..... 160

Figure 5-65: Comparison of CFD Simulation to Measured Data at the Furnace Exit..... 161

Figure 5-66: Oxygen Stratification at Furnace Outlet for Three Gas Phase Combustion Mechanisms 163

Figure 5-67: Carbon Dioxide Stratification at Furnace Outlet for Three Gas Phase Combustion Mechanisms..... 163

Figure 5-68: Carbon Monoxide Stratification at Furnace Outlet for Three Gas Phase Combustion Mechanisms..... 164

Figure 5-69: Boiler Mass and Energy Balance 166

Figure 5-70: Evaporator Heat Flux for Three Gas Phase Combustion Mechanisms..... 168

Figure 5-71: Comparison of CFD Predictions and Measurements on Burner E3 Centreline 170

Figure 5-72: NOx predictions on the Centreline of Burner E3..... 172

Figure 5-73: Particle Tracks for Different Size Fractions 173

List of Tables

Table 2-1: Specification of Coals Test in Transparent Wall Reactor [14] 31

Table 5-1: Reference Coal Proximate and Ultimate Analysis [56] 67

Table 5-2: Tabulated Experimental Devolatilisation Data for Reference Coal [13] 68

Table 5-3: DTF Devolatilisation Boundary Conditions.....71

Table 5-4: DTF Char Combustion Boundary Conditions.....81

Table 5-5: Char Reactivity Parameters 87

Table 5-6: One Step Mechanism Values 94

Table 5-7: Two Step Mechanism Values.....98

Table 5-8: Five Step Mechanism – Reaction 1 Definition 104

Table 5-9: Five Step Mechanism – Reaction 2 Definition 105

Table 5-10: Five Step Mechanism – Reaction 3 Definition 105

Table 5-11: Five Step Mechanism – Reaction 4 Definition 106

Table 5-12: Five Step Mechanism – Reaction 5 Definition 106

Table 5-13: Volatile Species Molecular Weight and Standard State Enthalpy 107

Table 5-14: PSCTF Sub Model Settings.....114

Table 5-15: PSCTF Flow Boundary Conditions.....115

Table 5-16: PSCTF Particle Size Distribution.....116

Table 5-17: PSCTF Temperature Measurements – Experiment and Prediction.....119

Table 5-18: Particle Burnout for Three Different Gas Phase Combustion Mechanisms.....126

Table 5-19: Sub-model Specification for Full Boiler Model 136

Table 5-20: Particle Size Distribution Per Burner 136

Table 5-21: 200MWe Boiler Process Conditions 138

Table 5-22: Process Conditions for each Burner 139

Table 5-23: Burner Inlets Swirl Angles 142

Table 5-24: Heat Exchanger Specifications 151

Table 5-25: Average Values of Boiler Parameters 165

Table 5-26: Particle Burnout in Full Boiler Model 172

Nomenclature

Symbol	Explanation
ε_p	Particle emissivity (-)
ε_f	Furnace wall emissivity (-)
ρ_p	Particle Density (kg/m^3)
σ	Stefan-Boltzmann constant (W/m^{2}K^4)
A	Arrhenius pre-exponential constant (kg/s)
A_p	Particle surface area (m^2)
C_p	Particle heat capacity (J/kg.K)
$Coal_{LCV,daf}$	Lower heating value of reference coal [J/kg]
$Char_{LCV,daf}$	Lower heating value of char [J/kg]
D_p	Particle diameter (m)
E	Arrhenius activation energy (J/KgK)
f_p	Particle scattering factor (-)
h	Convective heat transfer coefficient [W/mK]
h_{CO2}	Formation enthalpy of carbon dioxide [J/kmol]
h_{H20}	Formation enthalpy of water[J/kmol]
h_{SO2}	Formation enthalpy of sulphur dioxide [J/kmol]
D_O	Oxygen diffusion coefficient [cm^2 s^{-1}]
k	Arrhenius rate constant (1/s)

m_p	Particle mass flow (kg/s)
$MW_{volatile,daf}$	Molecular weight of volatile species [kg/kmol]
R	Universal gas constant [atm cm^3 mol^{-1} K^{-1}]
R_{diff}	Diffusion reaction rate diffusion constant [g cm^{-2} s^{-1} atm^{-1}]
R_c	Chemical reaction rate coefficient [g cm^{-2} s^{-1} atm^{-n}]
T_∞	Bulk temperature (K)
T_p	Particle temperature (K)
T_g	Gas temperature (K)
U_c	U_c – Fraction of unburnt carbon [ ]
$U_{VM,c}$	$U_{VM,c}$ – Fraction of unburnt combustibles (volatiles and carbon) [ ]
V	Instantaneous volatile matter content (kg)
V_∞	Final volatile matter content (kg)
Volatile $Weight_{daf}$	Mass fraction volatile material [ ]

Acronyms

AR	As received
AD	Air Dried
ASTM	American Society of Testing Materials
CFD	Computational Fluid Dynamics
C NMR	Carbon 13 Nuclear Magnetic Resonance

CoE	Centre of Excellence
CPD	Chemical Percolation Devolatilisation Model
CV	Calorific Value
DAEM	Distributed Activated Energy Model
d.a.f	Dry ash free
DPM	Discrete Phase Model
DTF	Drop Tube Furnace
EPPEI	Eskom Power Plant Engineering Institute
ESP	Electrostatic precipitator
FFP	Fabric filter plant
FG-DVC	Functional-Group Depolymerization, Vaporization, Cross-Linking
GDP	Gross Domestic Product
MCR	Maximum Continuous Rating
PA	Primary Air
PSCTF	Pilot Scale Combustion Test Facility
RT&D	Research Test and Development
RTS	Return to Service
SA	Secondary Air
TA	Tertiary Air
TDP	Tabulated Devolatilisation Process (Model)
TGA	Thermogravimetric Analysis
UDF	User Defined Function
WSGGM	Weighted Sum of Gray Gases Model

Definitions

As received	Coal quality based on the how it received from the mine
Air Dried	As received coal with surface moisture evaporated
Dry Ash Free	Coal properties stated in terms of zero ash and moisture content

1 Introduction

As the world population increases and significantly more people move to urban areas or big cities, there is a commensurate rise in the demand for reliable sources of energy. From the onset of the first industrial revolution, the combustion of fossil fuels and particularly coal, has been the mainstay of producing power and process heat. However due to rapid industrialisation in the western world, the pitfalls of burning fossil fuels became readily apparent i.e., prodigious amounts of pollution in the form of harmful gases as well as particulate emissions in the case of coal combustion. The situation has been exacerbated by the rise of developing nations in recent decades. China and India, for instance fed their rapid and continued industrialisation through extensive use of fossil fuel combustion.

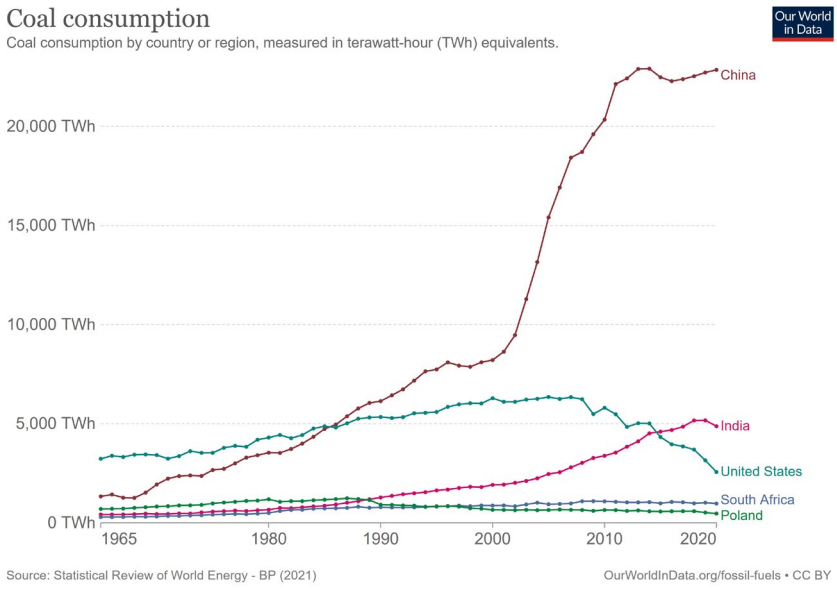

Figure 1-1: Historical Coal Consumption of Selected Countries [1]

These trends are shown in the historical coal consumption data of the selected countries. Post 2000, both India and China increased their coal consumption prodigiously in line with the observed growth in the respective countries. At the same time the coal usage in the United States declined at the start of the same period. This may be due to a larger uptake in renewable energy. But most likely corresponds to the shift to shale gas which the US had successfully exploited at this time. Also, an implicit shift of energy intensive and consequently polluting industries, was relocated from developed nations like the US and European Union to the new mass manufacturing centres in China and India. South Africa and

Poland have similar populations and industrial profiles. Poland is the last European nation with a significant dependence on coal for power generation. Their coal consumption trend is included in Figure 1-1, to demonstrate that even though the net consumption is far less than the larger economies, it is still significant. Also, the reliance on coal has been consistent for several decades. The impact of coal usage is seen in the annual CO_2 emissions (see Figure 1-2).

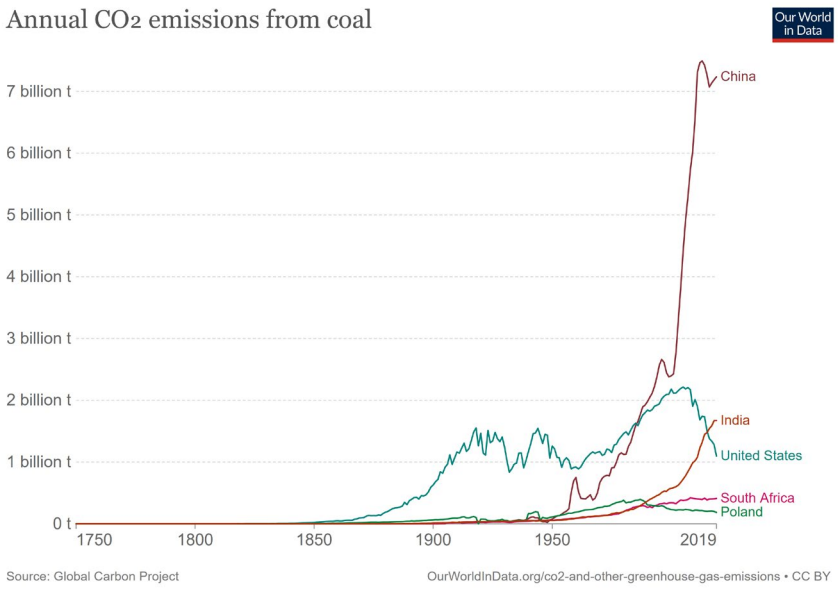

Figure 1-2: Annual CO_2 Emission from Coal for Selected Countries [2]

The emissions form the largest expanding economies in the world have increased substantially. Poland has reduced CO_2 emissions in recent decades, but South Africa has done the opposite.

However, the overall consumption must be related to output to create a fair measurement criterion. This can be done by using the energy intensity calculation which relates the total power generated from fossil fuels to gross domestic product. This is shown in Figure 1-3. A lower energy intensity shows that a particular country uses more efficient and effective industrial processes to generate GDP. Unfortunately, this indicates that South Africa is less energy intensive than China. Given the vast difference in the size of economies, this implies that South Africa is one of the worst CO_2 emitters based on population and GDP.

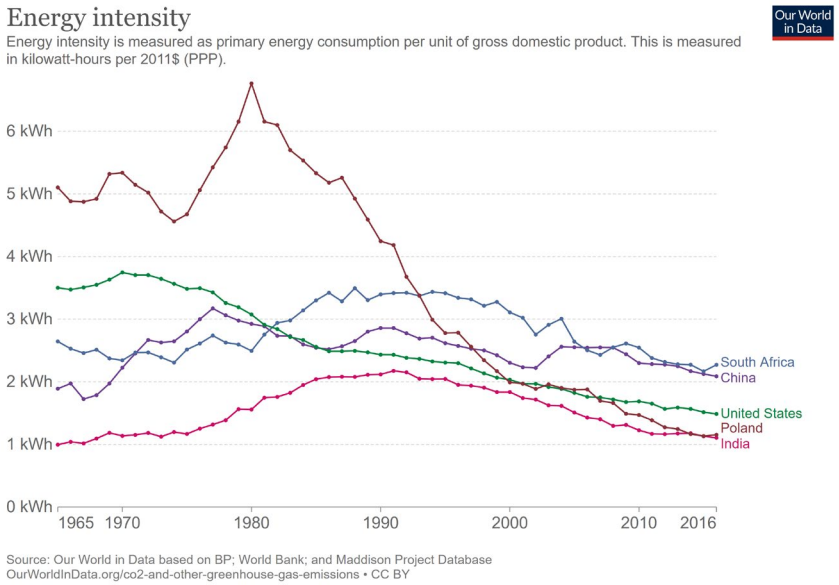

Figure 1-3: Energy Intensity for Selected Countries [3]

However, the status quo is being challenged. There is a global scientific consensus that climate change due the excessive emission of carbon dioxide and other greenhouse gases is causing a rapid increase in temperatures that in turn is having a detrimental effect on the weather patterns and consequently affecting the wellbeing of societies through scarcity of potable water and access to food. This is topical and complex issue that is being debated and researched in depth.

The immediate reaction to this impending catastrophe is to rapidly move away from burning fossil fuels to generate electricity and rather adopt renewable energy sources such wind turbines, concentrated solar power generation and photovoltaic solar electricity generation. On face value, this proposition is very attractive as it promises an abundant supply of energy with little to no emissions. However, there are still significant challenges within the sphere of renewable energy technologies that prohibit their large-scale adoption. It is also crucial to note that renewable energy production is inherently non-dispatchable. Notwithstanding the rapid improvement in energy storage technology and the potential to leverage hydrogen production, there is still a need to provide a baseload production capability that has historically been provided by nuclear, gas and coal fired power generation.

Hence it is necessary to take a pragmatic approach to the planning of the energy production in a nation state. In the case of South Africa, the country is still heavily reliant on coal fired electricity production. About 90% of the electricity generated in South Africa originates in the coal fired fleet of the state-owned power utility, Eskom. The South African Department of Energy has outlined its future energy plans in its Integrated Resource Plan Document of 2019 [4]. This plan shows there will still be a heavy reliance on coal fired energy production for some decades to come. Therefore, there is still an urgent need to research the field of coal combustion and ensure the maximum efficiencies are attained and the best possible efforts are made to reduce or contain emissions. The latter is a legislative matter, and the associated emissions regulations dictate the permissible releases to the environment.

Coal combustion will be used extensively in South Africa for some time to come. It is essential that important research into understanding the combustion process is conducted to aid the exploitation of this technology, and that it may be applied to reduce its harmful impact on the environment. Hence there is still a need to refine the available tools to improve the performance of coal fired power plants and understand what the key limitations are in operating on an electricity grid with diverse sources of energy. The introduction of renewable energy sources to the grid will require the existing coal fired plants to operate in different modes (e.g., low load) and there is a need to support the practical testing and optimisation of the plants with analysis tools.

1.1 Background

The physical process of combusting coal is complex. Several fundamental physical and chemical processes must be considered to construct framework to describe the combustion of coal. This allows for the processes to be modelled using tools such as computational fluid dynamics (CFD). By addressing the various phenomena using effective sub models, CFD can be used to gain insight into wide variety of combustion problems.

The fundamental processes occurring during the combustion of coal in a furnace were summarised by Smoot [5] and is shown schematically in Figure 1-4:

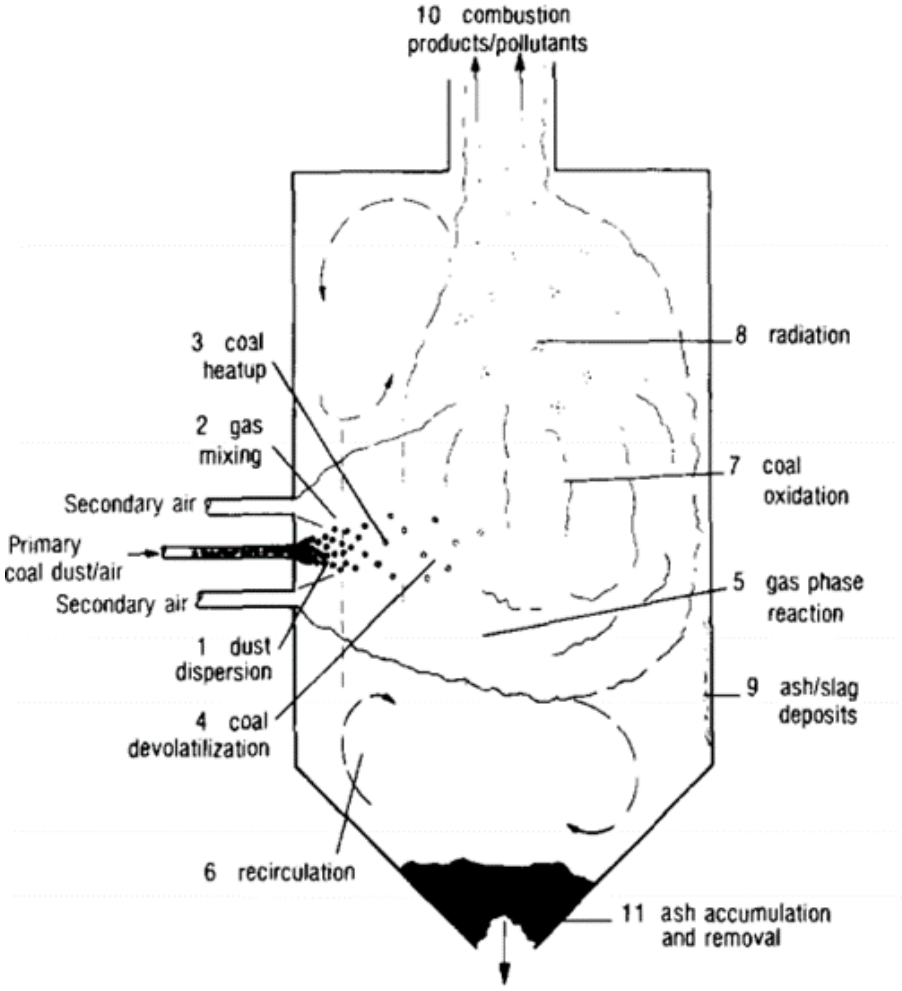

Figure 1-4: Typical Processes in a Pulverised Coal Fired Boiler [5]

The process of coal combustion in a typical pulverised coal furnace begins with the pneumatic transport of coal that is injected into a preheated furnace with combustion air support that has been aerodynamically tailored for optimum performance. The coal combustion may require initial support from a pilot oil flame.

The processes are described in more detail below [5]

1. **Pulverised Fuel (PF) Dispersion.** This relates to pneumatic transport of the PF particles through burner ducting and its delivery into the furnace region.

2. **Gas Mixing.** The flow at the mouth of a pulverised coal burner is typically of a high Reynolds number and hence the region may be considered one of turbulent mixing and this will have a bearing on the gas phase combustion as well as the heat transfer rates.

3. **Coal Heat-up.** This process refers to the modes of heat transfer between the environment and coal particles. This is important as the chemical reactions are temperature dependent.

4. **Coal Devolatilisation**. This refers to the phase of the coal combustion process where the particles are heated to a certain temperature, and they release volatile gaseous materials into gas phase.

5. **Gas Phase Reaction**. This is where the combustible materials in the gas phase react with each other. This is typically hydrocarbon combustion, and the rates and intensities of these reactions must be known.

6. **Recirculation.** The flow field with a boiler is complex and the various circulatory flows are essentially to bring back the combusting constituents back to the burner mouth to increase the heat rate to the fresh incoming PF and so enhance the devolatilisation rate.

7. **Coal Oxidation**. This is the portion of the combustion process where a large part of heat is released after devolatilisation ended. It is essentially the oxidation of the Char that is present in the Raw Coal and is governed by oxygen diffusion within the char particle through the channels that have been created during devolatilisation. Unlike

the gaseous phase combustion, this is a surface/volume related process and hence it requires its own set of rate parameters to be modelled.

8. **Radiation.** This is most dominant heat transfer mode when considering how heat is transferred from the fireball to un-combusted particles that are being introduced into the furnace region. It is quite complex as the gaseous combustion region is not optically clear due to the presence of the particulates and hence it is considered a participating media in the radiation process.

9. **Ash and Slag Deposits.** This is an issue of operational importance as the slag that attached to the boiler tubes in the furnace region reduces the heat transfer capacity of the said tubes. The production of the slag is dependant of the furnace temperature, the flow field and the properties of the coal being burnt.

10. **Combustion Products and Pollutants**. Apart from the products of the major heat generating reactions, there are also secondary processes that form pollutants such as oxides of nitrogen (NOx) and oxides of sulphur (SOx). It is important to understand how these are produced because their release to the atmosphere must be limited due to their adverse effect on the environment.

11. **Ash Accumulation and Removal**. A necessary by-product of coal combustion is the production of significant quantities of ash. The ash is not combustible, and it must be removed at a rate close to what it is produced at ensure that boiler is mechanically able to sustain the combustion process. Hence it is important to form an understanding of the properties of ash as it differs from raw coal and consequently the contribution it makes to radiation transmission within the furnace. Ash transport and accumulation must also be modelled correctly.

The processes described above only relate to the gas side combustion field in the furnace. The water/steam side of the furnace i.e., the heat exchangers and interface with the steam turbines is also important. However, as will be described in detail in later sections, the focus of this research is on the gas side.

The description above is intended to give the reader an appreciation of the complexity of the combustion process. This complexity must be contextualised in terms of the applications that

are typical of a coal fired furnace. For instance, a deep understanding of the combustion phenomena is required to optimise the performance of a low NOx burner and the implications of emissions release over a wide range of operating conditions. Furthermore, there should be a link between the modelling strategies and the inherent properties of the coal being burnt.

From an industrial perspective, CFD models that have an improved level of predictive capability can be used to optimise the entire combustion system. This can be in terms of improving combustion efficiency or emissions characteristics. The models can also be used to gain insight into the heat transfer mechanisms in the furnace when trying to find reasons for performance levels that do not correspond with the design specifications. Hence, there are a plethora of benefits to developing an efficient and accurate predictive tool for coal combustion.

1.2 Gaps Identified

The study of coal combustion is a mature field that has been researched extensively. However, much of the research has been directed at conditions more akin to the burning of coals mined in the northern hemisphere. These coals differ substantially in their combustion characteristics from the southern hemisphere that are prevalent in South Africa.

Hence the following gaps were determined from the literature what was reviewed:

- There is need to tailor the combustion models used in CFD, to account for the specificities of South African coals.
- Hence there is a need to extend the characterisation of the coals, specifically with respect to the devolatilisation and char combustion reaction kinetics, for use in CFD codes.
- The use of more detailed gas phase combustion mechanisms has not been tested in the context of South Africa coals and typical pulverised coal furnaces.

1.3 Research Questions

The following research question are pertinent to the current study:

1. What is the effect of different gas phase combustion mechanisms on the prediction of flame characteristics? This is specifically with regard to temperature and species distribution and the subsequent influence on pollutant prediction.

2. Can the prediction of carbon monoxide be improved by using more accurate coal characterisations and advanced gas phase chemistry?

3. Are there any apparent scale effects that can be ascertained from pilot scale to full scale combustion simulations?

2 Literature Review

It was described in section 1.1, that the process of burning coal on an industrial scale is inherently complex. It is necessary to formulate a workable computational baseline based on the previous research that has been conducted in this field. This chapter aims to assess the various aspects and phenomena that occur during the combustion of coal and subsequently present a best practice towards modelling these.

2.1 State of the Art in Coal Combustion Modelling

In their paper published in 2001, Williams et. al. [6], note that although modelling techniques have improved greatly, combustion modelling has not progressed to point where it could be used as a deterministic tool to predict coal combustion behaviour and hence it is not able to be used to accurately model the characteristics of combustion systems. Whilst they concede that CFD codes of the era did predict flow distributions and heat transfer well, they did not predict the rate of char burnout with sufficient accuracy. However, CFD has still been used extensively for the research of coal combustion behaviour and the design of boiler systems despite these limitations. This was most likely done by incorporating empirical data and operational experience to calibrate the models. The modelling of coal combustion requires an implementation of several sub-models to characterise the fundamental processes of inert heating, devolatilisation and char combustion. Further models are required to predict the development and transport of harmful pollutants such as NOx and SOx. Evidently, the key to improve the overall predictive capability of CFD codes with respect to coal combustion is to put attention to the individual sub-models, several studies have been conducted to build systemic models of the furnace region of coal fired boilers by incorporating advanced methods to improve the prediction of devolatilisation and char combustion. Backreedy et.al. [7] developed a model to predict the combustion behaviour of several test coals in a 1 MW furnace fired by a low NOx burner. The models developed included the use of a network pyrolysis code (FG-DVC) to improve the prediction of the devolatilisation step. Effort was also made to tailor the Char combustion models for the coals being tested using the intrinsic model developed by Smith [8]. The aim of this research was to predict the carbon in ash residue at the exit of the furnace and corelate that with observations. The models predicted the flow field and heat transfer well but highlight the sensitivity of the char burnout to correct selection of reaction mechanisms. Sankar et.al. [9] provided a

comprehensive review of computational fluid dynamics techniques that are relevant to the simulation of pulverised coal furnaces. The authors recognised the complexity of a coal fired combustion simulation and proposed the functional breakdown of the essential elements of a typical modelling technique, as shown in Figure 2-1.

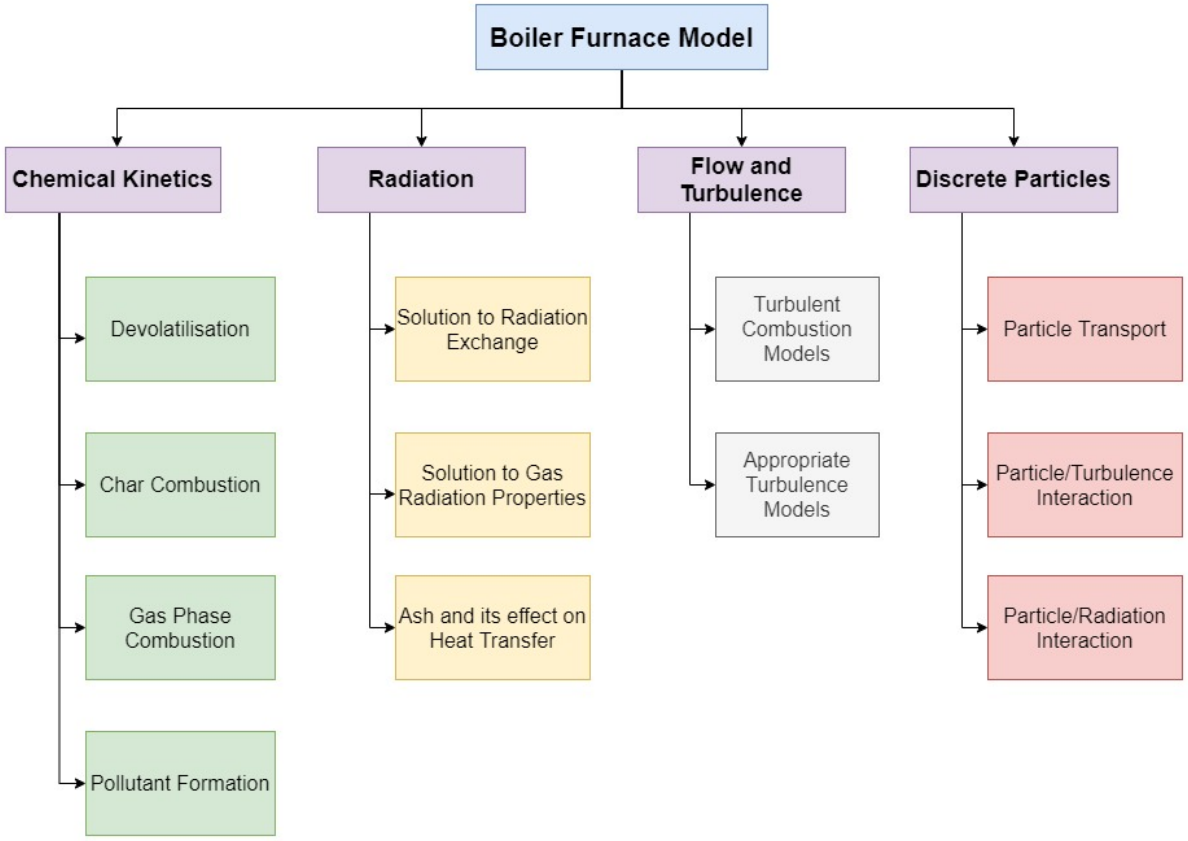

Figure 2-1: Essential Elements of a Coal Fired Furnace Simulation (adapted from [9])

The rate and manner of combustion of a coal particle is dependent on the chemical and physical transformation that it undergoes. These sub-processes are the devolatilisation of the raw coal particle and the subsequent burning of the residual char. Inherent to these processes is the transfer of matter from the solid phase to final combustion products that reside in the continuous (or gas) phase. The mechanism of these processes is governed by chemical kinetics and must be modelled using an appropriate formulation. Pollutant formation is also a highly topical area of research and hence models must be developed to predict the emission of oxides of nitrogen and sulphur. This sub processes will be discussed in detail in subsequent sections. It should be noted that the inherent moisture (see Figure 2-2) in the coal is evaporated initially and is accepted to occur before devolatilisation.

This devolatilisation process occurs rapid under the typical particle heating rate conditions seen in a furnace i.e., ~15000 K/s

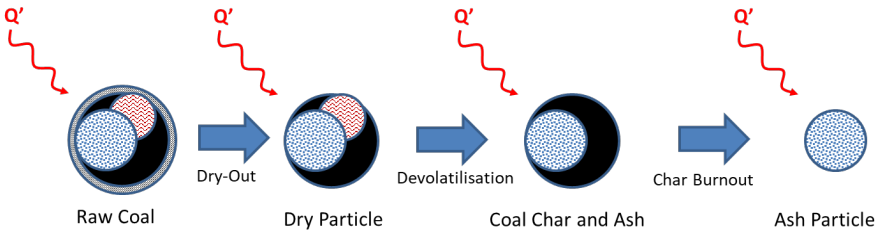

Figure 2-2: Combustion Process for a Single Coal Particle [10]

The heat transfer within the furnace is largely controlled by the radiation, due to high temperatures (1500 to 1800 °C) involved. Hence it is important to ensure that those techniques employed to simulate the radiation phenomena take into typical furnace conditions i.e., the presence of gas species (CO_2 and H_2O) that participate in radiation. Furthermore, unlike the combustions of gaseous fuels, the burning of a solid fuel such as coal results in a significant quantity of inert coal particles (several hundred tons/hour in a typical power generation furnace in South Africa) and these particles have a distinct effect on the radiation mechanisms with the furnace.

This also highlights the need to address the transport of coal particles from the burners into the furnace and finally the removal of the ash from the back end of boiler. Several methods have been used to couple the flow and particle transport. These are based on Euler/Euler methods where both phases (particle and gas) are modelling as continuous mediums. The alternative is the Euler/Lagrangian method that considers the particles as discrete and hence models their trajectories using fundamental Newtonian mechanics. The latter is more computationally intensive but considered feasible given current high performance computing capability.

Finally, the fluid flow through the furnace must be accurately modelled with a key focus on the implementation of turbulence. The gas phase combustion models are inextricably linked to flow turbulence models as they have a measurable effect on the calculated reaction rates. Hence care must be taken in finding a suitable turbulence that has satisfactory predictive capability in the free stream as well at the near-wall regions.

2.2 Combustion Modelling Framework in CFD

The complex physical interactions shown in Figure 1-4, must be modelled by the computational fluid dynamics code being used to study the facets of pulverised coal combustion. The CFD code must firstly satisfy the basic physical requirements of mass and energy conservation in an environment with multiple species and phases that are undergoing chemical reactions and releasing heat. It should be noted in the context of this study "phase" refers to either continuous medium (gases) or discrete medium (particles), as opposed to the traditional reference to changing of state of matter. For non-reacting flows, Reynolds averaging of the transport equations allows for the closure of the turbulence problem using models [11]. However, there is additional complication when dealing with non-premixed (this is the appropriate regime for the combustion of pulverised coal) combustion which is that the release of chemical energy causes large temperature gradients that are highly localised. This in turn creates significant fluctuations in the density. Versteeg and Malalasekera [11] give a comprehensive derivation of the flow equations, but the key additional mathematical feature is the implementation of Favre averaging, i.e. density averaging. The Favre averaging for a generic flow variable is shown in eq. 2.1.

$$\tilde{\phi} = \frac{\overline{\rho\phi}}{\bar{\rho}} \tag{2.1}$$

It can be shown that the continuity equation modified for reactive flow can be given as:

$$\frac{\partial \bar{\rho}}{\partial t} + \frac{\partial (\bar{\rho}\, \widetilde{u_i})}{\partial x_i} = 0 \tag{2.2}$$

The conservation can be described by the following equation:

$$\frac{\partial}{\partial t}(\bar{\rho}\, \widetilde{u_i}) + \frac{\partial}{\partial x_i}(\bar{\rho}\, \widetilde{u_i}\widetilde{u_j}) = -\frac{\partial \bar{p}}{\partial x_i} + \frac{\partial}{\partial x_j}\left(\bar{\tau}_{ij} - \overline{\rho u_i^{"} u_j^{"}}\right) \tag{2.3}$$

The enthalpy equation is given by:

$$\frac{\partial}{\partial t}(\bar{\rho}\,\tilde{h}) + \frac{\partial}{\partial x_j}(\bar{\rho}\,\widetilde{u_i}\tilde{h}) = -\frac{\partial}{\partial x_j}\left(\Gamma_h \frac{\partial \tilde{h}}{\partial x_j}\right) + \overline{S_h} \qquad 2.4$$

Where $\Gamma_h = (\mu/\sigma + \mu_t/\sigma_h)$ and σ_h is the turbulent Prandtl number.

And finally, the general species conservation is given by:

$$\frac{\partial}{\partial t}(\bar{\rho}\,\widetilde{Y_k}) + \frac{\partial}{\partial x_j}(\bar{\rho}\,\widetilde{u_j}\widetilde{Y_k}) = -\frac{\partial}{\partial x_j}\left(\bar{\rho}\,D_k \frac{\partial \widetilde{Y_k}}{\partial x_j}\right) + \widetilde{\dot{\omega}_k} \qquad 2.5$$

2.3 Sub Models for Chemical Kinetics of Coal Combustion

Sankar et.al. [9] put forward a concise review of the sub-models that are required to simulate the coal combustion processes. This is shown in Figure 2-3.

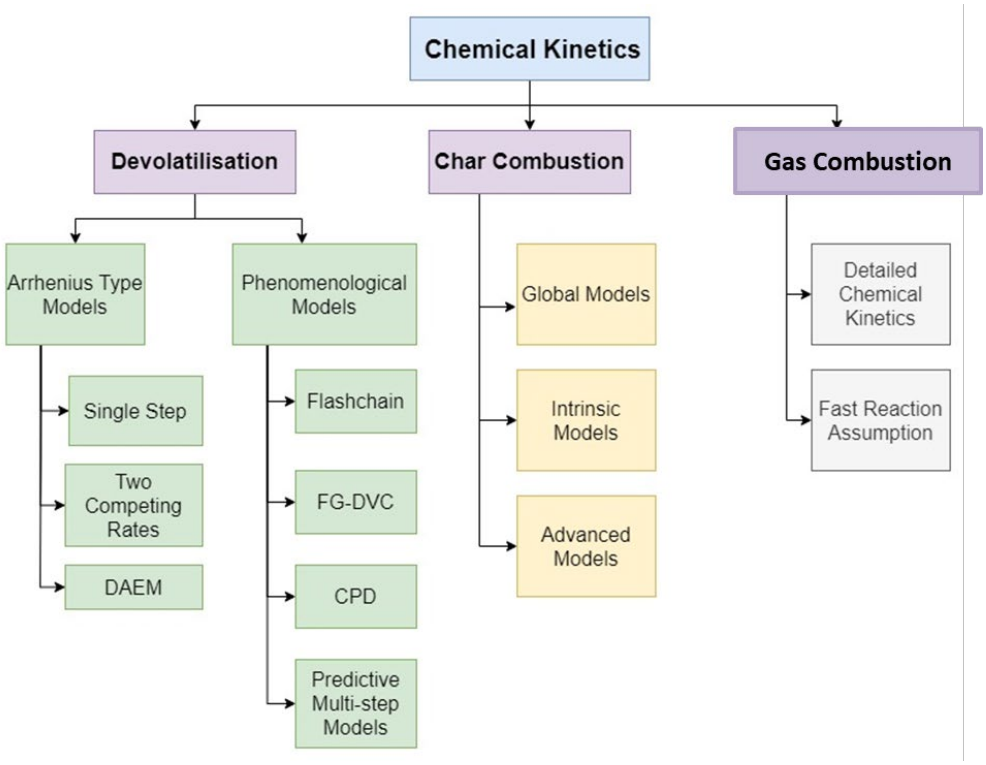

Figure 2-3: Chemical Kinetics Sub Models (adapted from [9])

Modelling strategies are required for the simulation of the devolatilisation process, the subsequent burnout of the coal char as well as the intermediate models to account for the gas phase reactions as result of the mass transfer of combustible materials from the first two processes. The modelling techniques for these processes will discussed in detail in the following sections.

2.3.1 Devolatilisation of Coal Particles

Coal is inherently a heterogeneous substance and as such it has a complex physical and chemical structure, and this is dependent on where the coal was mined. During the devolatilisation process volatile gases and non-condensable tars are released from the particle when the particle undergoes a physical transformation. The particle fragments and the volatile components are rapidly released from the particle in what appears to be a jet-like flow structure. This is shown in Figure 2-4.

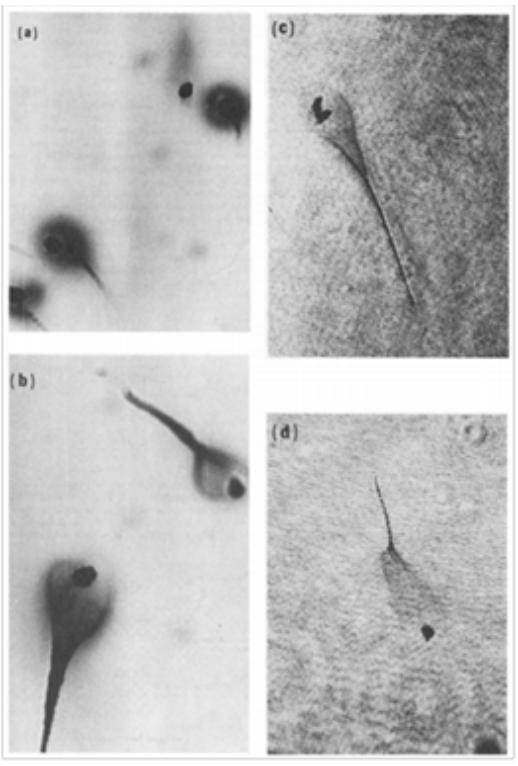

Figure 2-4: Volatile Release from Coal Particles for Typical North American Coals [8]

This release characteristic creates a cloud of combustible gaseous matter around the particle. This has an implication of the ignition characteristics of pulverised coal as in a typical combustion scenario there would be many particles adjacent to one another and the clouds of volatile matter would interact with each other. This effect was studied by Taniguchi et.al. [12] using a purpose designed laser ignition furnace and visualisation system. Eighteen different kinds of coal were tested and combusted in either air or oxygen. A visualisation of the experimental results is shown in Figure 2-5.

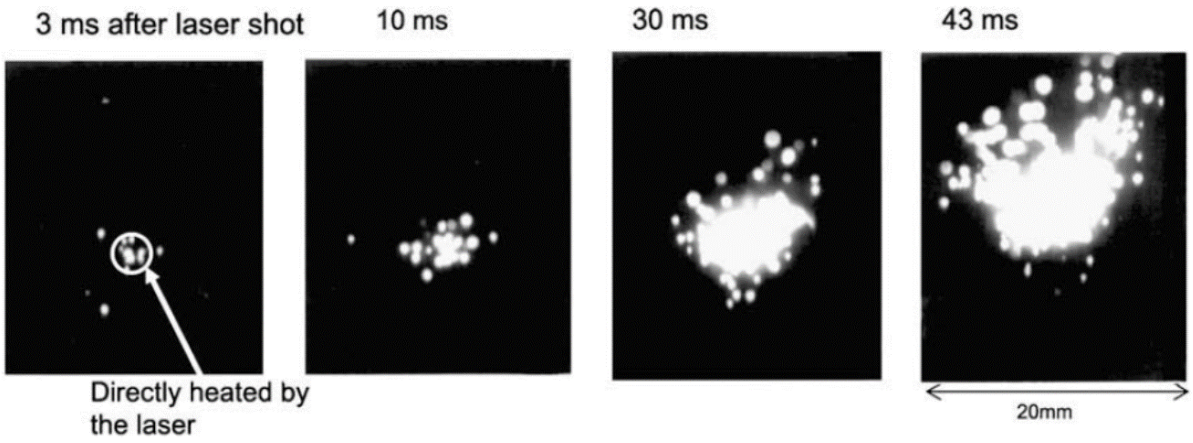

Figure 2-5: Ignition and Burning Characteristics of Pulverised Coal [12]

Taniguchi et.al. [12] also put forward a model to describe the ignition process. This model postulates that if the rate of volatile release is sufficiently high in relation to particle and gas velocities; there will be an opportunity for the volatile clouds to overlap and hence create a sustained chain reaction of sorts. This is shown in Figure 2-6.

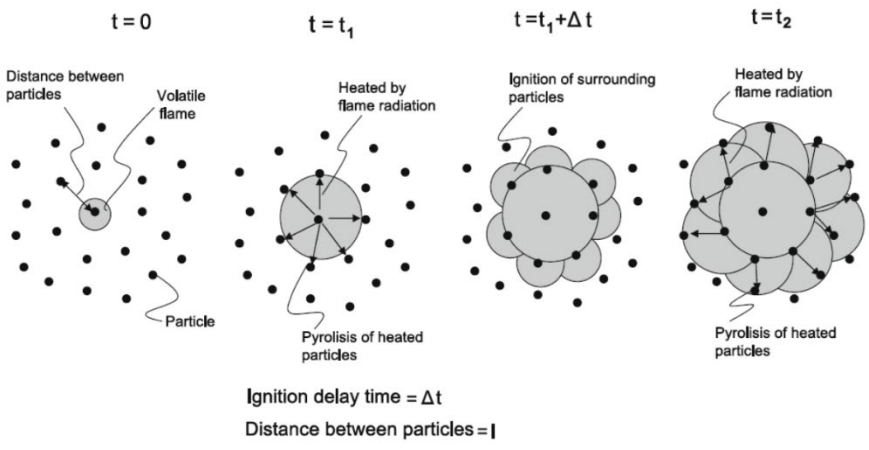

Figure 2-6: Flame Propagation Model [12]

The findings of the research were that a flame propagation velocity could be defined as well as a lean limit of flame propagation. The latter is useful to determine if combustion will be sustained at the outlet of a low NOx burner for instance. The key outcome was that both parameters were dependent on the rate of volatile release. The best-known modelling techniques are discussed in section 2.3.2 along with the empirical data needed to support the development of the models.

A further factor that must be considered is the characteristic of the coal. Coals from different parts of the world have different compositions and structures that in turn, affect the way they burn. Peta [13] investigated the ignition characteristics of several South African coals and a North American Coal using a transparent wall reactor. The results showed that under the specified test conditions the North American coal was more reactive that the South African coal, whose behaviour was more akin to anthracite. The proximate and ultimate analysis of the coals of interest are highlighted in Table 2-1. The U.S. coal is characterised by significantly higher volatile content and conversely a lower ash content. This indicates that the U.S. coal is of a higher grade than the South African coal.

Table 2-1: Specification of Coals Test in Transparent Wall Reactor [14]

Dray basis quantities		Unit	S.A. power generation coal				U.S. coal	Aus. coal
			A	B	C	E	D	F
Proximate	IM	%	-	-	-	-	-	-
	Ash	%	44.3	36.9	31.4	15.9	6.1	14.9
	Volatiles	%	20.0	24.8	21.1	24.8	43.7	31.1
	FC	%	35.7	38.3	47.5	59.4	50.2	54.0
Ultimate analysis	Carbon	%	40.8	49.8	55.7	70.1	64.9	69.0
	Hydrogen	%	1.7	2.7	2.4	3.6	5.1	4.9
	Oxygen	%	11.0	8.5	8.2	8.2	22.4	9.1
	Nitrogen	%	0.9	1.0	1.2	1.8	1.0	1.5
	Sulphur	%	1.2	1.1	1.1	0.4	0.5	0.6
	Fuel ratio	-	1.78	1.54	2.25	2.39	1.14	1.73

The experimental results from the transparent wall reactor are shown in Figure 2-8. The U.S coal is clearly more reactive than the South African coal and exhibits a larger more intense

flame and a higher flame propagation velocity. Based on the volatile content, this supports the ignition and flame propagation theory proposed by Taniguchi et.al.[15] .

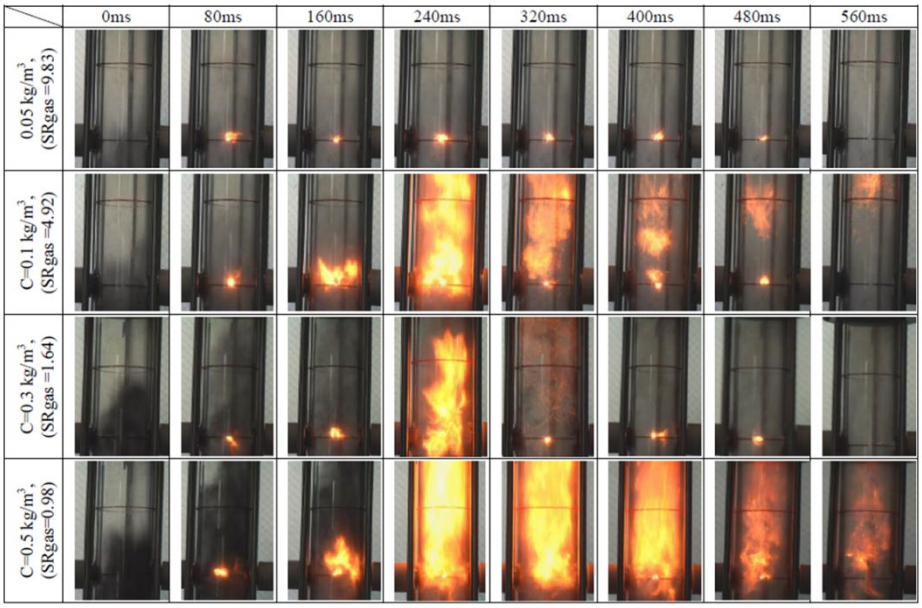

Figure 2-7: Ignition Characteristic of U.S. Coal in Transparent Wall Reactor [13]



Figure 2-8: Ignition Characteristic of South African Coal in Transparent Wall Reactor [13]

However, there is caveat to the research presented above. This apparently “poorly reactive” South African coal is routinely burnt with great success in a 600 MW South African

pulverised fuel furnace for several decades. This was described by Falcon and Ham [16]. This alludes to the fact that determining the combustion characteristics of a coal cannot be done solely using a proximate an ultimate analysis. The inherent structure of the coal must be considered as well. Elements of the theory of coal structure will be presented in section 2.5, and this will provide reasons for why this coal does indeed burn successfully.

Despite the complexities of predicting the combustion behaviour of coal, a modelling framework can be developed by using experimental data to calibrate the simulated physical behaviour. The rate of volatile release can be determined experimentally and the methods and tools to do this will be discussed below.

2.3.2 Modelling Techniques for Coal Particle Devolatilisation

Coal particle devolatilisation involves two stages i.e., low temperature pyrolysis where gaseous material and tars are released and then secondary pyrolysis that occurs at higher temperatures in which the coal char is formed due to a repolymerisation process. As described by Sankar et. al. [9] (Shown in Figure 2-3), the modelling techniques to predict the rate of devolatilisation can be broadly split into two groups i.e. Arrhenius methods or Phenomenological models. The former allows for the staged release of the volatiles whilst the latter considers more detail about the coal structure and the intrinsic mechanism of devolatilisation. Hence phenomenological models can further extend the devolatilisation information to include the relative proportions of gases, tars, and char in the volatile composition.

At this point it is important to consider how these models are validated. There are several experimental techniques that can measure the rate of volatile release under controlled conditions. These are the thermogravimetric analyser (TGA) and the drop tube furnace (DTF). The TGA uses a very precise amount of coal sample and heats it to a specified temperature at accurately controlled heating rates. The pyrolysis products can be accurately measured in the device by extensive use of gas analysers. The TGA, however, employs a heating rate that is significantly lower than that seen in a full-sized pulverised coal furnace. Hence the devolatilisation rates obtained using this method cannot be assumed to be fully representative of the true behaviour. Hence the DTF becomes a valuable tool to

experimentally determine volatile release rates that are industrially relevant. However, Czajka et.al. [17] demonstrated that devolatilisation rates obtained from a TGA could be adjusted to follow the trends shown in a DTF using extensive mathematical manipulation and assumptions based in the theory of coal structure. However, it is preferable to obtain high heating rate data from a DTF. Peta [13] used drop tube analysis extensively to determine the volatile release characteristics of selected South African coals.

The schematic of the drop tube furnace used is shown in Figure 2-9.

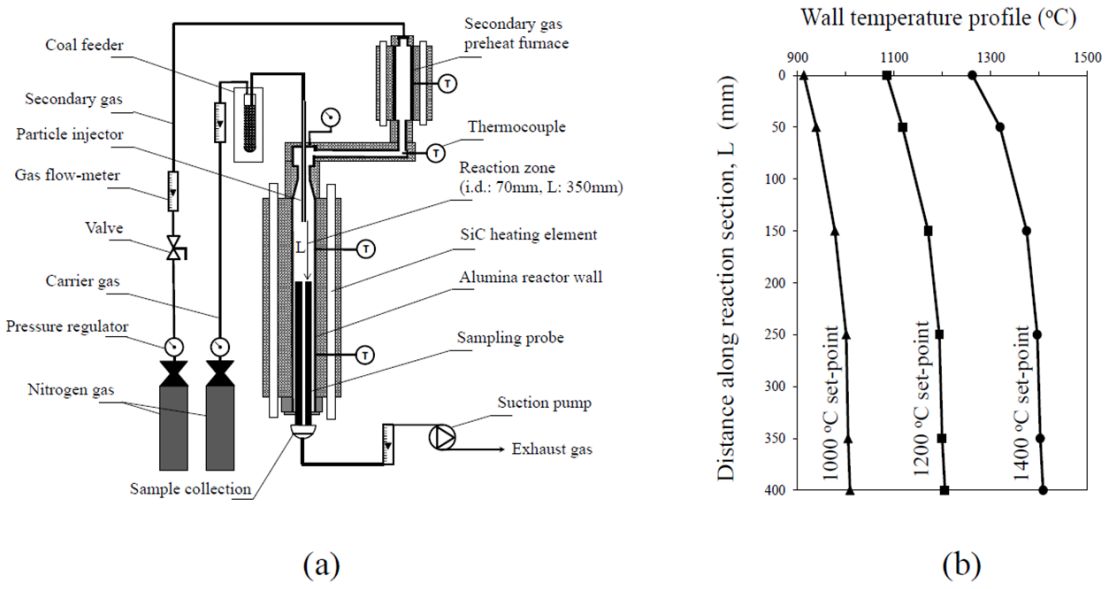

Figure 2-9: Schematic of the DTF (a) and Typical Wall Temperature Variation in the Test Section (b)

The devolatilisation of pulverised coal particles is conducted in an inert environment i.e., the working fluid is nitrogen. The reason for this is that is to avoid the onset of char combustion should any oxygen be present. Size graded coal particles are fed into test region of the DTF using a vibration feeder that attempts, ideally, to introduce the particles (typically 75µm) one at a time. This is practically, very difficult to achieve but as long of a steady stream of coal is achieved and the exact mass of coal used for a test run is known, the results will be acceptable. The nitrogen flow in the DTF test section is staged into two components i.e., the feeder gas to transport the particles and the secondary gas which is preheated to furnace temperatures. The wall of the DTF is electrically heated to achieved temperatures seen in industrial furnaces. By design this temperature should be constant, but as seen in Figure 2-9,

there is an inlet effect, and the wall temperature stabilises to the set point some distance downstream. This effect must be considered when modelling the drop tube. The coal particle will devolatilise, and the residual char is trapped in the collector vessel. The collector vessel can be moved closer to the injection point to test for a lower particle residence time. The collected char is then analysed in the lab to determine the ash content. Hence, using the ash tracer method, the original content of volatiles in coal can be determined. By considering the time of flight of the particle, the rate of volatile release can be determined. Gas species can also be measured if the sensors are available although it would be impossible to separate the products of primary and secondary pyrolysis as the tars would have had time to evolve.

Ideally, it would be expected that the quantity of volatiles released would be the same as that predicted by the proximate analysis. However, it has been shown that this is not the case at higher heating rates that are typically seen in a furnace i.e., > 10^4 K/s and above. The amount of volatiles measure is higher than the proximate value. This was first observed by Kobayashi [18] and it was rationalised that the increase in measured volatiles is due to some of the fixed carbon in the particle evolving with the gaseous phase. This higher volatile release is termed the high temperature volatile yield.

Typically, Arrhenius techniques would model the rate of release up to the defined maximum volatile yield. However, if more detail were required about the breakdown to the volatile composition, then phenomenological models would have to be considered as they consider the fundamental processes involved in devolatilisation.

2.3.2.1. Arrhenius Models for Devolatilisation

The main assumption applied to Arrhenius type models is that the rate of heating is faster than the rate of the chemical reactions involved in the devolatilisation process. This implies these models are merely mathematical interpretations of the physical behaviour and contain no intelligence with regard the structural changes that occur. Hence these models must be supported by empirical work to measure the rate of volatile release e.g., DTF experiments.

The most elementary of models employed by most CFD codes is the single rate approach developed by Badzioch and Hawksley [19] in which the rate of change of volatile matter is assumed to be proportional to the remaining volatile matter.

$$\frac{dV}{dt} = k(V_\infty - V) \quad 2.6$$

Where V is the volatile matter present and V_∞ is the total amount of volatiles that have evolved.

The rate constant k is given by:

$$k = Ae^{\frac{-E}{RT}} \quad 2.7$$

Where A is the pre-exponential exponent, E is activation energy, R is the gas constant and T is the temperature of the particle. However simple this model is, it is widely used in research since it produces good results if the parameters are supported by reliable empirical data. This modelling technique has been extended to consider the different phases of devolatilisation with respect to particle temperature. Kobayashi et. al. [18], noted that the process may be divided into two competing reactions i.e. one rate is determined for the decomposition step and another for the char formation step. It was shown experimentally that the latter reaction is more prevalent at temperatures below 1300°C whilst the former became dominate at higher temperatures. This model was employed by Peta [13] to characterise the devolatilisation behaviour of high ash South African coals. However, it should be noted that this researcher had also conducted comprehensive drop tube furnace tests and hence had reliable empirical data.

A more elaborate method to simulate the devolatilisation process was proposed by Anthony et.al., [20] where they considered that the process comprised of many parallel and independent reactions each with their own activation energy that was determined by using a continuous distribution function. The model was named the *Distributed Activated Energy Model* (DAEM). However, this model requires detailed measurements of the species distribution in relation to the particle distribution. As such it is difficult to generalise the mode to a wide variety of coals, without extensive testing.

More recently, a newer technique was developed by Hashimoto et. al.,[21], called the Tabulated Devolatilisation Process Model (TDP). The advantage of this model is that it addresses a fundamental limitation of the single rate model i.e., that the rate constant (k) is a function of only a single temperature. Clearly this is incorrect, since each coal particle would

experience a range of temperatures as it progresses through the combustion zone. This has implications for predicting the correct rate of release of volatiles especially in the areas where there are large temperature gradients as is typically seen in the ignition zone. The TDP model requires a look up table to be developed that comprises of the volatile rate release characteristics over a range of temperatures. The CFD code must be augmented to interpolate within this table based on the current particle temperature and hence reading a more appropriate rate constant for that scenario. This model adds resolution to the devolatilisation simulation; however, it requires a significant amount of input data.

Arrhenius models take a global approach to modelling devolatilisation. However, they require calibration using extensive empirical data. Due to the intrinsic heterogeneous nature of coal this implies that each of the models developed are coal specific and cannot find general application. Hence phenomenological models were developed to address this shortcoming.

2.3.2.2. Phenomenological Models for Devolatilisation

The key difference between phenomenological models and Arrhenius is that the former takes in into account the actual physical processes inherent to devolatilisation and in turn considers the chemical reactions to act on a faster time scale than that of the heating rate. The coal chemical structure is interpreted to be a macromolecular system of aromatic structures which are connected by aliphatic bridges. An example of this structure is shown in Figure 2-10.

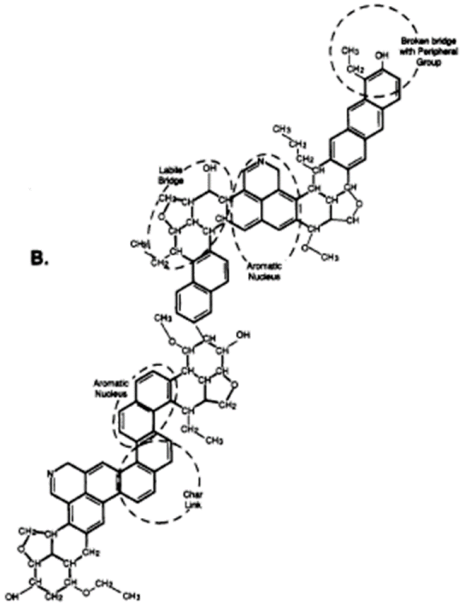

Figure 2-10: Chemical Structural Model of Bituminous Coal [22]

The main phenomenological models of interest are:

1. FV-DVC - Functional-Group Depolymerization, Vaporization, Cross-Linking [23]
2. CPD - Chemical Percolation Devolatilization Model [24]
3. Flashchain® – part of the PC Coal Lab® suite of analysis tools [22]

FG-DVC was developed by Solomon [23] and combines two existing theories i.e. the functional group method (FG) to determine the evolution of gas species and the depolymerization, vaporization cross linking (DVC) to use statistical methods to determine the evolution tars. Later the model was further developed to be able to predict behaviour of coals that were not initially part of the experimental test set. The CPD model developed by Grant et. al. [24] took a different approach in that the individual coal particles were considered to be a macromolecular array of aromatic rings that varied in size and configuration. These groupings of particles are connected by chemical bridges, which when broken during the devolatilisation process release the gaseous and tar products. Unfortunately, the input for this model relies on input form C NMR spectroscopy, which makes it difficult to apply to coals that have not been extensively tested. The generality of the model has been improved by correlating the C NMR spectroscopy data with basic ultimate and proximate analyses of the coals. The applicability of this model to the southern hemisphere must be demonstrated by further research. The Flashchain® model proposes a different strategy. Here the coal particles are comprised of several key structures i.e., aromatic nuclei, labile bridges, char links and peripheral groups. Although the coals used to test the code were initially sourced from the U.S., later research Peta [13] and Smit [25] has shown that it has applicability to South African coals.

Hence from the above descriptions. phenomenological models have an advantage over Arrhenius type models as they can predict gas yield compositions in addition to the rate of release. They can also predict secondary pyrolysis and the effects of char reactivity on the overall combustion process.

Flashchain® is the devolatilisation modelling tool chosen to be used in the current research study.

2.3.2.3. Flashchain®

Flashchain is part of a comprehensive suite of coal characterisation software called "PC-Coal Lab®" that was developed by Stephen Niksa [26]. The software is a commercial offering although it has found widespread use amongst coal research groups globally. The predictive capabilities span the devolatilisation, char combustion and gasification of a wide range of coals and biomass variants. The main parameters that are predicted during the devolatilisation phase are the yield and the release rate of the major products of primary pyrolysis. This includes nitrogen species, which is of great interest in the study of pollutant formation. The elemental composition of the char and tar products is also provided. PC-Coal Lab® only requires the proximate (as received) and ultimate analysis (d.a.f) of the coal to exploit the in-built solver and correlations and provide the above-mentioned predictions. The theoretical basis of the Flashchain® method is well documented in [26], [20] and [21]. Further elaboration on the detailed workings of the method is beyond the scope of this research study.

Chen and Niksa [29] found that the products of primary pyrolysis are tars and light gases that are driven out of the particle in a heated but inert environment (typical DTF operating conditions). These light gases tend to CO_2, CO, H_2O as well as light hydrocarbons (C1–C4).

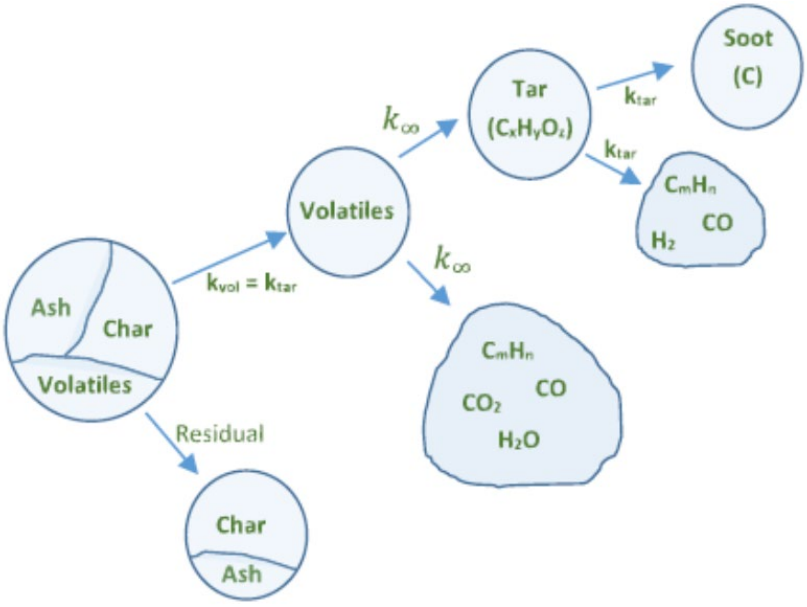

Figure 2-11: Primary and Secondary Pyrolysis Processes [30]

This behaviour is shown in Figure 2-11. Modliński and Hardy [30] elaborated on this modelling approach to simulate primary and secondary pyrolysis. Initially the embedded volatile matter is driven out of the particle under high heating rates and primary devolatilisation occurs producing the light gases. The tar compounds are heavy hydrocarbons and they pyrolyze later to form further light gases and soot. Modliński and Hardy [30] used FG-DVC to extend the single rate devolatilisation model to include the additional species considered to be devolatilisation products. The benefit of using PC-Coal lab® is that this work may be extended by incorporating an alternative method of calculating the breakdown of the volatile matter and their associated elemental compositions, all of which is essential information to implement this devolatilisation technique into a CFD code. PC-Coal Lab® was extensively validated using predominantly northern hemisphere coals. This is shown in Figure 2-12 where the total volatile yield (or the tar yield) is plotted against the carbon content of the coal. The results shown excellent corelation and hence predictive ability. Peta [13] and Smit [25] used the code extensively in analysing South African coals and hence confirmed the applicability of PC-Coal lab to southern hemisphere coals.

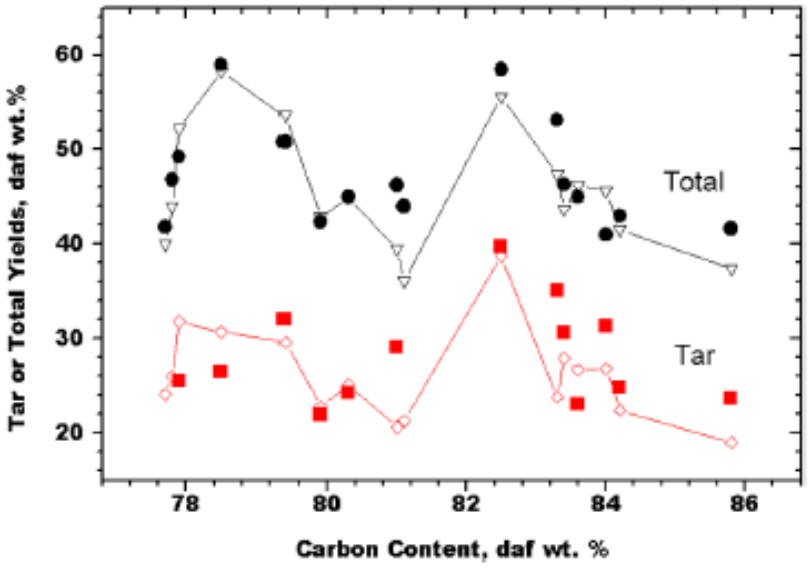

Figure 2-12: Validation of PC-Coal Lab® Devolatilisation Capability [22]

2.3.3 Modelling Techniques for Coal Particle Char Combustion

After the devolatilisation phases and the initiation of combustion, the combustion of the char in the coal particle takes over as the major energy release mechanism. The char combustion

process is slower than that of devolatilisation. The char combustion process in a typical power generation furnace usually only begins when the particles reach the centre, and the boiler is designed to ensure that the char combustion is complete before the particle laden flue gas reaches the first superheater. Sankar et.al. [9] proposed that char combustion can be segmented into three zones. In Zone 1, the temperatures are low, and the char consumption is governed by the chemical reactions which are happening slowly enough such that the supply of oxygen on the outside of the particle can be replenished. In Zone 2, the temperatures are higher and chemical reactions and pore diffusion contribute equally to the consumption of char. Since the temperatures are higher the rates of reaction are higher, and the experimentally derived activation energy of char is half of the actual value. In Zone 3, the combustion occurs at a higher temperature still. Here the reactions are very fast and the mass transfer from the particle to the continuous medium is rate controlling. The apparent activation energy is also very low. The visualisation of a coal particle at various stages of the combustion process was studied by Williams et. al. [31]. The images show how dramatically the physical structure of the particles changes and it alludes to physical transitions that any proposed char combustion models should consider. This is shown in Figure 2-13.

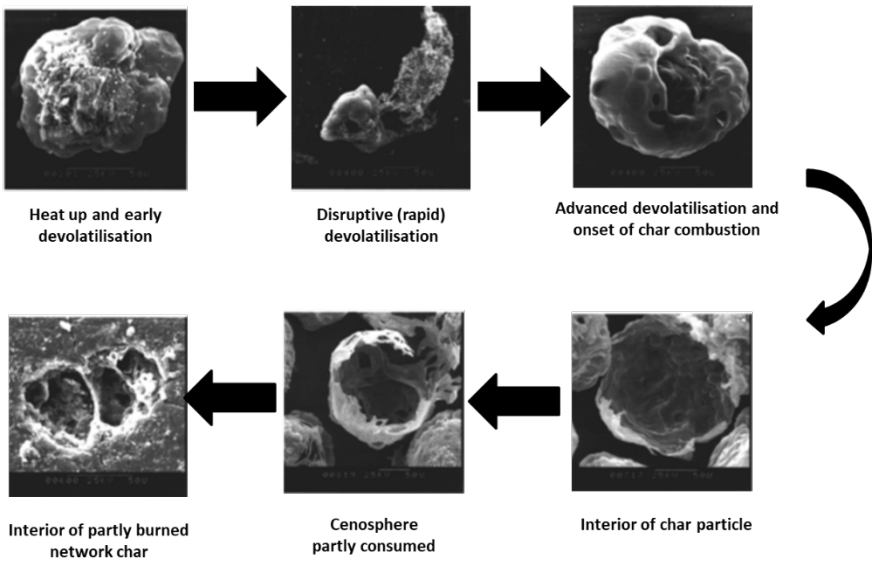

Figure 2-13 : Scanning electron microscope images of a coal particle at different phases of the combustion process (Adapted from [31])

The same level of experimental characterisation and modelling as for the devolatilisation process, is required to develop models that accurately predict the combustion of coal chars. As the char reacts with oxygen, it must be considered whether this is a surface reaction or some sort of diffusion phenomena that implies that the char particle burns form the inside out. Research into the field of char combustion has revealed that the overall process is dependent on several factors, such as the ash content and the intrinsic composition of the coal particles in terms of the presence of different maceral groups. The diffusion of oxygen into the pores of the particle also changes the rate of combustion and there is also a sensitivity to temperature at which the particle burns at. Hence the physical characteristics of the coal must be considered when formulating a model that predicts the kinetics of char combustion. Conversely, when detailed information about the char such as pore size and porosity and surface area is not available, it wise to employ a global mechanism that is supported by relevant experimental data.

It is well accepted in the research community that basic char combustion reactions are:

$$C + 0.5O_2 \rightarrow CO \quad (2.8)$$

$$C + CO_2 \rightarrow 2CO \quad (2.9)$$

$$C + O_2 \rightarrow CO_2 \quad (2.10)$$

It was shown in the extensive work of Walker et.al. [32] that the production of carbon monoxide occurs within the pores of the particle whilst the conversion of carbon monoxide to carbon dioxide is driven by the fluid mechanics within the boundary layer around the particle. From a modelling perspective successful research has been conducted using two classes of char combustion models i.e., i) Single film models and ii) Double film models. Single film models assume that all particle consumption is due to the localised oxygen concentrations. The formation of CO and CO_2 only occurs in the freestream for this model. The double film model on the other hand assume that the CO_2 produced blankets the particle and prevents the ingress of oxygen into the pores via the surface of the particle. Hence in this case the concentration of CO_2 controls the rate of char combustion. However, Mitchell [33] rationalised that for particles smaller than 130 μm the double film model is not valid. Since

typical pulverised coal combustion furnaces, which are the focus of this research, typically fire with mean particle size around 75 μm, only the single film models should be considered.

2.3.3.1. Global Models for Char Combustion

Hurt and Mitchell [34] proposed that char combustion kinetics can be represented by a rate in the form of:

$$q = k_s P_s^n \qquad 2.11$$

Where q is the burning rate per unit area, P_s is the partial pressure of oxygen (atm), and n is reaction order. The overall reaction rate coefficient is given by k_s which takes the familiar Arrhenius form:

$$k_s = A_a e^{\frac{-E_a}{RT}} \qquad 2.12$$

Where A_a is the pre-exponential exponent, E_a is activation energy, R is the gas constant and T is temperature of the burning particle. Most researchers have applied an apparent reaction order of unity, but recent studies have shown that this value may range between 0.1 and 0.2 for bituminous coal chars. Since the reaction order has a direct bearing on the rate of char combustion it was noted by Sankar et.al [9] that further research be conducted to evaluate what is the appropriate value high ash Indian coals. The situation is applicable to high ASH South African coals as well.

The model of Baum and Street [35] has found extensive application in many research studies. This model was based on the apparent activation energy of the char and the mathematical model was derived from experimental data of pulverised coal being combusted in a tube furnace at temperatures up to 1770 °C.

The model uses the following relationship to determine the mass loss of the particle:

$$\frac{dm}{dt} = -\pi D_p^2 \rho RT \left(\frac{X_{O2}}{M_{O2}}\right)\left(\frac{1}{R_{diff}} + \frac{1}{R_C}\right) \quad 2.13$$

Where:

- D_p – Particle diameter [cm]
- ρ – Particle density [g/cm^3]
- R – Universal gas constant [atm cm^3 mol^{-1} K^{-1}]
- T – Temperature of the reaction [K]
- X_{O2} – Oxygen mole fraction [ ]
- M_{O2} – Molecular weight of oxygen [gmol^{-1}]
- R_{diff} – Diffusion reaction rate diffusion constant [g cm^{-2} s^{-1} atm^{-1}]
- R_c – Chemical reaction rate coefficient [g cm^{-2} s^{-1} atm^{-n}]

The chemical reaction rate coefficient is expressed in the Arrhenius form:

$$R_c = A_f \varphi e^{-Ea/RT} \quad 2.14$$

Where:

- A_f – Pre-exponential factor [ ]
- φ – Ratio between the reacting surface and external surface area of the particle [ ]
- Ea – Apparent activation energy [J mol^{-1} K^{-1}]

The diffusion reaction rate is calculated by the following expression:

$$R_{diff} = \frac{2\Phi D_O M_C}{RT_0 D_p}\left(\frac{T_p + T_g}{2}\right)^{0.75} \quad 2.15$$

Where:

- Φ – Mechanism factor [ ]
- D_O – Oxygen diffusion coefficient [$cm^2\ s^{-1}$]
- M_C – Particle mass [g]
- T_p – Particle surface temperature [K]
- T_g – Gas temperature [K]

Baum and Street [35] also concluded that char combustion happens at constant diameter and fragmentation is only considered later in particle time history. However, issues related to changing particle size distributions and the swelling of the particles is not considered. This model is implemented in ANSYS Fluent® and is called the "kinetic/diffusion-limited surface reaction rate model" in the user interface. The code also offers a simplified version of the model where the kinetic contribution to the surface reaction rate is ignored, this model is named the "diffusion-limited surface reaction rate model" in the user interface. One other global char combustion model of interest is one developed by Mitchell et. al. [36] where the char combustion process was modelled using 43 elementary reactions.

All of the global char combustion models described in this section are limited in that [9]:

i. They do not account for the effects of pore structure.

ii. They do not account for the intrinsic reactions occurring on the surface of the particle.

iii. They do not account for fragmentation of the particles.

Despite these limitations, global models for char combustion can be useful if they are calibrated with reliable experimental data e.g., with char kinetics derived from drop tube furnace tests. This is approach that was be adopted in this study.

2.3.3.2. Intrinsic Model of Char Combustion and Other Advanced Models

Intrinsic models are more powerful than global models because they consider the pore structure within the particle and hence can incorporate more detail of the char combustion process. The model distinguishes between different pore sizes and the implication of oxygen diffusion with the particle. An appropriate oxygen diffusion modelling technique is used for the size range of the pores being considered. Smith [8], based his model on the shrinking core concept which allowed the model to be formulated independently of pore size and surface area. The model is given by:

$$\rho_c = \eta\gamma\sigma_a A_g R_i (C_G(1-\chi))^m \qquad 2.16$$

Where:

- ρ_c – Rate of char combustion per unit of external surface area of the particle [g/cm^{2}s]
- η – Effectiveness ratio
- σ_a – Characteristic size of the particle [m]
- A_g – Total surface area [m^2]
- Cg – Oxygen concentration in the bulk gas [g/cm^3]
- χ – Fraction char burnout
- R_i – intrinsic reaction rate coefficient that is expressed in Arrhenius form.
- m – True reaction order [ ]

This model did not correlate with the findings of Baum and Street [35] in that it proposed that at normal combustion temperatures the rate of char combustion is governed by diffusion and chemical reaction rate. The application of this model is limited as the rate is based on average surface area and moreover several of the parameters in eq. 2.16 require extensive laboratory work and hence each application is coal specific. This study will not consider the use of the intrinsic model of char combustion.

Several other more advanced models were developed to overcome the shortcomings of the model of Smith [8]. These are summarised by Sankar et.al. [9] and were not considered any further in the current study.

2.3.4 Gas Phase Combustion Mechanisms

The current research project was focussed on the mechanism of combustion of the various combustible species released during the burn out of pulverised coal particles. In non-premixed reacting turbulent flows (the regime applicable to PF combustion), the local time-dependent mixing and chemical reaction of the species as well as the heat transfer away from the reaction area, determine the effectiveness of the combustion process.

The main modelling challenge in computing gas phase combustion is how to determine that sources terms that feature in the transport equations, as well as the associated rates of reaction? A further complication is that rates of reaction are computed by using the average values of highly non-linear local reaction rates. The simplest approach is to assume infinitely fast chemistry. This is a plausible assumption as most species produced during combustion reach equilibrium very fast when reacting in high temperature fields. Hence under these assumptions it may be concluded that the rate of chemical reactions is governed by turbulent mixing and consequently, no kinetic data is required.

Two implementations of this type of reaction scheme are the single-step and two-step approaches. These are typically implemented as the default techniques in codes such as ANSYS Fluent® [37] and Siemens Simcentre Star CCM+® [38]. They provide sufficient to modelling detail to simulate bulk temperatures in conditions that ensure effective, complete combustion.

The single-step reaction process is described below:

$$C_m H_n O_x N_y S_z + a_1 O_2 \rightarrow a_2 CO_2 + a_3 H_2 O + a_4 N_2 + a_5 SO_2 \qquad 2.17$$

Where:

- *m,n,x,y,z* – Mole fraction of Carbon, Hydrogen, Oxygen, Nitrogen and Sulphur, respectively [ ]

- a_1, a_2, a_3, a_4, a_5 – Stochiometric coefficients of the reactants and products. [ ]

whilst the two-step reaction process is given by:

$$C_mH_nO_xN_yS_z + b_1O_2 \rightarrow b_2CO_2 + b_3CO + b_4H_2O + b_5N_2 + b_6SO_2 \quad 2.18$$

$$CO + \frac{1}{2}O_2 \rightarrow CO_2 \quad 2.19$$

Where:

- m,n,x,y,z – Mole fraction of Carbon, Hydrogen, Oxygen, Nitrogen and Sulphur, respectively [ ]

- $b_1, b_2, b_3, b_4, b_5, b_6$ – Stochiometric coefficients of the reactants and products. [ ]

The detailed implementation of these models is described in section 5.3.

The simple schemes shown above rely on the assumption that turbulent mixing plays the dominant role in the initiation of combustion. Hence once the fuel and oxidiser stream meet, combustion is assured. This is known as the "*mixed is burnt"* assumption. This assumption becomes less applicable when trying to predict the evolution of species such as carbon monoxide for instance. CO is known to oxidise very rapidly at high temperatures with sufficient oxygen supply. Conversely it does not oxidise to CO_2 as effectively when temperatures are lower, or the turbulent mixing conditions are subdued. Furthermore, at high temperatures that are typical in a coal fired furnace, the effect of the dissociation reactions become more pronounced. In this scenario it is necessary to consider the rate of chemical reactions and hence modelling of finite rate chemistry must be considered. This is particularly relevant when trying to predict the combustion behaviour of low NOx burners, where the flow field is typically comprised of a wide range of temperatures and fuel ratios.

Finite rate chemistry is important when considering the combustion mechanisms of even overtly simple reactions like the reaction of methane and oxygen to form water vapour and carbon dioxide. This reaction consists of hundreds of sub-reactions that may be reversible. It

is possible to model these many steps, but it tends to be computational expensive and does not lend itself towards being a flexible engineering analysis tool. This complex chemistry framework is implemented in the GRI-Mech 3.0 database [39], which lists the relevant reactions and their reaction parameters. Although comprehensive reaction mechanisms such as this do provide exceptional detail within the combustion field, they are computationally expensive and can become inappropriate for the design and optimisation environment. Hence several researchers have recognised this limitation and proposed reduced order gas phase combustion mechanisms. These mechanisms aim to represent the combustion flow field with a sufficient degree of fidelity for the required application.

The combustion of solid fuels such as coal, produce devolatilisation products that are highly dependent on the structure of the coal and consequently the geographical source. Hence there is no comprehensive mechanism that account for the variations in composition and hybrid models must be used.

Hautman et. al. [40] proposed a reaction scheme for the combustion of heavy and light hydrocarbons as well as subsequent CO using a four step process. The reaction rates are functions of the concentrations of the reactants and products as well as empirical constants. Modliński and Hardy [30] demonstrated that these gas phase reactions can be adapted for use in coal combustion by including a tar reaction proposed by Shaw [41] et. al. as shown below:

$$Volatiles \rightarrow \upsilon_{C_xH_yO_z} C_xH_yO_z + \upsilon_{C_mH_n} C_mH_n + \upsilon_{CO_2} CO_2 + \upsilon_{CO} CO + \upsilon_{H_2O} H_2O \qquad 2.20$$

$$C_xH_yO_z + \left({}^{x}/_{2} - {}^{z}/_{2}\right)O_2 \rightarrow xCO + {}^{y}/_{2}\, H_2 \qquad 2.21$$

$$C_mH_n + \left({}^{m}/_{2} + {}^{n}/_{4a}\right)O_2 \rightarrow mCO + {}^{(1-a)n}/_{2}\, H_2 + {}^{n}/_{2a}\, H_2O \qquad 2.22$$

$$H_2 + {}^{1}/_{2}\, O_2 \rightarrow H_2O \qquad 2.23$$

$$CO + {}^{1}/_{2}\, O_2 \rightarrow CO_2 \qquad 2.24$$

The corresponding rate expressions are given by:

$$R_1 = k_1[Volatiles] \qquad 2.25$$

$$R_2 = k_2[C_m H_n][O_2] \qquad 2.26$$

$$R_3 = k_3[CO]^{1.0}[O_2]^{0.25}[H_2O]^{0.5} \qquad 2.27$$

$$R_4 = k_4[H_2][O_2]^{0.5} \qquad 2.28$$

$$R_5 = k_5[CO][O_2]^{0.5}[H_2O]^{0.5} \qquad 2.29$$

Modliński and Hardy [30] also reviewed the work of Jones and Linstedt [42] and noted that they used an extended approach that used five steps and found that it was able to predict the combustion field for both lean and rich fuel conditions. Förtsch et.al. [43] developed a nine-step model that explicitly modelled secondary pyrolysis where the tar products oxidised to form soot, light hydrocarbons, hydrogen, and carbon monoxide. The production of the species was governed by a set of competing reactions.

The reaction rates that determine the source terms in species transport equations are predicted using generalised models to incorporate the effects of chemical kinetics and/or turbulent mixing.

One approach is to use the *Eddy Dissipation Model* as implemented in ANSYS Fluent® [37]. In this model the rate of reaction of species is assumed to be governed by turbulent mixing and by implication that the chemical timescales are fast. This is an efficient method as it avoids the additional computational overhead incurred by modelling Arrhenius type models for the reaction rates. This approach should only be used with one or two-step reaction schemes if realistic results are to be produced.

The more complicated multi-step models require that the chemical timescales be considered. Hence the more advanced turbulent combustion model known as the *Eddy Dissipation Concept*, should be used. The premise of this model is that the entire simulation domain in divided into the regions with fine turbulence structures and the remaining fluid volume. The areas of fine turbulence structures are treated as perfectly stirred reactors with a residence time that is directly related to local turbulence level. Both modelling approaches were used in the current research work.

2.3.5 In-Furnace Radiation

During the combustion of coal, the furnace of a typical power station is filled with air (N_2 and O_2, mainly), coal particles at various stages of burnout as well as the gaseous combustion products. Unlike burning natural gas or oil, coal combustion leaves behind an un-reactive remnant i.e., the ash particles. The quantity of ash is significant for most coals such that the ash particles play a role in the radiative heat transfer in the furnace. This factor is particularly important when considering South African coals which typically have high ash contents compared to northern hemisphere coals. This characteristic is well known by researchers studying South African coals and it is contextualised extensively by Falcon and Ham [16]. Sankar et.al.[9] also noted this issue in the context of the Indian coal fired power industry. Utilities in India and South Africa tend to burn coals of similar qualities and are accustomed to address the complexities introduced by burning high ash coals. If the effect of ash is not considered in a full scale CFD simulation of a boiler it could provide inaccurate heat transfer results that do not corelate with onsite observations. Furthermore, using these predictions as a basis of optimisation of the actual plant may lead to deleterious results. The heat flux at the furnace exit could be underestimated by 30% and cause deviations of up to 20% with the heat transfer from the fireball to the evaporator walls. The latter has significant influence on the ultimate electrical output of the power plant. Hence the effect of ash must be considered in the simulation of the combustion of coal particles.

From a fundamental perspective the heat transfer interactions with coal particles and their surrounds are dependent on the amount of radiative energy that is absorbed and scattered. The former can be estimated by considering an equivalent particle size parameter which will govern the diffraction of radiation and the latter is a consequence of diffraction of the incident radiation. These parameters may be determined using intensive mathematical techniques encompassed by *Mie Theory* which is described in detail in the doctoral research of Gronaz [44]. Further discussion of this technique is beyond the scope of the current research but suffice to say, Mie Theory can provide the absorption and scattering phase functions needed to characterise the particle radiation, albeit with significant computational cost. One notable advantage of Mie Theory is that it can incorporate the effect of the composition of the ash particles which is important since, like raw coal, the ash produced can vary widely.

The radiation mechanism for a coal particle is shown schematically in Figure 2-14.

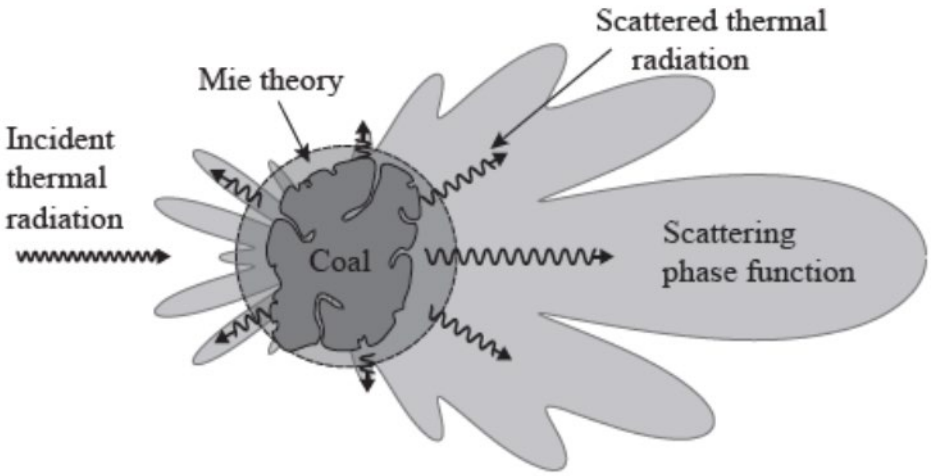

Figure 2-14: Coal Particle Radiation Mechanism [44]

Coal particles transition from raw coal to ash during the combustion process. The initial material and final combustion products have different radiative properties. Hence it is necessary to account for the transition in radiative properties as the particle traverses the furnace volume. These paths are tortuous and are affected by turbulence and several interacting swirling flows, notwithstanding the large density changes in the gaseous medium. Hence it is possible there will be a spatial and temporal distribution of raw coal and ash within the furnace.

Laubscher and Rousseau [45] simulated a South African utility boiler that burns a high ash coal (~41%) and showed that the inclusion of variable particle radiation properties in the simulation improved the prediction of heat take up in the furnace by approximately 7% compared to a simulation using constant properties. This result is highly topical to the current research. Laubscher and Rousseau [45] reviewed the literature and arrived at the correlations of Yin [46] and Lockwood [47]. The correlations are defined in equations 2.30 and 2.31.

$$\varepsilon_p = 0.4U_c + 0.6 \quad (2.30)$$

$$f_p = 0.9U_{VM,c} + 0.6(1 - U_{VM,c}) \quad (2.31)$$

Where:

- ε_p – Particle emissivity [ ]
- f_p – Particle scattering factor [ ]
- U_c – Fraction of unburnt carbon [ ]
- $U_{VM,c}$ – Fraction of unburnt combustibles (volatiles and carbon) [ ]

Laubscher [48] implemented the above relationships into an ANSYS Fluent® user defined function. This coding will be employed in this study. The solution of the radiation problem in the CFD code requires that the radiation transfer equation must be incorporated into the finite volume scheme. This method is explained in detail in the work of Yin [46]. This is in turn solved numerically by the CFD code. For this research the discrete ordinates radiation model [37] was used as it provides the capability required to model the complex interaction between the particles, gases and surfaces inside the furnace. Some of the gases that make up the combustion products absorb and scatter radiation. These are CO_2 and H_2O in this case. This effect was modelled using the Weighted Sum of Grey Gases model [37].

The solution methods listed above are considered the best practice in solving for the radiation heat transfer in a coal fired furnace and are implemented accordingly in this study.

2.4 The Principle of Operation of a Low NOx Burner

Environmental legislation is becoming stricter in terms of the allowable release of pollutants such as NOx. Even though South African legislation is currently not as strict as the European rules for fossil fuel emissions, for instance, they are still a challenge to satisfy. This is in context of a fleet of ageing plants and insufficient maintenance that makes operation at design conditions difficult. There is a structural change in the energy landscape underway in many nations, including South Africa, as they are moving towards replacing fossil fuel sourced electricity with that of renewables such as solar and wind energy. However, when one considers realistic projections considering the multitude of factors specific to the South African economy, it is very likely that coal fired power stations will be supplying base load power for several decades to come. Hence it imperative that coal fired utility operator still put attention to reducing harmful emissions whilst remaining within the economical envelope of operation.

Several researchers have concluded that the majority of NOx in a flue gas stream originates in the coal itself [49],[50]. As elaborated in section 2.3.4, when a coal particle ignites it releases tar and light gases during the devolatilisation process, into the continuous medium. These tars and light gases could oxidise to NOx products if the conditions are conducive. During the subsequent burnout of the char component of the particle, the nitrogen bound to the particle structure is released and can in turn form NOx. The NOx released during the devolatilisation process dominates the overall NOx inventory, in that it contributes between 60% and 80% of that value [51].

The common methods that have been developed to reduce NOx emissions are selective catalytic and non-catalytic method that relies on the injection of ammonia or urea into the flue gas stream, which in turn initiates the NOx reduction chemistry. The second method is to stage the air flows in the flame region. However, because char oxidation is a heterogeneous process the staging of air is not effective. Burner designers have overcome this limitation with modern low NOx burners by implementing designs that create a fuel rich NOx reduction zone. This technology has proven to be effective in reducing NOx emissions. But as always there are trade-offs. Because the final combustion of char is delayed due to the introduction of the staged air at the back of the flame region, there is an inherent propensity of low NOx burners to increase the amount of unburnt carbon at the back end of the boiler.

There are several different designs of low NOx burners. However, they all have the common operational objective of staging the airflows within the flame zone so as promote the chemical reduction of NOx products. The goal is converting the harmful NOx products into benign N_2.

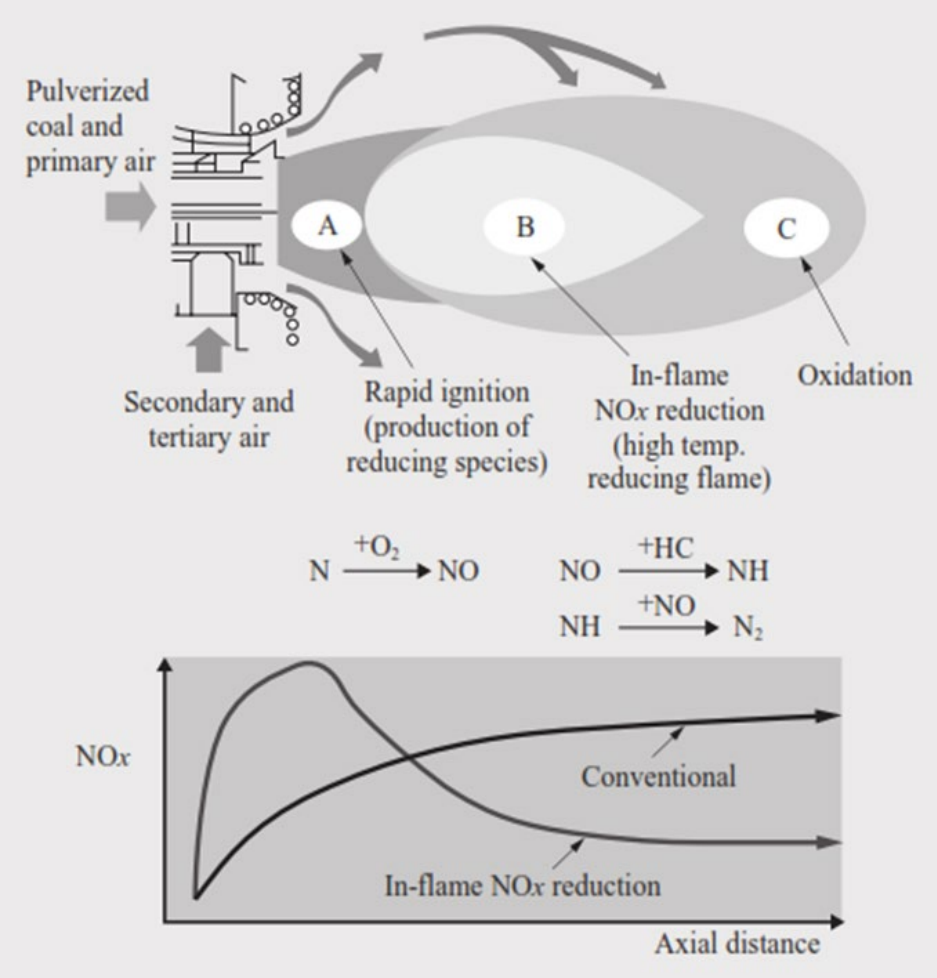

Figure 2-15: Principle of Operation of a Low NOx burner [52]

The three important regions in the staged low NOx flow field as shown in Figure 2-15 are:

A – This is the region right at the exit of the burner it necessary to encourage effective ignition that will in turn produce a stable flame.

B – This region is called the NOx reduction zone, and this created by ensuring that there is high coal particle concentration i.e., a higher concentration reduces the mean free path

between the particles and hence enhances ignition and promote better flame stability through better flame propagation.

C – This region sees the re-introduction of the staged air into the flame region and this necessary to ensure a high level of particle burnout.

The phenomenological reasoning for the process of NOx reduction requires an understating of the various paths and conversion the nitrogen oxides undergo in a reactive flow field. These chemical mechanisms are shown in Figure 2-16. The fuel rich mechanism that encourages the direct conversion of volatile and char nitrogen to N_2 is highlighted in Figure 2-16.

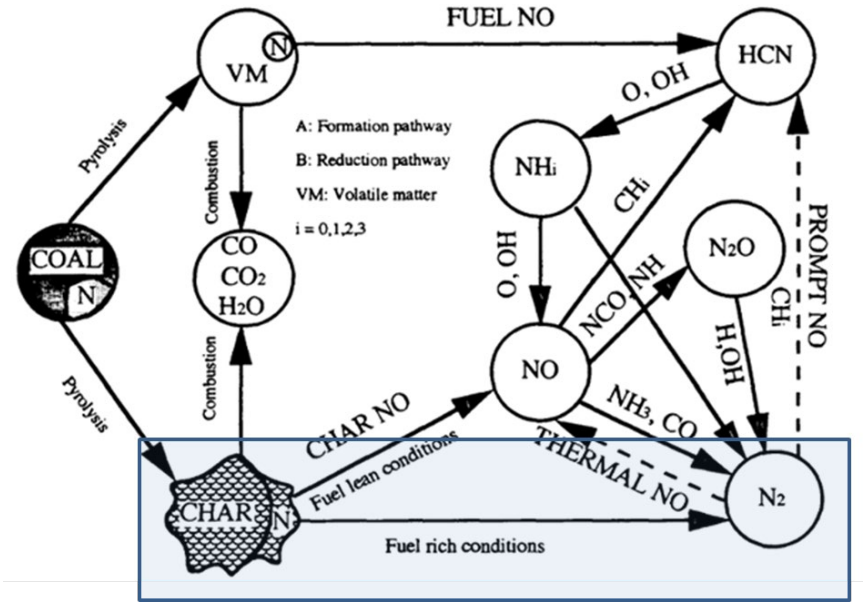

Figure 2-16: NOx formation and Reduction Pathways [53]

Abbas et. al.[53] state that key factor that must be taken into account when designing a low NOx burner is to ensure that the bulk of the coal particle devolatilisation and ignition occurs in the fuel rich region and hence expedites the conversion to N_2. Industrial low NOx burners are designed using extensive empirical input and it would be useful to be able to predict the amount of NOx in a tool such as CFD. The influence of the gas phase mechanisms in this regard could be substantial.

The typical temperature field in 550MW pulverised coal field boiler as well as the geometric layout of the low NOX burners is shown in Figure 2-17.

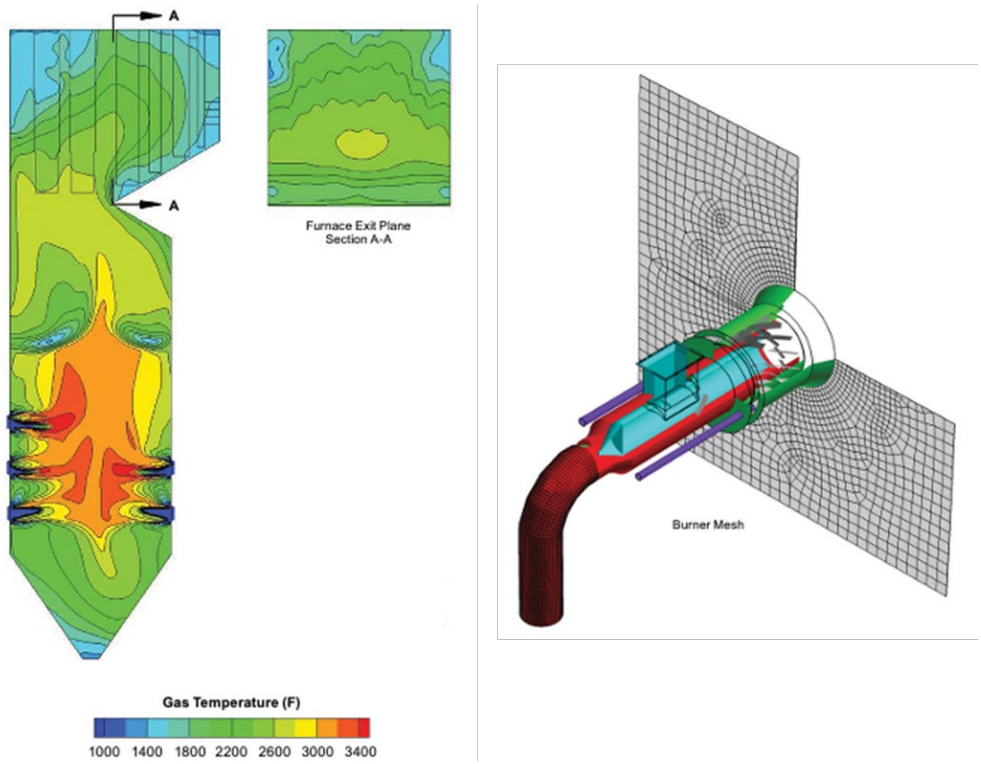

Figure 2-17: 550 MW Coal Fired Boiler CFD Simulation [54]

The corresponding temperature and velocity fields in the near burner region are shown in Figure 2-18. Note the location of the fuel rich zone as well as air staging that promotes the particle burn-out.

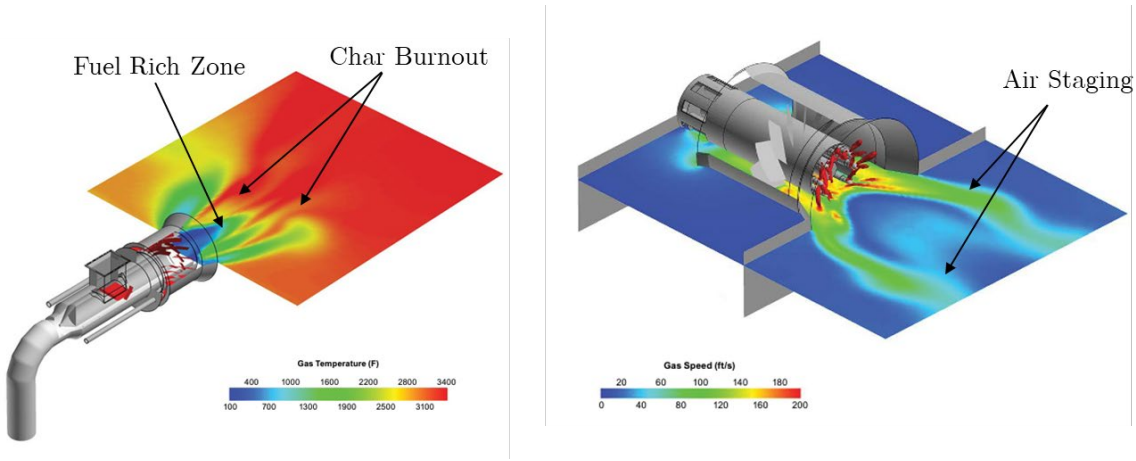

Figure 2-18: Low NOx Burner Temperature and Flow Field [54]

2.5 The Characteristics of Coal – A South African Perspective

Coal is a heterogeneous solid fuel that is comprised of combustible and non-combustible matter. Coal was formed by the compaction of a variety of organic materials under elevated pressures and temperatures over a long period of time. Hence the composition of coal is dependent on the geology of the region and its formation history. Smoot and Smith [51] noted that of the 1200 coals characterised by the Bituminous Coal Research Institute, no two had exactly the same chemical composition. Coal is considered to comprised of Carbon 65- 95%, Hydrogen 2-7%, Nitrogen 1-2%, Oxygen up to 25% and Sulphur up to 10% [55]. Coal particles can contain inorganic mineral matter (ash) in quantities up to 50% of the total mass, but typical northern hemisphere coals range between 5 and 15% ash. Moisture levels are typically in the range of 2 to 20%.

Coal is classified according to its rank as defined by the American Society of Testing Materials (ASTM) i.e., the inherent quantity of fixed carbon. This is shown in Figure 2-19.

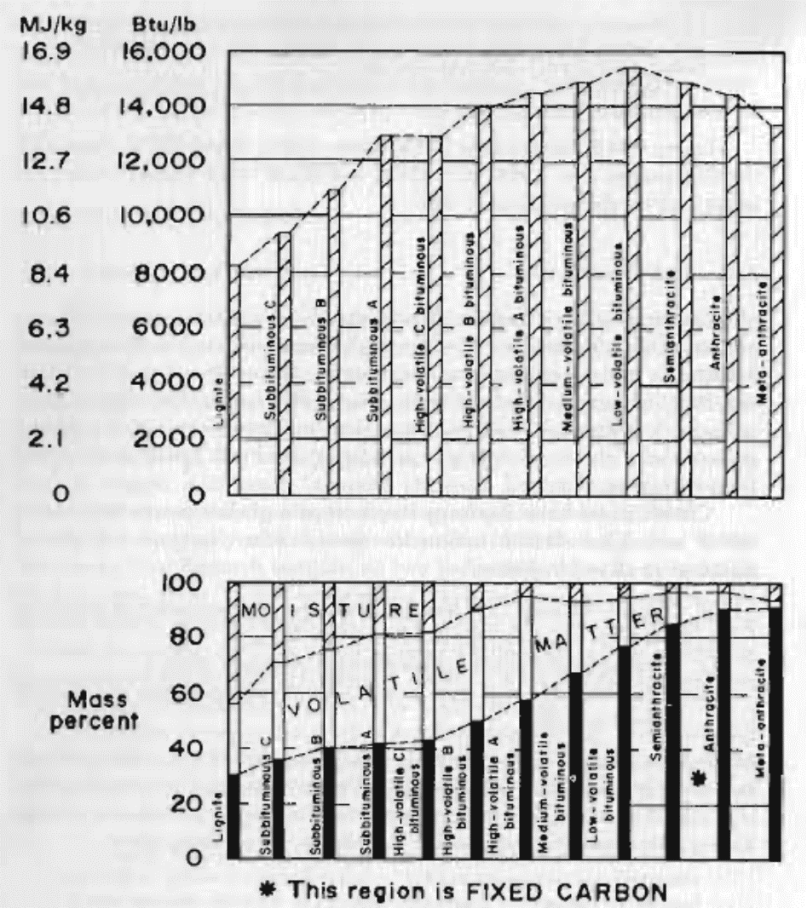

Figure 2-19: Energy Content and ASTM Rank of Various Coals [51]

Figure 2-19 shows the increase in coal rank from lignite on the left to anthracite on the right. This is matched with a commensurate increase in the fixed carbon content. Although there is a link between the volatile content and a calorific value of the coal being considered, the higher heating value is most likely specifically linked to the hydrogen content in the volatile gases that are released during combustion.

Since coal is highly dependent on where and how it was formed it is likely there will be a fundamental difference in the structure of the fuel from different parts of the world. This difference is dealt with at length by Falcon and Ham [16]. They focused on the fundamental differences between South African coals and their northern hemisphere counterparts. The issue at hand is that coals from the two regions exhibit different combustion characteristics and these must be accounted for in the design of combustion systems. The combustion characteristics of a given coal cannot reliably, be determined by its proximate and ultimate analyses only. Both are empirical techniques conducted under laboratory conditions. The proximate analysis (or "first analysis") provides a breakdown of the coal make up in terms of inherent moisture, ash, volatile matter and fixed carbon. The ultimate analysis provides an indication of the final chemical composition of the coal in terms of its carbon, hydrogen, oxygen, nitrogen and sulphur contents. Further important analysis of the coal is required to determine its calorific value and swelling index. Falcon and Ham [16] emphasise that further insight into the organic composition of coals is essential to augment the understanding of the combustion behaviour. This is typically done to quantify the organic constituents known as macerals which can be broadly grouped into either liptinite (exinite) or vitrinite. This information is obtained from a petrographic analysis of the coal. Inorganic material is defined as the mineral content and has a direct bearing on the quality of ash that is produced during firing. A further important factor is the "Rank" of the coal which gives an indication of the degree of metaphorphism. South African coals show a higher degree of diversity with respect to maceral and mineral content as well as rank when compared to typical northern hemisphere coals [16]. This diversity adds to the complexity of determining the combustion behaviour of South African coals. Macerals are typically grouped into reactive and un-reactive groups. The former has the propensity to devolatilise and ignite rapidly in the presence of oxygen whilst the latter tends to resist structural changes and requires a higher energy input to react. According to Falcon and Ham [16], the main reactive macerals are the vitrinite and exinite groups. The un-reactive macerals are termed the inertinite groups.

However, studies have shown that up to 60% of the constituents of the inertinite group are semi-reactive. Hence it is apparent that the terms *reactive* and *unreactive* are relative and not absolute. It further re-enforces the notion that a prudent and comprehensive test regime is required to faithfully characterise the combustion behaviour of coal at true combustion conditions.

Hence the need to perform thermogravimetric analysis (TGA) and drop tube furnace tests (DTF). The latter device is designed to replicate the heating rates experienced by a coal particle in a typical pulverised fuel furnace. Peta [13], performed extensive DTF tests on various coals including typical South African coals. The research showed the typical devolatilisation characteristics of the coals and emphasised that the low rank, high ash coal with higher inertinite contents tended to devolatilise more slowly. Smit [56] also used the DTF extensively but extended its use to also determine the char combustion kinetics of a single South African coal.

The volatile matter in the coal is derived from both the maceral and mineral constituents. During combustion this volatile matter is released from a coal particle and manifests as tars, oils, hydrocarbon gases, hydrogen, and oxides of carbon. This fundamental composition and subsequent break-up were a key focus area of the current research.

Falcon and Ham [16] gives practical context for applying more in depth methods to characterise coals by noting that the Lethabo Power Station (6 x 600MW) is designed to burn a coal with an ash content of up to 55% and a volatile content as low as 9%. By any conventional metric this would be a very poor choice of coal for steam generation. However, Eskom has been able to operate the boilers successfully to levels as low as 45% MCR, both safely and reliably. This combined with typically, 0.5% of unburnt carbon. Much of this success may be attributed to the fact Eskom's engineers and operators at the time, acknowledged the unique characteristics of South African coal and implemented design modifications to the plant during the construction phase. This included increasing the height of the boiler and optimising the mills to provide a finer product; typically, an average of 75 μm pulverised fuel particles.

Falcon and Ham [16] rather elegantly summarise the issues raised by stating: *"The evidence summarized in this paper indicates that the coals of the Gondwana region, and Southern Africa in particular, are not necessarily poor - only different"*

3 Hypothesis

The choice of gas phase combustion mechanisms (and consequently the assumed physics) will influence the structure of a pulverised coal flame. This may be evident by differing temperature distributions as well as the formation combustion products and pollutant species.

4 Research Objectives

The overall objective of this research was to develop a baseline computational fluid dynamics (CFD) approach to model the combustion of a typical South African coal. This entailed a multi-scale study to determine the most appropriate inputs for the model in the CFD code and subsequently apply this to pilot scale and full-scale simulations. The pilot scale simulations provided insight into the dynamics of the flame in a controlled one megawatt test rig whilst the full-scale simulation will consider the effects of a large combustion volume and complex aerodynamics introduced by multiple burners in a reactive, turbulent, swirling flow field.

Hence the objectives explicitly put, are:

1. Develop a detailed characterisation of the reference coal to be used in the study. This will entail comprehensive devolatilisation and char kinetics.

2. Development of a representative model of the 1 MW Pilot Scale Combustion Test Facility situated at Eskom RT&D. The output of the model should be to provide insight into flame characteristics and to confirm the measured burn-out time of the coal. The influence of the gas phase combustion mechanisms on the behaviour of the single burner flame will be studied.

3. Development of a representative model of the complete furnace of a typical 200 MWe, South African pulverised coal fired boiler. This model will provide detailed insight into the complex aerodynamics, thermodynamics and chemical

reactions occurring within the furnace. The influence of the gas phase combustion mechanisms in a multi-burner environment will be explored.

The research objectives are shown schematically in Figure 4-1, where the commensurate increase of complexity that accompanies an increase in scale is emphasised.

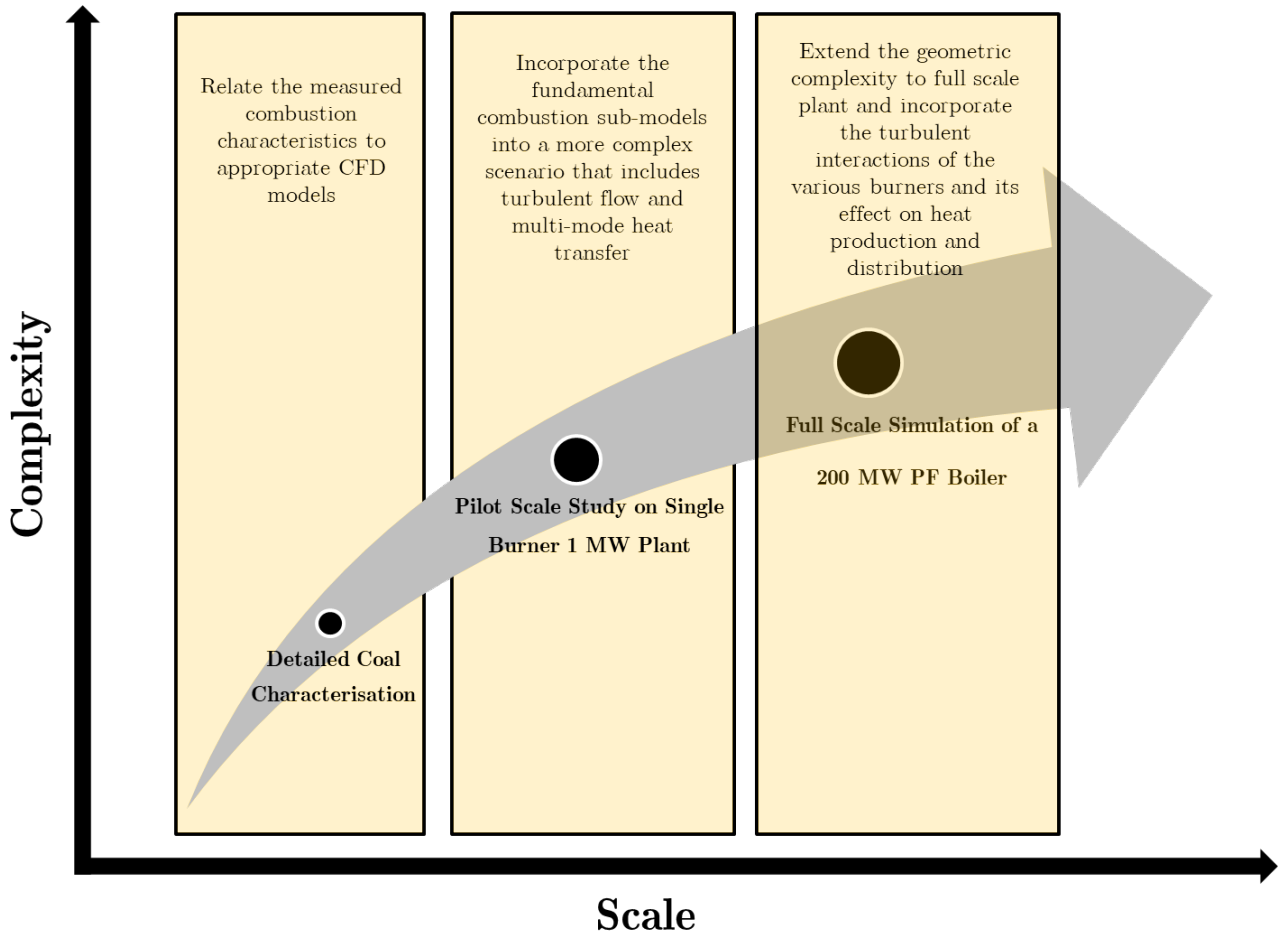

Figure 4-1: Research Objectives: Complexity vs Scale

5 Research Method and Results

Chapter 5 will describe the research methodology employed during this study. It will be structured in such a way as to describe the progression of analysis from laboratory scale to pilot scale and finally full-scale simulations. The method presented will explore the combustion characteristics of a reference coal at these scales.

5.1 Research Tools

The following tools were used to conduct the current research study:

1. The primary CFD tool was ANSYS Fluent® v19.2
2. A secondary CFD tool in Siemens Star CCM+ v13® was also employed.
3. Solidworks® 2020 for CAD development.
4. Mathcad® v15.0 for systemic calculations.
5. PC-Coal Lab® V4.3
6. Microsoft Excel® for general data processing and presentation.

Experimental data was used for validation and model development purposes from the following plants:

1. The Eskom RT&D Drop Tube Furnace was used to develop the coal devolatilisation and char combustion characteristics.
2. The Eskom RT&D Pilot Scale Combustion Test facility was used to validate the CFD model of the same plant and draw parity between simulated and experimental coal burnout times as well as the predicted temperatures.
3. A 200 MWe Pulverised Coal Boiler in the Eskom fleet was used as the basis of the full-scale study and measurements on the plant were used for validation purposes. Experimental data for temperature and combustion product species concentrations will be used for comparison.

5.2 Drop Tube Furnace Simulations

5.2.1 Background

The purpose of the DTF simulations is to correlate the experimental data with a reference CFD simulation. This in turn provides the analytical basis for determining the appropriate kinetic parameters for the devolatilisation and char combustion phases of the coal particle combustion process. This kinetic data will be used in the more complex CFD simulations. What is important to note is that this not merely a curve fitting exercise to find the required Arrhenius equation parameters. Rather it is a structured method to incorporate analytical tools such as PC-Coal Lab® and ANSYS Fluent® to replicate the coal devolatilisation and char combustion characteristics in an accurate representation of the Eskom DTF. The challenge is to replicate the same experimental behaviour whilst simultaneously simulating the flow and temperature field in an accurate representation of the DTF geometry as well as the mass and heat transfer interface with the devolatilisation and char combustion sub-models

5.2.2 DTF Rig Layout and Operation

The layout of the Eskom DTF is shown in Figure 5-1:

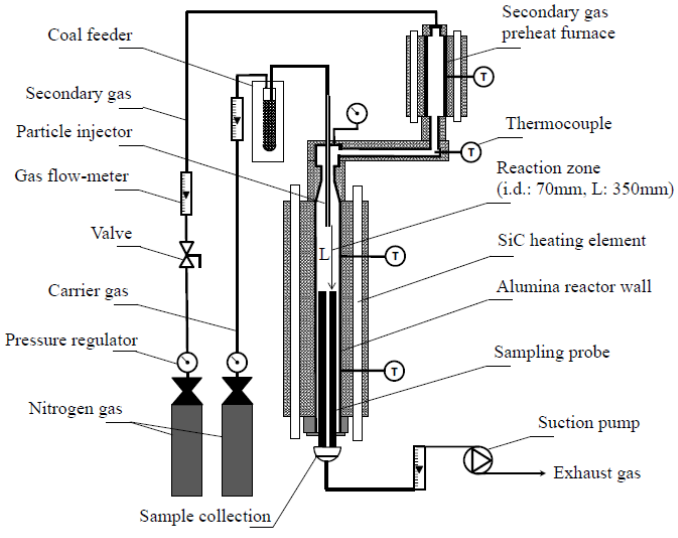

Figure 5-1: Layout of the Eskom Drop Tube Furnace [13]

The purpose of the DTF is to simulate the devolatilisation of a single coal particle at heating rates that are like those seen in a full-scale furnace. This is achieved by introducing the coal particles into the electrically heated test section. The internal diameter of the furnace region is 70mm and is lined by a ceramic (alumina) tube. The particle feeder uses high frequency vibrations to as best as possible, inject the particles one at a time. Nitrogen gas is used for the both the feeder line and carrier gas. Hence the devolatilisation occurs in an inert environment and therefore the char combustion process does not occur. However, there is some evolution of the volatile products as there may be oxygen released during devolatilisation. This is very difficult to prevent in a DTF. The resultant experiment essentially performs a separate effects test to only consider the devolatilisation process. The DTF has a water-cooled collection funnel that can be raised and lowered relative to injection point to perform tests at varying particle residence times. One other notable feature of the DTF is that it is run under laminar flow conditions and the particle quickly reaches its terminal velocity and hence travels at a constant velocity through the furnace for a large proportion of the residence time. This infers that the convective heat transfer coefficient is predictable, and the particle has enough opportunity to approach the furnace set point temperature. The governing heat transfer for the coal particle is given in equation 5.1. The term on the left-hand side represents the transient heating of the particle whilst the first term on the right-hand side is the convective term whilst the second represents the thermal radiation heat transfer,

$$\frac{4}{3}\pi r_P^3 \rho_P c_p \frac{dT_p}{dt} = 4\pi r_P^2 h(T_\infty - T_P) + 4\pi r_P^2 \sigma(\varepsilon_f T_f^4 - \varepsilon_P T_P^4) \qquad 5.1$$

Where:

- r_p – Particle radius [m]
- ρ_p – Particle density [kg/m^3]
- c_p – Particle specific heat [J/kgK]
- T_p – Particle temperature [K]
- T_∞ - Far field gas temperature [K]
- h – Convective heat transfer coefficient [W/mK]

- σ – Stefan- Boltzmann Constant [5.67 x 10^{-8} $W^{-2}K^{-4}$]
- ε_f – Furnace wall emissivity [ ]
- ε_p – Particle emissivity [ ]

Since coal combustion typically occurs at high temperature i.e., above 1400 °C, the radiation heat transfer term dominates i.e., it contributes to 90% of the overall heat transfer. An important observation is that emissivity of the coal particle and furnace wall place an important role in determining the radiative heat transfer. For all simulations considered in this study, the raw coal particle density was assumed to be 1200 kg/m^3 and the specific heat was 1100 J/kgK. The particle swelling factor was always set to 1.2.

The properties of the reference coal used in this study is collated in Table 5-1:

Table 5-1: Reference Coal Proximate and Ultimate Analysis [56]

		As Received	**Air Dried**	**Dry**	**Dry Ash Free**
Proximate Analysis					
Inherent Moisture	[%]	7.85	3.30	0.00	0.00
Ash	[%]	27.73	29.10	30.09	0.00
Volatile Matter	[%]	19.54	20.50	21.20	30.33
Fixed Carbon	[%]	44.88	47.10	48.71	69.67
Ultimate Analysis					
Carbon	[%]	52.89	55.50	57.40	82.1
Hydrogen	[%]	2.73	2.86	2.96	4.2
Oxygen	[%]	6.43	6.75	6.98	10.0
Nitrogen	[%]	1.21	1.27	1.31	1.9
Sulphur	[%]	1.16	1.22	1.26	1.8
Carbon	[%]	0.00	0.00	0.00	0.0
Gross CV	[MJ/Kg]	20.90	21.93	22.68	32.44

The reference coal is a typical South African steam coal, characterised by a relatively high ash content and low volatile content. This coal was tested by Smit [56] in the Eskom DTF and the devolatilisation characteristics were determined for three temperature i.e., 1000 °C, 1200 °C and 1400 °C. The data is presented in the form of a particle mass loss versus residence time and indicates the percentage of volatiles released relative to the original particle weight. The particles are introduced to the DTF in a dry state. Further detail on the execution of the DTF tests can be found in the work Smit [56] and Peta [13].

The experimental devolatilisation curves for the reference coal are shown in Figure 5-2 and the data is listed in Table 5-2.

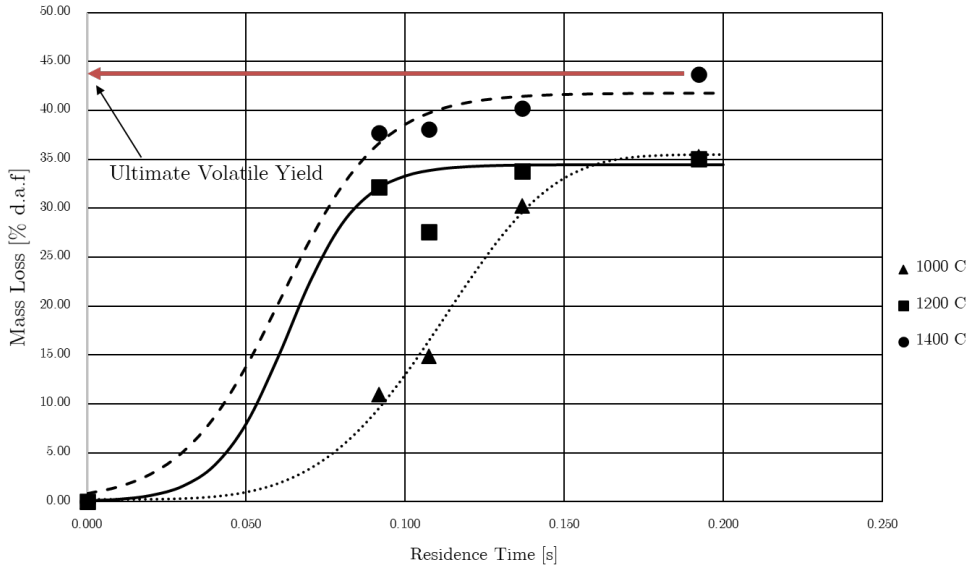

Figure 5-2: Reference Coal Experimental Devolatilisation Characteristic [13]

Table 5-2: Tabulated Experimental Devolatilisation Data for Reference Coal [13]

		Particle Mass Loss [%] (d.a.f)		
		1000 °C	1200 °C	1400 °C
Residence Time [s]	0.000	0.00	0.00	0.00
	0.092	10.95	32.16	37.67
	0.107	14.85	27.62	38.10
	0.137	30.27	33.80	40.25
	0.192	35.28	35.04	43.66

For the purposes of the current research work, only the 1400 °C curve is of interest as it relevant to normal operation on a full-scale boiler. It should be noted that peak experimental mass loss value, 43.66% d.a.f. is significantly higher than the value in the proximate analysis, 30.33% d.a.f. This is a demonstration of the well accepted phenomenon known as the high temperature volatile yield, which was noted by Kobayashi [18]. It is postulated the reason for this disparity is caused by test conditions i.e., the proximate test is done under even temperature conditions, whereas the DTF more closely follows actual furnace conditions. This implies that the particle passing through the DTF experiences a significantly higher heating rate and this causes ruptures in the porous structure of the coal particle and additional volatile material is released. The high temperature volatile yield is defined in equation 5.2.

$$High\ Temperature\ Volatile\ Yield = \frac{Peak\ Experimental\ Yield}{Proximate\ Yield} \tag{5.2}$$

The high temperature volatile yield for the reference coal is 1.44 or 44%.

5.2.3 CFD Model of the Drop Tube Furnace

The next phase of the research study was to develop a CFD model of the Eskom DTF and correlate the numerical predictions with the experimental findings.

A three-dimensional, 360-degree model of the DTF was created in ANSYS Design Modeller and Mesher ® and solved using ANYS Fluent® V19.2. The geometry of the model including a view of the mesh is shown in Figure 5-3. The mesh is comprised of 2 095 776 hexahedral cells of a high quality. The test section is 400 mm for the devolatilisation cases as the collection cup is in its position closest to the injection nozzle. This was done to ensure that the lowest residence times could be achieved. Although the model operates at a laminar Reynolds number, the simulation was conducted using the standard k-epsilon model with low inlet turbulence. It was necessary to do this to enable the species transport combustion model in ANSYS Fluent®. The model consists of three flow boundaries i.e., a carrier gas inlet that introduces a nitrogen gas stream as well as the coal particles. The second inflow boundary is that of the secondary gas, which enters the DTF after being preheated in the gas pre-heater. Finally, the gases and devolatilised coal particles exit the model by passing through the collector outlet. Since radiation is the dominant heat transfer mechanism in the furnace it was

important to resolve it sufficiently. Hence the discrete ordinate model was used with the standard discretisation. This radiation model allows for the usual wall to wall interactions but also provided a way to account for particle radiation and its effect on the local thermal and flow field.

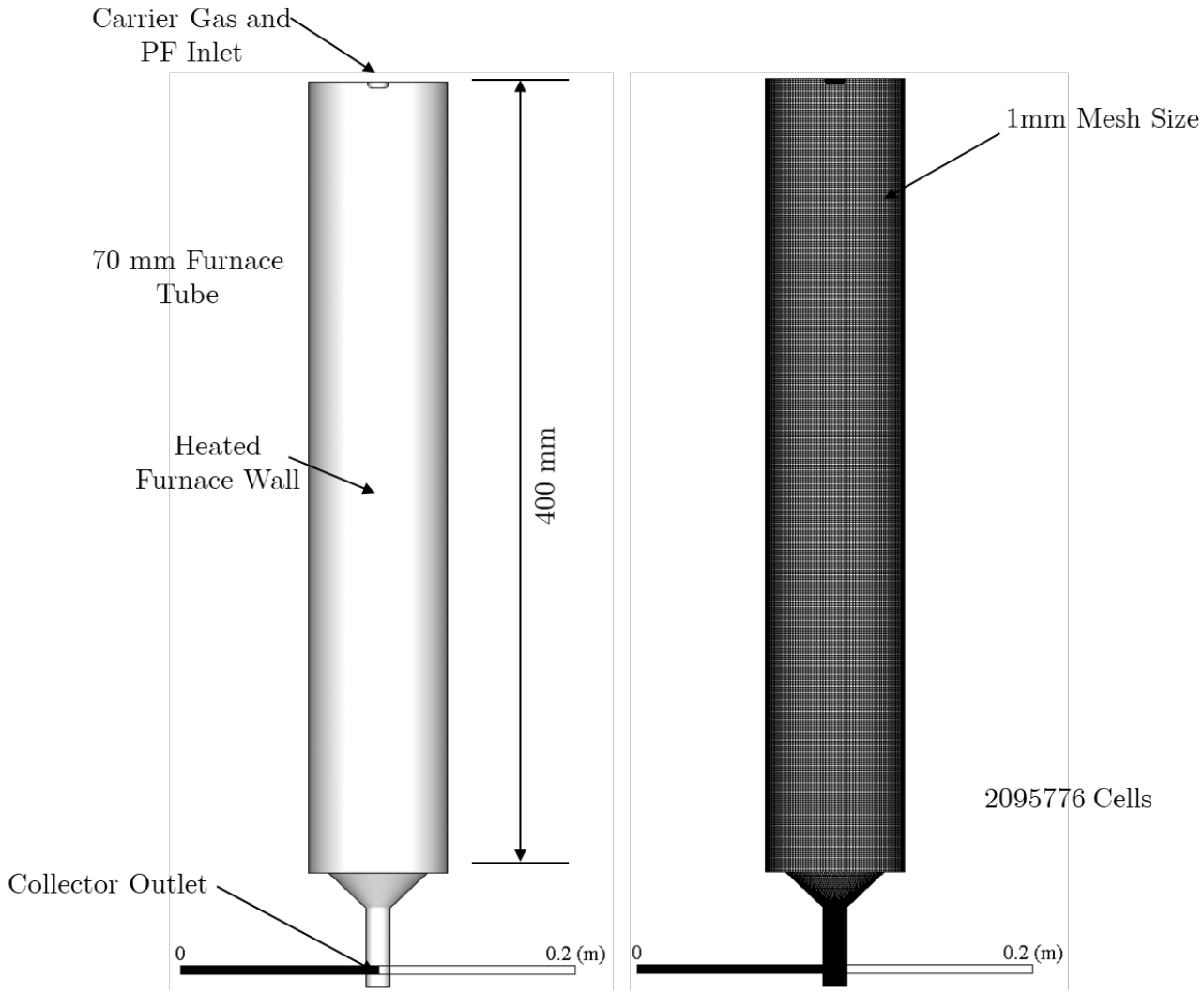

Figure 5-3: CFD Model of Eskom DTF

The input values for each of the boundaries is listed in Table 5-3. Additionally, all walls were assigned an emissivity value of 0.8. The flow boundary conditions are consistent with experimental work done by Peta [13].

Table 5-3: DTF Devolatilisation Boundary Conditions

Carrier Gas Inlet (Velocity Inlet)	
Inlet Velocity	1.59 m/s
Inlet Temperature	25 °C
Hydraulic Diameter	0.02 m
Turbulent Intensity	5 %
Nitrogen Mass Fraction	100 %
Secondary Gas Inlet (Velocity Inlet)	
Inlet Velocity	1.9 m/s
Inlet Temperature	1170 °C
Hydraulic Diameter	0.06 m
Turbulent Intensity	5 %
Nitrogen Mass Fraction	100 %
Collector Outlet (Pressure Outlet)	
Static Pressure	85 kPa (Absolute)
PF Injection (Point Injection)	
Particle Size (Constant)	90e-5 m
Particle Temperature	25 °C
Particle Flow Rate	1.96e-5 kg/s

A constant particle size was simulated, and this was taken as the mean of the measured size distribution. The furnace of the DTF is a ceramic tube that is heated by a coiled electrical element. Ideally it would be desirable for the heater to work with 100% effectiveness and impart the set point temperature to the entire furnace wall. Due to design limitations, the heating element does not impart a uniform temperature to the wall. This is a crucial aspect of the model as the heat radiated from the walls has a direct bearing on the heating rate of the particle and hence the devolatilisation rate. Hence the measured wall temperature [13] profile was implemented in the model to account for the variation of temperature along the length of the furnace.

The implementation of the measured furnace wall temperature is shown in Figure 5-4. Only the 1400 °C furnace set point is of interest to the current research study. The variable temperature boundary was applied to the ANSYS Fluent® model with the use of user defined functions (UDFs). The simple code needed to accomplish this is listed in Appendix A.

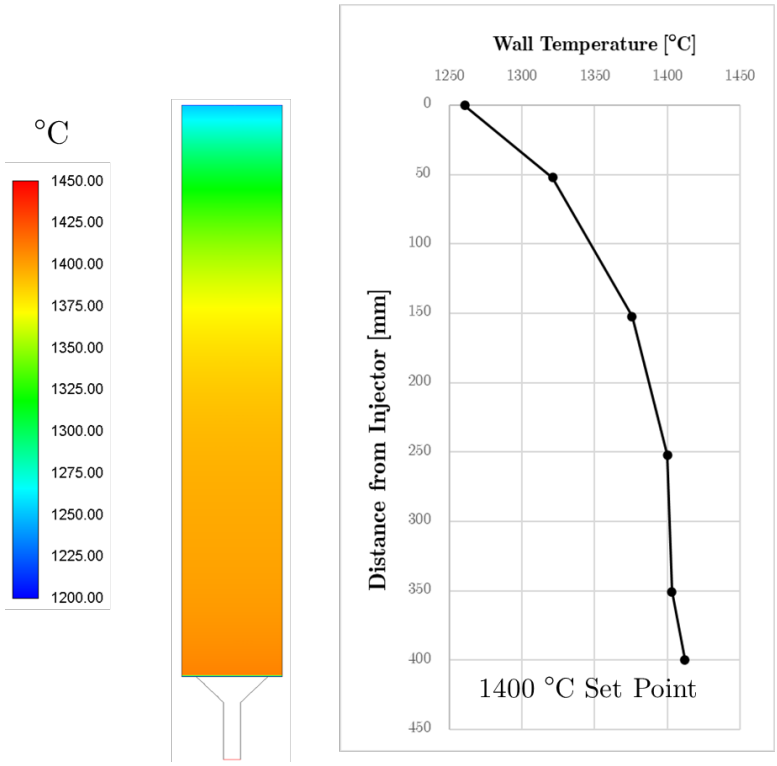

Figure 5-4: Implementation of Measured Furnace Wall Temperature (Devolatilisation)

5.2.4 Devolatilisation Results

The results from the devolatilisation simulations are presented in this section. The flow and temperature fields as well as the devolatilisation process for a single particle was analysed. The velocity magnitude contours on a plane slice through the centre of the DTF is shown in Figure 5-5.

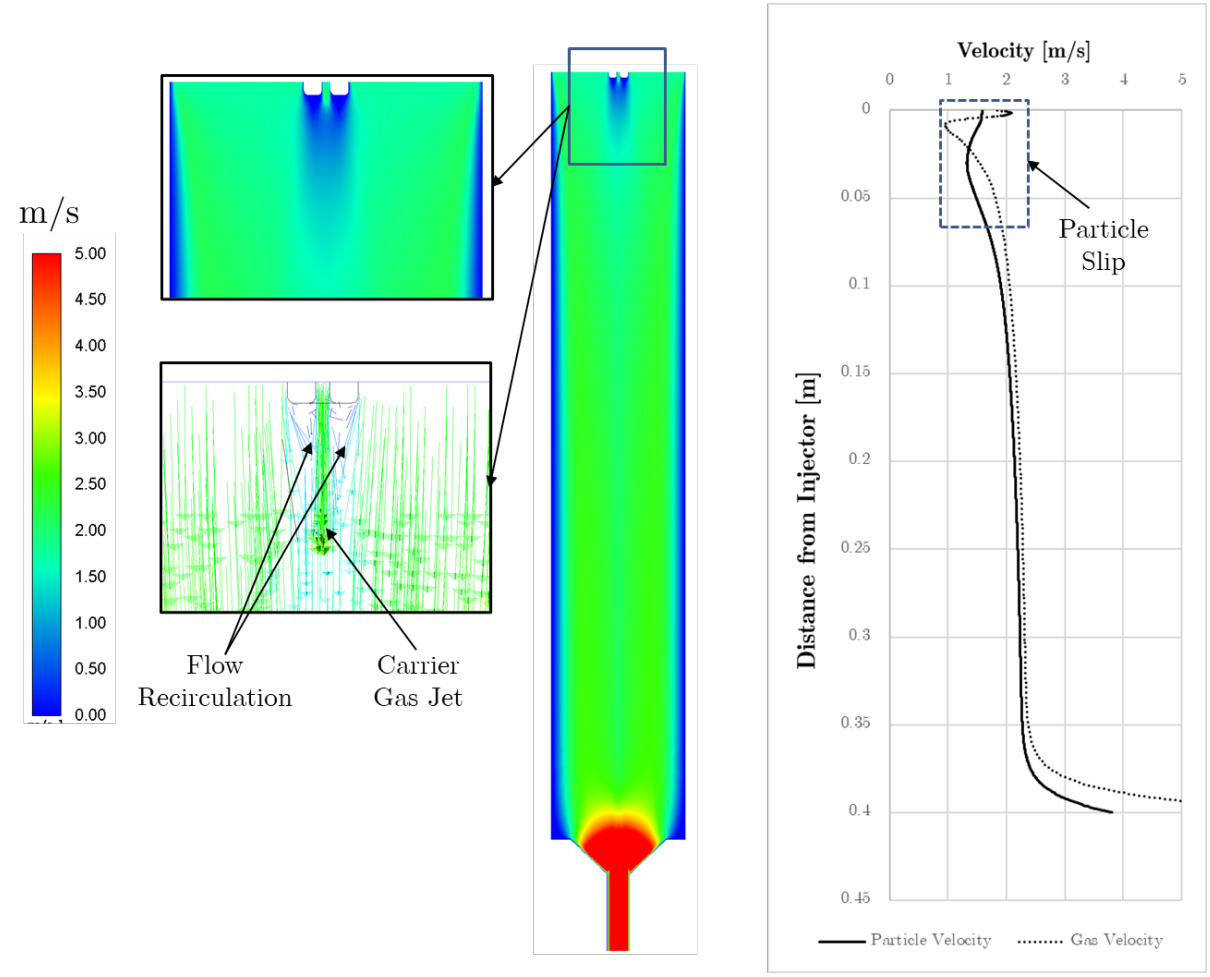

Figure 5-5: DTF Velocity Profiles During Devolatilisation

As expected, the injection nozzle produces a well-defined jet structure that penetrates the furnace region. A notable feature is the recirculation zone just after the bluff body structure of the nozzle section. This recirculation prevents the carrier gas from assimilating to the secondary flow stream. This is evident in the enlarged vector plot of Figure 5-5. Rather it causes a disturbance that creates a mismatch in the particle and gas velocities immediately at the exit of the nozzle. This mismatch is known as particle slip and it will have an effect on the local convective heat transfer coefficient on the particle. This region lasts for approximately

the first 0.05s of the particle trajectory. There after the gas and particle velocities settle into a stable and near constant velocity as the particle travels down furnace at its terminal velocity. The increase in the velocity at the end of the furnace is due to the constriction created by the collector probe.

The temperature field in the DTF is shown in Figure 5-6.

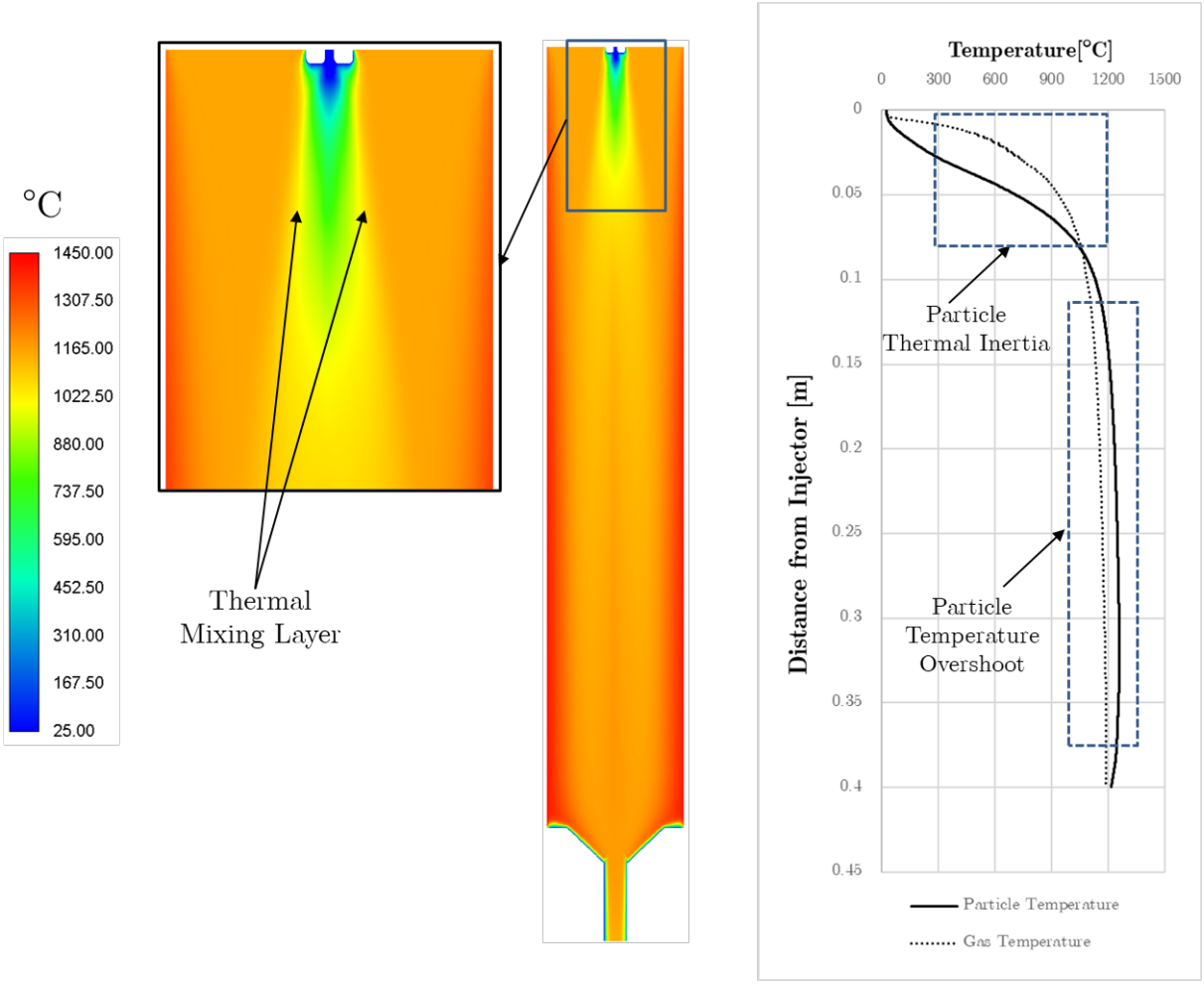

Figure 5-6: DTF Temperature Profiles During Devolatilisation

The carrier gas and secondary gas have a large temperature differential. This is evident in the contour plot shown in Figure 5-6. Here the colder carrier gas jet forms a distinct thermal mixing layer with the surrounding fluid, and this gradually allows the centreline gas temperature to increase to the vicinity of the set point temperature as the two streams mix. The particle temperature on the other hand increases at a slower rate and this is indicative of the thermal inertia associated with particle and perhaps also adverse convective heat transfer

initiated by the recirculation zone near the nozzle exit. The scenario reverses once into the lower sections of the furnace as the particle temperature rises marginally higher than that of the gas. This may be attributed to radiative heat exchange becoming dominant and hence allowing the particle temperature to approach the wall temperature. The gas temperature lags since it mainly consists of nitrogen (a small fraction of volatile gases and tars), which is a pure gas and is not considered to participate in radiation. This is consistent with the application of the weighted sum of grey gases model (WSGGM) that is being employed.

The evolution of the volatile gases as they are released form the solid particle to the continuous gas phase is shown in Figure 5-7.

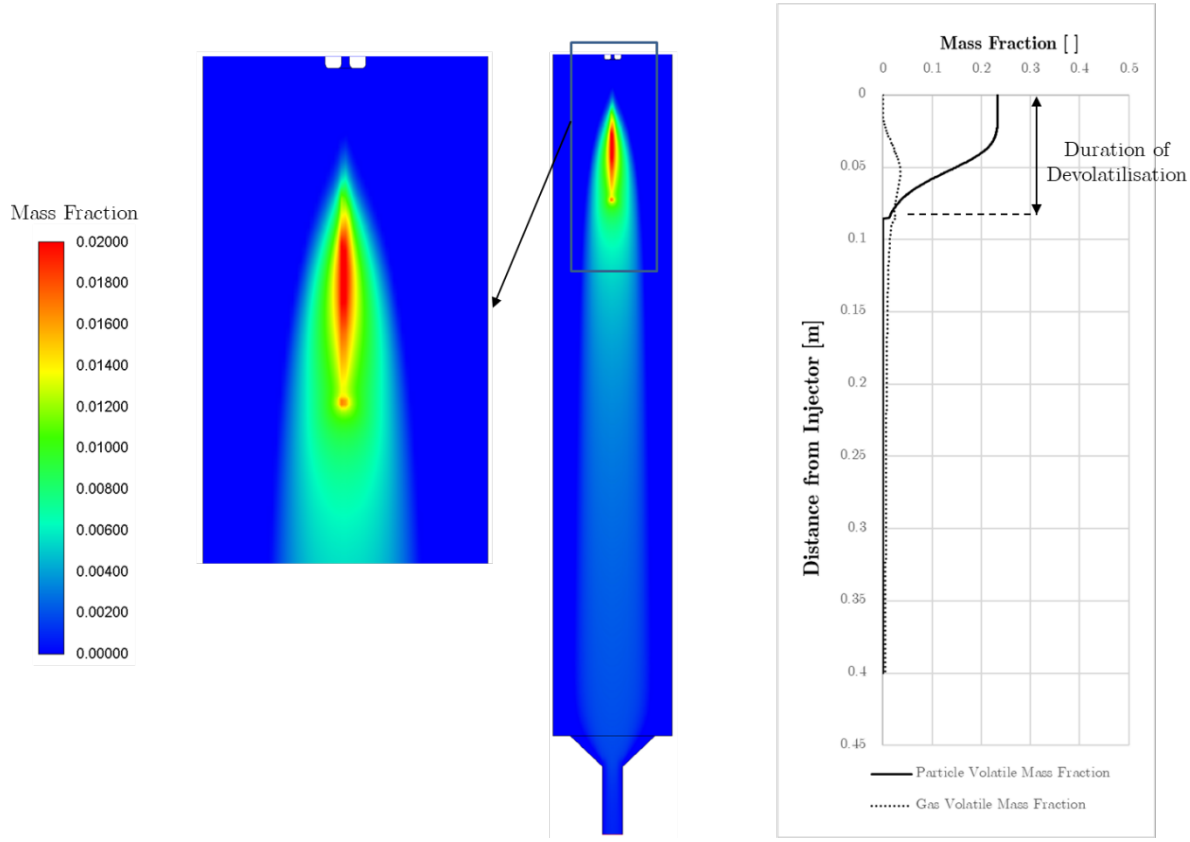

Figure 5-7: Volatile Gas Species Evolution During Devolatilisation

Volatile release is modelled in ANSYS Fluent® by assigning a pseudo-gas species to represent the combined volatile gases and tars. The rate of release of this species, known as the volatile species, is determined by the applied kinetic parameters. Hence the main task of the devolatilisation numerical experiments is to determine the Arrhenius equation parameters for the single rate devolatilisation model described in section 2.3.2.

The physical behaviour shows that there is lag in terms of the onset of volatile release, which can be seen in Figure 5-7 i.e., there is a distinct offset from the exit of the injection nozzle. This is typical of low volatile, high ash South African coals. The devolatilisation period is within a range of 0 to 100ms which is also in line with known coal particle behaviour. The rate of release of volatile material from the particle (Particle volatile mass fraction) and the uptake of these volatile gases into the continuous medium are shown in Figure 5-7. It should be noted that these values differ since the gaseous components are diluted by the nitrogen content in the stream.

An iterative algorithm was developed to synergise the advanced kinetics calculation capability of PC-Coal Lab® and the full three-dimensional flow and heat transfer modelling of ANSYS Fluent®. This process is described in the flow chart shown in Figure 5-8.

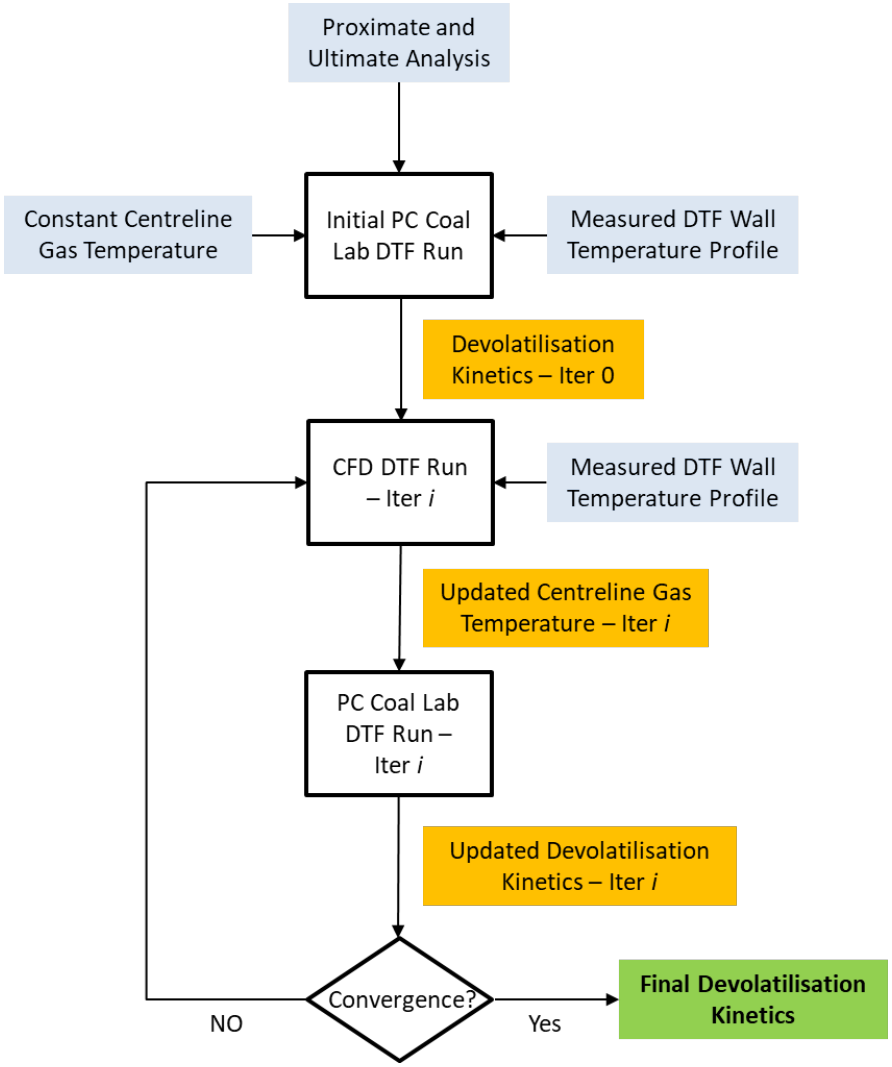

Figure 5-8: Iterative Algorithm for Optimisation of Coal Devolatilisation Kinetics

The description of the iterative algorithm is as follows:

1. The process begins with a baseline PC Coal Lab run. The inputs to this run are the proximate and ultimate analyses of the coal. The wall temperature is user defined since the measured wall temperature is known. The centreline gas temperature is set at a constant value equal to the DTF setpoint temperature. The output is the devolatilisation kinetics i.e., pre-exponential constant A [1/s] and the activation energy Ea [J/kmol].

2. This kinetics are implemented into the CFD model of the DTF and a more realistic centreline gas temperature profile is extracted.

3. Then PC Coal Lab® is run with the updated centreline gas temperatures and once again the devolatilisation kinetics are the output.

4. The CFD simulation is run with the updated kinetics and the output is an updated centreline gas temperature profile.

5. This iterative cycle is repeated until there is no change in the devolatilisation kinetics and convergence is found.

This algorithm was applied using the reference coal and experimental devolatilisation results for the 1400 °C setpoint.

The results are shown in Figure 5-9.

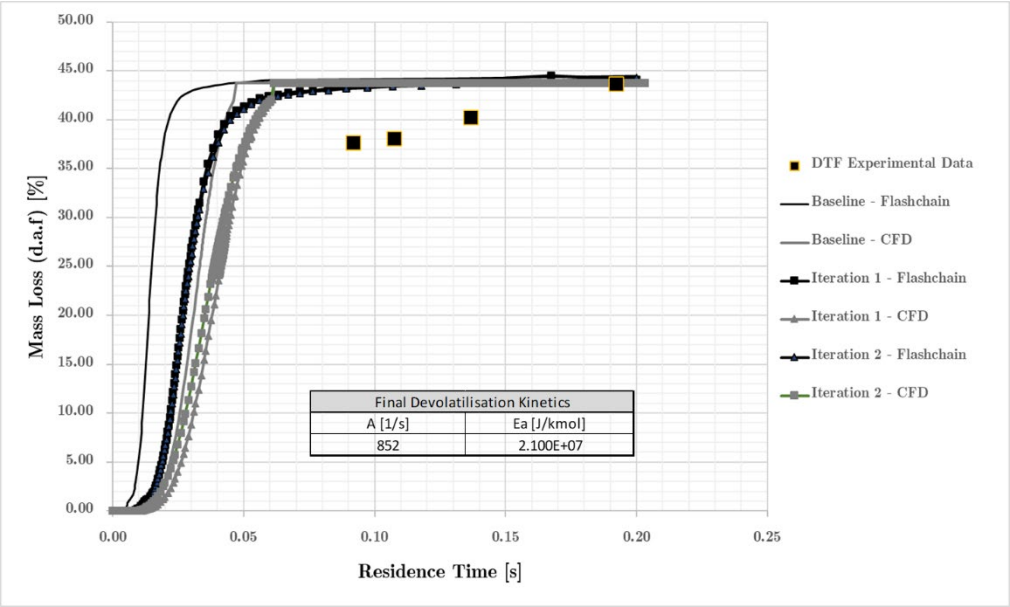

Figure 5-9: Devolatilisation Characteristic for the Reference Coal

Firstly, the algorithm corrected the PC Coal Lab® prediction to a less rapid and more realistic devolatilisation rate. This was due to applying the CFD calculated centreline gas temperature to the PC Coal Lab® model and hence not employing the in-built gas temperature prediction This resulted in kinetics that in turn improved the CFD prediction. The second iteration of the algorithm already showed that there was no change in the predicted kinetics and hence convergence was achieved. The final devolatilisation kinetic parameters are shown in Figure 5-9. These results may be justified when considering the heating rates of the particles in the both the simulation methods. The heating rate is defined as the time averaged temperature of the particle from the injection of the particle to the point where devolatilisation ceases. This is shown in Figure 5-10. The plot shows the temperature history of the particles in both simulation tools. Initially the Flashchain model predicted a significantly higher heating rate i.e., 42368 K/s. However, the CFD simulations consistently predict a heat rate that is between 17000 and 21000 K/s. This is because the CFD simulation is solving the full three-dimensional heat transfer problem as well as resolving the mixing of the carrier and injection gas streams more realistically than the one-dimensional approach employed by PC Coal Lab®.

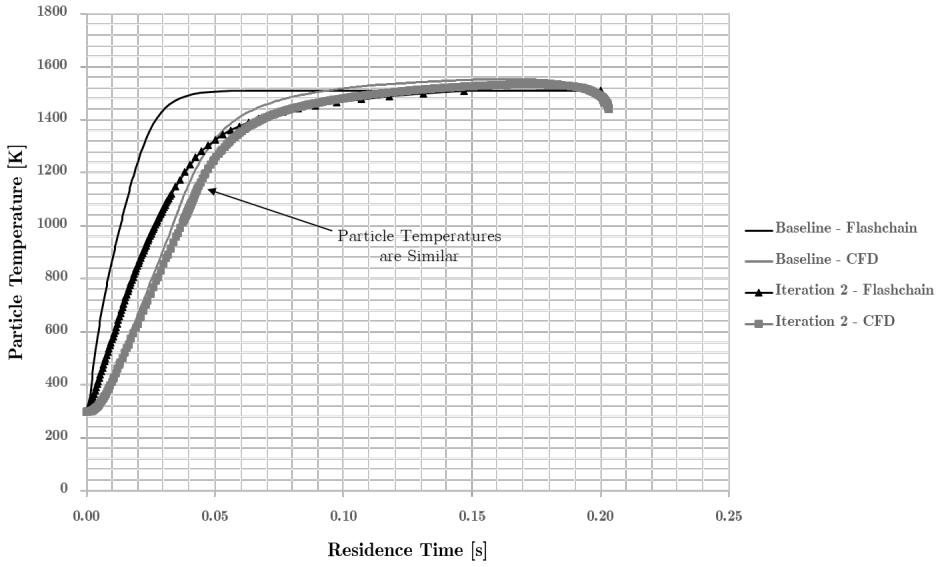

Figure 5-10: Particle Temperature History for Flashchain and CFD DTF Simulations During Devolatilisation

This is further emphasised when considering the consistency of the gas temperature prediction in the CFD code, as seen in Figure 5-11.

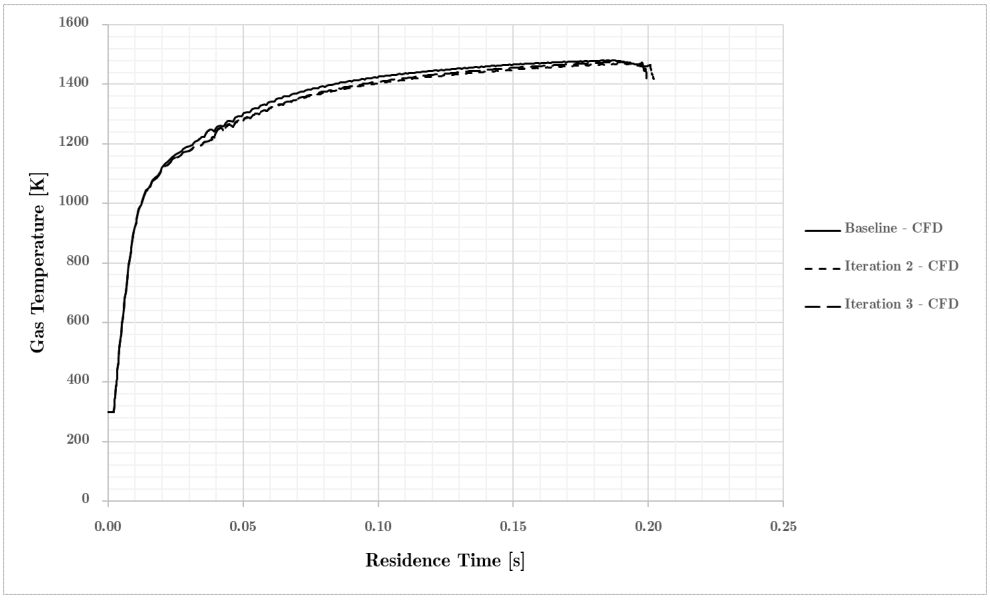

Figure 5-11: Gas Temperature Profiles for CFD DTF Simulations During Devolatilisation

The final heating rates are 20106 K/s and 17567 K/s for PC Coal Lab® and CFD, respectively.

5.2.5 Char Combustion Results

A similar algorithmic process as in the case of devolatilisation, was following for the prediction char combustion kinetics. However, the parameters used for iterative calculations differ, most notably, the inclusion of the predicted centreline O_2 concentration. Char combustion tests on the DTF are conducted at O_2 levels similar to that found in a full-scale furnace. Hence the operating gas species composition has been altered to represent the oxygen concentrations found in a typical coal fired furnace. Hence 3.4% (by mass) of oxygen is included in the carrier and injection gas streams. Char combustion occurs on a timescale in the order of seconds, whereas devolatilisation is much faster i.e., in the order of milliseconds. Hence the test conditions employed for the char combustion tests in the DTF must be adapted to ensure that sufficient residence time is allow for complete burn out of the char particle. This is accomplished by lowering the collection cup to its lowest position i.e., 1.2 m from the injection nozzle as well as reducing the flow rate of the secondary gas.

The geometry used for the char combustion runs is consistent with that shown in Figure 5-3, with the exception that it is significantly longer. The experimental data used in this section was retrieved from the work of Smit [56]. The measured DTF wall temperature profile as applied to the char combustion CFD model is shown in Figure 5-12. A fifth order polynomial was found to be a good fit for the data and the subsequent inclusion into the UDF (see Appendix B).

Table 5-4: DTF Char Combustion Boundary Conditions

Carrier Gas Inlet (Velocity Inlet)	
Inlet Velocity	1.59 m/s
Inlet Temperature	25 °C
Hydraulic Diameter	0.02 m
Turbulent Intensity	5 %
Oxygen Concentration (by Mass)	3.4 %
Secondary Gas Inlet (Velocity Inlet)	
Inlet Velocity	0.53 m/s
Inlet Temperature	1396 °C
Hydraulic Diameter	0.06 m
Turbulent Intensity	5 %
Oxygen Concentration (by Mass)	3.4 %
Collector Outlet (Pressure Outlet)	
Static Pressure	85 kPa (Absolute)
PF Injection (Point Injection)	
Particle Size (Constant)	47e-5 m
Particle Temperature	25 °C
Particle Flow Rate	1.96e-5 kg/s

The behaviour of the gas and particle flow within the DTF during char combustion was explored by looking at key parameters. The results presented are the for the case with the final char combustion kinetics. The CFD simulations use the single rate char combustion model described in section 2.3.3.

The velocity flow field is shown in Figure 5-13. The same jet behaviour is evident as in the case for the devolatilisation run, however due to less of a mismatch in velocities between the carrier gas and secondary gas velocities, the recirculation behind the nozzle bluff body is replaced with more of a gas entrainment. This less chaotic flow field manifests in lower particle slip as shown in Figure 5-16.

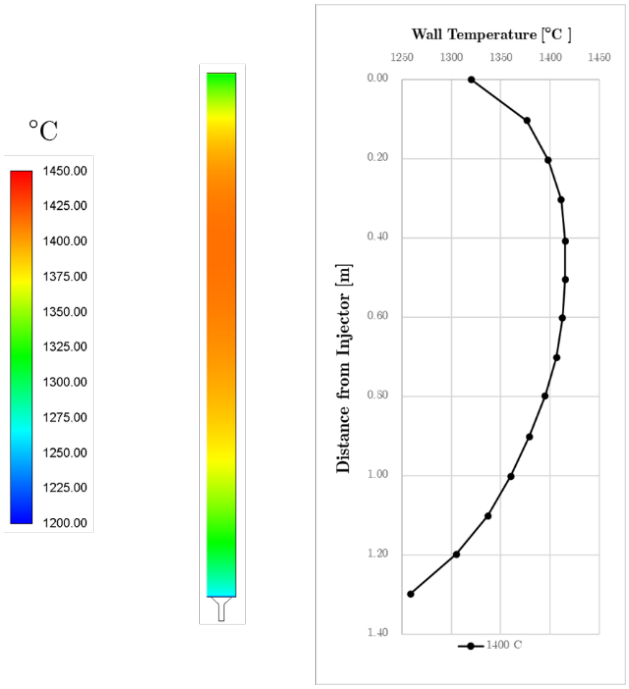

Figure 5-12: Implementation of Measured Furnace Wall Temperature (Char Combustion)

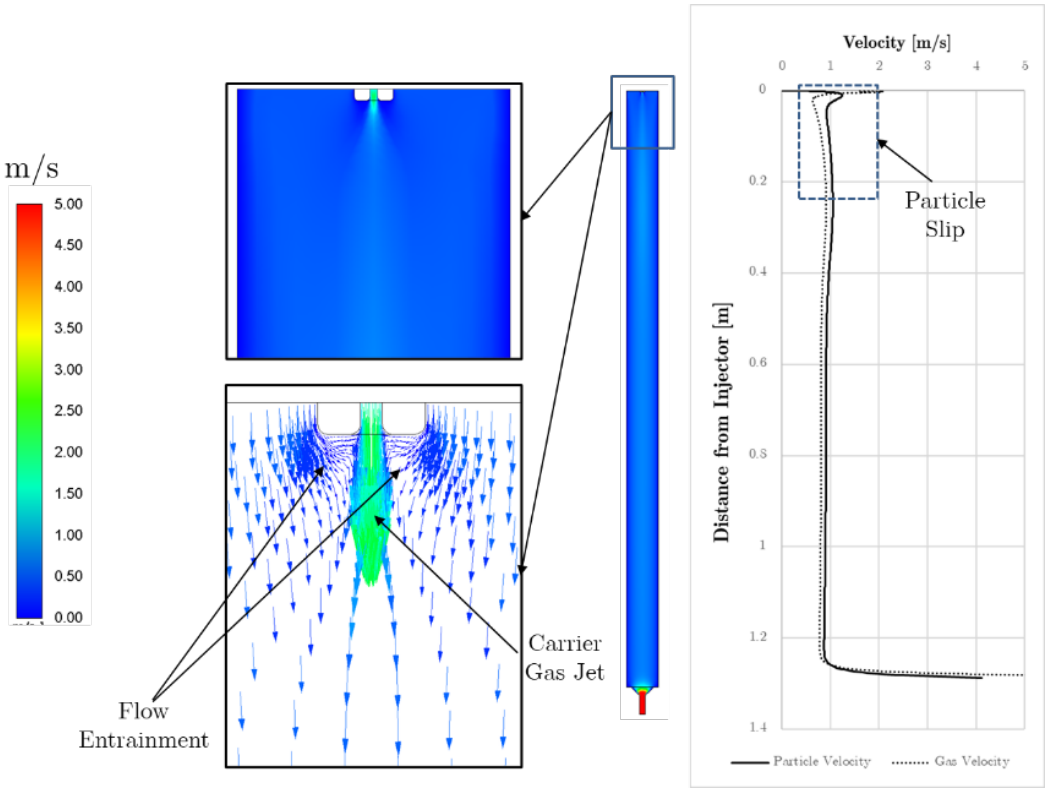

Figure 5-13: DTF Velocity Profiles During Char Combustion

The temperature field for the char combustion run is shown in Figure 5-14.

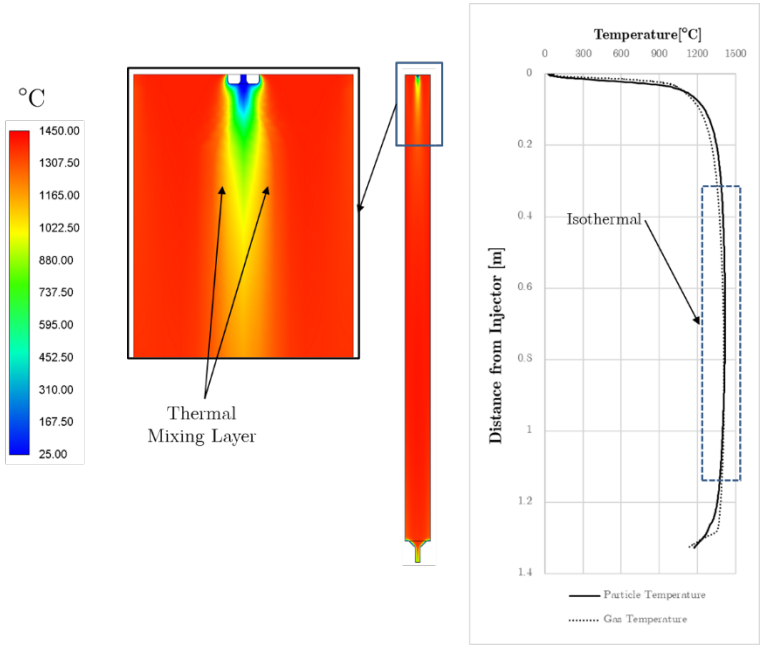

Figure 5-14: DTF Temperature Profiles During Char Combustion

The colder carrier gas jet penetrates the DTF furnace region and is rapidly mixed with the carrier gas flow. Because the char combustion run occurs in a significantly longer test section than the devolatilisation test, the particles have more time to assimilate to the thermal conditions in the furnaces. In this regard, the particle experiences a near constant temperature throughout most of its journey through the DTF.

The next parameters of interest are the centreline oxygen concentrations as well as the rate of char consumption in the furnace. This may be seen in Figure 5-15. The oxygen profile shows a steady decrease in the O_2 concentration measured in the vicinity of the particle down the centreline of the DTF. There is an inflection in this curve between 0.2 m and 0.4 m from the injection point. This may be attributed to variable mixing conditions and the entrainment of the secondary gas O_2 into the centreline region. The char consumption of the particle is also shown, and it indicates that the particle burnout is near linear from the injection point to the exit of the DTF. This indicates that the reference coal has a slow burnout characteristic. A fast burnout would manifest as peak in the consumption of char and O_2 near the injection point.

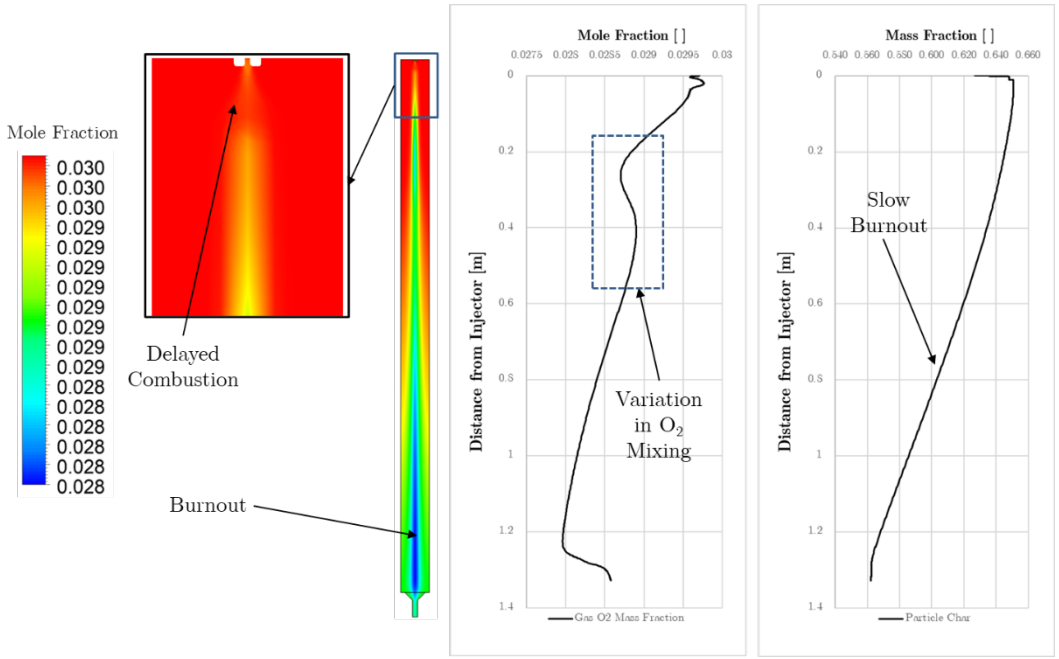

Figure 5-15: Oxygen Concentration and Char Consumption during Char Combustion

The char combustion kinetics were improved by using an iterative algorithm to leverage the predictive capabilities of the CFD code as well as PC Coal Lab®. The latter tool employs the CBK-E [22] model of char combustion. The iterative algorithm is similar in structure to the one used for the devolatilisation calculations. However, the key parameters that effect the char reactions are not only the centreline gas temperature and DTF wall temperature, but also the centreline O_2 concentration. The char combustion kinetics optimisation algorithm is shown in Figure 5-16.

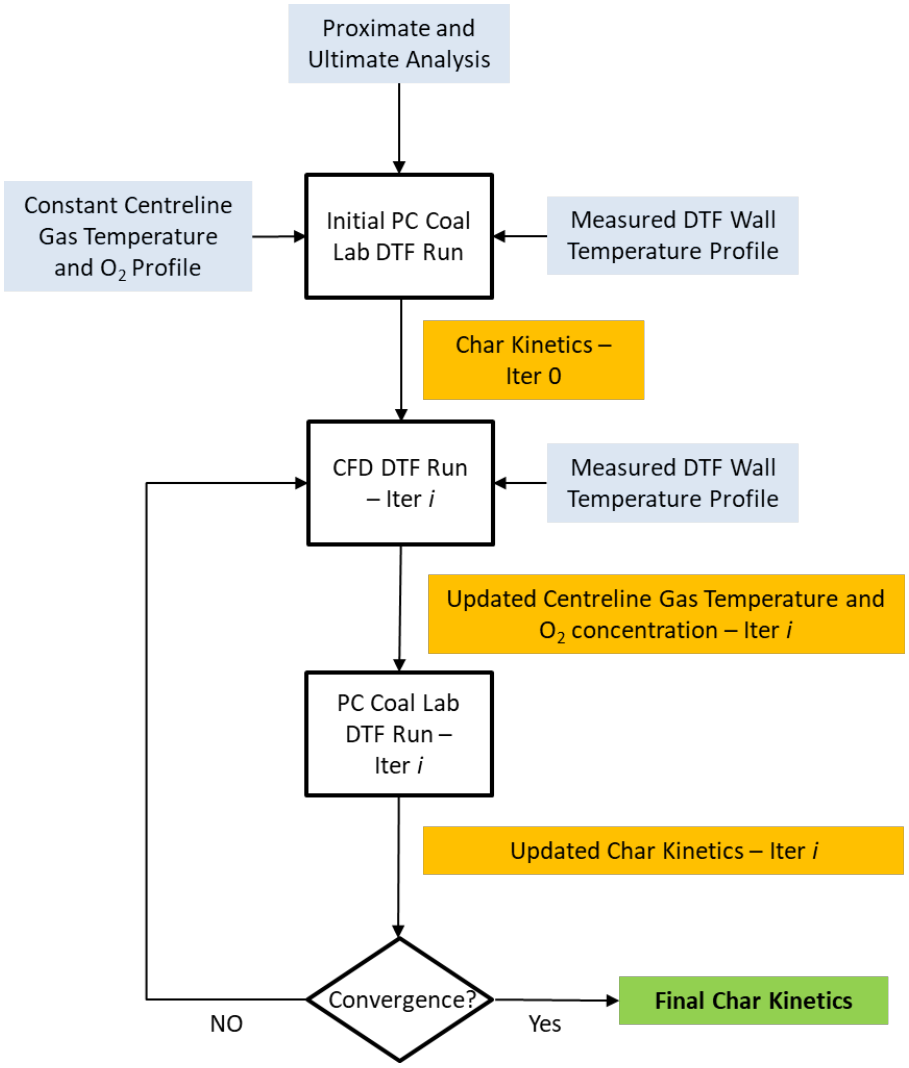

Figure 5-16: Iterative Algorithm for Optimisation of Coal Char Combustion Kinetics.

The description of the iterative algorithm is as follows:

1. The process begins with a baseline PC Coal Lab run. The inputs to this run are the proximate and ultimate analyses of the coal. The wall temperature is user defined since the measured wall temperature is known. The centreline gas temperature is set at a constant value equal to the DTF setpoint temperature. The centreline O_2 concentration is calculated by PC-Coal Lab®. The output is the char combustion kinetics i.e., pre-exponential constant A [1/s] and the activation energy Ea [J/kmol].

2. This kinetics are implemented into the CFD model of the DTF and a more realistic centreline gas temperature and O_2 profile is extracted.

3. Then PC Coal Lab is run with the updated centreline gas temperatures and the O_2 profiles and once again the devolatilisation kinetics are the output.

4. The CFD simulation is run with the updated kinetics and the output is an updated centreline gas temperature and O_2 profile.

5. This iterative cycle is repeated until there is no change in the char combustion kinetics and convergence is found.

The iterative algorithm only provided part of the solution to the char kinetics problem. It will be shown that further tailoring was required to account for the peculiar combustion characteristic of the reference coal. The reference coal exhibits a very slow burn-out rate for a sub-bituminous coal. This is evident when interrogating the experimental data points in Figure 5-18. The iterative algorithm is only effective in improving the PC-Coal Lab® prediction marginally, whilst the CFD calculation (the baseline and iteration 1 curves are coincident) is insensitive to changes. At this point it appears that limit has been reached regarding the predictive capability of the codes. However, the Author engaged with the developer of PC Coal Lab®, Dr Stephen Niksa [57], and he was able to provide insight that would be used to improve the numerical predictions. Dr Niksa provided the following:

"When you compare the results, you will see that the variable conditions definitely slow down the burnout, as expected. But there is still a very large discrepancy with the measured values. However, this is not due to a problem with PC Coal Lab. As you correctly implemented in your CFD simulation, these conditions definitely sustain film diffusion limited burnout for all but the latest stages, and that is consistent with the combustion histories from CBK/E. This observation raises the question, "Why are the measured values markedly inconsistent with diffusion limited burnout?" One possibility is that the very high ash level in this coal retards burnout even more than predicted by CBK/E."

Dr Niksa postulated that the slow burnout rate could be a consequence of the high ash content in the reference coal. High ash coal is common to South Africa and is routinely burnt in the coal fired furnaces in the power generation industry. The recommendation from Dr Niksa was to modify the char oxidation reactivity of the coal as used by PC Coal lab®.

The default char reactivity is given by equation 5.3. This correllation was developed from extensive testing of coals [22]. “C” is the carbon content in the coal on a dry ash free basis. Whether this expression is valid for high ash South African coals is a question for further research and is beyond the scope of this study.

$$A_{30} = 10^{(14.38-0.0764*C)} \quad 5.3$$

The values tested for the char reactivity sub-study are listed in Table 5-5.

Table 5-5: Char Reactivity Parameters

A_{30}	Value [1/s]
Default	1.28e8
Iteration 1	1e10
Iteration 2	5e7
Iteration 3	3e7
Iteration 4	2e7
Iteration 5	1.5e7
Iteration 6	1.4e7

The final char combustion simulation from the iterative procedure was adapted to run with the various char oxidation reactivities shown in the table above. The effect on the burnout charactersitic of the coal is shown in Figure 5-17. It can be seen that the prediction from PC-Coal Lab® simulation improves substantially when lowering the the char oxidation reactivity from the default value i.e., 1.28E8 /s to 1.4E7 /s. The lower limit for the reactivity value was found when the code displayed the onset of numerical instability. Despite the improvement the char combustion kinetics still did not agree well with the experimental data.

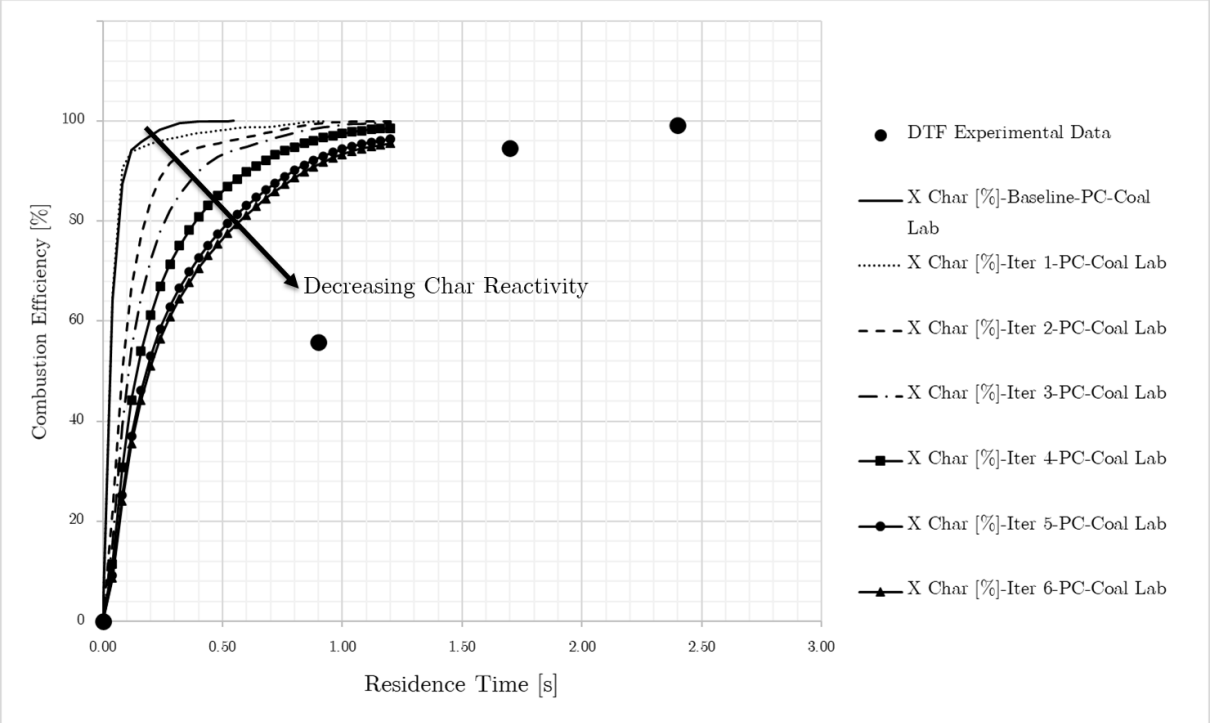

Figure 5-17: Effect of Varying Char Oxidation Reactivity on Particle Burnout

The final step of tailoring the char kinetics lay in the CFD code. The parameters available for user input to the single step char oxidation model as described in section 2.3.3.1, are the Arrhenius inputs as well as the mass diffusion-limited rate constant. The latter value has profound effect on the rate of char oxidation. A wide range of values were tested for this constant and the best result was achieved by changing the default value of 5e-12 to 4.5e-13. The physical interpretation of this change is that the transport of oxygen to the particle surface is retarded and hence combustion is also slowed.

As stated previously the iterative algorithm is not sufficient to modify the char combustion kinetics to an extent that the numerical simulations agree with the experimental data. The final kinetics curve that employs both the PC Coal Lab® reactivity calibration and the modified mass diffusion-limited rate constant effectively capture the slow and gradual nature of the char combustion characteristics of the reference coal. Importantly, these kinetics values ensure that realistic a burn-out time calculated. This can be seen in Figure 5-19 and it is evident that only the final char combustion kinetics that were developed, produce a burnout time commensurate with the experimental data.

The final char combustion characteristic for the reference coal is shown in Figure 5-18.

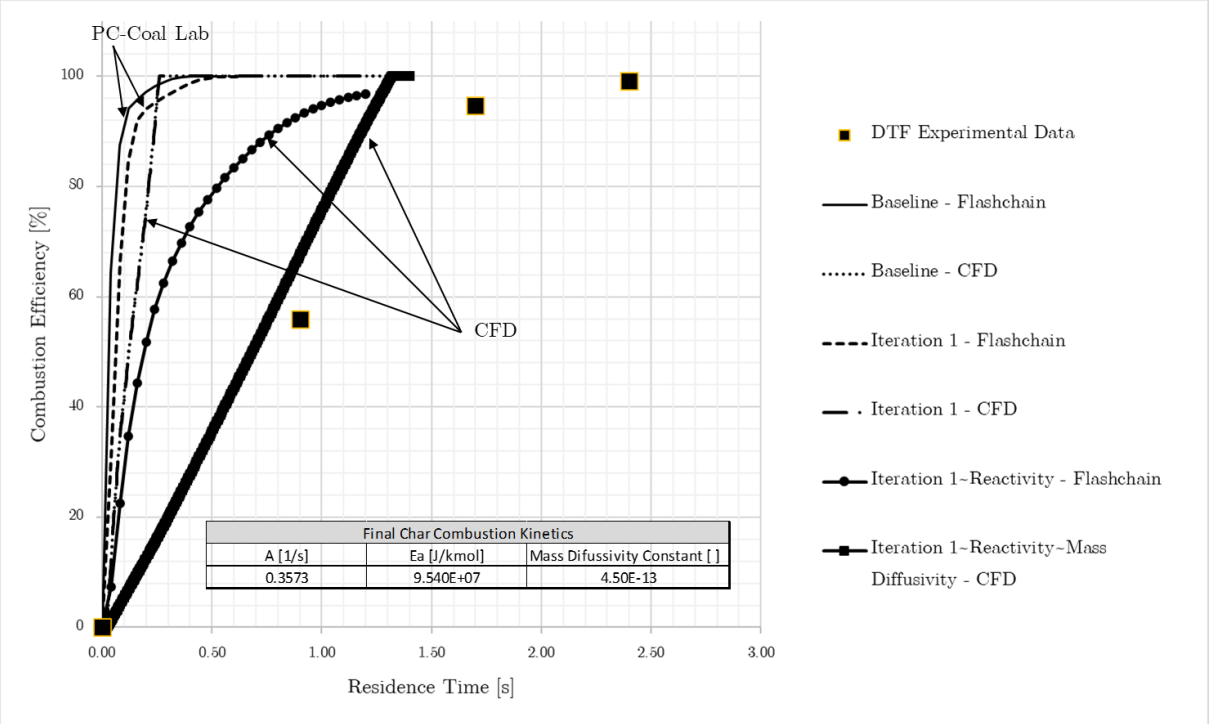

Figure 5-18: Char Combustion Characteristic for the Reference Coal

The intermediate techniques produce a burnout time that is obviously not in line with the combustion nature of this South African coal. This behaviour is further confirmed when analysing the oxygen consumption profile in the vicinity of the char particle (see Figure 5-20). The final char kinetics consumes oxygen at a lesser rate which is in line with its slow rate of burnout.

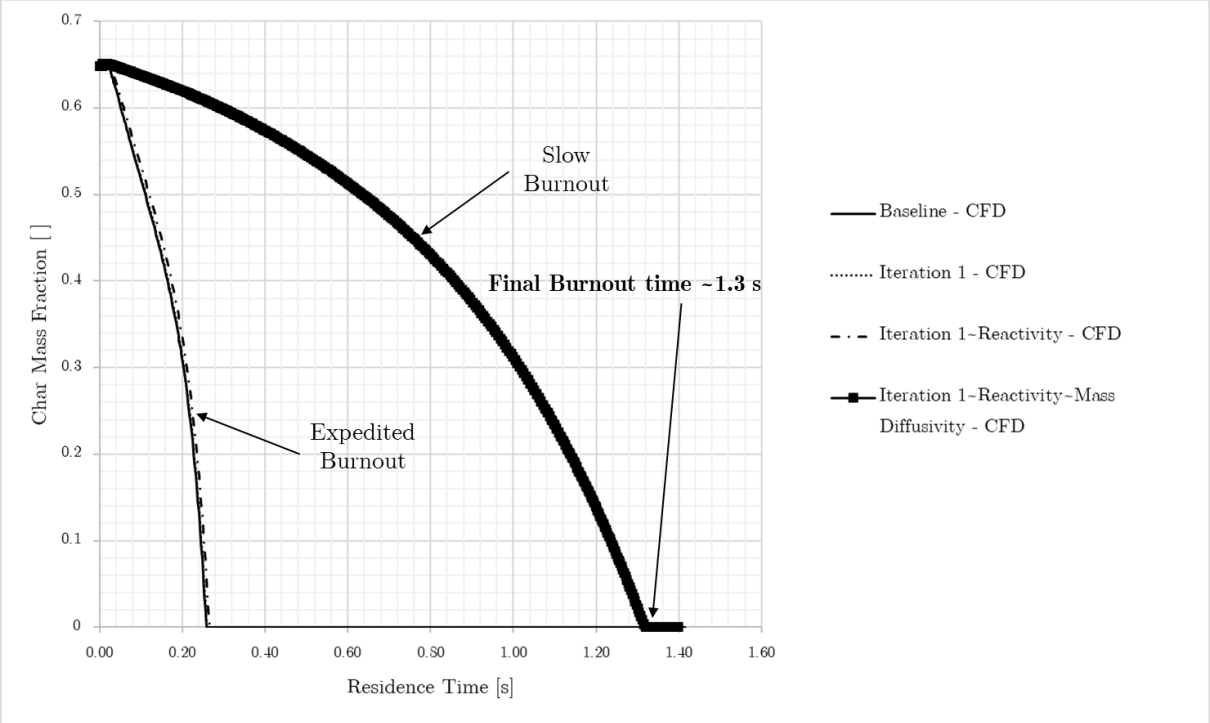

Figure 5-19: Particle Burnout for Reference Coal for Different Char Combustion Kinetics

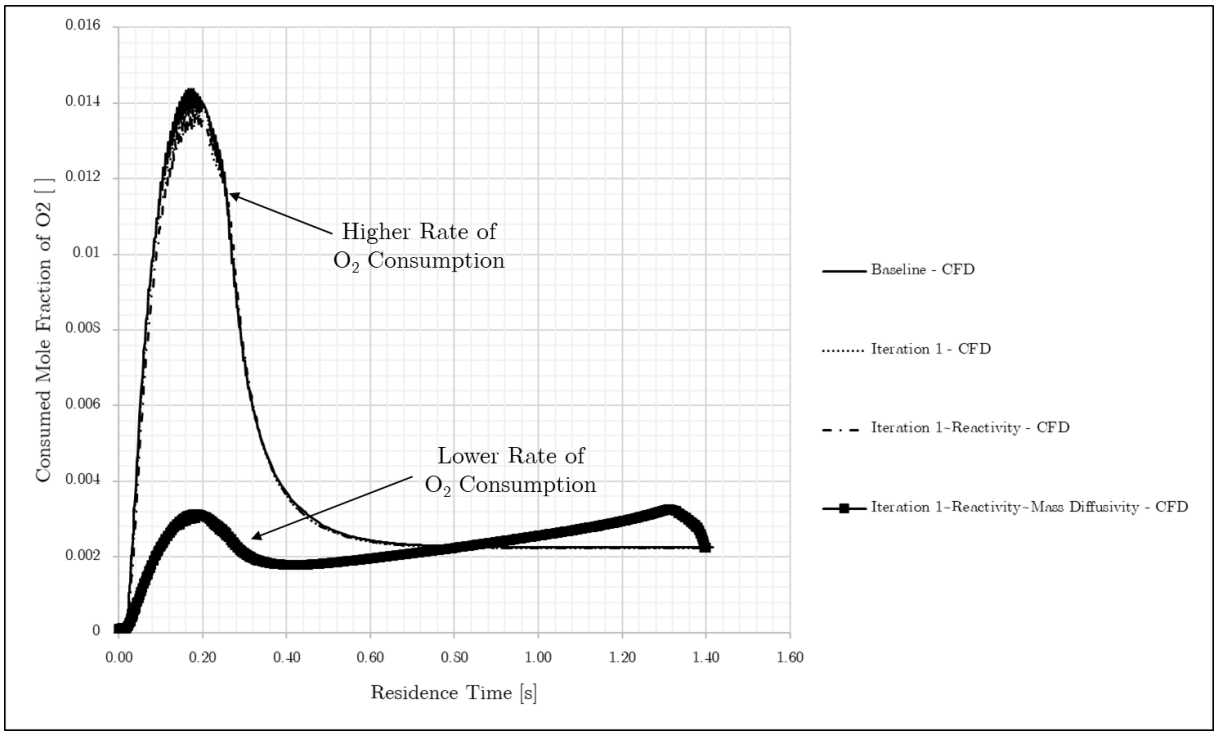

Figure 5-20: Oxygen Consumption Profiles for Different Char Combustion Kinetics

5.2.6 Discussion of Drop Tube Simulation Results

The modelling of the devolatilisation and char combustion processes of the reference coal was successfully completed. The devolatilisation data followed the expected behaviour and follows the slightly retarded onset of volatile release associated with some South African coals. The char combustion results on the other hand provided additional challenges as the predictive tools needed to be tailored to improve the correlation with the experimental data. It was shown that PC Coal Lab® does not provide satisfactory predictions in its default state. This was improved by modifying the char reactivity rates. This was done in a methodical manner and the results showed that when the char reactivity is reduced, PC Coal Lab® provides a better correlation with the experimental data. This was, however, still not acceptable, and further development was required, by modifying the mass diffusion-limited rate constant in the char combustion model of ANSYS Fluent®. This parameter has a profound impact on the rate that the char burns in the DTF. Hence, by methodical investigation, an appropriate value was determined. The devolatilisation and char reaction kinetics were determined and fixed for implementation into the pilot and full-scale combustion models.

The most important learning from this section of the research work was that South African coals require careful characterisation and the standardised values employed by analysis codes must be interrogated critically. Very often this default kinetics are derived for northern hemisphere coals. The codes must be shown to predict the behaviour derived by experiments, when modelling the combustion of South African coals. This outcome is consistent with the conclusions described in section 2.5.

5.3 Gas Phase Combustion Modelling

The current section outlines the calculation method in implementing the various gas phase combustions that were studied. These sub-models define the specific species that are released during the devolatilisation process and their subsequent combustion mechanisms. The modelling approach used in study was to use a pseudo volatile species to represent the combustible matter that is released from the solid coal particle. The rate of this release is governed by the devolatilisation kinetics derived in section 5.2.4. This pseudo species is assumed to decompose rapidly into the pyrolysis products and as such does not affect the subsequent stages of gaseous combustion.

The current research is focused on implementing three fundamentally different gas phase combustion mechanisms i.e.:

- One-step reaction mechanism
- Two-step reaction mechanism
- Five-step reaction mechanism

The different mechanisms assume a different set of combustion products, and this plays a role as to how the pulverised coal flame is calculated.

5.3.1 One-Step Combustion Mechanism

The one step reaction is the simplest form of volatile combustion in that the pseudo volatile species is assumed to react with oxygen and directly forms the final combustion products. This method has an advantage of being simple to implement and is also computationally efficient. The method proposed is also suggested by ANSYS [37].

The one step reaction scheme is shown in equation 5.4:

$$C_m H_n O_x N_y S_z + a_1 O_2 \rightarrow a_2 CO_2 + a_3 H_2 O + a_4 N_2 + a_5 SO_2 \qquad 5.4$$

Where:

- *m,n,x,y,z* – Mole fraction of Carbon, Hydrogen, Oxygen, Nitrogen and Sulphur, respectively [ ]

- a_1, a_2, a_3, a_4, a_5 – Stochiometric coefficients of the reactants and products. [ ]

The formation enthalpy of the volatile species is given by:

$$h_{volatile} \rightarrow mh_{CO_2} + \frac{1}{2}h_{H_2O} + zh_{SO_2} + \frac{Coal_{LCV,daf} - Char_{LCV,daf} * FC_{daf}}{Volatile\ Weight_{daf}} * MW_{volatile,daf} \quad 5.5$$

Where:

- h_{CO2} – Formation enthalpy of carbon dioxide [J/kmol]
- h_{H20} – Formation enthalpy of water[J/kmol]
- h_{SO2} – Formation enthalpy of sulphur dioxide [J/kmol]
- $Coal_{LCV,daf}$ – Lower heating value of reference coal [J/kg]
- $Char_{LCV,daf}$ – Lower heating value of char [J/kg]
- Volatile $Weight_{daf}$ – Mass fraction volatile material [ ]
- $MW_{volatile,daf}$ – Molecular weight of volatile species [kg/kmol]

The stoichiometric coefficients are calculated by balancing the number of constituent atoms on either side of the reaction equation:

$$a_1 = \frac{1}{2}\left(2m + \frac{1}{2}n + 2z - x\right) \quad 5.6$$

$$a_2 = m \quad 5.7$$

$$a_3 = \frac{1}{2}n \quad 5.8$$

$$a_4 = \frac{1}{2}y \tag{5.9}$$

$$a_1 = \frac{1}{2}\left(2m + \frac{1}{2}n + 2z - x\right) \tag{5.10}$$

$$a_5 = z \tag{5.11}$$

The important outputs of the one step mechanism calculation are shown in Table 5-6.

Table 5-6: One Step Mechanism Values

Parameter	Value
a_1 [ ]	3.145
a_2 [ ]	2.307
a_3 [ ]	2.215
a_4 [ ]	0.071
a_5 [ ]	0.059
$h_{volatile}$ [J/kmol]	-9.008e7

It should be noted that this formulation of the formation enthalpy is exothermic. This is consistent with the transition directly to final combustion products. A detailed description of the calculation process can be found in Appendix C. It should be noted that the sulphur content is assumed to be completely converted to sulphur dioxide. This is consistent with what is observed on coal fired power plant. The finite rate/eddy dissipation turbulent combustion model was employed. By implication, the reaction rates of the gaseous species are limited by turbulent mixing. This is of course immaterial in the case of the single step reaction mechanism as the volatiles are immediately converted to the final combustion

products. It should also be noted that in this case, the char combustion model must be set to oxidise the char in the coal particle directly to carbon dioxide.

5.3.2 Two-Step Combustion Mechanism

The two-step combustion mechanism extends the one-step mechanism, marginally by incorporating the carbon monoxide into the products of pyrolysis. This added feature allows for a more natural development of the burnout of the coal particles as the carbon monoxide must react with oxygen to form carbon dioxide. Firstly, this mechanism can in fact predict the transport and distribution of carbon monoxide, but it also allows for the flow field to play a more significant role in developing the flame structure.

The two-step reaction scheme is shown in equation 5.35:

$$C_m H_n O_x N_y S_z + b_1 O_2 \rightarrow b_2 CO_2 + b_3 CO + b_4 H_2 O + b_5 N_2 + b_6 SO_2 \qquad 5.12$$

Where:

- *m,n,x,y,z* – Mole fraction of Carbon, Hydrogen, Oxygen, Nitrogen and Sulphur, respectively [ ]
- $b_1, b_2, b_3, b_4, b_5, b_6$ – Stochiometric coefficients of the reactants and products. [ ]

The calculation of the formation enthalpy of the volatile species in the case of the two-step method must be formulated to recognise that carbon monoxide and carbon dioxide are combustion products.

The formation enthalpy of the volatile species is given by:

$$h_{volatile} \rightarrow m(1-\alpha)h_{CO_2} + m(\alpha)h_{CO}\frac{1}{2}h_{H_2O} + zh_{SO_2} + \frac{Coal_{LCV,daf} - Char_{LCV,daf} * FC_{daf}}{Volatile\ Weight_{daf}} * MW_{volatile,daf} \qquad 5.13$$

Where:

- h_{CO2} – Formation enthalpy of carbon dioxide [J/kmol]
- h_{CO} – Formation enthalpy of carbon dioxide [J/kmol]
- h_{H20} – Formation enthalpy of water [J/kmol]

- h_{SO2} – Formation enthalpy of sulphur dioxide [J/kmol]
- $Coal_{LCV,daf}$ – Lower heating value of reference coal [J/kg]
- $Char_{LCV,daf}$ – Lower heating value of char [J/kg]
- Volatile $Weight_{daf}$ – Mass fraction volatile material [ ]
- $MW_{volatile,daf}$ – Molecular weight of volatile species [kg/kmol]

To complete the calculation, the ratio of carbon monoxide to carbon dioxide released during pyrolysis must be specified. This is the α value. This value was derived from experimental observations and insights gained from the char combustion models described in section 2.3.3.

The method of calculating the α value was a rudimentary adaption of the one proposed by Peters and Weber [58]:

$$\alpha = \left(1 - \frac{12 f_o}{16 f_c}\right) \qquad 5.14$$

Where:

- α – ratio of CO to CO_2 produced during primary pyrolysis [ ]
- f_o – Mass fraction of oxygen in the coal volatiles [ ]
- f_c – Mass fraction of carbon in the coal volatiles [ ]

Peters and Weber [58] justify this approximation by reasoning that it often assumed that most the volatile bound oxygen is already associated spatially with the bound carbon monoxide. Hence a small of amount the volatile material will oxidise directly to carbon dioxide. They go on to cite the work of Smith (explained in detail in section 2.3.3) where the combustion of a pulverised coal particle occurs when all the released volatile carbon monoxide is oxidised to carbon dioxide in the thin boundary layer around the particle. Furthermore, the work of Waters et. al. [59] showed that a small portion of the volatile carbon does react directly to carbon dioxide. But since the particle boundary layer on a sub-micron pulverised coal particle is very small and considering the mixing effect of the turbulent eddies in the vicinity of the

particle; this would promote rapid oxidisation to the final product of carbon dioxide. Hence the conclusion is that most of the volatile material will be released as carbon monoxide. This now poses a contradiction to the basis of the single step reaction mechanism as it does not follow observed behaviour. However, the implications of this will be explored in the latter parts of this work.

Using the specification of the reference coal (see Table 5-1), the α value is calculated to be 0.9. In this case the char oxidation model is specified to oxidise the char particles to carbon monoxide. Once again, a detailed description of the calculation process may be found in Appendix C.

The second step of this mechanism is oxidising the carbon monoxide released during the pyrolysis process:

$$CO + \frac{1}{2}O_2 \rightarrow CO_2 \tag{5.15}$$

The stoichiometric coefficients for the two-step combustion mechanism are calculated as follows:

$$b_1 = \frac{1}{2}(m(2-\alpha) + \frac{1}{2}n + 2z - x) \tag{5.16}$$

$$b_2 = m(1-\alpha) \tag{5.17}$$

$$b_3 = m\alpha \tag{5.18}$$

$$b_4 = \frac{1}{2}n \tag{5.19}$$

$$b_5 = \frac{1}{2}y \tag{5.20}$$

$$b_6 = z \quad 5.21$$

The calculated inputs for the two-step model are listed in Table 5-7.

Table 5-7: Two Step Mechanism Values

Parameter	Value
b_1 [ ]	2.107
b_2 [ ]	0.231
b_3 [ ]	2.076
b_4 [ ]	2.215
b_5 [ ]	0.071
b_6 [ ]	0.059
$h_{volatile}$ [J/kmol]	4.98e8

In contrast to the one-step combustion mechanism, the two-step variant shows that the primary pyrolysis process is endothermic.

5.3.3 Five Step Combustion Mechanism

The objective of the five-step combustion mechanism is to introduce more of the actual physics at play during the processes of primary and secondary pyrolysis and the subsequent burnout of the combustible species. The basis of the technique to assume that the initial mass transfer of the pseudo-volatile species undergoes a primary pyrolysis and disintegrates into its light hydrocarbon (gas) and heavy hydrocarbon (tar) species. The heavy hydrocarbons undergo a secondary pyrolysis at disintegrate into light hydrocarbons. The light hydrocarbons oxidise to the final combustion products.

A detailed and annotated MathCAD calculation describing the current calculation is documented in Appendix D.

The first step in the formulation of the technique is to input the basic coal qualities i.e. The coal calorific value as well as the proximate and ultimate analyses of the coal. This data is consistent with that specified in Table 5-1 i.e., the reference coal for this study.

For the purposes of mathematical expediency this coal data is arranged into three column vectors:

$$char = \begin{bmatrix} C_{char} \\ H_{char} \\ O_{char} \\ N_{char} \\ S_{char} \end{bmatrix} \quad tar = \begin{bmatrix} C_{tar} \\ H_{tar} \\ O_{tar} \\ N_{tar} \\ S_{tar} \end{bmatrix} \quad gas = \begin{bmatrix} C_{gas} \\ H_{gas} \\ O_{gas} \\ N_{gas} \\ S_{gas} \end{bmatrix} \qquad 5.22$$

The *char* column vector represents the elemental composition of the fixed carbon in the coal. Whereas the *tar* column vector represents the elemental composition of the heavy hydrocarbons, whilst *gas* column vector does the same for the light hydrocarbons.

The individual elemental compositions of these products of pyrolysis are derived from the output of the PC Coal lab® run that corresponds to final devolatilisation characterisation as specified in section 5.2.4. Firstly, the distribution by mass of the three pyrolysis products is calculated by PC Coal lab®. This can be seen in Figure 5-21.

The species that constitute the non-condensable gases are also provided by PC Coal Lab®. These gases are CO_2, H_2O, CO, HC and HCN. HC is the cumulative species for the hydrocarbons released. The mass distributions of these gases are shown in Figure 5-22.

DROP TUBE SIMULATION WITH PC COAL LAB

FULL DYNAMICS

FDC1WT1.rpt

COAL CHARACTERISTICS: REFERENCE COAL

Ultimate, daf wt.%		Proximate, as rec wt.%	
%C	82.1	Moisture	3.3
%H	4.2	Vol. Mat.	20.5
%O	10.0	Ash	29.1
%N	1.9	Fixed C	47.1
%S	1.8		

OPERATING CONDITIONS:

90. micron particles at 25. C are entrained in N2
with 0.0 % O2 at 1170. C in a furnace at 1400. C
for .200E+00 s. The ambient pressure is 0.10 MPa.

User-specified conditions were implemented during devolatilization.

Thermal History Time,s	Tmp,C	Wt.Loss daf wt.%	Products, daf wt.% Ygas	Ytar	Ychr
.000E+00	25.	0.0	0.0	0.0	100.0
.165E-02	61.	0.0	0.0	0.0	100.0
.371E-02	117.	0.0	0.0	0.0	100.0
.576E-02	177.	0.0	0.0	0.0	100.0
.782E-02	238.	0.0	0.0	0.0	100.0
.988E-02	297.	0.2	0.1	0.2	99.8
.119E-01	357.	0.8	0.1	0.7	99.2
.140E-01	420.	1.3	0.3	1.1	98.7
.160E-01	478.	2.2	0.5	1.7	97.8
.181E-01	533.	4.1	0.9	3.2	95.9
.201E-01	583.	6.6	1.5	5.1	93.4
.222E-01	632.	10.1	2.3	7.7	89.9
.243E-01	677.	14.3	3.4	10.8	85.7
.263E-01	721.	18.9	5.0	13.9	81.1
.284E-01	762.	23.1	6.4	16.7	76.9
.305E-01	803.	26.8	7.5	19.4	73.2
.330E-01	847.	30.6	8.6	22.0	69.4
.424E-01	988.	39.2	11.6	27.6	60.8
.561E-01	1091.	42.0	13.1	28.8	58.0
.763E-01	1158.	42.9	13.9	29.0	57.1
.118E+00	1218.	43.5	14.6	29.0	56.5
.200E+00	1239.	44.2	15.3	29.0	55.8

Figure 5-21: Mass fractions of Char, Tar and Gas as predicted by PC Coal Lab®

DROP TUBE SIMULATION WITH PC COAL LAB

FULL DYNAMICS

FDC1NG1.rpt

COAL CHARACTERISTICS: REFERENCE COAL

Ultimate, daf wt.%		Proximate, as rec wt.%	
%C	82.1	Moisture	3.3
%H	4.2	Vol. Mat.	20.5
%O	10.0	Ash	29.1
%N	1.9	Fixed C	47.1
%S	1.8		

OPERATING CONDITIONS:

90. micron particles at 25. C are entrained in N2
with 0.0 % O2 at 1170. C in a furnace at 1400. C
for .200E+00 s. The ambient pressure is 0.10 MPa.

User-specified conditions were implemented during devolatilization.

Thermal History Time,s	Tmp,C	Wt.Loss daf wt.%	Noncondensibles, daf wt. % Ygas	Yco2	Yh2o	Yco	Yhc	Yhcn
.000E+00	25.	0.0	0.0	0.0	0.0	0.0	0.0	0.00
.165E-02	61.	0.0	0.0	0.0	0.0	0.0	0.0	0.00
.371E-02	117.	0.0	0.0	0.0	0.0	0.0	0.0	0.00
.576E-02	177.	0.0	0.0	0.0	0.0	0.0	0.0	0.00
.782E-02	238.	0.0	0.0	0.0	0.0	0.0	0.0	0.00
.988E-02	297.	0.2	0.1	0.0	0.0	0.0	0.0	0.01
.119E-01	357.	0.8	0.1	0.0	0.1	0.0	0.0	0.01
.140E-01	420.	1.3	0.3	0.1	0.1	0.0	0.1	0.01
.160E-01	478.	2.2	0.5	0.1	0.2	0.0	0.1	0.01
.181E-01	533.	4.1	0.9	0.2	0.4	0.1	0.2	0.02
.201E-01	583.	6.6	1.5	0.3	0.7	0.1	0.4	0.02
.222E-01	632.	10.1	2.3	0.5	1.1	0.2	0.5	0.02
.243E-01	677.	14.3	3.4	0.7	1.6	0.3	0.8	0.03
.263E-01	721.	18.9	5.0	1.0	2.3	0.5	1.2	0.03
.284E-01	762.	23.1	6.4	1.3	2.9	0.6	1.5	0.03
.305E-01	803.	26.8	7.5	1.5	3.4	0.8	1.7	0.04
.330E-01	847.	30.6	8.6	1.7	3.8	1.0	2.0	0.04
.424E-01	988.	39.2	11.6	2.2	4.9	1.8	2.5	0.07
.561E-01	1091.	42.0	13.1	2.3	5.2	2.4	2.7	0.10
.763E-01	1158.	42.9	13.9	2.3	5.3	2.7	2.7	0.15
.118E+00	1218.	43.5	14.6	2.4	5.3	2.9	2.7	0.23
.200E+00	1239.	44.2	15.3	2.4	5.3	2.9	2.9	0.29

Figure 5-22: Mass fractions of the Non-Condensable Gases as predicted by PC Coal Lab®

The hydrocarbon composition was also provided and is shown in Figure 5-23.

DROP TUBE SIMULATION WITH PC COAL LAB

FULL DYNAMICS

FDC1HC1.rpt

COAL CHARACTERISTICS: REFERENCE COAL

Ultimate, daf wt.%		Proximate, as rec wt.%	
%C	82.1	Moisture	3.3
%H	4.2	Vol. Mat.	20.5
%O	10.0	Ash	29.1
%N	1.9	Fixed C	47.1
%S	1.8		

OPERATING CONDITIONS:

90. micron particles at 25. C are entrained in N2
with 0.0 % O2 at 1170. C in a furnace at 1400. C
for .200E+00 s. The ambient pressure is 0.10 MPa.

User-specified conditions were implemented during devolatilization.

Thermal History		Wt.Loss	Hydrocarbon Gases, daf wt. %							
Time,s	Tmp,C	daf wt.%	HCs	CH4	C2H4	C2H6	C3H6	C3H8	H2	H2S
.000E+00	25.	0.0	0.0	0.0	0.00	0.00	0.00	0.00	0.00	0.00
.165E-02	61.	0.0	0.0	0.0	0.00	0.00	0.00	0.00	0.00	0.00
.371E-02	117.	0.0	0.0	0.0	0.00	0.00	0.00	0.00	0.00	0.00
.576E-02	177.	0.0	0.0	0.0	0.00	0.00	0.00	0.00	0.00	0.00
.782E-02	238.	0.0	0.0	0.0	0.00	0.00	0.00	0.00	0.00	0.00
.988E-02	297.	0.2	0.0	0.0	0.00	0.00	0.00	0.00	0.00	0.01
.119E-01	357.	0.8	0.0	0.0	0.00	0.00	0.00	0.00	0.00	0.01
.140E-01	420.	1.3	0.1	0.0	0.01	0.00	0.01	0.00	0.00	0.03
.160E-01	478.	2.2	0.1	0.0	0.01	0.00	0.01	0.00	0.00	0.06
.181E-01	533.	4.1	0.2	0.1	0.03	0.00	0.02	0.00	0.00	0.11
.201E-01	583.	6.6	0.4	0.1	0.04	0.01	0.03	0.00	0.00	0.17
.222E-01	632.	10.1	0.5	0.2	0.06	0.01	0.05	0.00	0.01	0.27
.243E-01	677.	14.3	0.8	0.2	0.09	0.01	0.07	0.00	0.01	0.40
.263E-01	721.	18.9	1.2	0.3	0.13	0.02	0.10	0.00	0.02	0.58
.284E-01	762.	23.1	1.5	0.4	0.17	0.03	0.13	0.00	0.03	0.74
.305E-01	803.	26.8	1.7	0.5	0.19	0.03	0.15	0.00	0.04	0.87
.330E-01	847.	30.6	2.0	0.6	0.21	0.03	0.16	0.00	0.06	0.99
.424E-01	988.	39.2	2.5	0.7	0.26	0.04	0.20	0.00	0.18	1.32
.561E-01	1091.	42.0	2.7	0.7	0.27	0.04	0.20	0.00	0.41	1.47
.763E-01	1158.	42.9	2.7	0.7	0.26	0.04	0.20	0.00	0.71	1.52
.118E+00	1218.	43.5	2.7	0.7	0.26	0.04	0.20	0.00	1.12	1.53
.200E+00	1239.	44.2	2.9	0.8	0.29	0.05	0.22	0.00	1.52	1.54

Figure 5-23: Mass fractions of the Hydrocarbon Gases as predicted by PC Coal Lab®

Finally, PC Coal Lab provides the elemental compositions of tar and char. These are shown in Figure 5-24 and Figure 5-25 respectively.

DROP TUBE SIMULATION WITH PC COAL LAB

FULL DYNAMICS

FDC1TC1.rpt

COAL CHARACTERISTICS: REFERENCE COAL

Ultimate, daf wt.%		Proximate, as rec wt.%	
%C	82.1	Moisture	3.3
%H	4.2	Vol. Mat.	20.5
%O	10.0	Ash	29.1
%N	1.9	Fixed C	47.1
%S	1.8		

OPERATING CONDITIONS:

90. micron particles at 25. C are entrained in N2
with 0.0 % O2 at 1170. C in a furnace at 1400. C
for .200E+00 s. The ambient pressure is 0.10 MPa.

User-specified conditions were implemented during devolatilization.

Thermal History		Wt.Loss	Tar Characteristics						
Time,s	Tmp,C	daf wt.%	Ytar	Mn,g/m	% C	% H	% O	% N	% S
.000E+00	25.	0.0	0.0	0.0	0.0	0.0	0.0	0.0	0.0
.165E-02	61.	0.0	0.0	0.0	0.0	0.0	0.0	0.0	0.0
.371E-02	117.	0.0	0.0	0.0	0.0	0.0	0.0	0.0	0.0
.576E-02	177.	0.0	0.0	0.0	0.0	0.0	0.0	0.0	0.0
.782E-02	238.	0.0	0.0	0.0	0.0	0.0	0.0	0.0	0.0
.988E-02	297.	0.2	0.2	169.6	81.5	3.2	11.4	1.9	2.1
.119E-01	357.	0.8	0.7	170.7	80.1	4.6	11.4	1.9	2.0
.140E-01	420.	1.3	1.1	178.4	80.0	4.8	11.3	1.9	2.0
.160E-01	478.	2.2	1.7	205.0	80.1	4.9	11.1	1.9	2.0
.181E-01	533.	4.1	3.2	240.1	80.3	5.0	10.8	1.9	1.9
.201E-01	583.	6.6	5.1	262.3	80.5	5.1	10.6	1.9	1.9
.222E-01	632.	10.1	7.7	284.5	80.8	5.1	10.4	1.9	1.9
.243E-01	677.	14.3	10.8	301.1	81.1	5.1	10.0	1.9	1.8
.263E-01	721.	18.9	13.9	309.8	81.7	5.1	9.6	1.9	1.7
.284E-01	762.	23.1	16.7	313.3	82.3	5.2	9.0	1.9	1.6
.305E-01	803.	26.8	19.4	314.0	82.8	5.2	8.5	1.9	1.5
.330E-01	847.	30.6	22.0	314.0	83.4	5.1	8.0	2.0	1.4
.424E-01	988.	39.2	27.6	308.9	84.6	5.1	7.0	2.0	1.3
.561E-01	1091.	42.0	28.8	306.0	84.9	5.1	6.7	2.0	1.2
.763E-01	1158.	42.9	29.0	305.4	84.9	5.2	6.7	2.0	1.2
.118E+00	1218.	43.5	29.0	305.4	84.9	5.2	6.7	2.0	1.2
.200E+00	1239.	44.2	29.0	305.4	84.9	5.2	6.7	2.0	1.2

Figure 5-24: Elemental Composition of Tar as predicted by PC Coal Lab®

DROP TUBE SIMULATION WITH PC COAL LAB

FULL DYNAMICS

FDC1CC1.rpt

COAL CHARACTERISTICS: REFERENCE COAL

Ultimate, daf wt.%		Proximate, as rec wt.%	
%C	82.1	Moisture	3.3
%H	4.2	Vol. Mat.	20.5
%O	10.0	Ash	29.1
%N	1.9	Fixed C	47.1
%S	1.8		

OPERATING CONDITIONS:

90. micron particles at 25. C are entrained in N2 with 0.0 % O2 at 1170. C in a furnace at 1400. C for .200E+00 s. The ambient pressure is 0.10 MPa.

User-specified conditions were implemented during devolatilization.

Thermal History		Wt.Loss		Char Composition, daf wt.%				
Time,s	Tmp,C	daf wt.%	Ychar	% C	% H	% O	% N	% S
.000E+00	25.	0.0	100.0	82.1	4.2	10.0	1.9	1.8
.165E-02	61.	0.0	100.0	82.1	4.2	10.0	1.9	1.8
.371E-02	117.	0.0	100.0	82.1	4.2	10.0	1.9	1.8
.576E-02	177.	0.0	100.0	82.1	4.2	10.0	1.9	1.8
.782E-02	238.	0.0	100.0	82.1	4.2	10.0	1.9	1.8
.988E-02	297.	0.2	99.8	82.1	4.2	10.0	1.9	1.8
.119E-01	357.	0.8	99.2	82.2	4.2	9.9	1.9	1.8
.140E-01	420.	1.3	98.7	82.3	4.2	9.8	1.9	1.8
.160E-01	478.	2.2	97.8	82.5	4.2	9.7	1.9	1.7
.181E-01	533.	4.1	95.9	82.8	4.1	9.5	1.9	1.7
.201E-01	583.	6.6	93.4	83.2	4.1	9.2	1.9	1.6
.222E-01	632.	10.1	89.9	83.8	4.0	8.7	1.9	1.6
.243E-01	677.	14.3	85.7	84.7	3.9	8.0	2.0	1.4
.263E-01	721.	18.9	81.1	86.0	3.8	6.9	2.0	1.2
.284E-01	762.	23.1	76.9	87.3	3.6	6.0	2.0	1.1
.305E-01	803.	26.8	73.2	88.3	3.5	5.2	2.1	0.9
.330E-01	847.	30.6	69.4	89.4	3.4	4.4	2.1	0.8
.424E-01	988.	39.2	60.8	92.7	2.9	1.9	2.2	0.3
.561E-01	1091.	42.0	58.0	94.7	2.4	0.6	2.2	0.1
.763E-01	1158.	42.9	57.1	95.7	1.9	0.2	2.2	0.0
.118E+00	1218.	43.5	56.5	96.6	1.2	0.1	2.1	0.0
.200E+00	1239.	44.2	55.8	97.5	0.4	0.0	2.1	0.0

Figure 5-25: Elemental Composition of Tar as predicted by PC Coal Lab®

The elemental composition of the gas pyrolysis product is calculated by mass weighting the various gaseous components predicted by PC Coal Lab®. Care was taken to make sure all the atoms were accounted for the respective mass fractions summed to unity.

The column vectors shown in equation 5.22, are further conditioned according to the techniques proposed by Modliński and Hardy [30]. The first aspect of the vector manipulation was to eliminate sulphur from the elemental compositions. This was done as sulphur does not play a role in the gaseous combustion process. The sulphur mass fraction is added to the that of the carbon in the char product. This is shown mathematically below:

$$C_{char} = C_{char} + S_{char}\frac{W_C}{W_S} \qquad S_{char} = 0$$

$$C_{tar} = C_{tar} + S_{tar}\frac{W_C}{W_S} \qquad S_{tar} = 0 \qquad 5.23$$

$$C_{gas} = C_{gas} + S_{gas}\frac{W_C}{W_S} \qquad S_{gas} = 0$$

Hydrogen is eliminated from the char and moved to the tar product. This is shown below:

$$H_{tar} = H_{tar} + H_{char} \quad H_{char} = 0 \tag{5.24}$$

Finally, nitrogen is eliminated from each of the elemental definitions in the column vectors representing the products of pyrolysis. The column vectors are now conditioned to be in form that enables the calculation of the molecular formulations of the light and heavy hydrocarbons. This can be seen below:

$$char^* = \begin{bmatrix} C_{char^*} \\ 0 \\ 0 \\ 0 \end{bmatrix} \quad tar^* = \begin{bmatrix} C_{tar^*} \\ H_{tar^*} \\ O_{tar^*} \\ 0 \\ 0 \end{bmatrix} \quad gas^* = \begin{bmatrix} C_{gas^*} \\ H_{gas^*} \\ 0 \\ 0 \\ 0 \end{bmatrix} \tag{5.25}$$

It is now possible to specify the atomic makeup of the tar and gas species. The tar is assumed to be of the form: $C_xH_yO_z$ and is predominantly made up of C_7 hydrocarbons. The gas species is assumed to be of the form: C_mH_n. It should be noted the gas species only considers that hydrocarbon components. Hence CO_2 and H_2O must be accounted for separately.

The heating values for the overall volatile pseudo-species, tar and gas are calculated using the approach proposed by Modliński and Hardy [30]. The lower heating value of the volatile species is given by:

$$LHV_{volatile} = \frac{LHV_{coal_{daf}} - f_{char} LHV_{\ char}}{f_{volatile}} \tag{5.26}$$

Where:

- $LHV_{coal,daf}$ – Low heating value of the reference coal [MJ/kg]
- F_{char} – mass fraction of char in the coal (d.a.f) [ ]
- $F_{volatile}$ –fraction of volatile material in the coal (d.a.f) [ ]
- LHV_{char} – Lower heating value of the char [MJ/kg]

The LHV_{char} is assumed to be the same as pure carbon.

The lower heating value of the tar compounds is given by:

$$LHV_{tar} = \frac{LHV_{volatile} - \left(y_{gas} LHV_{gas} + y_{CO} LHV_{CO}\right)}{y_{tar}} \quad 5.27$$

Where:

- y_{gas}, y_{tar}, y_{CO} – mass fractions of the gas, tar and carbon monoxide species respectively [ ]
- LHV_{gas} – Lower heating value of the gas species [MJ/kg]
- LHV_{CO} – Lower heating value of the carbon monoxide [MJ/kg]

The LHV*gas* is assumed to be the same as for methane i.e., 50 MJ/kg.

After some mathematical manipulation (see detailed calculation in Appendix D) the stoichiometry of the five reactions that make up this combustion mechanism (see section 5.3.3) was determined. The summarised input specification is listed below:

Table 5-8: Five Step Mechanism – Reaction 1 Definition

$\mathbf{1kmol\ Volatiles \longrightarrow s_{tar}mv_{tar} + s_{gas}mv_{gas} + s_{CO}mv_{CO} + s_{CO_2}mv_{CO_2} + s_{H_2O}mv_{H_2O}}$						
Species	**Stoich. Coefficient**	**Rate Exponent**	**Species**	**Stoich. Coefficient**	**Rate Exponent**	**Arrhenius Rate**
mv_vol	1	1	mv_tar	s_{tar} = 0.316	1	A = 1.00e13 s-m-kmol T_b = 0.00 Ea = 0.00
			mv_gas	s_{gas} = 0.178	1	
			CO	s_{CO} = 0.128	1	
			CO_2	s_{CO2} = 0.069	1	
			H_2O	S_{H2O} = 0.309	1	

Table 5-9: Five Step Mechanism – Reaction 2 Definition

$1kmol\ mv_{tar} + s_{21}O_2 \longrightarrow s_{22}CO + s_{23}H_2$						
Species	**Stoich. Coefficient**	**Rate Exponent**	**Species**	**Stoich. Coefficient**	**Rate Exponent**	**Arrhenius Rate**
mv_tar	1	1	CO	$S_{22} = 7$	1	A = 3.80e7 s-m-kmol $T_b = 0.00$
O_2	$S_{21} = 3.294$	1	H_2	$S_{23} = 2.917$	1	Ea = 5.6463e7

Table 5-10: Five Step Mechanism – Reaction 3 Definition

$1kmol\ mv_{gas} + s_{31}O_2 \longrightarrow s_{32}CO + s_{33}H_2O$						
Species	**Stoich. Coefficient**	**Rate Exponent**	**Species**	**Stoich. Coefficient**	**Rate Exponent**	**Arrhenius Rate**
mv_gas	1	1	CO	$S_{32} = 7$	1	A = 2.33e11 s-m-kmol $T_b = 0.50$
O_2	$S_{31} = 2.932$	1	H_2O	$S_{33} = 4.864$	1	Ea = 1.6737e8

Table 5-11: Five Step Mechanism – Reaction 4 Definition

$1kmol\ CO + s_{41}O_2 \longrightarrow s_{42}CO_2$						
Species	**Stoich. Coefficient**	**Rate Exponent**	**Species**	**Stoich. Coefficient**	**Rate Exponent**	**Arrhenius Rate**
CO	1	1	CO	$S_{42} = 1$	1	A = 1.30e11 s-m-kmol T_b = 0.00 Ea = 1.252e8
O_2	$S_{41} = 0.5$	0.5	H_2O	$S_{43} = 0.00$	0.5	

Table 5-12: Five Step Mechanism – Reaction 5 Definition

$1kmol\ H_2 + s_{51}O_2 \longrightarrow s_{52}H_2O$						
Species	**Stoich. Coefficient**	**Rate Exponent**	**Species**	**Stoich. Coefficient**	**Rate Exponent**	**Arrhenius Rate**
CO	1	1	CO	$S_{52} = 1$	1	A = 1.00e7 s-m-kmol T_b = 0.00 Ea = 8.368e6
O_2	$S_{51} = 0.5$	1	H_2O			

The char in the coal particle is assumed to oxidise to CO and thus would require further reaction to form CO_2.

The main characteristics of the pseudo volatile matter and the tar and gas components are summarised below:

Table 5-13: Volatile Species Molecular Weight and Standard State Enthalpy

Species	Molecular Weight [kg/kgmol]	Standard State Enthalpy [J/kgmol]
mv_vol	46.563	-5.8145e8
mv_tar	96.560	-1.20322e9
mv_gas	21.817	-4.7895e8

Thus, the main input parameters are defined, and the five-step mechanism is ready for implementation into ANSYS Fluent®.

5.4 Pilot Scale Combustion Test Facility Simulations

5.4.1 Background

The Pilot Scale Combustion Test Facility (PSCTF) simulations allow for the study of the combustion of the reference coal in a turbulent, swirling flow field that is similar to the conditions seen in a full-size plant. The PSCTF has a single burner in a refractory lined combustion chamber and consequently the flame has significant thermal support from the radiating walls. The PSCTF can be very useful in correlating the realistic burnout times of various coals with the behaviour seen on full size boilers. From a research perspective the simulations of the PSCTF provide the first opportunity to test the influence of gas phase combustion mechanisms on the complete combustion process. The current section will detail the development of the CFD model with the necessary input data.

5.4.2 PSCTF Rig Layout and Operation

The PSCTF is fired by a down-shot low NOx burner into a refractory lined radiative furnace section. The resultant flue gas passes through a water-cooled convective section where it is cooled and passed through a bag filter to remove particulates and eventually released into the atmosphere via the stack. The radiative section has several ports that allow access to the furnace during operation. This is where gas and particulate samples are obtained using gas pyrometry and iso-kinetic particle sampling. The gas temperature is also logged at several of these points. A schematic description of the PSCTF is shown in Figure 5-26.

Other notable characteristics of the PSCTF are:

- The plant has its own on-site coal handling facility where raw coal can be prepared in terms of obtaining a representative sample and subsequently milling the coal to the required fineness. The coal preparation is not an online process and rather, is done as a batch process. Hence all the coal required for a combustion test is milled beforehand and is expended during the firing of the coal. This also means the coal particle size and the inherent coal quality can be controlled.

- The PSCTF was designed using the concept of *residence time scaling*. This is to ensure that the temperature and combustion histories of the coal particles in the PSCTF, mimic that of a full-scale furnace.

- The plant has a capacity of $1MW_{th}$. It is also capable of running at low load conditions, dependant on the coal being fired and the minimum fuel flow rate required.

- The burner is a downward firing design that can operate in low NOx mode. The secondary and tertiary swirlers are radial in design and are operated manually by adjusting the position of the swirler blocks. The burner can transition from a pure jet burner (0° swirl) to a high swirl design (approximately 45° swirl). Any setting in between these end points can also be achieved.

- The primary air (35 °C to 105 °C) and secondary air streams (35 °C to 400 °C) are electrically pre-heated. This allows for a reasonable range of operation and the plant can maintain these conditions in a stable manner.

According to Rajoo [60], care was taken to ensure the conditions of similitude between the PSCTF and full scale plant, during the design and operation phases, several key parameters had to be considered. These included: inlet flow temperatures, PA and SA flow rates and hence SA/PA ratios, excess air ratios, PF fineness and ultimately the particle residence time in the combustion zone.

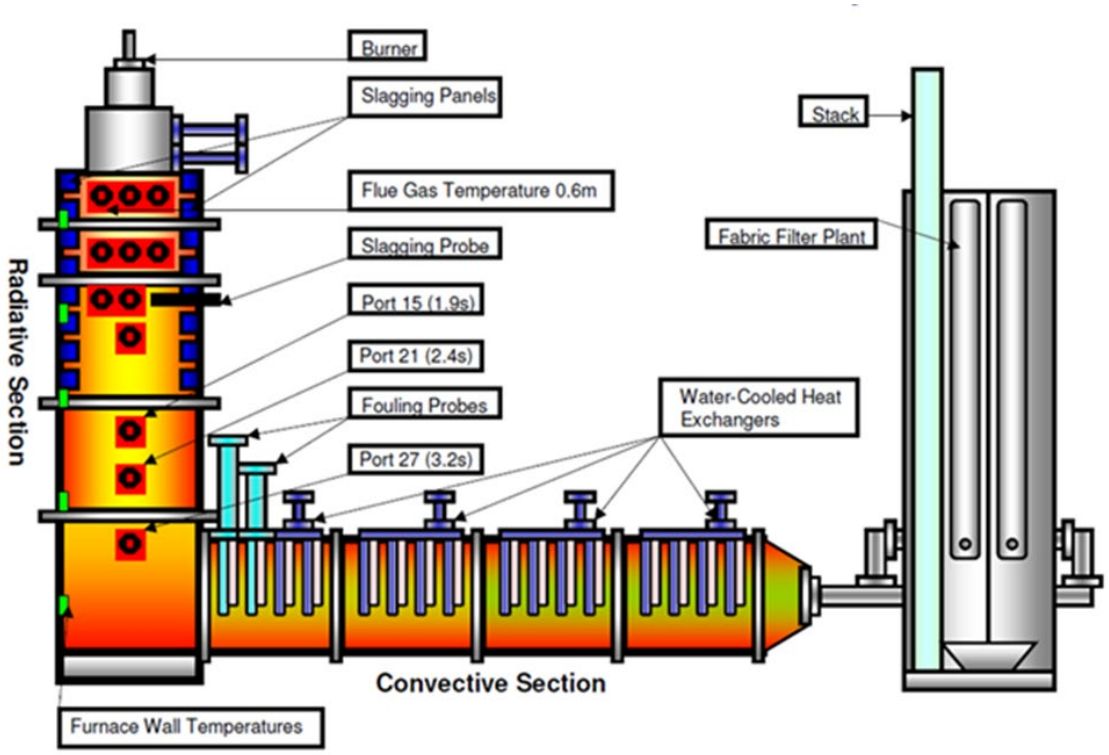

Figure 5-26: Schematic of the PSCTF [60]

5.4.3 PSCTF CFD Model

A CFD model was developed in ANSYS Fluent® V19.2 to simulate the combustion of the reference coal at full load i.e., 1 MW_{th} firing capacity. The CFD model faithfully captures the internal dimensions of the furnace region, which is refractory lined. The back pass was modelled to allow for the evacuation of the combustion products. The focus area of this study is the furnace region and particularly the region near the burner exit. In lieu of this, the low NOx burner was modelled explicitly with attention being paid to the flow inlets, including the coaxial core air and primary air pipes. At the time of this study there was no data available to characterise the swirl emanating from the burner. Hence the secondary and tertiary air swirlers are modelled in detail to predict this.

A schematic of the CFD model is shown in Figure 5-27.

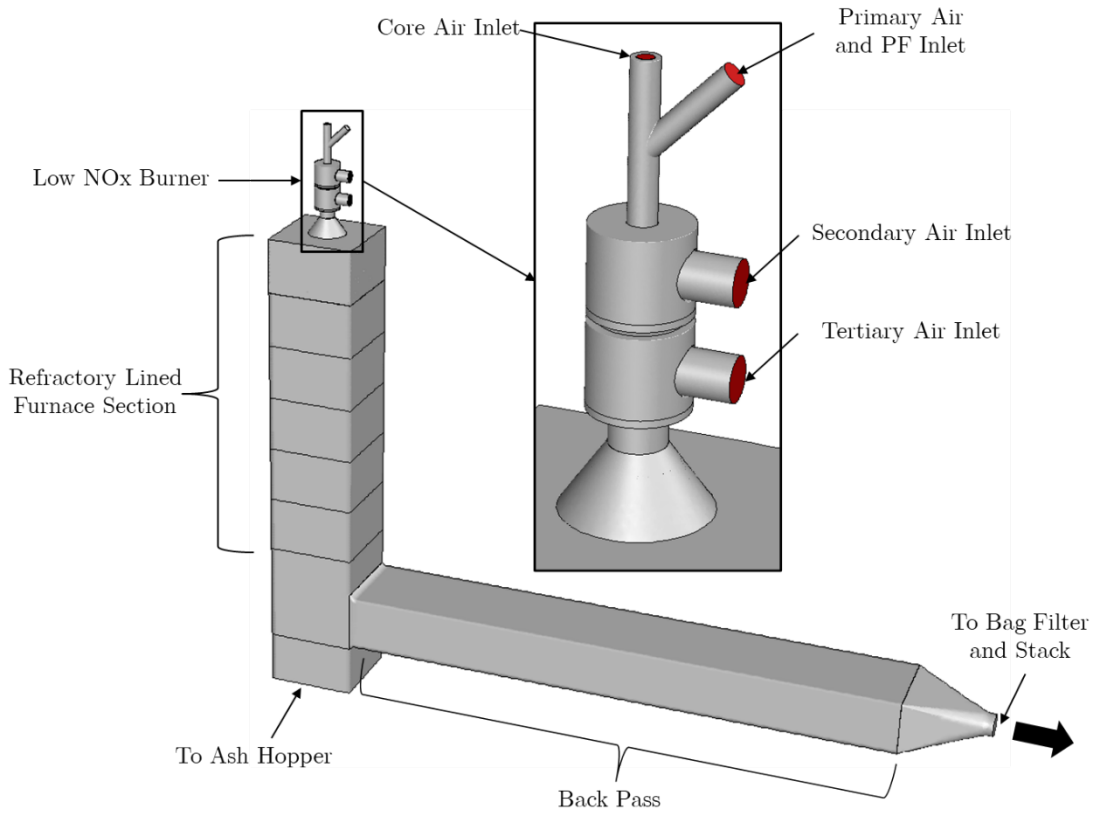

Figure 5-27: CFD model of the Pilot Scale Combustion Test Facility

A hybrid computational mesh was used in the simulation of the PSCTF. This was to ensure that sufficient resolution was applied to the swirling flow region and the flows within the narrower section of the burner. As far as possible, a structured mesh was used for the rest of the model.

The reference mesh used over 4 million computational cells and the details are shown in Figure 5-28.

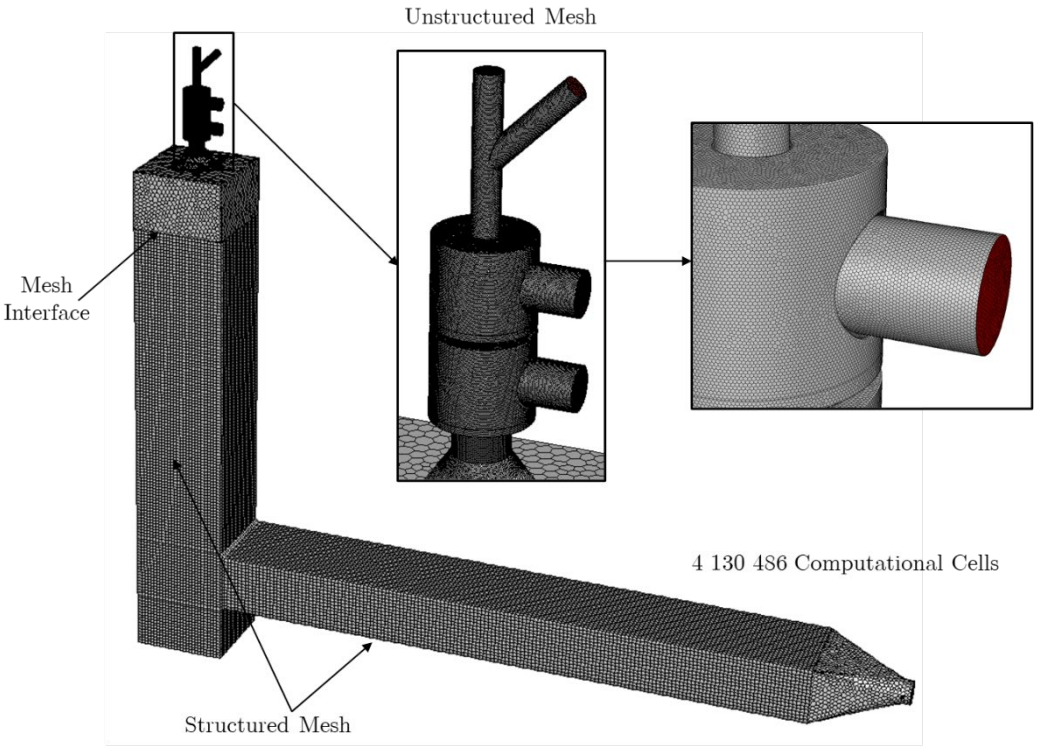

Figure 5-28: PSCTF Computational Mesh Details

The internal configuration of the secondary and tertiary swirlers is shown in Figure 5-29. The design of the low NOx burner on the PSCTF is such that the core air, primary air, secondary air, and tertiary air are configured to exit the burner in several coaxial streams. The secondary and tertiary air have swirl by virtue of the position of the swirler blocks. The primary air annulus will also produce an offset flow into the furnace due to the asymmetric positioning of the primary air and coal feeder tube. The secondary and tertiary swirler blocks are the same design albeit for the tertiary swirl having a larger diameter.

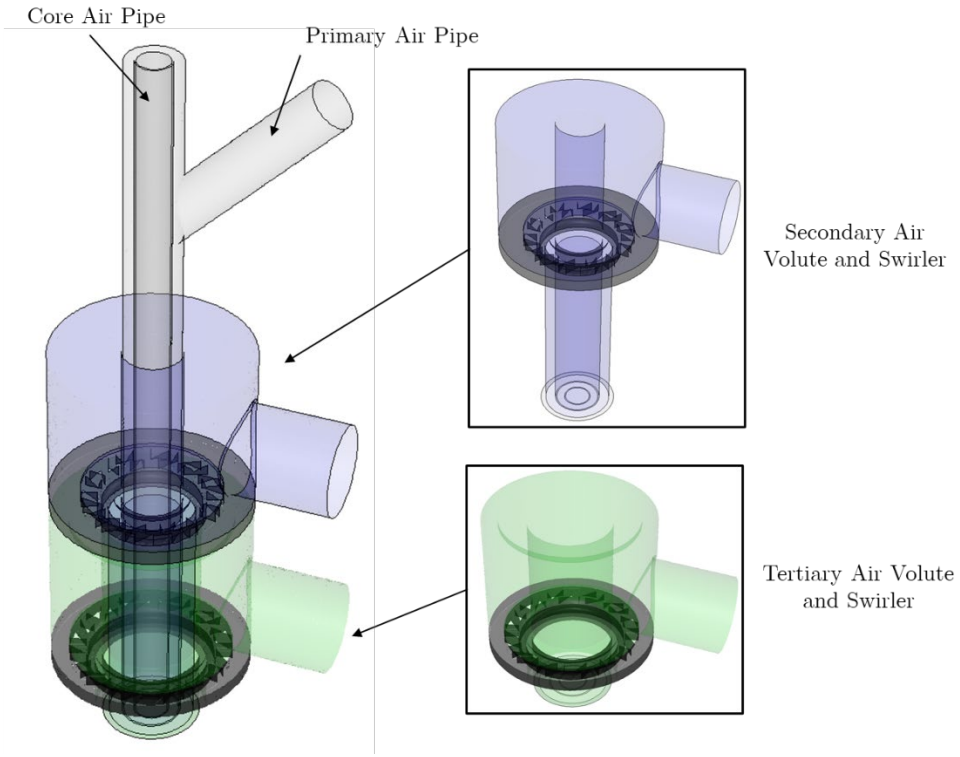

Figure 5-29: Secondary and Tertiary Swirler Configuration

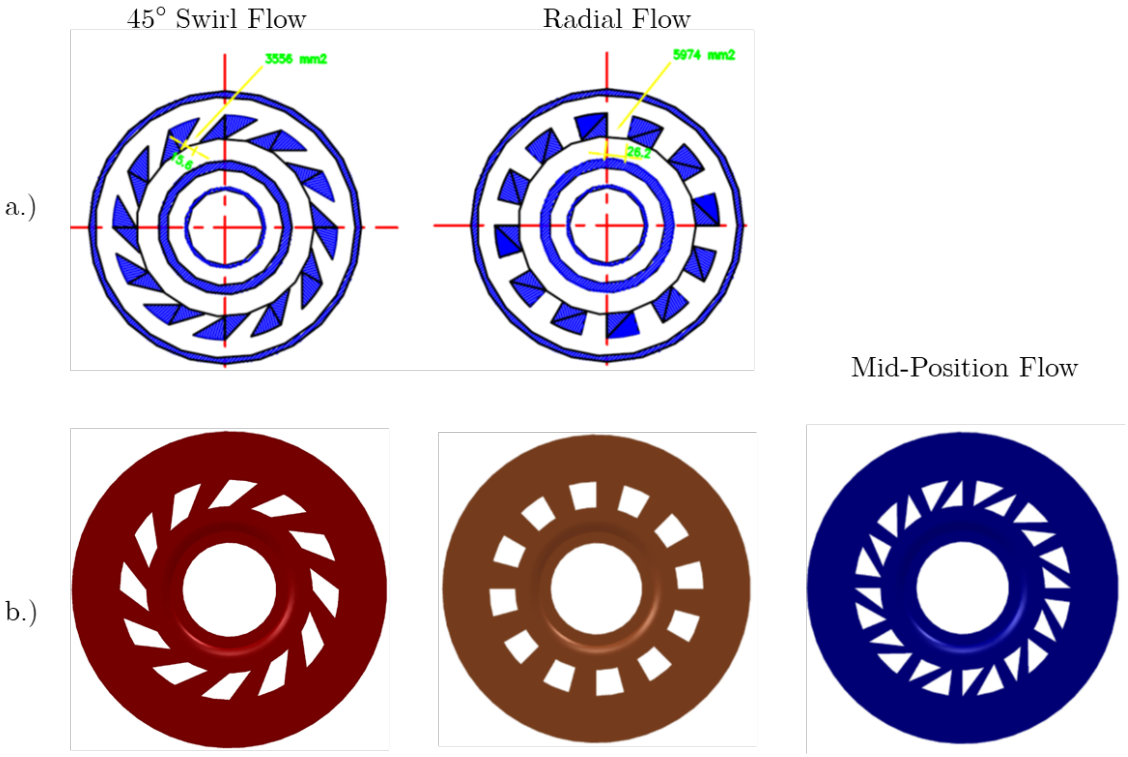

Figure 5-30: (a) Swirler Block Orientation for 45° and radial flow settings. (b) Fluid regions for 45°, radial and mid-positions as implemented in CFD model

The extreme positions of the swirler blocks are shown in Figure 5-30 (a). The swirler can be configured to operate in purely radial mode. The CFD model requires the inverse of the solid geometry i.e., the associated fluid volumes. The fluid volumes for each configuration are shown in Figure 5-30 (b). The mid position configuration is also shown, and this is swirler position used in all the simulations as this the setting employed on the PSCTF rig. It was chosen by Eskom Research as the best setting for optimal swirl rates.

Table 5-14: PSCTF Sub Model Settings

Sub - Model	Details
Solver	Steady State, Pressure based solver. SIMPLE pressure-velocity coupling using standard pressure discretisation. Second order discretisation was used for all transport equations. Operating pressure set to highveld conditions i.e., 85 kPa ambient pressure.
Turbulence	Realizable k-ε with enhanced wall functions.
Radiation	Discrete Ordinates with standard discretisation, with WSGGM for participating gases.
Discrete phase	Reacting solid fuel particles with coupled particle/fluid/wall radiation. Discrete particle size distribution applied. Discrete random walk model for turbulent dispersion.
Devolatilisation	Single step model as per settings defined in section 5.2.4
Char Combustion	Single step model (Baum and Street) as per settings defined in section 5.2.5

The flow boundary conditions applied to CFD model are listed in Table 5-15. The air and fuel flow are consistent with the definition of the $1MW_{th}$ operating point. Note the tertiary flow is reduced to the magnitude of a cooling flow. Hence under experimental conditions the PSCTF burner is operated as a swirl burner and not a low NOx burner. This operating principle was arrived at by Eskom Research after several years of operation, and it was shown to provide the necessary conditions to assess the burnout of the coal being tested.

The walls of the PSCTF are lined with refractory in the furnace region. Hence a great deal of the incident radiative heat emanating from the flame is in fact reflected into the flame zone. This is the concept of *flame support,* and it mimics the effect in a full-scale boiler where the surrounding flames in the burners provide radiative heat exchange to flame of interest. The

walls in the furnace region were modelled as coupled heat exchange surfaces i.e., the emissivity of the wall facing the flame was set to 0.6 and the effect of conduction through the refractory to outside surface of the PSCTF facing the atmosphere was modelled using the one-dimensional thermal resistance feature in ANSYS Fluent®. The refractory was modelled using an average thermal conductivity of 1.3 W/mK, which was obtained from the material specification [61]. Finally, the convective heat transfer coefficient on the outside wall facing ambient air is set 10 W/m^2K. This is consistent with natural convection conditions. The walls of the back pass were modelled as adiabatic walls as this region was not of interest for the current study.

The test conditions were documented by Eskom Research [62] and are summarised in Table 5-15.

Table 5-15: PSCTF Flow Boundary Conditions

Parameter	Value
Core Air Inlet Mass Flow [kg/s]	0.0022
Core Air Inlet Temperature [°C]	71.47
Primary Air Inlet Mass Flow [kg/s]	0.0950
Primary Air Inlet Temperature [°C]	71.47
Secondary Air Inlet Mass Flow [kg/s]	0.2487
Secondary Air Inlet Temperature [°C]	267.11
Tertiary Air Inlet Mass Flow [kg/s]	0.0170
Tertiary Air Inlet Temperature [°C]	202.11
PF Mass Flow [kg/s]	0.0460
PF Inlet Temperature [°C]	71.47

A discrete particle size distribution was implemented in the simulations. The size distribution from a size analysis performed on a representative pulverised fuel sample. Particle characterisation was implemented using 4 size bins i.e., 38µm, 75µm, 106µm and 150µm. The particles were introduced into the model from the primary air inlet (see Figure 5-27) at

the primary air temperature. The total PF mass flow was partitioned according to the size distribution (see Table 5-16). A particle injection was created for each size bin in ANSYS Fluent®.

Table 5-16: PSCTF Particle Size Distribution

Particle Size [mm]	Mass Flow [kg/s]	% of Total
38	0.0292	63
75	0.0064	14
106	0.0027	6
150	0.0077	17

The PSCTF model was developed to test the influence of implementing three different gas phase combustion mechanisms on the flame characteristics. The one-step, two-step and five-step combustion mechanisms (see section 5.3) were used. The results from these simulations are presented in the following section.

5.4.4 PSCTF Simulation Results

The results for 1 MW_{th} simulations of the PSCTF are presented in this section. Three different gas phase combustion mechanisms were tested, and temperatures extracted from the CFD simulations at several locations, was compared to experimental measurements at the same locations. The measurement data was obtained from tests [62] performed by Eskom Research at the PSCTF in Rosherville, Johannesburg.

The results are visualised by means of contour plots of several scalar quantities. The results are presented on planes that cross the midpoint of the furnace in two directions. The two viewing directions, front view and right-hand side view are shown in Figure 5-31.

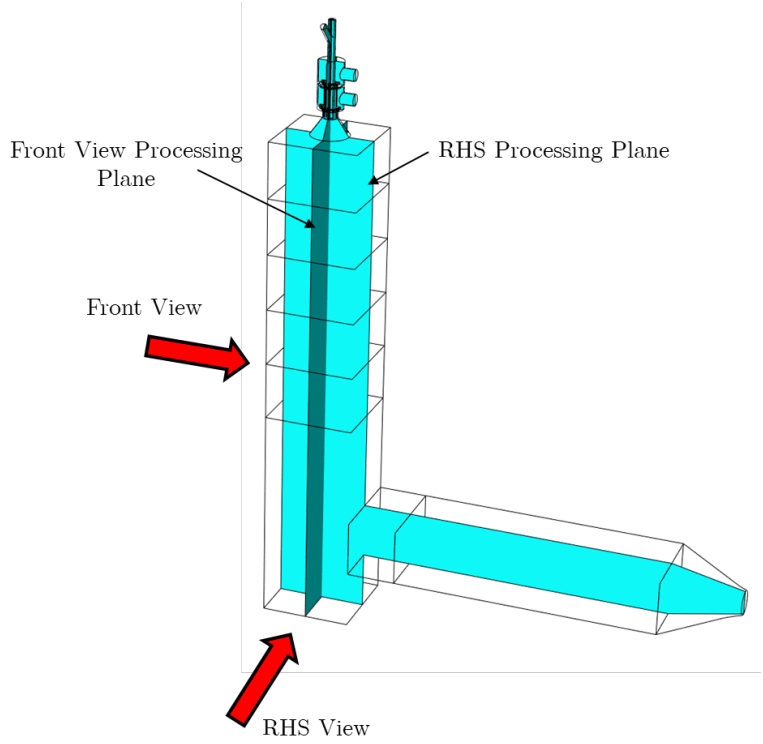

Figure 5-31: Reference Viewing Directions for the PSCTF CFD Model

The temperature contours for the PSCTF model are shown in Figure 5-32. The comparison with the experimental and predicted values are shown in Figure 5-33

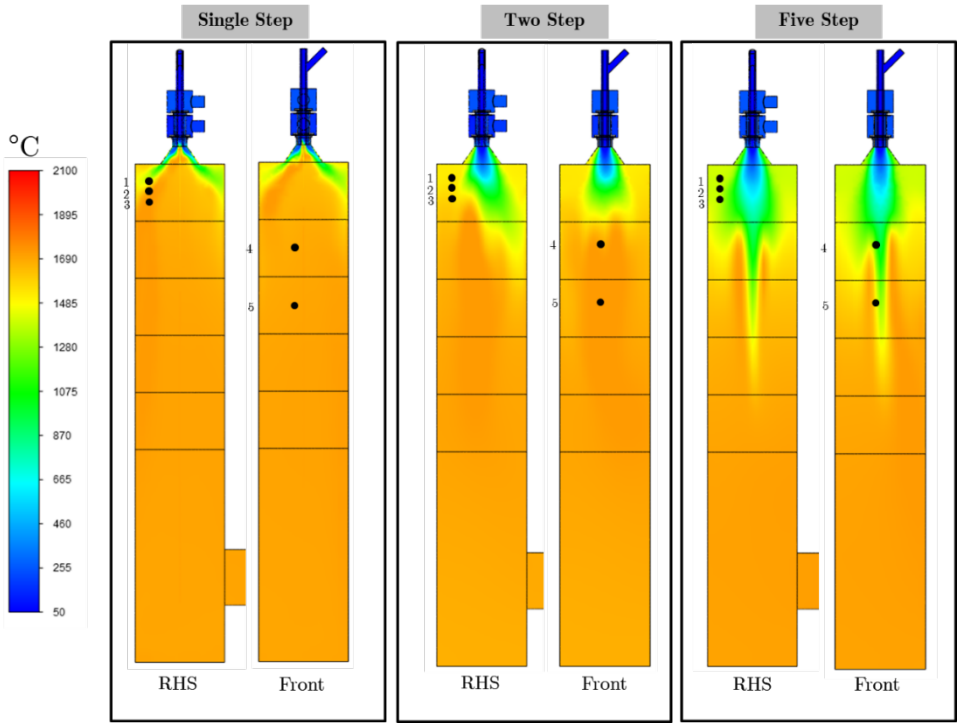

Figure 5-32: Temperature Contours on Mid-Section Planes for Three Different Gas Phase Combustion Mechanisms

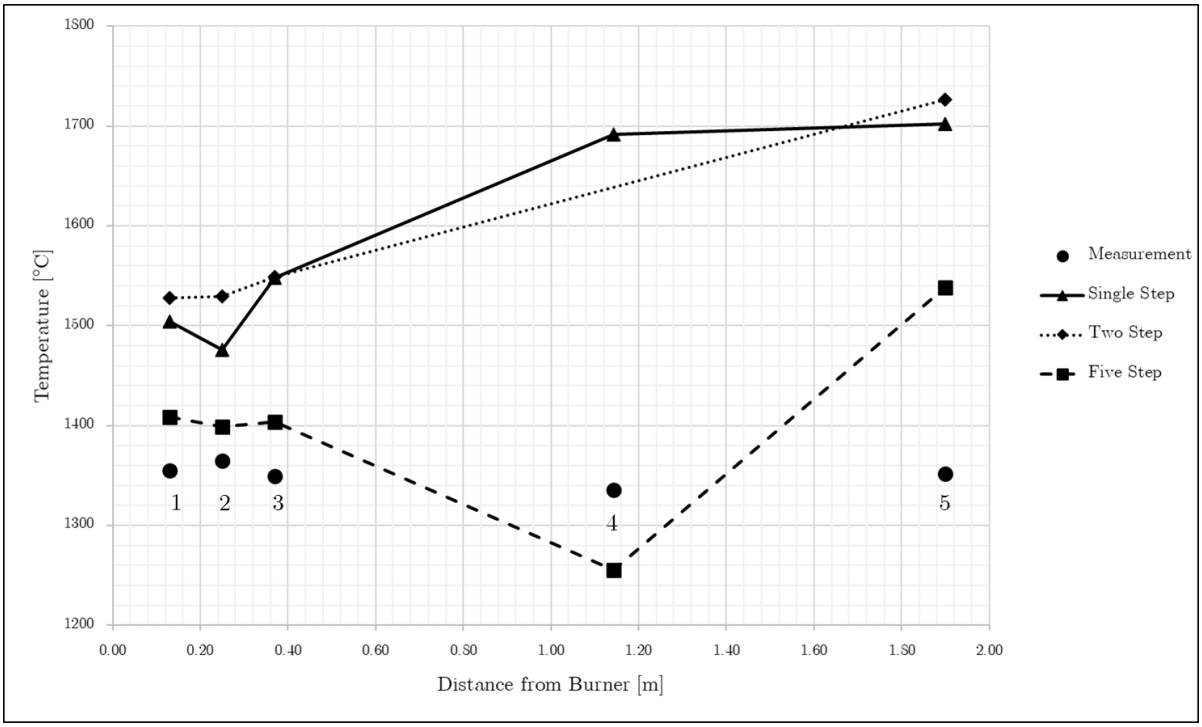

Figure 5-33: Temperature Measurements at Selected Points for Three Different Gas Phase Combustion Mechanisms

Measurements 1,2 and 3 are taken from thermocouples installed on the wall in the region of the furnace near the burner outlet. Measurement 4 and 5 are gas pyrometer readings at a distance of 450mm into the furnace. The position of these measurements is overlayed onto the temperature fields (see Figure 5-32) of the three simulations. The comparison of the experimental data to the predicted values, as well as the location of the measurement point relative to the burner outlet is shown in Table 5-17.

Table 5-17: PSCTF Temperature Measurements – Experiment and Prediction

Index	Measurement Name	Distance from Burner [m]	Experiment [°C]	Single-Step [°C]	Two-Step [°C]	Five-Step [°C]
1	Gas Temp 0.13m	0.13	1355	1504	1528	1408
2	Gas Temp 0.25m	0.25	1365	1476	1529	1399
3	Gas Temp 0.37m	0.37	1350	1548	1549	1404
4	Gas Temp Port 10	1.14	1336	1692	1727	1256
5	Gas Temp Port D	1.90	1352	1702	1727	1538

It can be seen from the temperature contours (see Figure 5-32) that the predictions for the three different mechanisms are starkly different. The single-step mechanism has a drastic flaring of the flow field immediately after the burner exit. The two-step mechanism predicts a flame that shows the typical behaviour. There is an indication of a flame root after a significant stand off from the burner mouth. The five-step mechanism predicts the flame root to be lower and the colder gas stream penetrates further down the furnace. The quantitative comparison with experimental data (see Figure 5-33), shows that the five-step mechanism provides the best corelation. The initial temperature in the zone after the burner exit and to the side is predicted better. Both the single-step and two-step mechanisms over predict the temperatures in that region. The five-step mechanism also has the best temperature for the experimental points obtained from the in-furnace gas pyrometry. All the mechanisms over predict the temperature at the lowest measurement location i.e., Port 10 at 1.90m from the burner outlet.

The adverse temperature field predicted by the single-step mechanism may be explained by considering how heat is released from the fuel as it exits the burner. The normalised heat release for all three mechanisms is shown in Figure 5-34. This contour allows the location of the heat release in the furnace to be visualised.

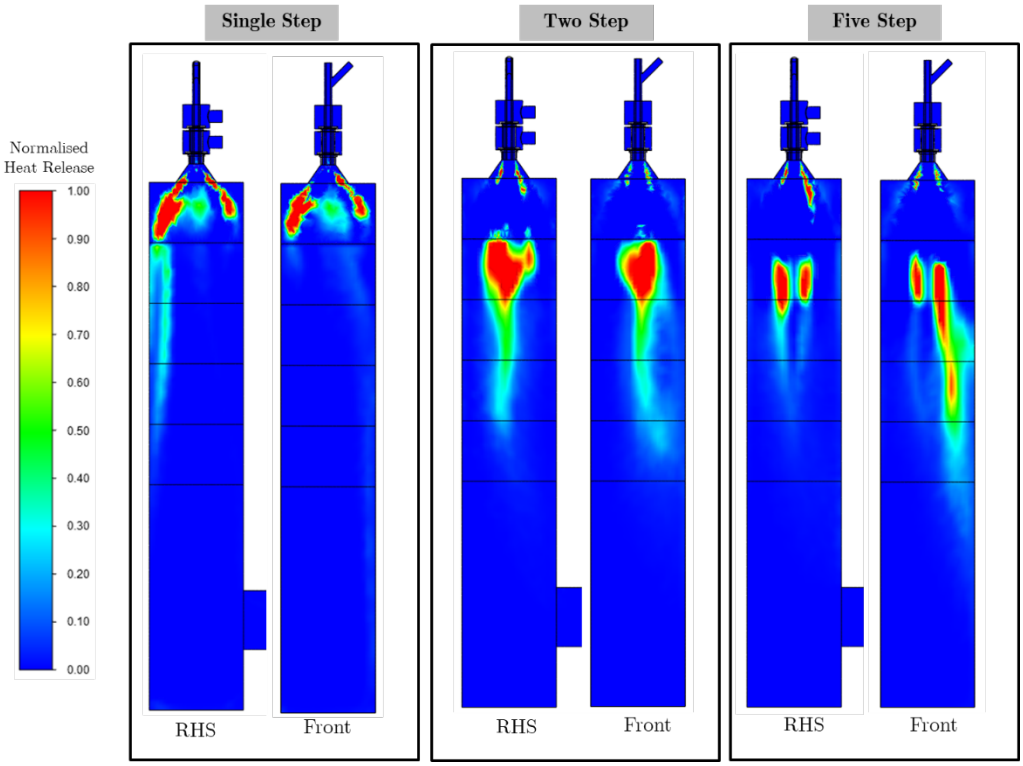

Figure 5-34: Normalised Heat Release for Three Different Gas Phase Mechanisms

The single-step mechanism differs from the other two mechanisms in that most of the heat release is near the burner outlet i.e., it is significantly premature compared to the other simulations. A reason for this may be that the devolatilisation reaction for the single-step mechanism is exothermic since all the volatiles transition instantaneously to the final combustion products. This rapid release of energy may be promoting large density changes in the swirl zone at the exit of the burner, and in turn promoting the flaring of the flow. The devolatilisation reactions for the two-step and five-step mechanisms are endothermic. The heat release for the two-step mechanism is conglomerated in region approximately 1.5m from the burner mouth. The five-step mechanism shows two distinct regions of combustion, and the reactions continue further down the furnace.

The particle trajectories for the three cases are shown in Figure 5-35. The particles are coloured by their char mass fraction. Hence it gives an indication of the burnout levels in the furnace.

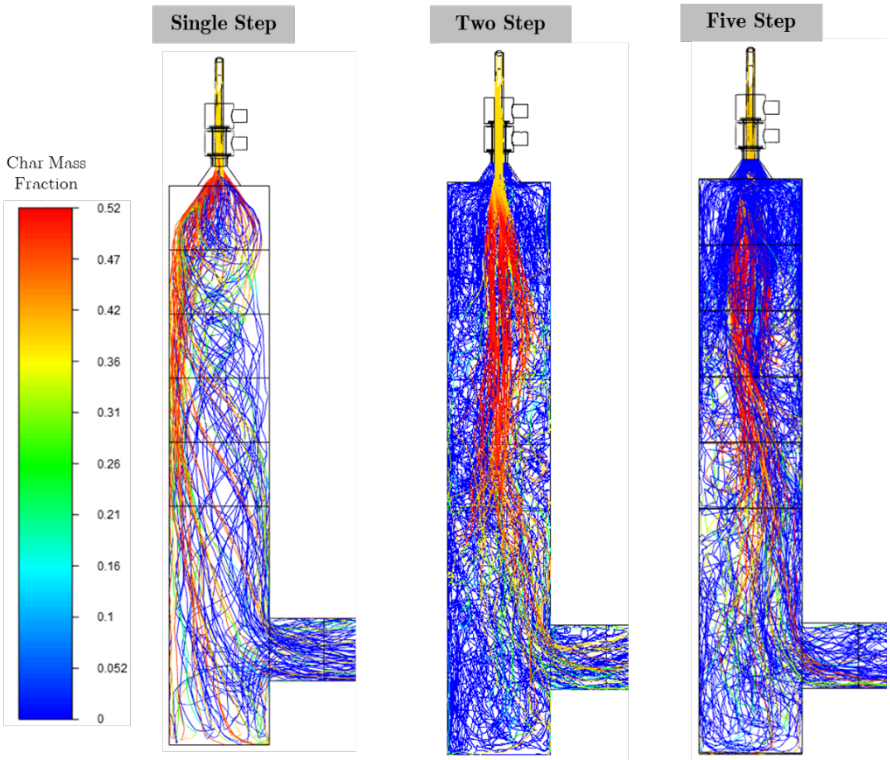

Figure 5-35: Particle Tracks Coloured by Char Mass Fraction for Three Gas Phase Combustion Mechanisms

In all cases 4400 particles were tracked through the domain. The single-step mechanism does not produce a credible flow field prediction and it is characterised by severe channelling of the particles toward the front wall. The particles are also evacuated through the exit of the furnace without much recirculation. The other two mechanisms produce a swirling core of particles that eventually burn out after recirculated in the furnace for some time. It should be noted that the reason the char mass fraction increases after it leaves the PA pipe and enters the furnace region, is that the particle undergoes a drying and devolatilisation process. Both of which imply a mass loss for the particle. Because the CFD code assumes that dry-out, devolatilisation and char combustion are sequential for a given particle, the char mass fraction must increase as the particle mass decreases and the commencement of char combustion has not occurred.

The distribution of the particles is further described in Figure 5-36. In this figure the particle concentration scalar is plotted on the two orthogonal planes through the centreline of the furnace.

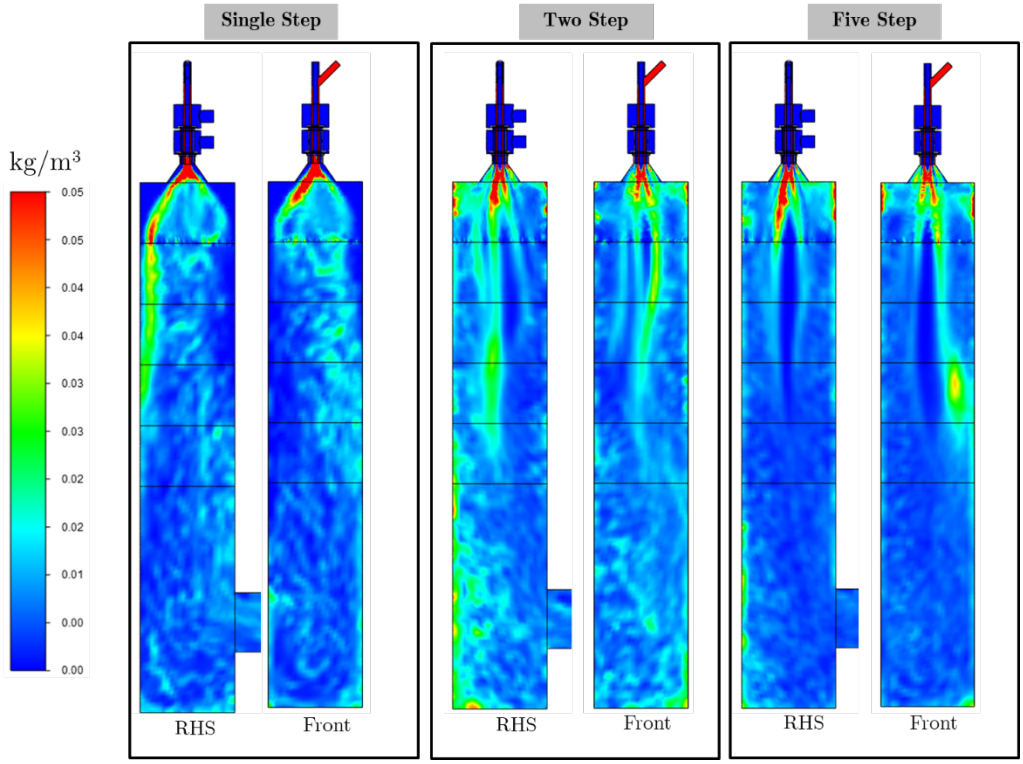

Figure 5-36: Particle Concentration for Three Different Gas Phase Mechanisms

As expected, there is a high concentration of particles at the exit of the PA tube. The particles rapidly disperse as they begin to react. The channelling of the particles in the single-step mechanism is again evident. The two-step and five-step mechanisms indicate that there is significant entrainment of the particles in the swirling flow, however the former also shows a higher concentration of particles at the bottom of the furnace. The particle concentration is somewhat analogous to locations of peak heat release in the furnace as this is where the combustion is occurring.

The distribution of gaseous volatile matter in the furnace is shown in Figure 5-37. All three simulations use the same volatile release kinetics that was developed in section 5.2.4.

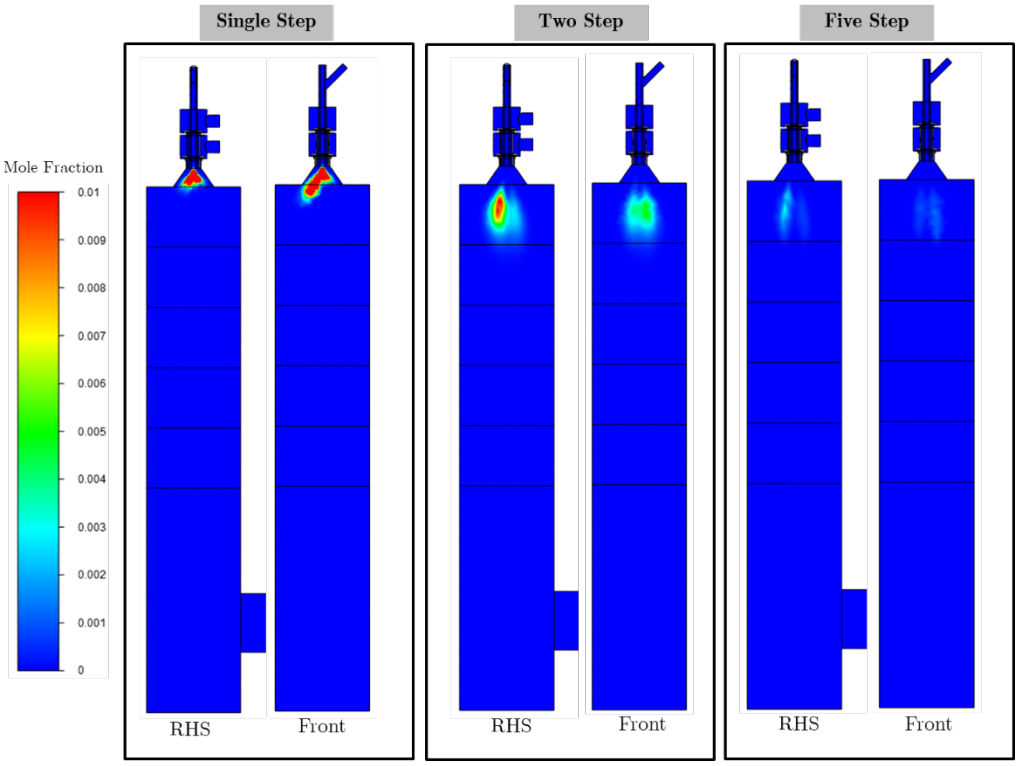

Figure 5-37: Volatile Species Distribution for Three Different Gas Phase Mechanisms

Hence the chemical rate of release of the pseudo-volatile species is the same. However, the distribution of the initial volatiles differs for the different techniques applied. The single-step mechanism again produces a result that lacks credibility. However, the other two techniques show the typical stand-off from the burner mouth associated with South African coals. The release of the volatile matter has a direct influence on the ignition of the coal particles, as explained in section 2.3.1. The release of the volatile matter is a precursor to the major heat release from the combustion of the coal i.e., the char combustion stage. The single-step mechanism is aggressive in its ignition characteristics as the volatile matter burns instantaneously to form the final combustion products. The two-step mechanism shows that the ignition point is shifted lower down the furnace when the intermediate conversion of volatiles to carbon monoxide is considered. The effects of local aerodynamics and heat transfer also play a greater role in the oxidation of the carbon monoxide to carbon dioxide.

The five-step mechanism has a higher degree of complexity since the volatiles are modelled in such a way that they first break down into the light hydrocarbon species (gases) and heavy hydrocarbon species (tars). This is explained in detail in section 5.3.3. It is important to note that light hydrocarbons react at a faster rate than the heavy hydrocarbons and this physical feature is modelled by using the appropriate Arrhenius parameters for the respective reactions. The distribution of the initial volatile species, the light hydrocarbons and heavy hydrocarbons is shown in Figure 5-38.

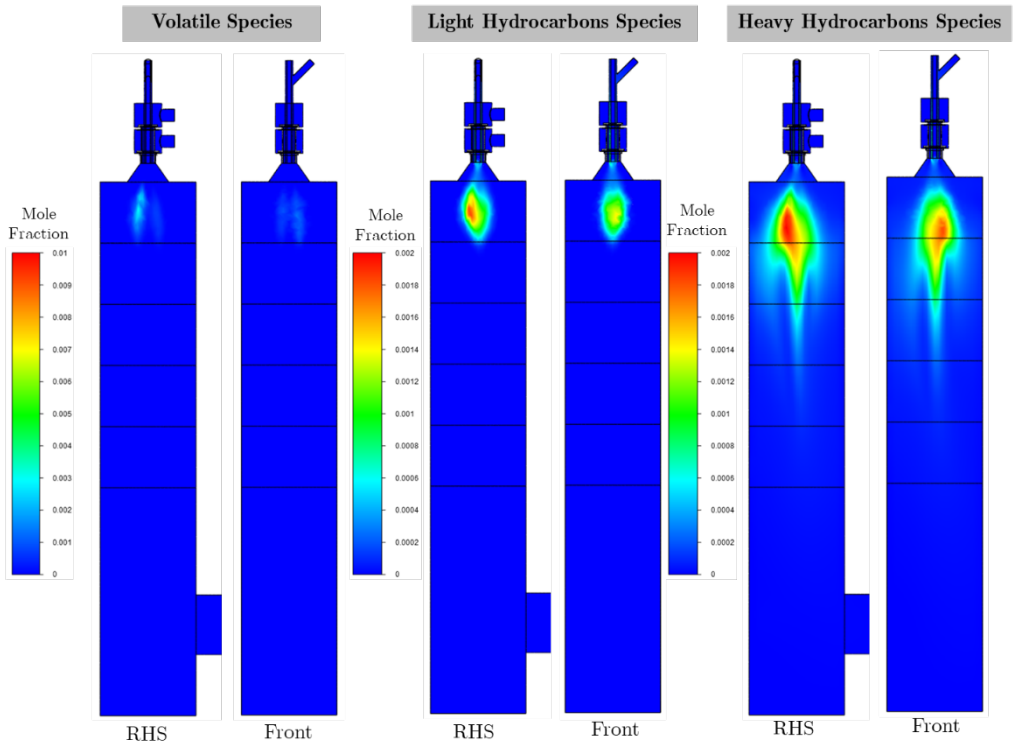

Figure 5-38: Distribution of Initial Volatiles, Light Hydrocarbons and Heavy Hydrocarbons for the Five-Step Gas Phase Combustion Mechanism

The initial volatile species is modelled to decompose into the light and heavy hydrocarbons quickly. As such it does not have a long residence time. The heavy hydrocarbons react at the slowest rate and hence have the longest residence time and consequently have a greater opportunity to be influenced by local heat transfer and aerodynamics inside of the furnace. These features were predicted because this approach used the eddy dissipation concept that included the effect of chemical kinetics on the overall reaction rates.

Since one of the main purposes of the pilot scale combustion test facility (see section 5.4.2) is to correlate burn out times measured during the drop furnace testing. The objective is to demonstrate that the burnout times are consistent both at the lab and pilot scales and then may be extrapolated to full scale furnaces. The industrial need for this is to ensure that burn-out time for a given coal matches the full-scale boiler that it will be burnt in. If, for instance, the burn-out time for the coal is too long for the furnace being considered, firing it would result in delayed combustion in the upper reaches of the furnaces and increase the temperatures at the heat exchangers. Provided it is within the capability of the mitigation systems, significant spray cooling water may be required to protect the reheaters and superheaters. If the power plant is pushed into this scenario, the long-term viability could be compromised due to material degradation of the heat exchangers due to thermal fatigue and there will be large efficiency losses due to bypassing water to the spray cooling systems and, potentially damaging the turbines if the steam is not completely dry at the intake. The solution is to source a more appropriate coal, which in most cases is economically unfeasible or rather implement design changes to boiler e.g., the increasing of the height of the Lethabo boilers as described in section 2.5.

The burnout characterisation for the three cases was accomplished by analysing the individual particle trajectories and interrogating the reduction of the char mass fraction as the particle burns. The dataset was, as expected, very large due to large number of particles analysed. An algorithm was developed to analyse the particle tracks and determine the average burn out time. The combustibles within particle were completely consumed when the particle mass fraction reaches zero. This analysis was extended to all the size fractions simulated. The results are listed in Table 5-18.

Table 5-18: Particle Burnout for Three Different Gas Phase Combustion Mechanisms

Mechanism	38μm		75μm		106μm		150μm	
	1.3 s [%]	2 s [%]	1.3 s [%]	2 s [%]	1.3 s [%]	2 s [%]	1.3 s [%]	2 s [%]
Single-Step	13	4	43	23	60	46	84	63
Two-Step	0	0	16	0	69	29	100	96
Five-Step	2	0	33	13	58	32	100	82

The values in the table represent the percentage of particles that still had some amount of unburnt char after 1.3 seconds and 2 seconds of residence time in the furnace. This must be interpreted in context of the mass loading of each size fraction described in Table 5-16. Hence it represents the percentage of particles of the specific size range that has not completely burnt out. The value of 1.3 seconds corresponds to the predicted burnout time calculated in section 5.2.5. The burnout value at two seconds was included to observe whether there were large changes in burnout further on in the particle trajectory.

The single-step results are compromised due to adverse flow field that was described previously. However, all three mechanisms demonstrate the trend that the smaller particles burn out to a greater extent. This is an intuitive result as a larger particle would contain more char and hence take longer to burn out. The 38μm particles are almost completely consumed when the two-step and five-step mechanisms are employed. It should be noted that the drop tube furnace tests that provide the char combustion results and the subsequent basis of the numerical prediction (the numerical prediction used a mean value of 47μm), are done using a size fraction with a mean of 38μm and second test with a mean size fraction in the range of 38μm to 75μm. Hence there two experimental sets of char combustion kinetic data available for the two size ranges. Since most of the particles fired in the PSCTF were in the 38μm and less range (see Table 5-16), the former set of kinetics was employed.

Hence the poor burnout of the larger particles may be justified by recognising that the char kinetics may not be best suited to that size fraction. This is a limitation of the current modelling technique. However, when a pragmatic approach is taken, the poor burnout is more likely due to size of the particles because the char kinetics is intrinsically linked to

composition of the coal. This result also suggests that most of the unburnt carbon exiting the furnace, would be due to the larger size fractions. This may play a role in how the ash particles are formed and hence change the characteristics of the fly ash.

From a numerical perspective, the model for char combustion developed at the laboratory scale (DTF) was shown to be consistent with the char combustion characteristics within the PSCTF i.e., the 38μm particles did indeed burnout in 1.3 seconds or less. This is an important result as it shows the modelling technique is valid at both the laboratory and pilot scales. The latter has significantly more complex flow structures due to the swirling turbulent flow emanating from the burner.

5.4.5 Discussion of PSCTF Results

The simulations of the PSCTF provided insight into the characteristics of the flow field in terms of the temperature distribution, and particularly the distribution of the volatile species.

The temperature profiles as well as the flame shape predicted by the three gas phase combustion mechanisms were starkly varied. These differences were rationalised to be due to the modelling assumptions and its effect on localised heat releases. The impact of aerodynamics was also considered a factor, particularly with the single and two-step mechanism which employed the eddy dissipation turbulent combustion model i.e., the combustion rates are limited by the turbulence levels. In contrast, the five-step mechanism employed the eddy dissipation concept and hence the effect of chemical kinetics was also considered. This would have played a role in the distribution of combustible species within the furnace and consequently the temperature profiles.

The most advanced technique, the five-step combustion mechanism justified its complexity and additional computational overhead, by providing the best correlation with the measured temperatures. It also produced burnout results that were intuitive. In this regard, the overall modelling strategy showed consistency in that the burnout times predicted in the DTF simulations were consistent in the more complex flow structures of the PSCTF. The single-step result produced an adverse flow field characterised by a severe flaring of the flow field coincident with the burner quarl. Hence the credibility of the results from this mechanism are in question and as a result it is not recommended for use in this scenario. The two-step

mechanism produced qualitatively similar results to the five-step mechanism but the prediction of the temperatures in the furnace compared to the latter was inferior.

The findings speak directly to hypothesis of this research work and specifically to research questions 1 and 3. It may be concluded that the choice of gas phase combustion mechanism does have distinct role in the prediction of the characteristics of the pulverised coal flame at the pilot scale. Furthermore, techniques employed to predict the burnout times were translatable between the laboratory and pilot scales.

5.5 Full Scale Simulation of a 200 MWe Pulverised Coal Fired Boiler

5.5.1 Background

A 200 MWe pulverised coal boiler that uses the reference coal as its fuel, was selected for the basis of the full-scale study. The boiler is a Babcock El-Paso design and does not employ reheat and rather relies on two stages of super heating to supply the require steam flow to the turbogenerator set. The boiler does have recuperative heat exchangers in the form of two banks of economiser tubes in the back pass of the boiler. The power station was commissioned in the 1970's and operated into the late 1980's when it was mothballed and put into cold reserve. This was due to an oversupply of power production at the time. South Africa underwent significant political and economic change between the 1980's and 2010's as this is well known and documented. The resultant impact on Eskom, was that it was required to return to service (RTS) several of the previously mothballed power stations. However, the original axial swirl jet burner designs were beyond repair. Due to dearth of the original burners, Eskom engaged with the boiler OEM to install the latest generation of low NOx axial swirl burners on the relevant units. The original burners would not meet the required emissions requirements in terms of NOx attenuation in any event. This provided significant challenges in interfacing the older existing technology and the newer one. The basis of the boiler model used for this study will be with the current operating and process conditions i.e., with the low NOx burners installed.

5.5.2 Modelling Objectives

The CFD model of the 200MWe boiler was developed to be fit for purpose and be able to produce the required data to support the comparison with measured data and provide key insight into the dynamics of combustion within the furnace. Explicitly put, the requirements were:

1. The model should capture the main dimensions of the furnace.
2. The model should be able to test various chemistry schemes for gas phase combustion.
3. The model should capture the important flow structures that influence ignition and burnout.

4. The model should have sufficient mesh resolution to ensure accurate results.

5. Conversely, the model should have a sufficiently economical mesh to ensure reasonable run times on the available high performance computing platforms.

5.5.3 Modelling Requirements

A complete boiler model requires the integration of several modelling techniques and sub-models to address a broad range of physics and chemistry. Each of thematic areas shown in Figure 5-39 were addressed when developing the comprehensive boiler model.

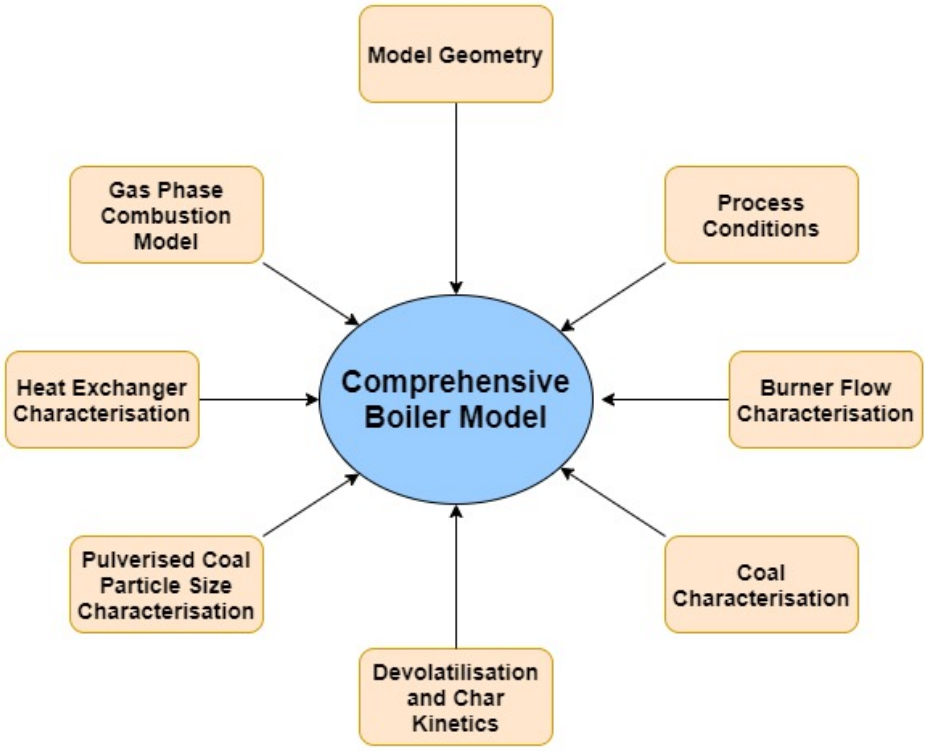

Figure 5-39: Required Focus Areas to Develop a Comprehensive PF Boiler Model

The explanation of these focus areas are as follows:

- **Model geometry** – a three-dimensional model of the boiler was created in CAD and transferred to the ANSYS Workbench ® environment. The source information comes from the general layout schematic of the plant. Bearing in mind that this plant was first commissioned in the 1970's, the drawings were typically old and of a poor quality. Hence it was necessary to confirm the key dimensions by an onsite

inspection. The areas of importance to the current study were the burner wind box and the layout and orientation of the low NOx burners.

- **Process conditions** – since this study is primarily focused on the gas side of the boiler, the most important parameters are the air and fuel flows. Some steam data was required to determine the heat rejection in the heat exchangers. Once again there was a challenge to ratify the older data in the original boiler C-schedule [63] with the more recent test conditions, post low NOx burner implementation.

- **Burner flow characterisation** – the design of the low NOx burner installed on the plant is such that it is not possible to determine flow details within the burner that are necessary be used to calculate the simplified boundary conditions applied to the boiler model. Hence it was necessary to develop a detailed model of the low NOx burners to determine the necessary flow rates to implemented in the full-scale model.

- **Coal characterisation** – the CFD model of pulverised coal combustion with the boiler requires the proximate and ultimate analyses of the coal. This data was taken from the work done in section 5.2.

- **Devolatilisation and Char Combustion Kinetics** – this data was also taken from the work done in section 5.2.

- **Pulverised coal particle size distribution** – the range of particle sizes produced by the PF mills varies significantly. It was necessary to determine from the particle size analyses on the resultant PF, suitable parameters that was conducive to input to the CFD code. This was obtained from data provided by Eskom Research [64]

- **Heat exchanger characterisation** – The furnace region was the area of interest for this study. However, it was still necessary to develop an uncoupled model of the various heat exchangers to ensure realistic attenuation of the fire ball within the furnace.

- **Gas phase combustion model** – three gas phase combustion models were developed to determine whether it has a role in determining the intrinsic characteristic of the pulverised fuel flame. This follows on from the work developed in section 5.3

5.5.4 Pulverised Coal Fired Boiler Geometry

The overall geometry developed for the simulation is shown in Figure 5-40.

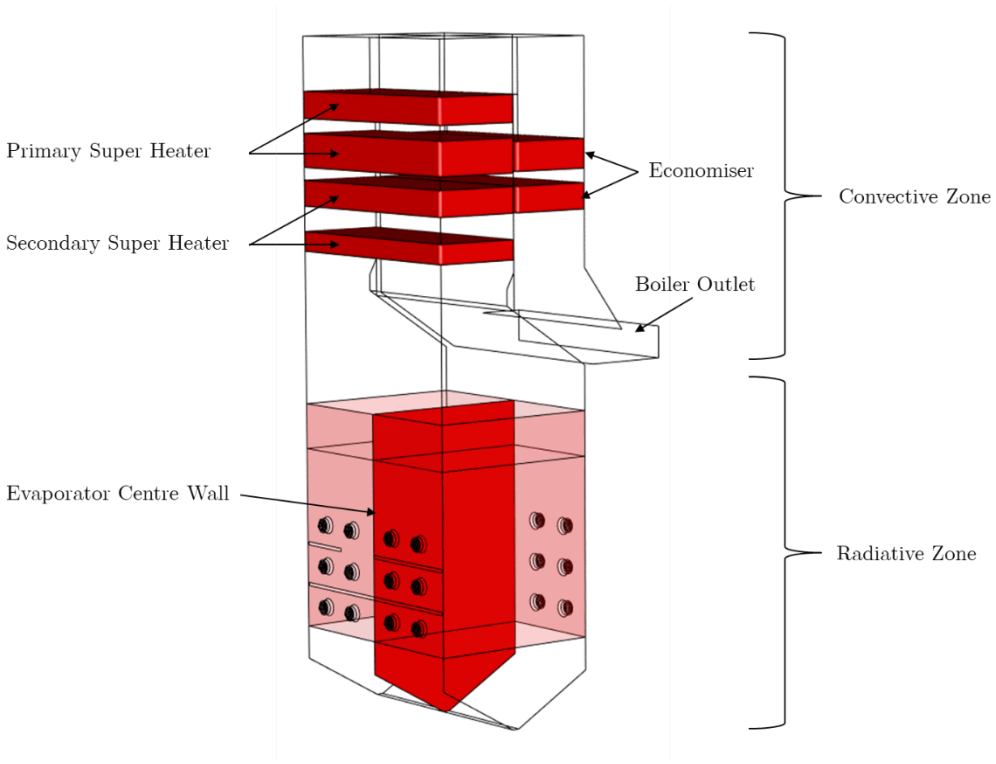

Figure 5-40: Boiler CFD Model Layout

The boiler is 200 MWe unit that operates in the sub-critical water/steam regime. The total height of the boiler is 49.00m. The furnace cross section at the burner belt line is 11m by 11m. The geometry is consistent with the boiler layout drawings [63] and onsite visual confirmations. The CFD model uses a simplified representation of the two stages of superheat and two stages of recuperative heat exchange through the economiser banks. As mentioned previously, there is no re-heat installed on this plant. The furnace area is split by a dividing wall that forms part of the evaporative heat exchanger. This spilt is also carried through the wind box feeding the burners with combustion air. There are six opposed burner rows on the front and back walls of the boiler. Each row comprises of four low NOx burners and each row is supplied with pulverised coal from a single mill. The mill has a static particle classifier and feeds four outlet pipes. There are six mills into total, but only five burner rows and five mills are required to achieve the maximum continuous rating. The burner orientation, naming

and swirl direction is shown in Figure 5-41 and Figure 5-42. Note the opposing swirl of adjacent burners.

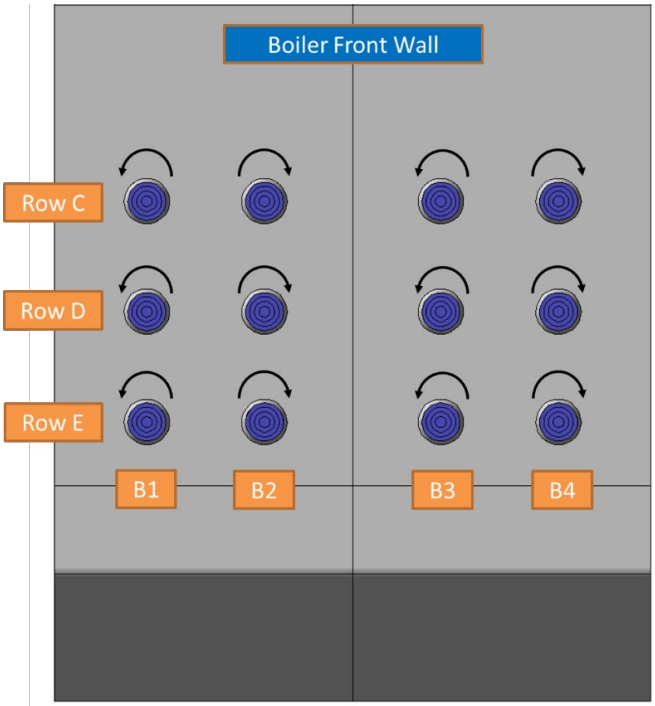

Figure 5-41: Front Wall Burner Details

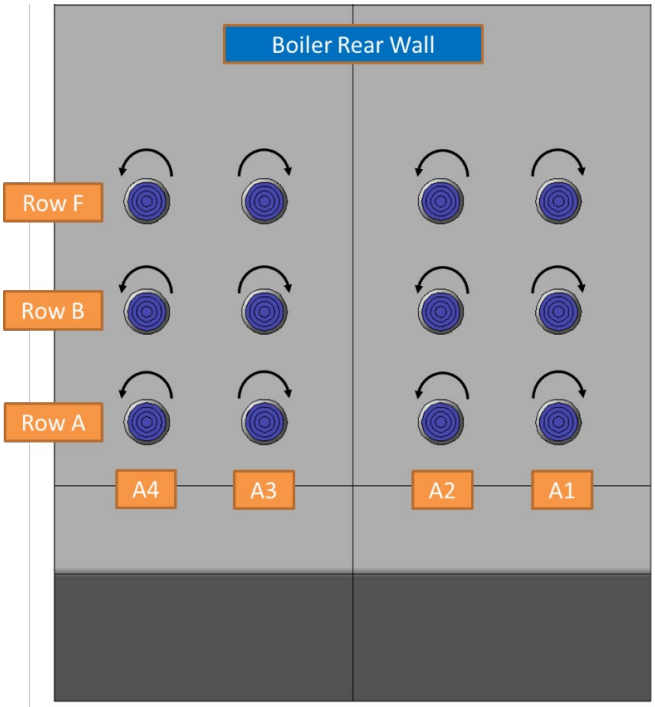

Figure 5-42: Rear Wall Burner Details

It is crucial that the burner swirl was implemented correctly, and this was verified per burner. An example of this is shown in Figure 5-43. The method of how the individual burner swirl angles were determined is described in section 5.5.6.

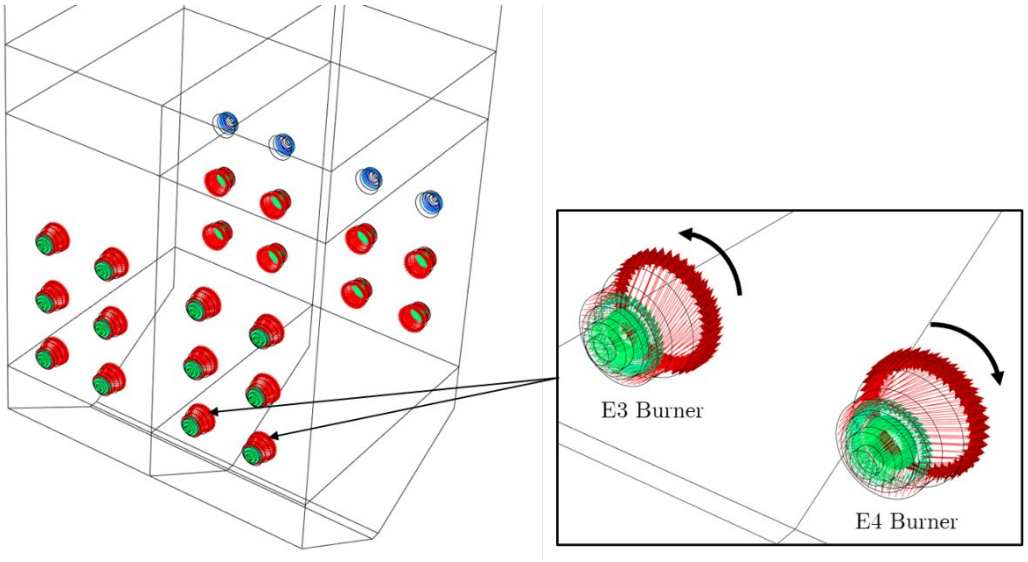

Figure 5-43: Burner Swirl Implementation

The model was developed in SolidWorks® and then transferred to the ANSYS Workbench ® environment. Extensive use of geometric decomposition was employed to enable the computational mesh to be generated in an automated fashion. This was also done to ensure that the resultant mesh was of a high-quality from a numerical perspective i.e., minimize cell skewness and aspect ratio. This decomposition, which mimics a block meshing technique, is shown in Figure 5-44.

The resultant mesh is shown in Figure 5-45. The mesh is largely structured, and this will contribute positively towards simulation stability and ease of numerical convergence. The model also makes use of mesh interfaces between the burner belt region and the convective and hopper regions, respectively. This was done to ensure that majority of the computational cells were concentrated in the burner belt region, to ensure there is sufficient mesh resolution where the largest temperature and velocity gradients exist.

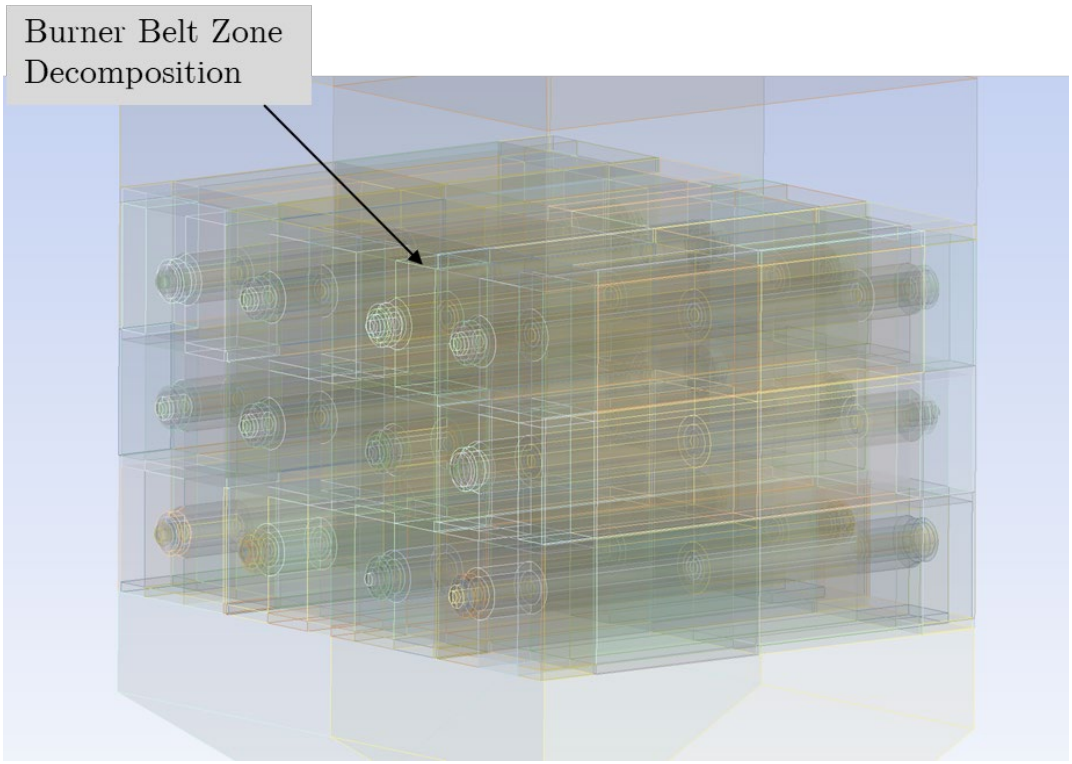

Figure 5-44: Boiler CFD Model Volume Decomposition

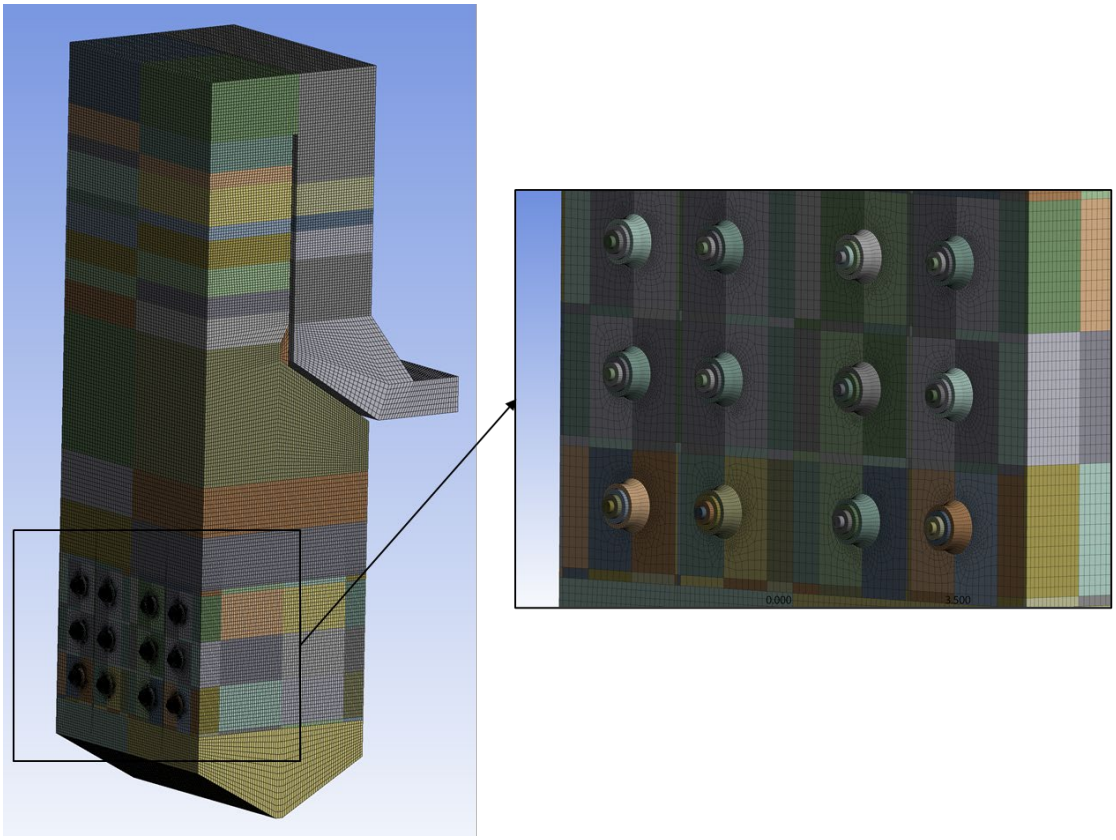

Figure 5-45: Boiler CFD Model Computational Mesh

The summarised sub model settings for the boiler simulation are listed in Table 5-19.

Table 5-19: Sub-model Specification for Full Boiler Model

Sub - Model	Details
Solver	Steady State, Pressure based solver. SIMPLE pressure-velocity coupling using standard pressure discretisation. Second order discretisation was used for all transport equations. Operating pressure set to highveld conditions i.e., 85 kPa ambient pressure.
Turbulence	Realizable k-ε with enhanced wall functions.
Radiation	Discrete Ordinates with standard discretisation, with WSGGM for participating gases.
Discrete phase	Reacting solid fuel particles with coupled particle/fluid/wall radiation. Discrete particle size distribution applied. Discrete random walk model for turbulent dispersion.
Devolatilisation	Single step model as per settings defined in section 5.2.4
Char Combustion	Single step model (Baum and Street) as per settings defined in section 5.2.5

The particle size distribution exiting the mills was determined by on-site testing. The mass flow distribution amongst the different size fractions is listed in Table 5-20. The values stated for each firing burner.

Table 5-20: Particle Size Distribution Per Burner

Particle Size [mm]	Mass Flow [kg/s]	% of Total
75	0.9579	67
106	0.2140	15
150	0.1892	13
300	0.0760	5

The walls of the evaporator were modelled with a constant temperature that is set to that of the inlet to drum. This is a reasonable approximately to simulate the high heat transfer

(boiling) conditions that exist on the steam side of the evaporator. The emissivity of the furnace walls was set to 0.7 as this was consistent with a well fouled boiler internal surface.

5.5.5 Process Conditions

The process conditions refer to the thermodynamic state at the load condition being considered. For the water-steam side of the plant, it is necessary to determine the pressure and temperatures of the working fluid entering and leaving the various heat exchangers to determine how much energy it is extracting from the flue gas side. These variables should also be known to determine the state of the steam (as well as the mass flow) entering the turbine to ensure that there is enough drive to the turbogenerator set to in turn deliver the rated power.

The current study was primarily focused on the phenomena occurring in the furnace on the gas side. Hence the parameters of interest are the mass flow rate of air and pulverised coal being introduced to the combustion zone.

The process conditions were extracted from the C-Schedule [63] and other supporting documentation [65] of the boiler plant as defined by the boiler OEM and refined after final commissioning.

The partition of the combustion air into secondary and tertiary annuli of the individual burners is not explicitly given in the plant documentation. Additional analysis was required to determine the values, and this is described in detail in section 5.5.6. The output of this analysis is pre-emptively listed in Table 5-22, where the overall process conditions are reduced to apply to each burner.

Table 5-21: 200MWe Boiler Process Conditions

Parameter	Value
Boiler Load MCR [%]	100.00
PF Mass Flow [kg/s]	28.74
Firing Capacity [MW_{th}]	600.64
Total Combustion Air [kg/s]	230.30
Air Coefficient at Furnace Exit	1.10
Number of Mills in Operation	5.00
Number of Burners in Operation	20.00
Burner Capacity [MW_{th}]	30.03
Total Primary Air Flow [kg/s]	49.60
Total Secondary, Tertiary Air Flow [kg/s]	175.30
Total Cooling Air Flow of Burners out of Operation [kg/s]	5.40
Total Core Air [kg/s]	0.20
Total Secondary Air [kg/s] and Tertiary Air[kg/s]	175.30
Total Secondary Air [kg/s]	36.52
Total Tertiary Air [kg/s]	138.78

The process conditions on a per burner basis is listed in Table 5-22.

Table 5-22: Process Conditions for each Burner

Parameter	Value
SA and TA Mass Flow Combined [kg/s]	8.77
Burner PF Mass Flow [kg/s]	1.44
Burner CA Flow [kg/s]	0.01
Burner PA Flow [kg/s]	2.48
Burner TA/SA Split Ratio	3.80
Burner SA Flow [kg/s]	1.83
Burner TA Flow [kg/s]	6.94
Cooling Air Flow per out of service burner [kg/s]	1.35
CA Out of Service [kg/s]	0.00
PA Out of Service [kg/s]	0.00
SA Out of Service [kg/s]	0.28
TA Out of Service [kg/s]	1.07

5.5.6 Burner Flow Characterisation

The low NOx burner installed on the boiler is designed to provide carefully staged tertiary air to supply air after the NOx reduction zone, to complete the combustion of the coal particles. Hence the burner relies on a complex arrangement of flow throttling sleeves and swirlers to achieve the required flow field. Since the burners are arranged in the wind box in pairs and they are supplied air by a common duct, it is not possible to know the split between the secondary and tertiary air without CFD modelling or experimental flow characterisations. The former approach was used in this study [66]. Hence a detailed model of a burner pair including the wind box section was created and run at the same process conditions seen on the boiler. This allowed the determination of the flow split between the tertiary and secondary air. The flow emanating from the burners is shown in Figure 5-46. The data is presented on a

horizontal slice through the midpoint of the burners. The model was simulated in Star CCM+ ® v13.

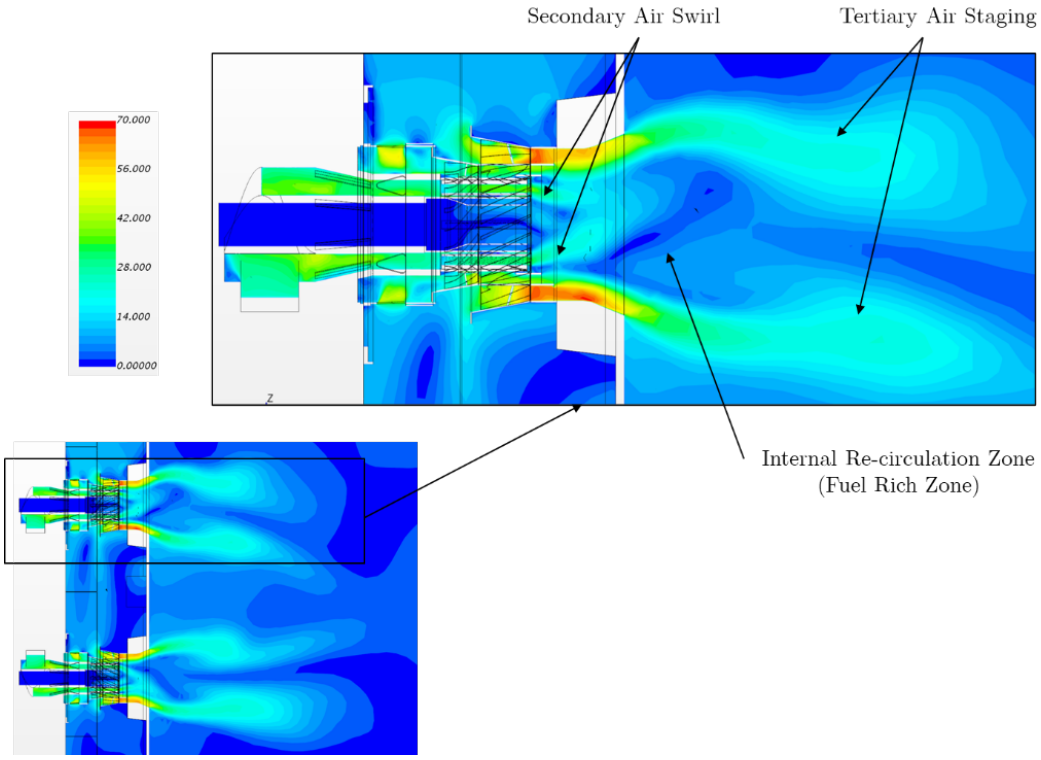

Figure 5-46: Velocity Magnitude Contours for Detailed Burner Model

The tertiary and secondary air split is summarized in Figure 5-47.

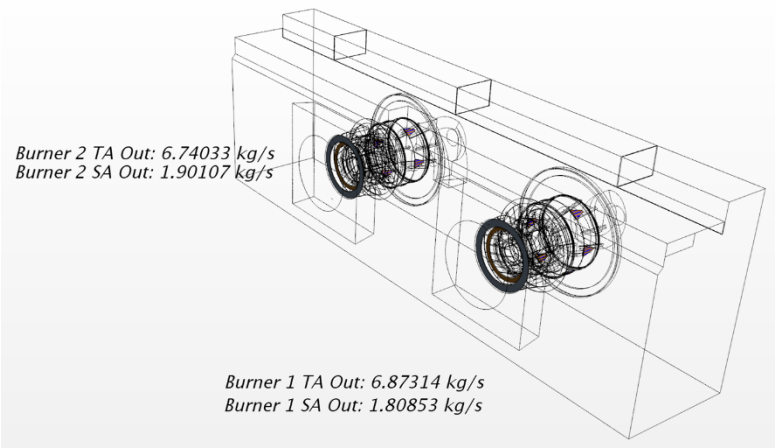

Figure 5-47: Tertiary and Secondary Air Split

From the simulation results the average TA/SA split ratio was determined to be 3.8. The model was also used to extract the SA and TA flow vectors at the exit of the respective

swirler sections. These values were required to implement a swirling condition on the simplified burner implemented on the boiler model. The reason the model was simplified is that the additional complexity of the detailed burner would require significantly more mesh cells and hence render the model difficult to work with and increase simulation times substantially.

The simplified burner layout is shown in Figure 5-48.

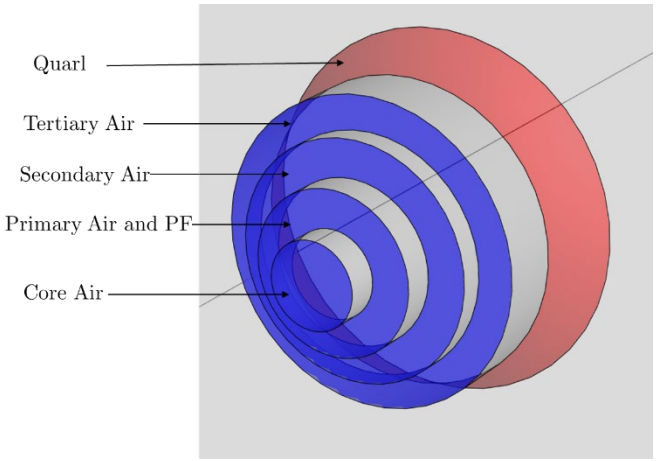

Figure 5-48: Simplified Burner Layout

The various flows were implemented on discrete surfaces where the mass flow was specified along with the appropriate flow vectors to induce a swirling motion. Over 2000 data points (this is related to the fine mesh used) were extracted from each SA and TA surface on the either burner, from the detailed model. Hence, it was deemed that the average value of the angle obtained in each case would be representative of the overall flow. Rudimentary vector algebra was required to compute the swirl angles from the extracted velocity vectors:

$$\alpha = arccos[(\boldsymbol{a} \cdot \boldsymbol{b})/(|\boldsymbol{a}| \times |\boldsymbol{b}|)] \qquad 5.28$$

Where:

- α - Swirl angle (Radians)
- **a** – Velocity vector at SA or TA surface [m/s]
- **b** – Unit vector in burner axial direction [ ]

The final swirl angles that were extracted from the detailed burner model is listed in Table 5-23. The swirl angles out of the secondary and tertiary swirlers of the detailed model are visualised using streamlines and this is shown in Figure 5-49. These values were applied to the simplified burners in the boiler model as part of the boundary condition specification and they are visually confirmed in Figure 5-49. In this figure, streamlines emanating from the SA and TA swirlers were visualised to show the difference in swirl angles.

Table 5-23: Burner Inlets Swirl Angles

Inlet Type	Swirl Angle [Deg]
Primary Air	0
Secondary Air	38.44
Tertiary Air	28.34

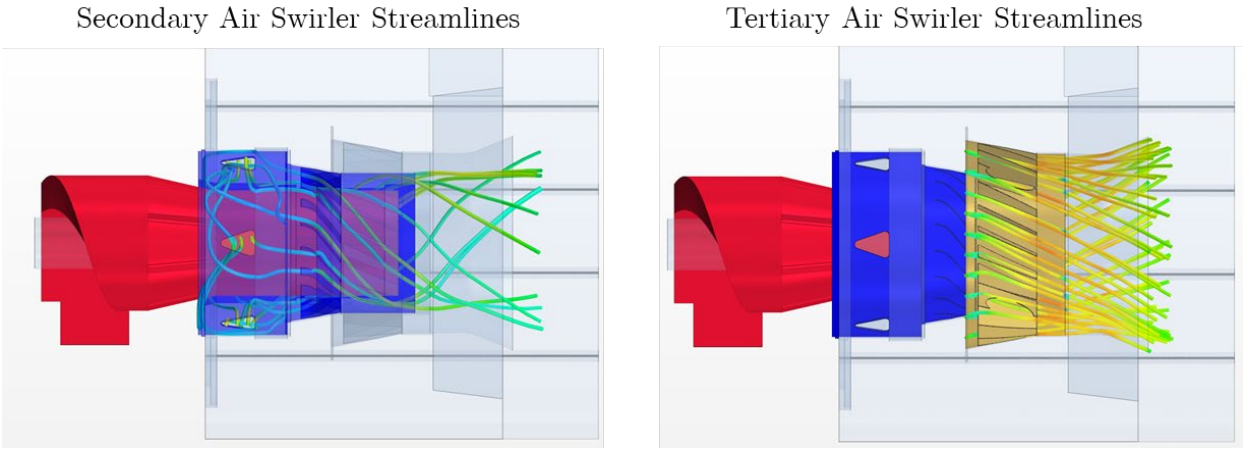

Figure 5-49: Secondary and Tertiary Swirl Visualised with Streamlines

It would be logical to consider whether the simplified burner re-creates the flow field produced by the detailed model. Hence the results were compared on a qualitative and quantitative basis. A comparison between the velocity profiles in the detailed and simplified burner models is shown in Figure 5-50. In both cases the flow field was simulation under "cold" conditions, i.e., with no combustion reactions included. The flows were introduced at their pre-heated temperatures. Burner 1 was used as the basis of comparison for the current sub-study,

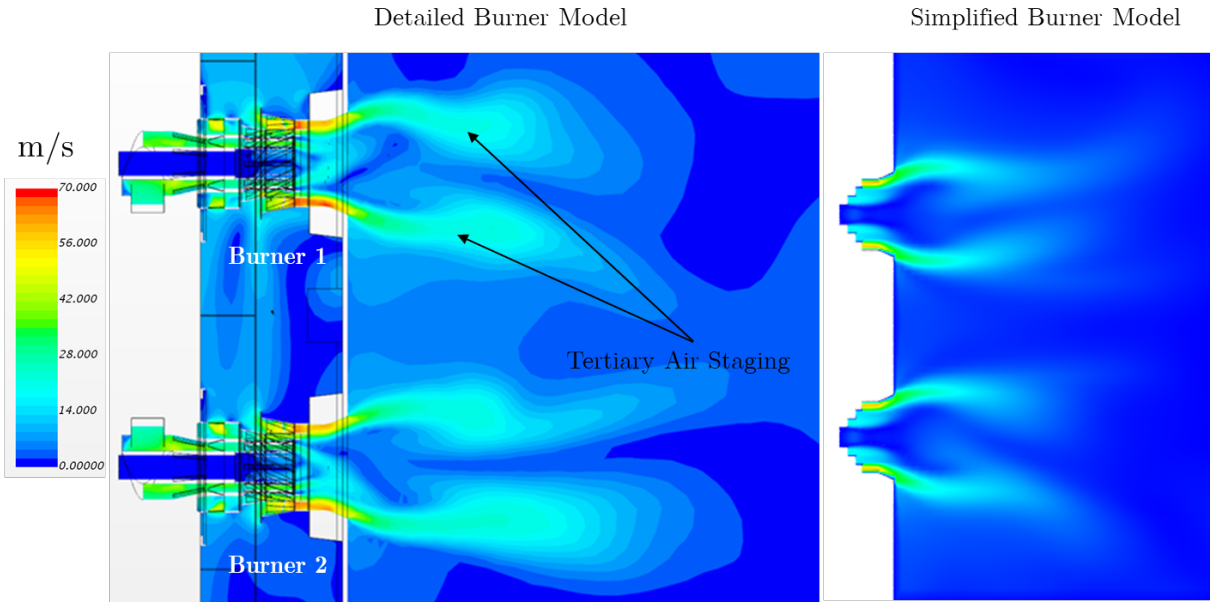

Figure 5-50: Comparison of Burner Flow Fields between Detailed and Simplified Models

The velocity contours shown in Figure 5-50 confirm that the simplified burner does indeed reproduce the overall flow field as with the detailed model. The major flow structures appear to be reproduced as well as the magnitudes of the velocities in that air staging region.

A quantitative assessment was also carried out on the models by extracting the velocity magnitude and turbulent kinetic energy values at various points in the flow field. The areas of interest were the burner centreline, and radial locations at the burner mouth and 0.5m and 1m from the exit of the burner. The data extraction points are shown in Figure 5-51.

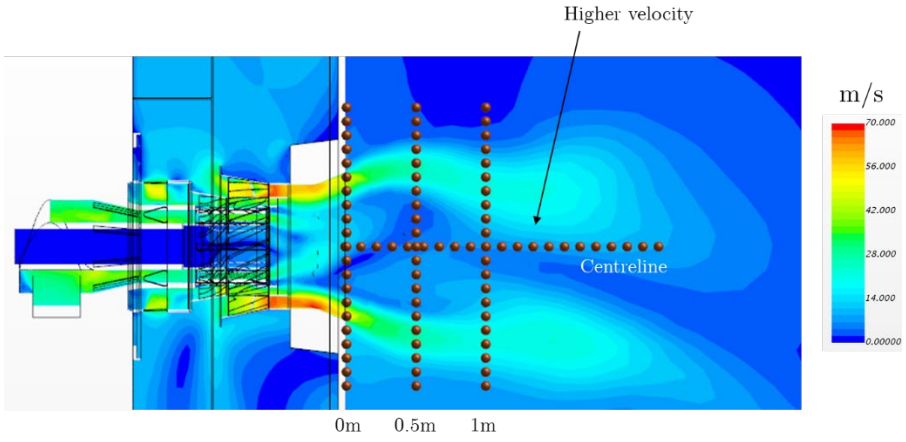

Figure 5-51: Data Extraction Location in the Burner Flow Field

A comparison of the velocity magnitude on the centreline of the detailed and simplified burner models is shown in Figure 5-52(a). The results show that the predicted velocity magnitudes compare well up approximately 1m from the burner mouth. The detailed model then predicts a higher velocity. This may be explained by considering that the staged velocity plume in the detail model "curls" back towards the centreline more substantially than the simplified model. This effect is shown in Figure 5-51.

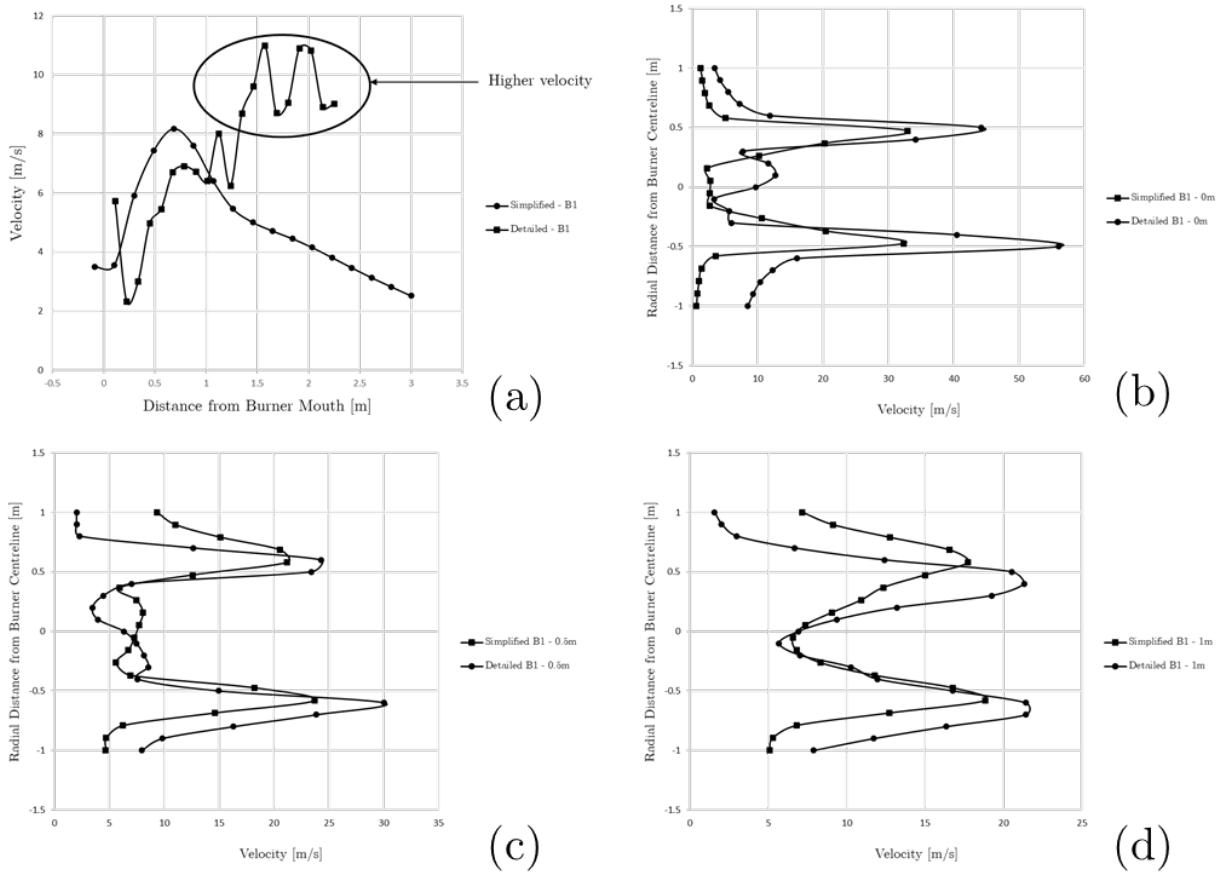

Figure 5-52: Comparison of Velocity Profiles for Detailed and Simplified Models. (a) Centreline Velocity, (b) Radial Velocity at 0m (c) Radial Velocity at 0.5m (d) Radial Velocity at 1m

The radial velocity distribution in the two models was also compared. Specifically, the velocity magnitude at several radial locations were extracted from the CFD models. These locations were: at the burner mouth (0 m), 0.5 m further downstream and finally a 1 m distance from the burner mouth. These results are shown in Figure 5-52 (b) to (d).

The velocity profiles are similar in trend and magnitude for both the detailed and simplified model. The standard deviation of the difference in point velocities between the models reduces from 10.48m/s at the burner mouth to 4.51m/s 1m metre downstream.

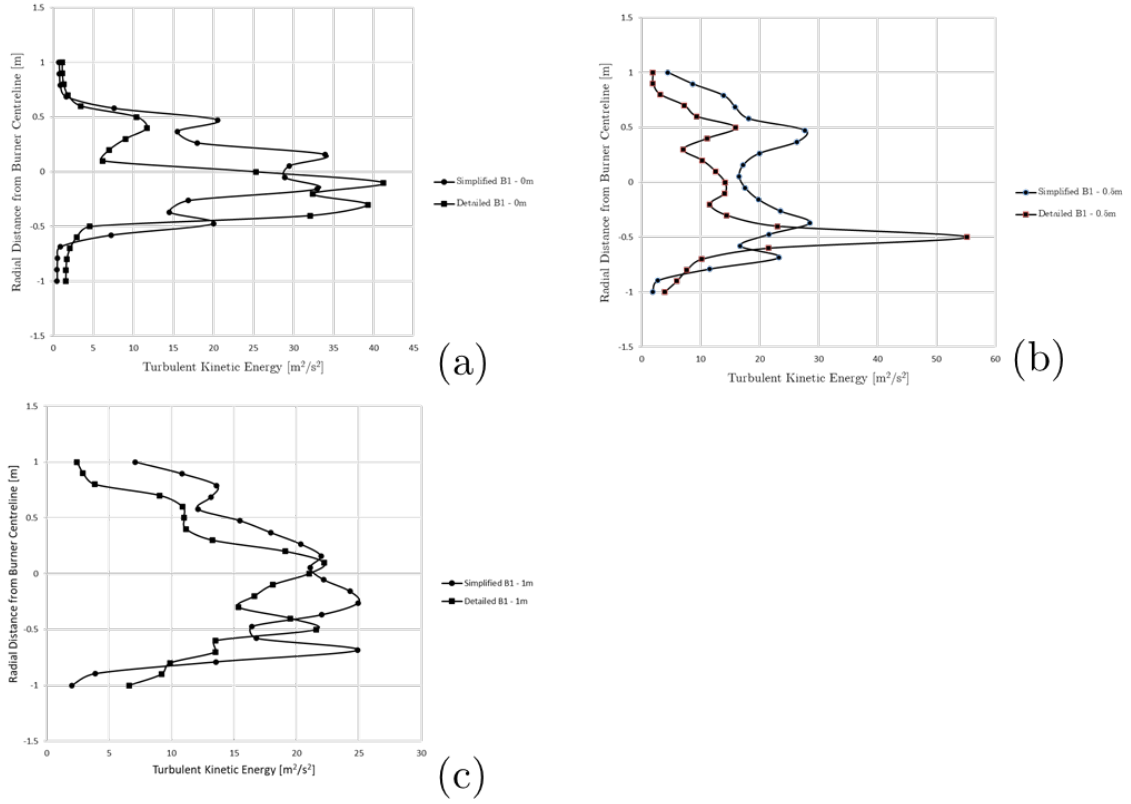

Figure 5-53: Comparison of Turbulent Kinetic Energy Profiles for Detailed and Simplified Models. (a) TKE at 0 m, (b) TKE at 0.5 m (c) TKE at 1 m

The turbulent kinetic energy profiles at the radial stations are shown in Figure 5-53. As with the velocity profiles the profiles follow a similar trend for both the detailed and simplified burner models. The turbulence kinetic energy is related to the mean velocity and as such it also exhibits a similar reduction in the standard deviation of the difference in predicted values between the two models. These results also indicate that similar levels of turbulence are sustained at a distance from the burner mouth. The variations are caused by deviations in modelled geometry as well as inherent fluctuations to be expected in a turbulent, swirling flow. Hence the sub-study demonstrates that the simplified burner replicates the flow field of the detailed burner to a sufficient degree.

5.5.7 Boiler Heat Exchanger Characterisation

An important facet in developing a comprehensive boiler model is the treatment of the various heat exchangers. The 200MWe boiler of interest to this study has two stages of superheating and two stages of economisation. The heat exchangers are arrangements of metal alloy tubes of significant wall thickness as they must sustain large, cyclic temperature variations and operate under high pressures. The production of steam and the associated boiling processes is beyond the scope of the current research. However, the heat exchangers pose a flow resistance to the flue gas as it passes through the convective sections and this back pressure will influence the flame dynamics within the furnace that would manifest in an attenuation of the fireball. Furthermore, the heat exchangers should reject heat from the flue gas, and this will result in large temperature gradients that would reduce the density of the flue gas and subsequently the velocity passing through the back pass. Hence it was necessary to develop a modelling strategy to account for these physical processes.

The heat exchangers in the boiler are comprised of multiple tube banks arranged in an in-line orientation. The key parameters that are required to model the pressure drop across the tube bundles are the outer diameter of the tube as well as the parallel and cross pitch relative to the flow. There are several techniques that could be used to develop an expression for the pressure loss in the tube bundles. These include physical experiments simulating different flow conditions; or conducting numerical experiments using CFD to obtain the necessary data. Both are time consuming and could be expensive if no pre-existing facilities are available. The numerical techniques would require substantial sensitivity studies and meshes with large number of cells to properly resolve the flow between the tube bundles. Another option is to use well accepted correlation-based methods to model the pressure drop. The latter strategy was employed in this study and the method was derived from the correlation developed by the VDI [67] and described in the published “Heat Atlas” reference work. The first step in using this model is to gather the necessary geometrical information for the actual heat exchangers used in the boiler. This information was sourced from the C-Schedule of the 200MWe boiler [63]. This document describes the as-built configuration and provided by the boiler OEM.

The in-line tube bundle is configured as shown in Figure 5-54.

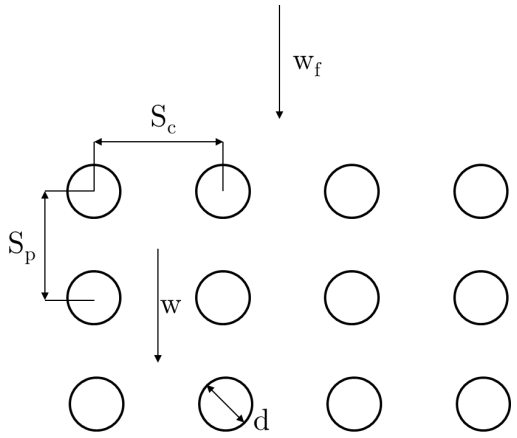

Figure 5-54: Heat Exchanger Tube Bundle Arrangement

The following parameters are described:

- w_f – free stream flow velocity approaching the tube bundle [m/s]
- w – the accelerated flow velocity within the tube bundle [m/s]
- S_c – cross flow tube pitch [m]
- S_p – parallel flow tube pitch [m]
- d – tube outer diameter [m]

The following intermediate variables must be determined to use to correlation:

$$a = \frac{S_c}{d} \tag{5.29}$$

$$b = \frac{S_p}{d} \tag{5.30}$$

$$w = \frac{a}{(a-1)} w_f \tag{5.31}$$

$$Re = \frac{\rho w d}{\mu} \tag{5.32}$$

where:

- ρ – Fluid density [kg/m^3]
- μ – Fluid dynamic viscosity [N.s]

The pressure drop across the tube bundle is given by:

$$\Delta p = \xi N_R \frac{\rho w^2}{2} \tag{5.33}$$

where:

- ξ – Drag coefficient [ ]
- N_R – Number of resistances in the flow direction [ ]

The drag coefficient is given by:

$$\xi = \xi_L + \xi_T \left[1 - exp\left(-\frac{Re + 1000}{2000}\right)\right] \tag{5.34}$$

The laminar portion of the drag coefficient is given by:

$$\xi_L = \frac{f_{a,L,f}}{Re} \tag{5.35}$$

And the laminar factor is given by:

$$f_{a,L,f} = \frac{280\pi(b^{0.5} - 0.6)^2 + 0.75}{(4ab - \pi)a^{1.6}} \tag{5.36}$$

The turbulent portion of the drag coefficient is given by:

$$\xi_T = \frac{f_{a,T,f}}{Re^{0.1(b/a)}} \tag{5.37}$$

And finally, the turbulent drag factor is given by:

$$f_{a,T,f} = \left[0.22 + 1.2\frac{\left(1-\frac{0.94}{b}\right)^{0.6}}{(a-0.85)^{1.3}}\right] 10^{0.47\left(\frac{b}{a}-1.5\right)} \qquad 5.38$$

Application of the equations above results in a pressure loss characteristic of a given tube bundle as a function of the free stream velocity. The curve for the bottom section of the primary superheater is shown in Figure 5-55.

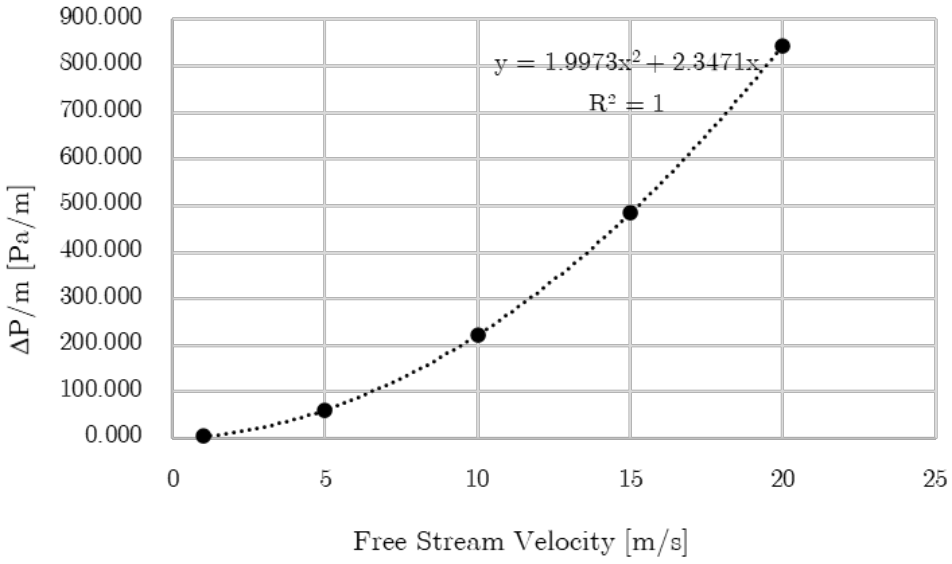

Figure 5-55: Primary Superheater Pressure Loss Characteristic

A 2nd order polynomial curve is easily fitted to the pressure loss characteristic and the quadratic and linear coefficients are used to calculate the porous media coefficients required to implement the pressure loss within the tube bundles using the modelling tool implemented in Ansys Fluent® [37].

The porous media coefficients are expressed as follows:

$$C_2 = \frac{2A}{l\rho} \tag{5.39}$$

$$\frac{1}{\alpha} = \frac{B}{l\mu} \tag{5.40}$$

where:

- C_2 – Inertial porous coefficient [1/m]
- $1/\alpha$ – Viscous porous coefficient [$1/m^2$]
- A – Quadratic curve fit coefficient
- B – Linear curve fit coefficient
- l – length of heat exchanger simulated [m]

The resultant inertial porous media coefficient for the primary superheater is 3.37 1/m whilst the viscous porous media coefficient is 127146.00 $1/m^2$. The complete calculation and pressure loss characteristics for all of the heat exchangers may be found in Appendix E.

The next step in completing the modelling of the heat exchangers was to implement a suitable heat sink in the volumes that represent each of the individual heat exchangers. Due to simplicity of the flow path within the boiler and the relatively attenuated recirculation zone around the nose region, it was possible to implement a simple volume energy sink in ANSYS Fluent® to reject the required amount of energy. The basis of this calculation was provided by using the OEM design data [68] that provided a prediction of the bulk temperature and mass flow rate of the flue gas entering and leaving the respective heat exchangers. It should be noted that the modelled heat exchangers are geometrically simplified and hence the reference volume for the heat sink calculation was taken from the CFD model. Hence the required heat sinks were calculated using the following expression:

$$Q_{sink} = \frac{\dot{m} C_p (T_{outlet} - T_{inlet})}{HX_{volume}} \tag{5.41}$$

The average heat exchanger temperatures and the calculated heat sinks are shown in Table 5-24.

Table 5-24: Heat Exchanger Specifications

Heat Exchanger	Inlet Temperature [°C]	Outlet Temperature [°C]	Q_{sink} [MW]
Secondary Superheater	1252.00	929.40	-110.00
Primary Superheater	929.40	582.20	-118.00
Economiser	557.00	310.00	-83.90

5.5.8 Full Boiler Simulation Results

A cold flow simulation (no fuel input) was conducted on the full boiler model. This was done to verify if the all the flow boundary conditions were implemented correctly. There are three flow boundaries (CA, PA, SA and TA) and one particle injection (per size fraction) per burner.

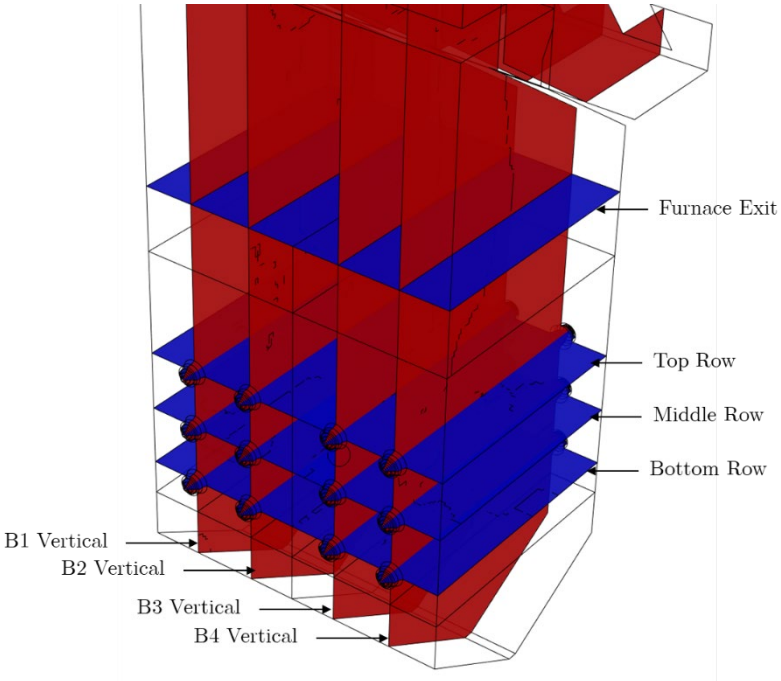

Figure 5-56: Visualisation Planes for Full Boiler Model

The velocity contours on vertical and horizontal planes (visualisation planes) through the burner centres are shown in Figure 5-57 and Figure 5-58. The relative position of the visualisation planes used on the model, are shown in Figure 5-56. Under cold conditions the burner flows are staging correctly and in a predictable way. This confirms that boundary conditions have been implemented correctly, specifically that the air flows on all the burners are balanced, as intended. Furthermore, the swirl direction verification was shown in Figure 5-43.

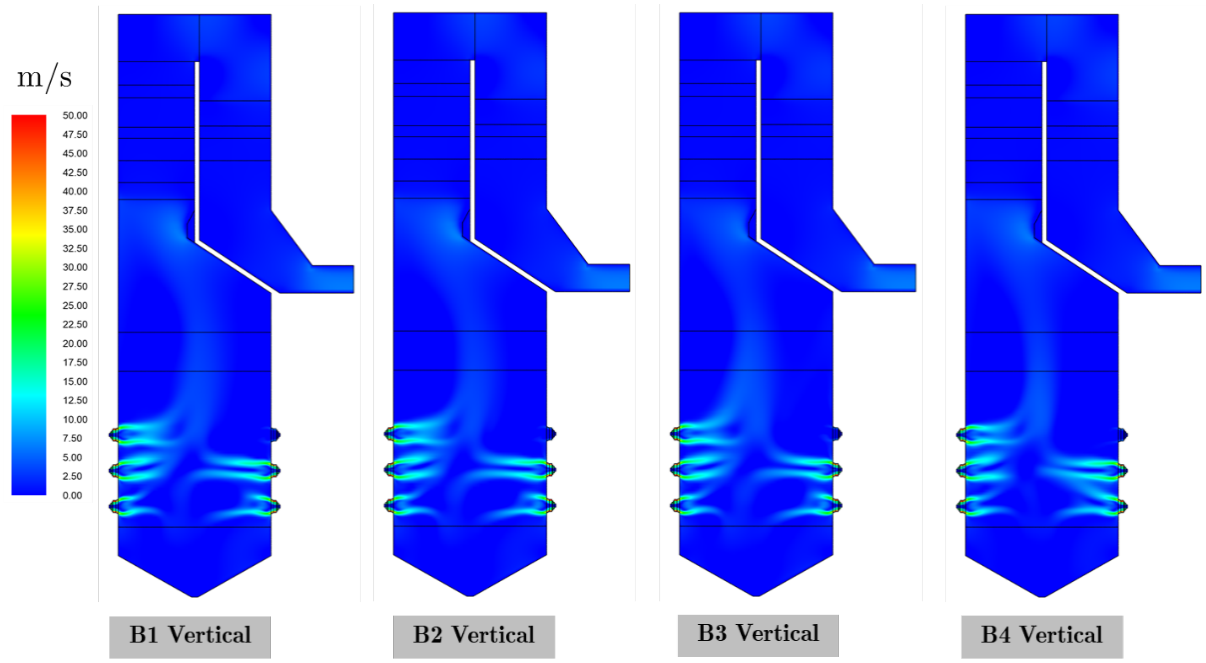

Figure 5-57: Velocity Contours on Vertical Section Planes through the Centrelines of the Burner 1 to 4 (Cold Flow)

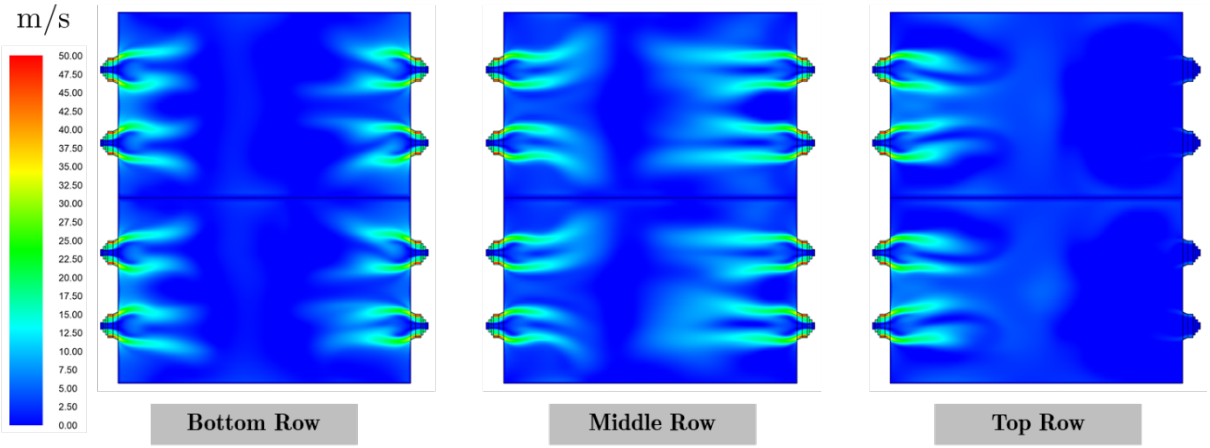

Figure 5-58: Velocity Contours on Horizontal Section Planes through the Centrelines of the Burner Rows (Cold Flow)

Thereafter the fully reactive simulations were run, and the three gas phase combustion mechanisms of interest were tested on the boiler model. The temperature contours on the horizontal and vertical sections are shown in Figure 5-59 and Figure 5-60 respectively.

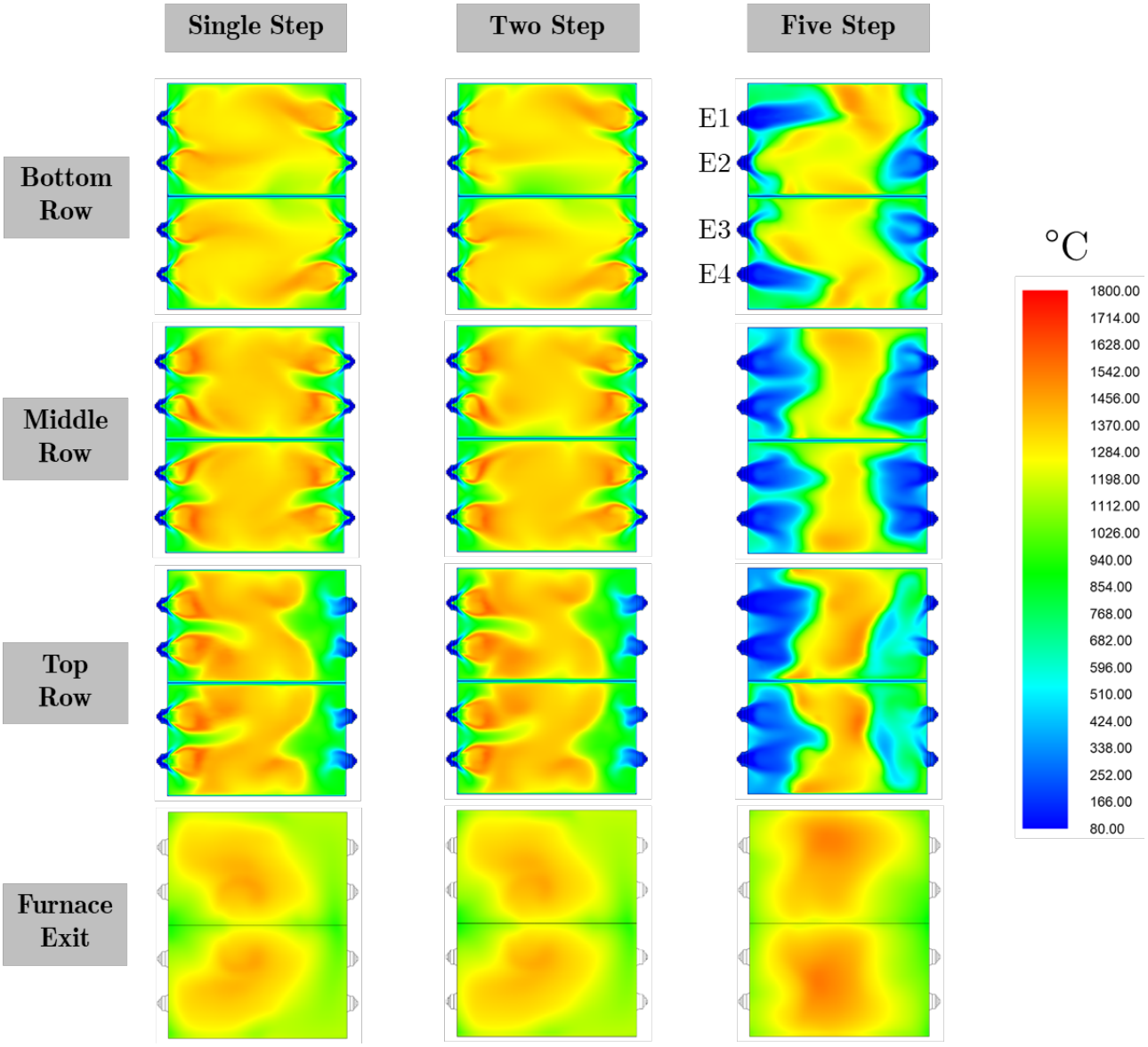

Figure 5-59: Temperature Contours on Horizontal Section Planes through the Centrelines of the Burner Rows

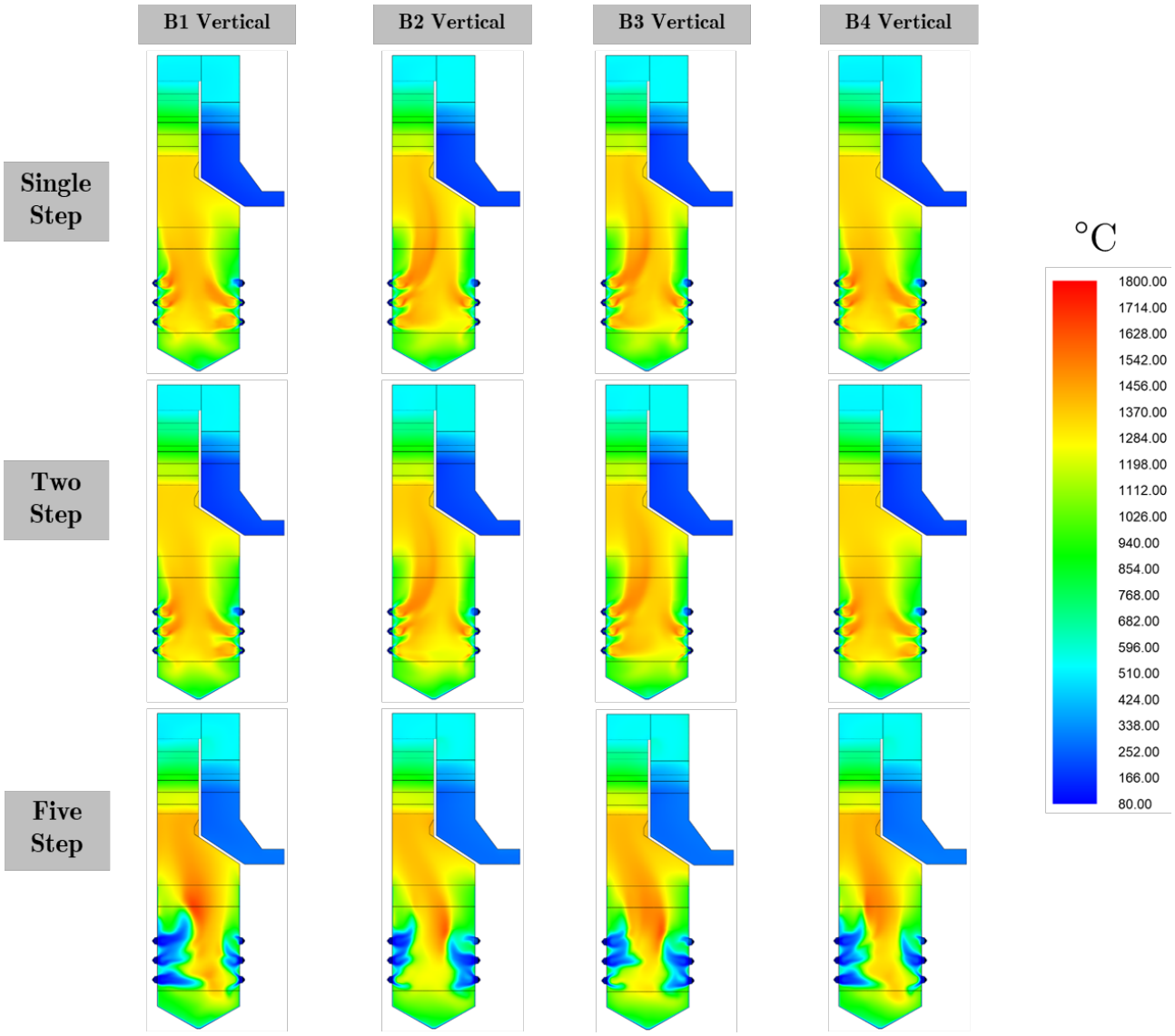

Figure 5-60: Temperature Contours on Vertical Section Planes through the Centrelines of the Burner 1 to 4

The single and two-step models produce similar temperature fields. The coal is igniting in a uniform manner and the flame root is very close to the burner mouth. This can be seen in the temperature contour plots for the bottom, middle and top rows in Figure 5-59. This is typical of the eddy dissipation turbulent combustion model, since the burner belt line has a high degree of turbulence and swirling flow, and this promotes rapid and stable combustion. The five-step mechanism produces a different temperature field than the first two mechanisms. Notably, there is a significant stand-off in the flame and the fireball is concentrated in the

middle of the furnace. This stand-off was noted during a measurement campaign conducted by Eskom Engineering [69] and it was stated that flame root is up to two metres into the furnace. An interesting flow structure can be seen on the temperature prediction of the bottom row using the five-step model i.e., there is what appears to be a flow instability in the adjacent burners. This is quite evident when considering the flame structure at burner E3 and E4 (see Figure 5-59). Burner E3 exhibits the typical delayed ignition associated with South African coals. However, burner E4 is displaying what could be considered blow-off. However, the burner is sustaining combustion and the flame front appears to be in the middle of the furnace. This flow structure is mostly mirrored on the left side of the boiler, because of the presence of the evaporator wall in the centre of the furnace. The middle and top rows show that all burners on these levels behave like burner E4, i.e., that fireball is shifted to a narrow corridor in the furnace. The temperature fields are further described in Figure 5-60. Here the temperature distribution is shown on the vertical planes. The five-step mechanism pushes the flame front into centre of the furnace. Once again, the single and two-step mechanisms show a stable combustion characteristic. The heat removal in the boiler heat exchangers is also evident as the temperature decreases as the flue gases make their way to the boiler exit.

The unexpected flow behaviour on the bottom row burners using the five-step mechanism required further investigation. Three plausible reasons were considered as to why there was such a difference in the behaviour of adjacent burners. After considering potential root causes the following influences were considered:

1. Mesh Sensitivity – The baseline was constructed with due cognisance of the need for high quality cells in the burner belt region. The model already comprised a significant number of computational cells i.e., 2 301 446. The cell quality was good. Hence it was deemed that mesh does not have a significant effect of the result.
2. The major development in this study was the refinement of the char combustion kinetics. Hence it was deemed prudent to test this effect and revert the mass diffusion constant to the default value.
3. The effect of swirl was also considered. It should be noted that the installed low NOx burners were not designed for this legacy power station. Hence there was most likely a compromise in terms of matching the burner characteristic to the requirements of

the boiler performance and characteristics. Hence it could be plausible that the burners did not perform as expected.

The effect of the parameters discussed in point 2 and 3 above is shown by means of assessing the effect on the temperature contours on the bottom row. This can be seen in Figure 5-61.

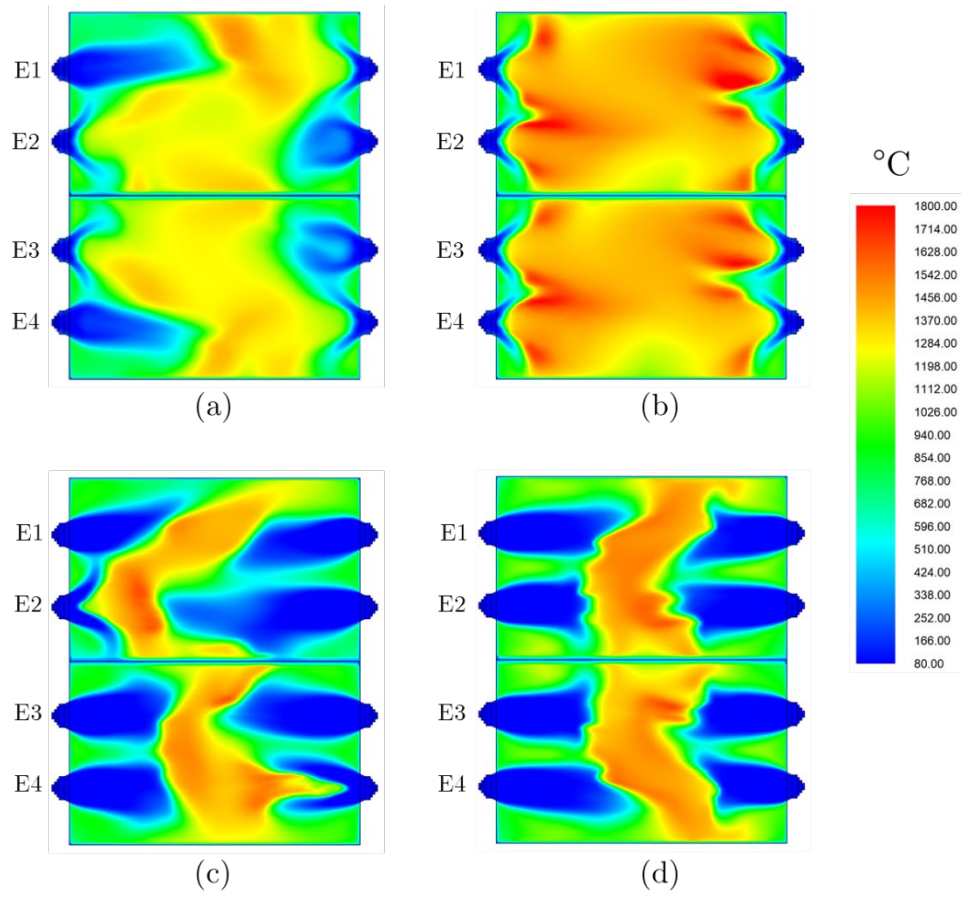

Figure 5-61: Parameter Study on Boiler Model using Five Step Combustion Mechanism: (a) Baseline result, (b) Default Mass Diffusion Constant, (c) Reduced Swirl - 15°, (d) Reduced Swirl - 5°

The effect of changing the mass diffusion constant in the char combustion model can be seen by comparing Figure 5-61(a) and Figure 5-61(b). There is an unequivocal change in the temperature field, and it resembles the prediction of the single and two-step mechanisms. The implication of the modelling change is that the coal burnout time (see Figure 5-19) is closer to ~0.3s as compared to the more realistic value of 1.3s. The single and two-step techniques use the eddy dissipation combustion model and hence the rates of burnout are controlled by the turbulence level and the above result also shows that without the specific char combustion

characteristics developed in this work, the advanced prediction capability of the eddy dissipation concept used in the five-step model, is nullified. This is an important observation, and it re-iterates the need to fully characterise South African coals for use in analysis, as well as choosing an appropriate turbulent combustion model to resolve the physics and chemistry occurring in the furnace.

The second facet of the parameter study was to consider the effect of the swirl rates implemented on the burners. The plant was originally commissioned with burners that were closer to swirling jet burners rather than the current low NOx burners with staged tertiary flows. Two stages of analysis were conducted i.e., with the SA and TA swirls on the all the burners set to 15° and subsequently 5°. These values are significantly less than the values derived from the detailed low NOx burner model (see Table 5-23) and coaxes the burners to behave like jet burners. The results can be seen by interrogating Figure 5-61(a) and progressing to Figure 5-61(c) to observe the effect of the 15° swirl, and finally Figure 5-61(d) for the 5° swirl angle. The results show that the adjacent burners of interest on the bottom row (E3 and E4) behave similarly, and the apparent flow instability found with the default swirl angles is obviated. This result improves the understanding of the behaviour of the boiler and particularly correlates the numeral results with the observations made during the test campaign conducted by Eskom Engineering [69] soon after the commissioning to the boiler with the newly installed, latest generation low NOx burners. The main observations were that there appears to be delayed combustion and the flame instability caused flame outs and back flow into the burner were causing significant damage. At the time of the on-site work the source of these problems was assumed to be poor air supply to the burners (due to the lack of *tightness* of the ducts and boiler casing brought on by the age of the plant) as well as poorly optimised swirl rates. The outcomes of this section of the study indicate that the slow burning nature of the reference coal plays a significant role in the combustion performance and that the burners were perhaps not the ideal design to be retrofitted i.e., it was not suited for the geometrical requirements of the furnace and the coal quality available. The latter was the result of the market constraints i.e., there were few options in terms of available burners from the OEM's.

The modelling results provided by the five-step model illuminated several of the finer details of the combustion flow field. It re-enforced the notion that combustion of micron sized coal particles exhibits behaviour that indicates a strong coupling between the aerodynamic,

thermodynamic, chemical and particle transport processes underway in the furnace. On further investigation it was thought that the concentration of coal particles at the exit of burner E3 and E4 may indicate a reason for the asymmetry in the flames.

The concentration of coal particles can be seen in Figure 5-62.

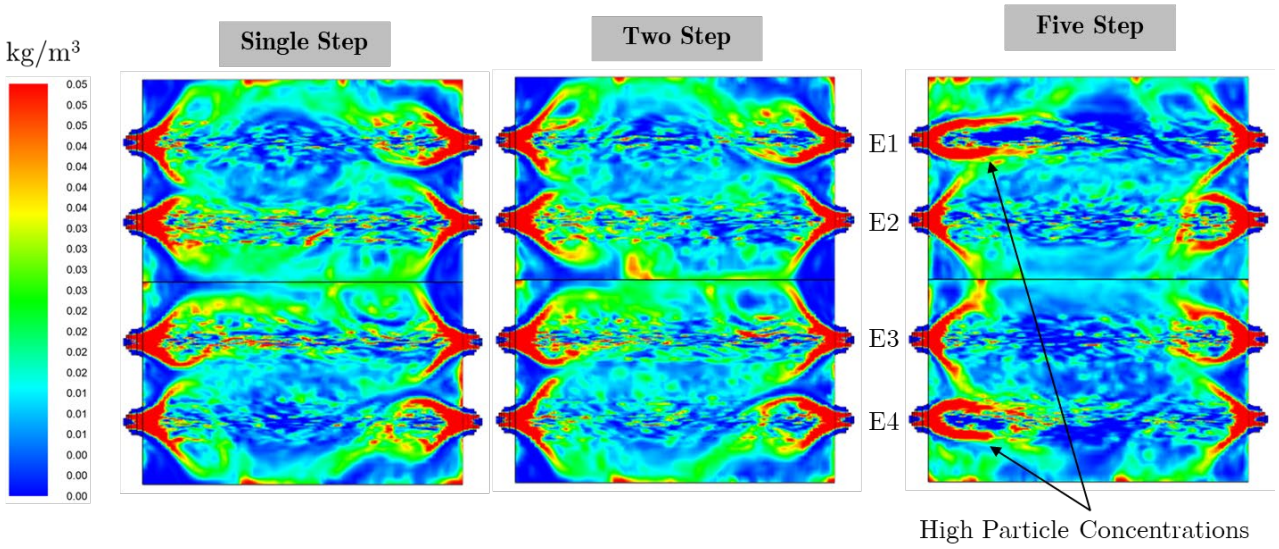

Figure 5-62: Coal Particle Concentrations on Bottom Burner Row for Three Different Gas Phase Combustion Mechanisms.

Burner E1 and E4 (five-step mechanism) produce a long concentration of particles that may be considered a *rope* structure. This effect is not evident when the single and two-step mechanisms are employed where the burners then diffuse the coal stream rapidly to produce stable flames that are positioned close to the burner mouth. In the case of the five-step mechanism, the concentration of particles was likely initiated by a complex interaction of the gas/particle aerodynamics and finite rate chemistry at the burner outlet. It should be noted that this is not a numerical artifact introduced by the pulverised coal injection boundaries, as they were confirmed to be implemented in an identical fashion (see Figure 5-57 and Figure 5-58. The result of the concentrated *rope* of particles is that the particles on the inner sections of this flow structure are shielded from incident radiation in furnace. Since this is the primary mode of heat transfer in the high temperature environment, it results in delayed combustion.

This idea is supported when the initial release of pyrolysis products is considered, and this may be seen in Figure 5-63.

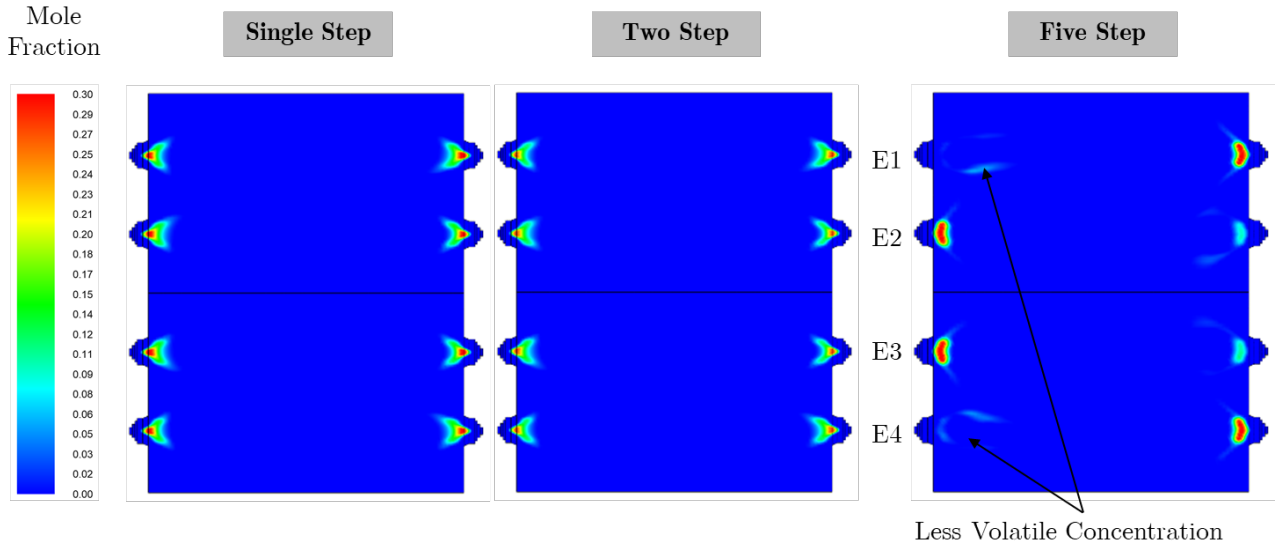

Figure 5-63: Initial Volatile Mole Fractions on Bottom Burner Row for Three Different Gas Phase Combustion Mechanisms.

Burner E1 and E4 have significantly less initial volatile release than the adjacent burners and this lack of combustible gases would retard ignition. Notably, the single and two-step mechanisms do not present this behaviour. The further break down of the initial volatile components to light and heavy hydrocarbons shows that there are combustible gases to establish combustion (see Figure 5-64) and hence the particle ignition is pushed to the centre of the furnace, which is consistent with the temperature profiles previously presented. Hence the E1 and E4 burners are experiencing severely delayed combustion but has not gone into a blow off situation as the coal is indeed burning, albeit very much later than in the case of burner E2 and E3.

The evolution of the volatile components for the five-step mechanism is shown in Figure 5-64.

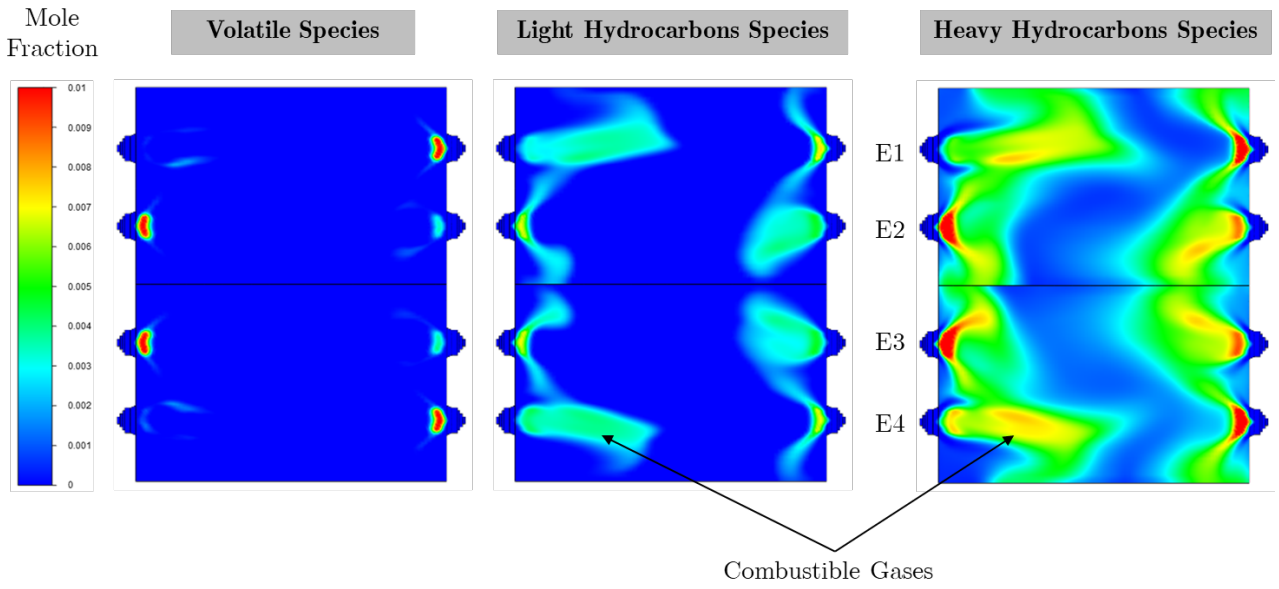

Figure 5-64: Predicted Initial Volatiles, Light and Heavy Hydrocarbons on the Bottom Burner Row using the Five-Step Combustion Mechanism.

Eskom Research conducted a test campaign [64] on the 200 MW Coal Fired Boiler modelled in this work and recorded measurements at the furnace exit and in flame measurements on the centreline of burner E3. The furnace exit data was obtained using gas pyrometry and sampling at a location close to the rear wall of the furnace, due to the availability of access hatches. The sampling probes were inserted 4m into the furnace. The measurements taken were gas temperature, oxygen concentration and carbon monoxide and carbon dioxide concentrations. The in-flame measurements on burner E3 were the same but included the nitric oxide concentrations. The work of Smit [25] provided an alternative set of temperature measurements on the centreline of burner E3. The comparison of the data extracted from the furnace exit for the three simulations, to the measured data is shown in Figure 5-65.

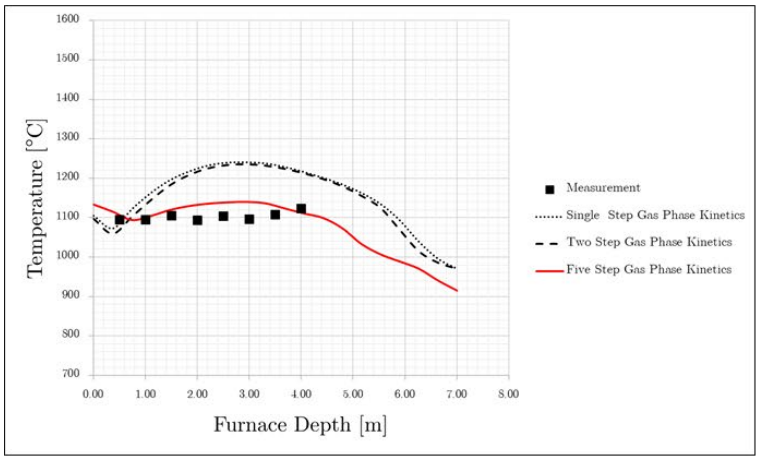

(a)

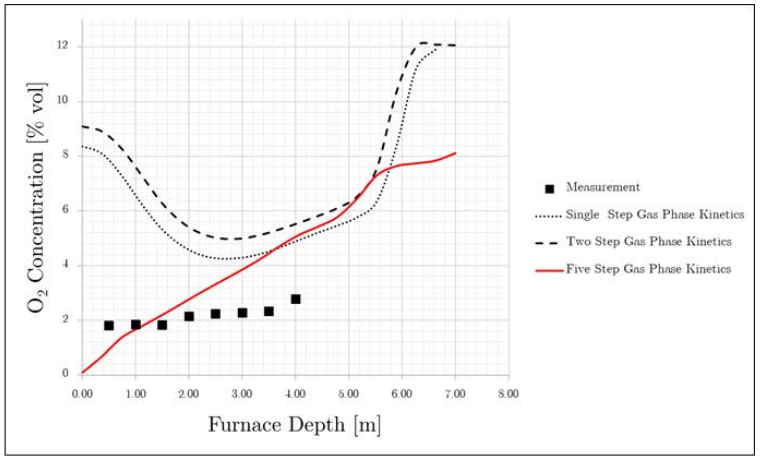

(b)

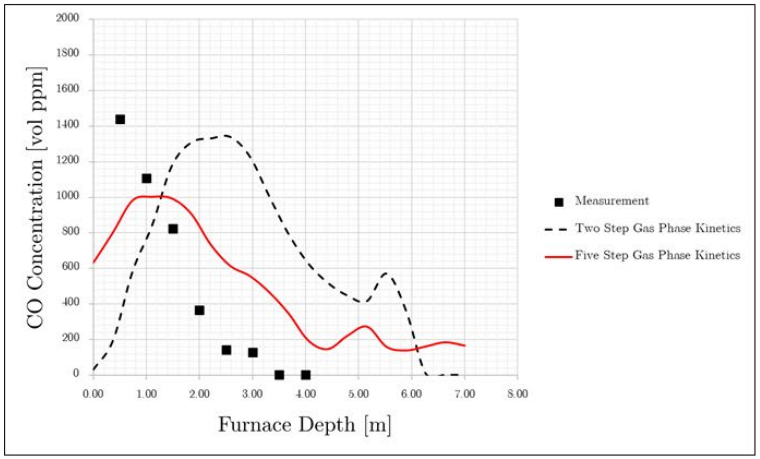

(c)

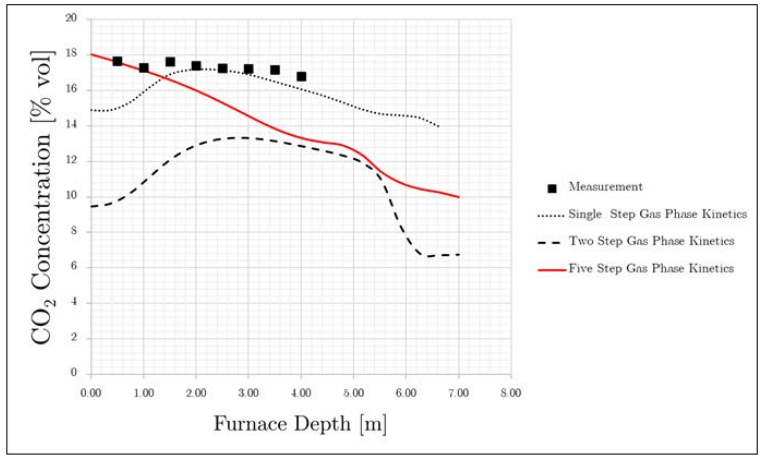

(d)

Figure 5-65: Comparison of CFD Simulation to Measured Data at the Furnace Exit

The comparison of the temperature prediction to the measured data is shown in Figure 5-65 (a). The five-step model produces the best agreement with the measured data, capturing the flat gradient. The single-step and two-step models predict a gradual increase until about 3 m into the furnace followed by a gradual decline in temperature. The burner belt is where there are large temperature and velocity gradients because the fuel is being injected and ignition and char burnout is occurring in this region. The products of combustion then mix extensively and travel towards the furnace exit region. The gradients are consequently less due to thermal equilibration as well as species mixing and evolution. This, however, does not preclude the existence of significant temperature stratification, as can be seen in Figure 5-59. This poses a fundamental challenge to arriving at a representative average temperature by measurement, as point readings could differ significantly depending on where the probes are inserted. Hence it is prudent for utilities to invest in reliable furnace exit temperature measurement equipment such as acoustic pyrometers.

The comparison of the CFD predictions to the measured oxygen values is shown in Figure 5-65 (b). All three mechanisms do not corelate with the measured values. However, the five-step mechanism does initially predict an oxygen value that is the correct magnitude. The single and two-step mechanisms generally over predict the oxygen concentration. The reason for the large variation in predicted oxygen values is that there is significant stratification at the furnace outlet. This is shown in Figure 5-66 along with the measurement location.

The carbon dioxide comparison is shown in Figure 5-65 (d). In this case the single-step model has the best overall correlation with the measured data. The five-step model initially predicts well but then indicates a decrease in carbon dioxide. The two-step model underpredicts the carbon dioxide concentration across the range of the measurement data. The single-step model immediately oxidises the released volatiles to the final product i.e., water and carbon dioxide. This occurs at the burner belt region and hence the carbon dioxide has more opportunity to mix and distribute in the furnace before it travels to the furnace outlet plane. The contours for this scalar are shown in Figure 5-67.

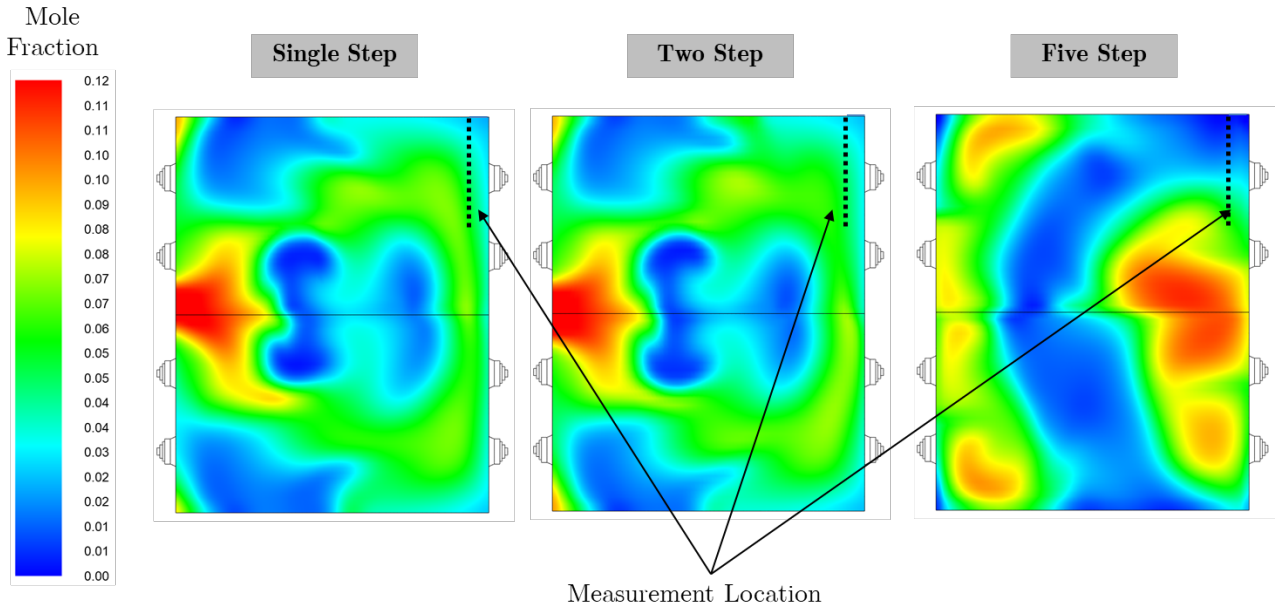

Figure 5-66: Oxygen Stratification at Furnace Outlet for Three Gas Phase Combustion Mechanisms

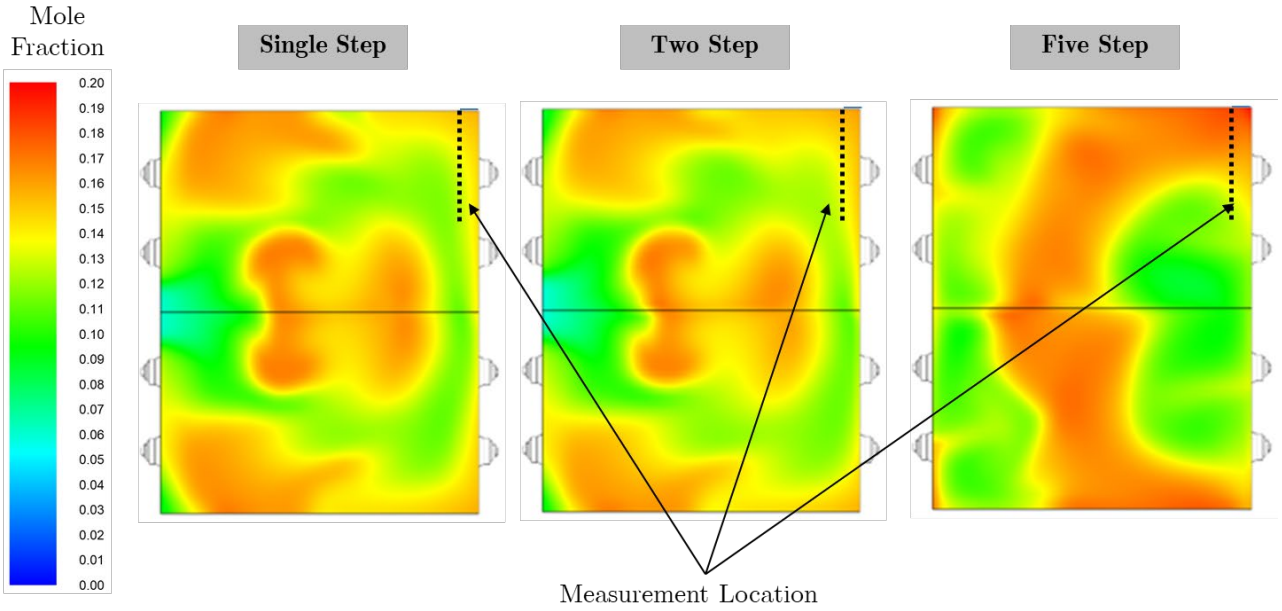

Figure 5-67: Carbon Dioxide Stratification at Furnace Outlet for Three Gas Phase Combustion Mechanisms

The carbon monoxide CFD prediction was compared against the measured values and this was only done for the two-step and five-step mechanisms since this species does not feature in the formulation of the single-step mechanism. The five-step mechanism shows the best comparison. It follows the trend and magnitude of the measured data well, except for the near wall region. Here the CFD predicts a decrease in carbon monoxide concentration. However, although underpredicted by both mechanisms, the five-step model does not go to zero concentration which is not likely since carbon monoxide is known to accumulate near the walls of coal fired furnaces and in turn promotes the onset of fireside corrosion. Hence this is an important predictive capability and five-step mechanism produces acceptable results. The contour plot of carbon monoxide on the furnace exit is shown in Figure 5-68. Here it is obvious that measurement is not located ideally to capture the peak carbon monoxide concentration. This issue emphasises the worth of CFD in understanding the behaviour of coal fired furnaces and how it may be used to inform the testing activities on the plant. The carbon monoxide level is an indication of incomplete combustion and under certain conditions can pose an explosion risk. Hence it is imperative that these values be well known during the operation of the plant.

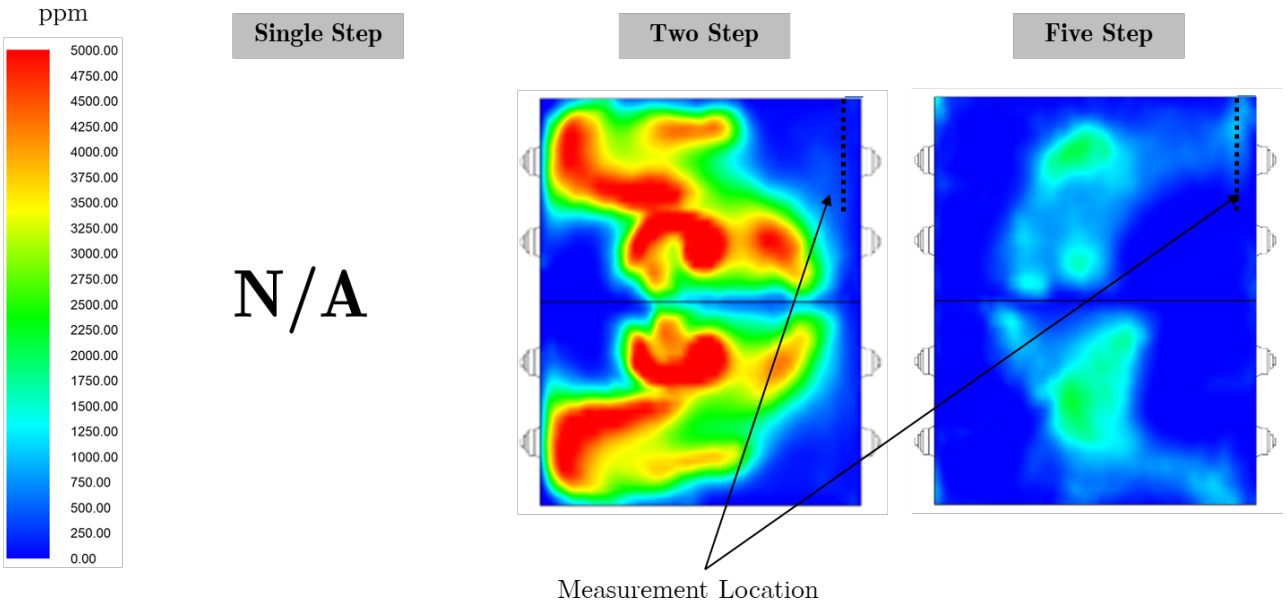

Figure 5-68: Carbon Monoxide Stratification at Furnace Outlet for Three Gas Phase Combustion Mechanisms

The average values of the important combustion parameters are shown in:

Table 5-25: Average Values of Boiler Parameters

Parameter	Single-Step Mechanism	Two-Step Mechanism	Five-Step Mechanism
Thermal Input [MW]	600	600	600
Electric Output [MWe]	200	200	200
CFD Heat Balance [W]	8.46E+05	2.61E+04	-5.09E+06
CFD Heat Balance Error [%]	0.42	0.01	-2.55
Boiler Outlet O_2 [% Vol]	2.49	2.54	2.61
Furnace Exit O_2 [% Vol]	3.82	3.85	3.95
Boiler Outlet CO [ppm]	N/A	620.72	2213.60
Furnace Exit CO [ppm]	NIL	3115.16	673.36
Boiler Outlet CO_2 [% Vol]	15.86	15.78	16.13
Furnace Exit CO_2 [% Vol]	14.53	14.32	14.95
FE Temperature [°C]	1306.34	1312.43	1344.48
Boiler Outlet Temperature [°C]	312.97	321.90	380.60
Heat Absorbed by Evaporator [MW]	216.64	217.88	190.83
Front Wall Heat Flux [MW/m^2]	0.12	0.12	0.08
Left Wall Heat Flux [MW/m^2]	0.19	0.19	0.17
Right Wall Heat Flux [MW/m^2]	0.16	0.16	0.13
Centre Wall Heat Flux [MW/m^2]	0.19	0.19	0.17
Back Wall Heat Flux [MW/m^2]	0.11	0.11	0.10

With reference to Table 5-25, The thermal input of the boiler is the total heat that is available by virtue of the coal flowing into the furnace. The electrical output is achieved at 100% MCR according to the boiler design. Mass and energy balances were done on each of the models.

The outline of this calculation is described in Figure 5-69.

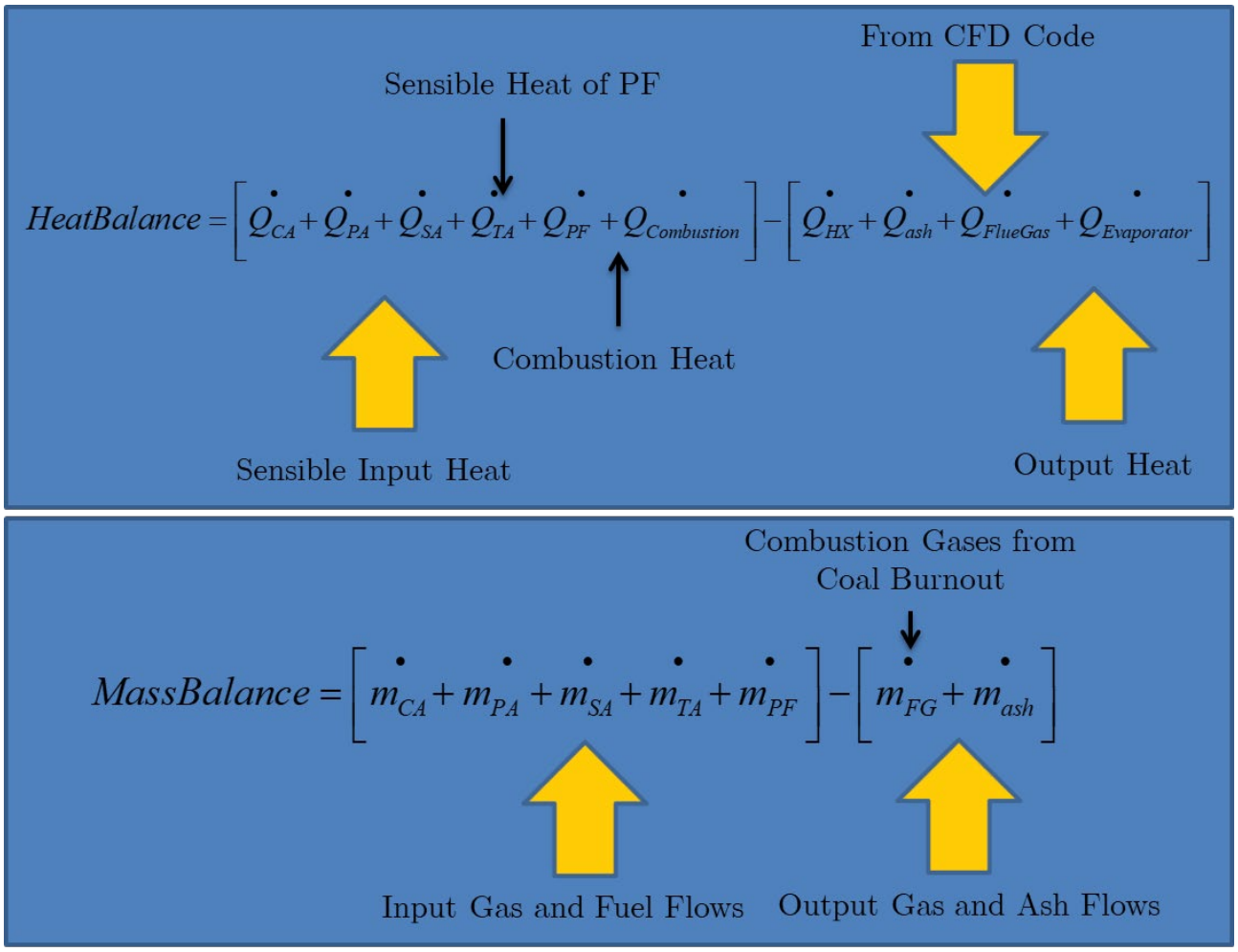

Figure 5-69: Boiler Mass and Energy Balance

The mass balance was not challenging to achieve and the CFD code produced good results early in the iterative calculation. The energy balance on the other hand required extensive run time (typically ~100 000 iterations) to be realised. Hence this parameter was used an indication of numerical convergence of the CFD code. The single and two-step mechanisms achieved excellent heat balances and the error was typically less than one percent. The five-step mechanism required further run time to converge due to its more complicated chemistry scheme. The heat balance error was -2.55% in this case and was deemed acceptable. The heat balance error is the ratio of heat balance value divided by 200 MW i.e., the design output of the plant.

The mass weighted averages of oxygen, carbon monoxide and carbon dioxide at the furnace exit and boiler outlet were extracted from the CFD simulations. The values were in-line with the design specifications [65]. The boiler outlet temperature was determined by the amount of energy extracted by the heat exchangers. A set point value of 310 °C was used to calculate the heat removal of the heat exchangers listed in Table 5-24. The single-step mechanism came within an acceptable range of the expected boiler outlet temperature. The two-step and five-step mechanisms predict higher boiler outlet temperatures. The two-step mechanism predicts a higher furnace exit temperature and hence the boiler exit temperature is higher. The same is the case for the five-step mechanism albeit that the furnace exit temperature is higher still. A possible explanation for this is the difference in heat absorption by the evaporator. The evaporator rejects 190.93 MW of heat when compared to the other mechanisms that reject in the range of 215 to 218 MW. This difference is due to fundamentally different flow and temperature fields and how it affects the heat absorption of the various parts of the evaporator. The evaporator heat flux for the three simulations is shown in Figure 5-70. The front evaporator wall rejects 0.08 MW/m^2 for the five-step mechanism, which is substantially less than the 0.12 MW/m^2 that the other two mechanisms predict. Hence this excess heat that must be taken up by the flue gas and particles and results in a higher furnace exit temperature for the five-step mechanism. This result indicates that the five-step mechanism can predict adverse heat transfer conditions in the furnace. This will be advantageous when off-design conditions need to be predicted, such as burner air and fuel flow imbalance.

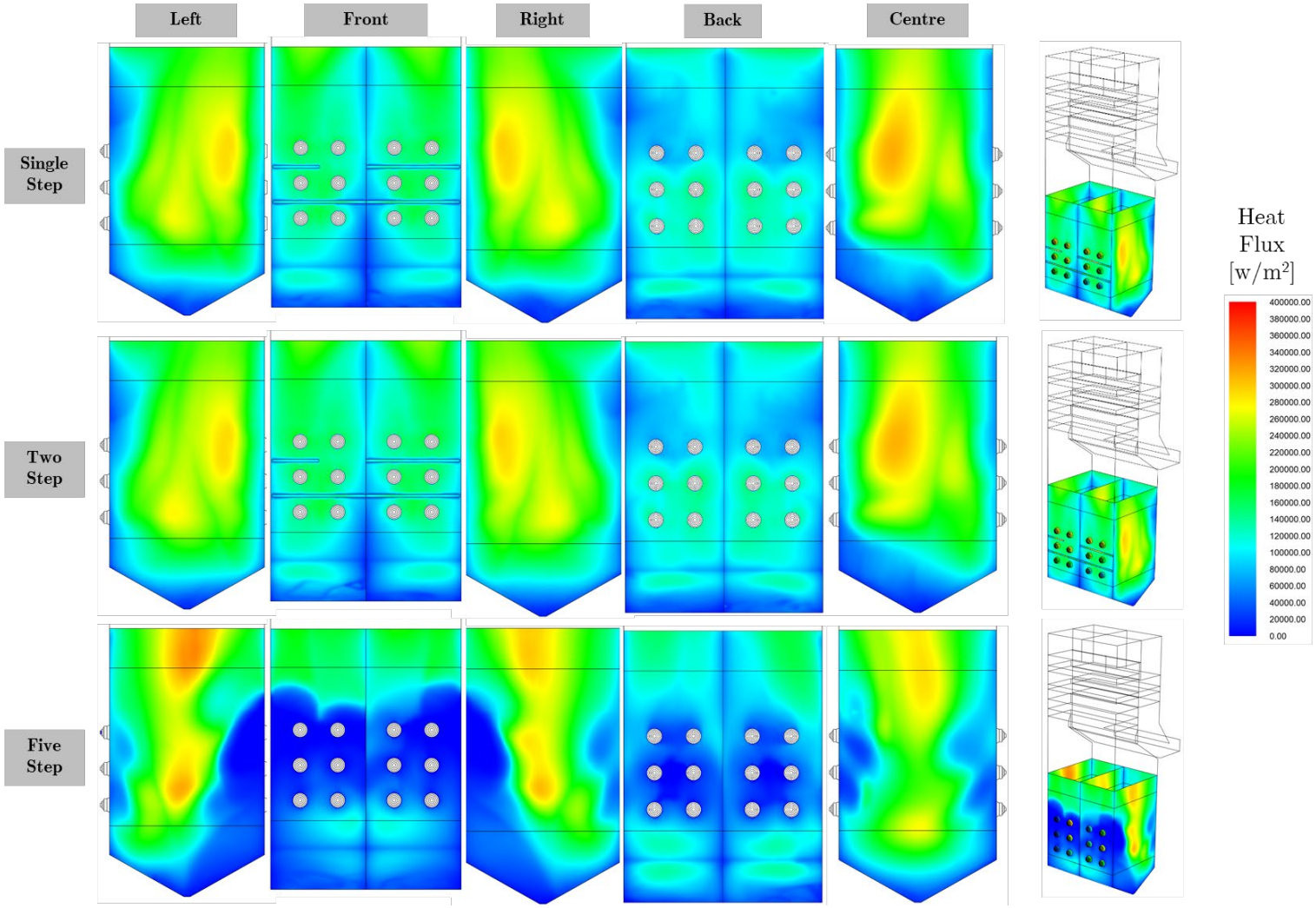

Figure 5-70: Evaporator Heat Flux for Three Gas Phase Combustion Mechanisms

The focus will now shift to measurements on the centreline of burner E3. This burner is on the front wall of the furnace and is used for measurements as it is accessible, and the required support equipment is available. The location of burner E3 is shown in Figure 5-41. The comparison with the predicted CFD results with the measurement data is shown in Figure 5-71. These in-flame measurements are done in a highly reactive, swirling turbulent flow field. In contrast to the furnace exit, here the coal is still igniting in the near burner region and consequently there are large temperature and velocity gradients.

Figure 5-71(a) shows the comparison between the predicted and measured centreline temperatures in the furnace. All three mechanisms predict the general trend, but the five-step mechanism produces the closet correlation with the measurements. On closer inspection, only the five-step mechanism can predict a realistic burner exit temperature i.e., the temperature is close to the primary air temperature. Because the one and two-step mechanisms release combustible matter immediately after pyrolysis, the flame is attached to the burner and hence produces exit temperatures of over 800°C. It should be noted that the measured data indicates that the temperature increases at a slower rate down the burner centreline. This indicates that the burner instability that was predicted by the five-step mechanism, could retard the combustion on burner E3 to larger extent. It appears the measured temperature data is somewhere in between the predictions on the adjacent E3 and E4 burners.

Figure 5-71(b) shows the oxygen profile on the burner centreline. The single and two-step mechanisms completely overpredict the consumption of oxygen and create an unrealistically lean combustion zone near the burner exit. This is typical of the eddy dissipation combustion model. Although the five-step mechanism prediction is significantly offset from the measurements, it does share the same trend and importantly predicts a realistic oxygen level at the burner outlet.

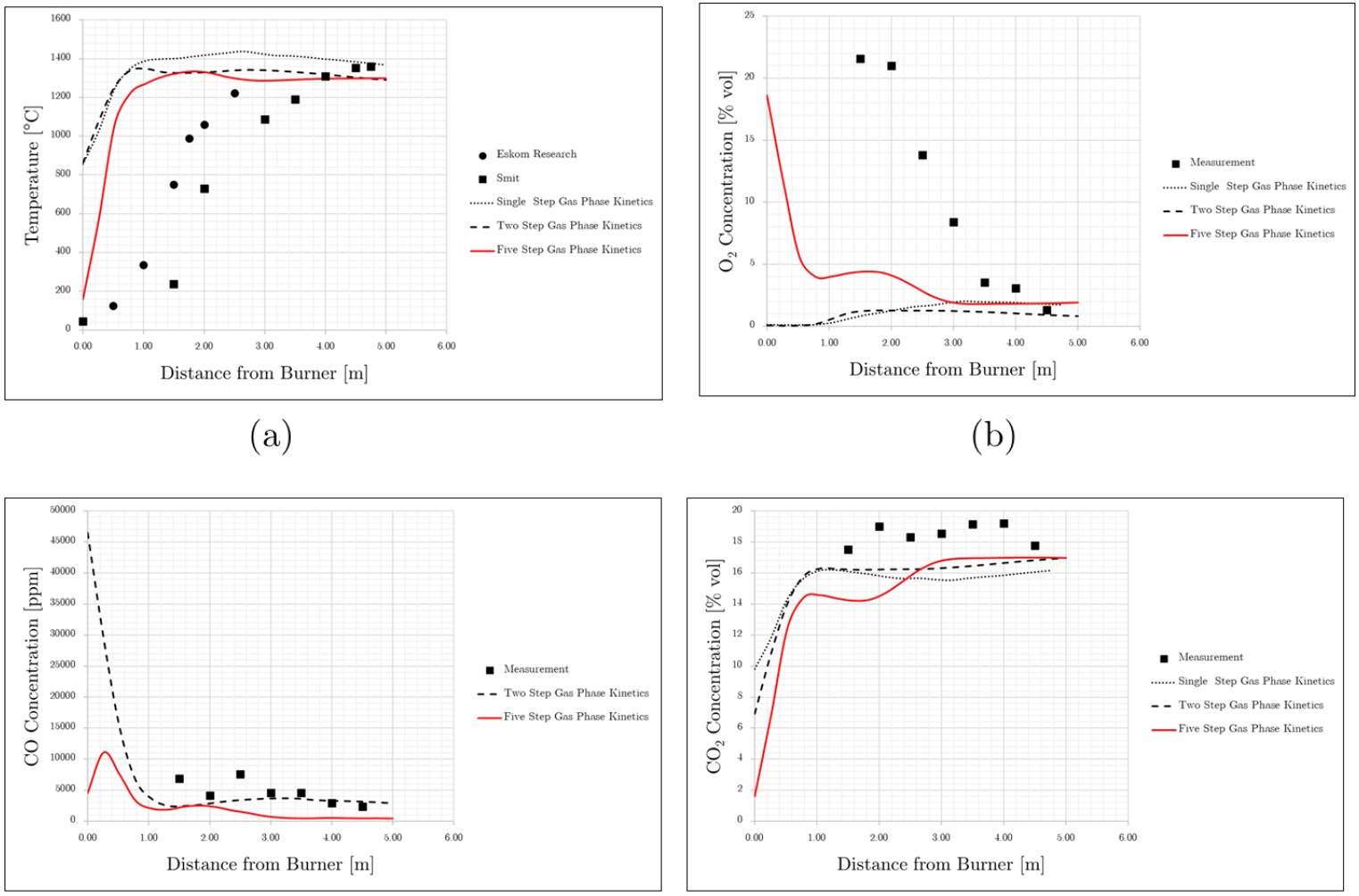

Figure 5-71: Comparison of CFD Predictions and Measurements on Burner E3 Centreline

Figure 5-71(c) shows the results from the carbon monoxide comparison. Only the two and five-step models can predict the formation of carbon monoxide. Both models show good agreement with the measured data about 1m and onward form the burner mouth. The two-step model predicts an unrealistic peak at the burner mouth, and this is because the model is designed to release carbon monoxide during pyrolysis. The five-step model shows a more natural evolution of carbon monoxide in that there is an initial peak after approximately 0.5m metres from the burner mouth. This due to the release of the light hydrocarbons which provide combustible gases to initiate ignition and subsequently support the char combustion process. The five-step mechanism does under predict the carbon monoxide levels later downstream of the burner. This indicates that reaction kinetics is promoting a rate of oxidation of carbon monoxide to carbon dioxide, that is too high. This could be altered based on more appropriate chemical rate data.

The profile of carbon dioxide gas down the centreline of burner E3 is shown in Figure 5-71(d). All three mechanisms predict the carbon dioxide levels past 1.5m from the burner mouth well. But once again, the assumptions of the one and two-step mechanisms are not appropriate for near burner predictions. This manifests in higher carbon dioxide levels at the burner mouth.

The NOx pollutant solver in ANSYS Fluent® was used to predict the nitric oxide concentration on the centreline of the burner. A rudimentary approach was taken in that only fuel NOx was considered. The volatile and char nitrogen fractions were calculated to be 0.0188 and 0.0191 respectively. The default value of the BET surface area was used i.e., 25000 m^2/kg. The fuel nitrogen species was assumed to be released into the gas stream with weighting of 30% HCN, 30% NH_3 and 40% NO. These values were arrived at by trial and error, and it produced a prediction that agreed with the measured values. The comparisons are shown in Figure 5-72.

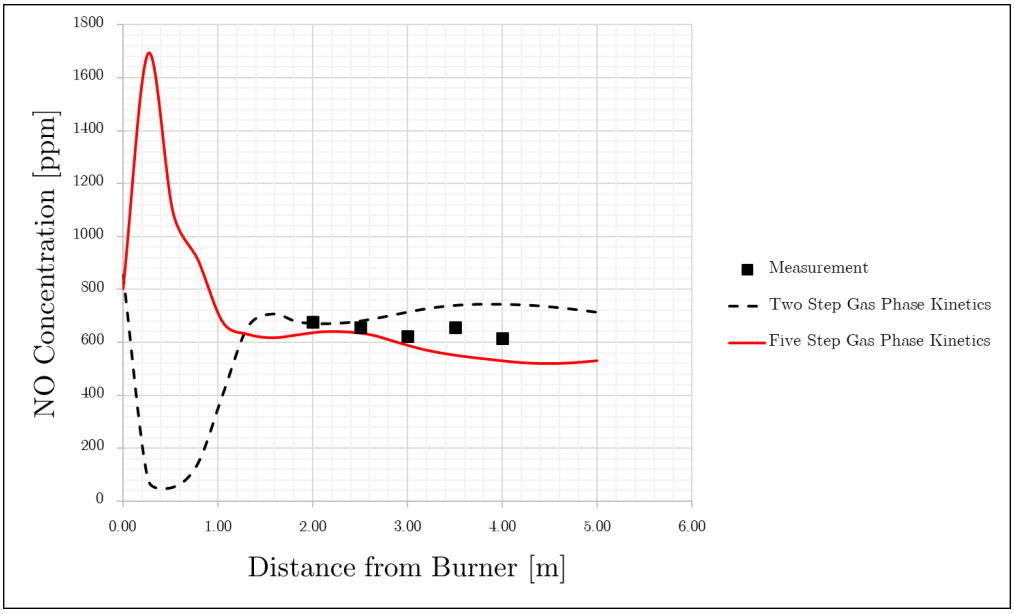

Figure 5-72: NOx predictions on the Centreline of Burner E3

The prediction of NOx pollutants is beyond the scope of the current study and future work should consider a phenomenological justification for the NOx formation based on the reference coal characteristics. The current result shows that the CFD NOx prediction models can be "tuned" to produce favourable correlations with the measured data.

Finally, the particle burnout rates were calculated for the boiler simulations. This was done in the same way as for the PSCTF analysis (see section 5.4.4).

Table 5-26: Particle Burnout in Full Boiler Model

Mechanism	**75µm**		**106µm**		**150µm**		**300µm**	
	1.3 s [%]	**3 s [%]**	**1.3 s [%]**	**3 s [%]**	**1.3 s [%]**	**3 s [%]**	**1.3 s [%]**	**3 s [%]**
Single-Step	32	0	96	15	100	84	100	84
Two-Step	26	0	96	12	100	83	100	86
Five-Step	9	0	93	9	100	80	100	87

Once again, lightest particles burn out effectively whilst the heavier particles do not get completely consumed, even after 3 seconds.

This result is shown graphically by visualising the particle tracks for each size fraction. The particle tracks are coloured by their char mass fraction. This is shown in Figure 5-73.

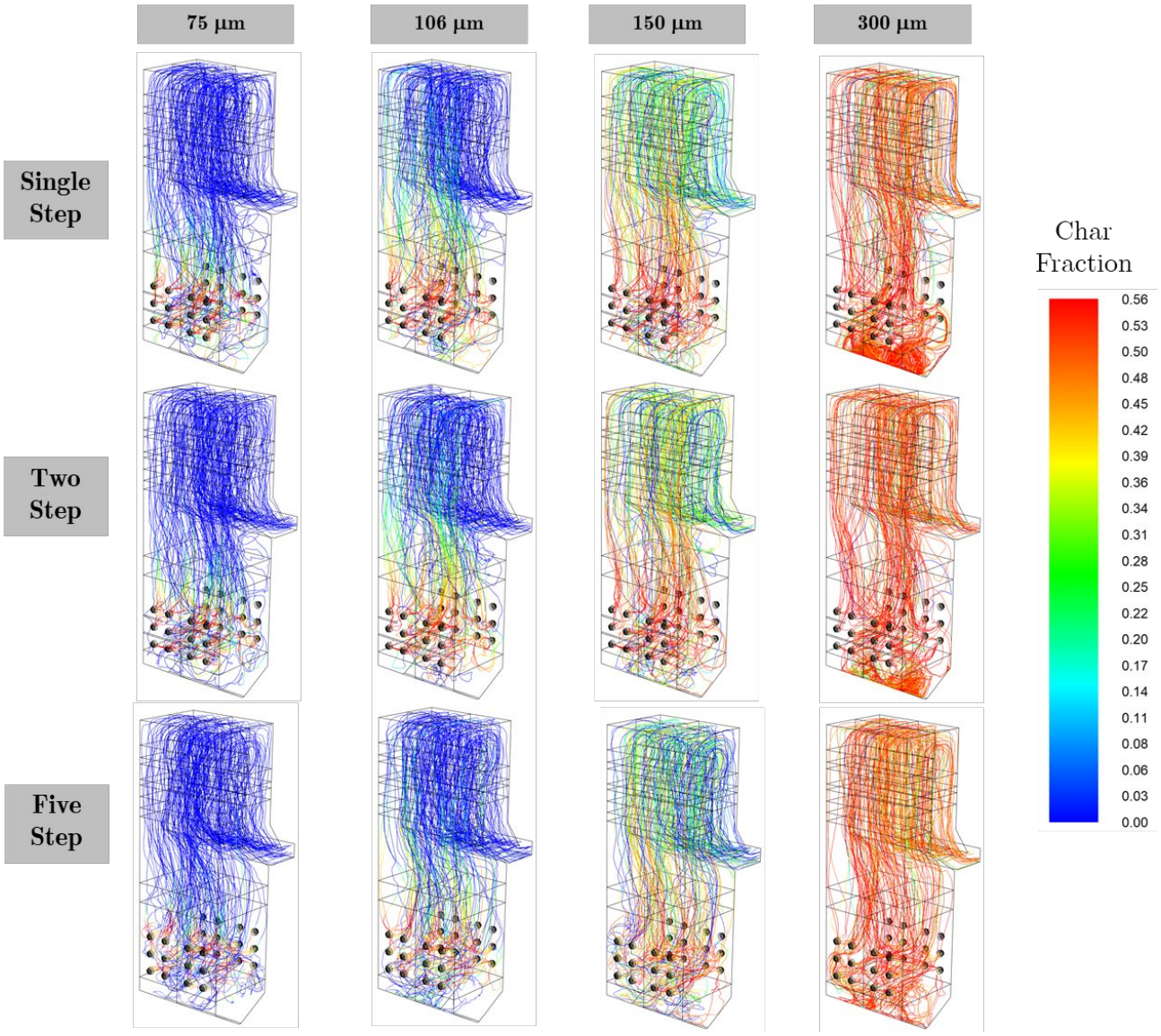

Figure 5-73: Particle Tracks for Different Size Fractions

A similar trend was observed when analysing the burnout characteristics of the reference coal at the pilot scale (see Table 5-18) and once again it demonstrates an intuitive behaviour i.e., that heavier particles would take longer to burn out. On the full-scale plant, when the mills are run past their service intervals and they start underperforming by producing the larger size fractions, it is observed the measured unburnt carbon at the boiler outlet increases. Hence it is postulated that most of the unburnt carbon originates in the larger particles.

5.5.9 Discussion of Full-Scale Boiler Results

The effect of the gas phase combustion mechanisms was shown on a full-scale pulverised coal boiler. The mechanisms produced different results and in general the five-step mechanism compared more closely with the measured data. Scale effects came to the fore, particularly when using the five-step mechanism. This was seen through the complex interaction of multiple, firing burners. The onset on asymmetry and perhaps instability in the flames emanating from the E3 and E4 (and E1, E2) burners on the bottom row of the furnace indicates that when the chemical kinetics of the reactions are accounted for, there is a more distinct coupling between the local thermodynamics and aerodynamics of the coal flames. This was shown when the coal rope was predicted coming out of burner E1 and E4. It was confirmed by the cold flow simulations that the flow boundary conditions were implemented correctly, hence this complex particle transport behaviour occurs due the local conditions. The single and two-step mechanisms do not predict this behaviour and should be used with caution when near burner conditions are to be predicted. The scale effect was not apparent on the PSCTF simulation as it comprised of a single burner. Hence the results demonstrate that whilst the PSCTF may be adept and confirming the burnout times of a given coal, its behaviour cannot be extrapolated to full scale burner interactions i.e., detecting flame instability in a multi-burner combustion flow field. The furnace exit is used on utility boilers as the main location to do measurements to confirm the combustion performance. In this regard, the five-step mechanism provided the best comparison with the measured data. The examination of the conditions at the furnace exit showed that five-step mechanism predicts the CO concentration better than the other two mechanisms. The CFD simulations also provide a deep level of insight into the flow structures in the boiler, particularly regarding stratification or abnormal concentrations of the gas species. Finally, it may be concluded that the full-scale simulation of the 200 MWe boiler successfully demonstrated that using an advanced gas phase combustion mechanism improves the quantitative prediction of gas species, even carbon monoxide. Furthermore, the use of the eddy dissipation concept draws in the influence chemical kinetics that showed a greater sensitivity to the inherent coupling between localised thermodynamics, aerodynamics, and particle dynamics. This in turn increased the predictive capability of the modelling technique. The significance of the detailed coal characterisation developed in the current work, was brought to the fore. The

influence of the predicted rate of char combustion was shown to be translatable between the laboratory (DTF), pilot (PSCTF) and full scales.

6 Conclusions

The current work demonstrated that the incorporation of advanced gas phase kinetics does improve the predictive capability of CFD when simulating pulverised coal combustion. The results show that there is an unequivocal influence on the flame characteristics in terms of temperature and species distribution. These results confirm the research hypothesis postulated in section 3. The prediction of most gas species showed better correlation with experimental data when the five-step gas phase kinetic mechanism was employed. This was particularly apparent for the prediction of carbon monoxide. These results answer the research question 1 and 2 described in section 1.3. A key feature of the current research was to investigate the effects of scale on the prediction of the pulverised coal combustion field. The comprehensive simulation of the 200 MWe boiler demonstrated that there is indeed a strong coupling between the aerodynamics, thermodynamics, particle dynamics and chemical reactions in a multi-burner environment. This result speaks to research question 3 (section 1.3), in that there are scale effects both in terms of overall temperature and species predictions, but also in terms of the spatial and temporal characteristics of the combustion zone. However, this coupling was only evident when the finite rate chemistry of the five-step mechanism was employed. The single-step and two-step mechanisms predicted stable flame characteristics across all the burner rows with the flames sitting comfortably within the burner quarl. When the five-step mechanism is employed, the flames are significantly offset to the centre of the furnace. This is consistent with on-site observations and shows that only the five-step mechanism can predict the effect of the relatively slow char burnout characteristics of the reference coal. This is particularly evident on the bottom row burners where a flow instability occurs. This behaviour was also noted during onsite investigations. Extensive work was done to confirm that the instability could be attenuated by reducing the swirl (relative to the burner axis) on the burners, which alluded to a coupling effect dominated by localised burner aerodynamics. This is somewhat counter intuitive as swirl rates are usually increased to reduce flame instability in industrial conditions. Hence the conclusion is that the single-step and two-step mechanisms may provide acceptable predictions of the average parameters such as furnace exit temperature, they cannot represent the complicated combustion dynamics in the burner region. This limitation is further emphasised when the reference coal is less reactive than the typical northern hemisphere coals for which the assumptions of the simpler mechanisms are more applicable. This brings

to the fore the importance of developing realistic devolatilisation and char kinetic characterisations for the coal being burnt. Hence it is essential to apply the advanced characterisation techniques described in the current work to faithfully represent the combustion characteristics of South African steam coals. Furthermore, care must be taken when localising OEM designs for use in the South African context to account for local coal characteristics and other factors such as ambient conditions i.e., South African power stations are not at sea level and the fluence of altitude must be considered.

In closing, it may be concluded that the current research study effectively highlighted the complexities involved in simulation the combustion of pulverised coal. The systematic research strategy used brought to the fore the need for advanced gas phase mechanisms to better predict the near burner flame behaviour. It also showed that models that represent the detailed physics such as the breakdown of volatile matter into light and heavy hydrocarbons as well as temperature and turbulence dependent chemical kinetics are required to simulate complex flow structures such as instabilities. It is particularly important when trying to determine combustion characteristics of diverse coals at varying scales. The former point is relevant when devising analysis strategies to investigate off-design conditions whilst the latter point is crucially important when considering South African coals. Conversely the simpler mechanisms may provide predictions that match the bulk temperature conditions at the furnace and boiler exits but are not capable of predicting the nuanced structures in the main combustion zones. In conclusion, the fidelity of the modelling technique must match the predictive capability it is expected to provide.

7 Recommendations for Future Research

The current research study made several important observations regarding the aerodynamics and heat transfer of pulverised coal flames at multiple scales. The research highlighted several key aspects that appear to play a significant role in the realistic prediction of the flame structures. There is merit in continuing the research effort to address these issues. Hence it recommended the following areas be considered for future research to improve the understanding of pulverised coal combustion:

1. The results from section 5.2.5 indicate that the char combustion characterisation of coals can be challenging if the coal exhibits non-typical behaviour. Hence it is recommended that the techniques applied to the reference coal be extended to a wider variety of South African and international coals. This is in conjunction with a review of the modelling limitations of PC Coal Lab® and its applicability to these coals may be explored.

2. The results from section 5.4.4 indicate that burnout times for the coal are predicted well for the size fraction that the experimental and numerical predictions are based. The particle size that is typically tested is 38μm. however the milling process for pulverised fuel rig produces a range of particle sizes i.e., up to 150μm. The results show that the larger particles do not match the expected burn out time. Hence it is proposed that the experimental philosophy be reconsidered to include the burn out characterisation of the larger particles. The simulation technique should also be extended to consider different particle char kinetics per size fraction. This problem may be approached from a *systems thinking* point of view, in that the influence and magnitude of the untested particle sizes must be juxtaposed against the realistic milling capabilities as well as the full-scale combustion of the coal.

3. Throughout the research presented in the current work, the numerical models were compared to experimental data. It should be noted that there is an associated error with the experimental data. The numerical work also has inherent error due to mesh sensitivity, modelling approximations and other numerical artifacts. Further work should focus on developing a best practice to evaluating these errors in the context of

the complex, multi-variate problem of experimenting with and simulating pulverised coal combustion.

4. The research study indicated that there is strong coupling between the chemical and aerodynamic processes. It would be informative to extend the gas phase mechanisms to the highest fidelity e.g., the use of the GRI-Mech complex chemistry scheme and corelate the results with the current research. Furthermore, it is recommended that this advanced chemistry is coupled with scale resolving flow simulations i.e., large eddy simulations. This would provide a high degree of insight into the fundamental processes occurring in a pulverised coal combustion zone.

8 References

[1] BP Statistical Review of World Energy, "Coal Consumption by Country," *Our World in Data*, 2021. [Online]. Available: www.ourworlindata.org/energy. [Accessed: 06-Sep-2021].

[2] Global Carbon Project, "Annual CO2 Emmissions," *Our World in Data*, 2021. [Online]. Available: www.ourworldindata.org/co2-and-other-greenhgouse-gas-emissions. [Accessed: 06-Sep-2021].

[3] BP, World bank, and Maddsion Project, "Energy Intensity," *Our World in Data*, 2021. [Online]. Available: www.ourworldindata.org/co2-and-other-greenhgouse-gas-emissions. [Accessed: 06-Sep-2021].

[4] Department of Energy Republic of South Africa, "Integrated Resource Plan," 2019.

[5] L. D. Smoot, *Coal Combustion and Gasification*. Plenum Press, New York and London, 1985.

[6] A. Williams, R. Backreedy, R. Habib, J. M. Jones, and M. Pourkashanian, "Modelling coal combustion : the current position," *Fuel*, vol. 81, pp. 605–618, 2001.

[7] R. I. Backreedy, L. M. Fletcher, L. Ma, M. Pourkashanian, and a. Williams, "Modelling Pulverised Coal Combustion Using a Detailed Coal Combustion Model," *Combust. Sci. Technol.*, vol. 178, no. 4, pp. 763–787, 2006.

[8] I. W. Smith, "The Combustion Rates of Coal Chars: A Review," in *19th International Symposium on Combustion, The Combustion Institute*, 1982, pp. 1045–1065.

[9] G. Sankar, D. S. Kumar, and K. R. Balasubramanian, "Computational modeling of pulverized coal fired boilers – A review on the current position," *Fuel*, vol. 236, no. September 2018, pp. 643–665, 2019.

[10] R. Naidoo, P. Rajoo, and W. Schmitz, "CFD Simulation of a Single Burner Pulverised Coal Combustion Test Facility," in *10th South African Conference on Computational and Applied Mechanics, Potchefstroom, 3rd - 5th October*, 2016.

[11] H. K. Versteeg and W. Malalasekera, *An Introduction to Computational Fluid Dynamics*, 2nd ed. Pearson Prentice Hall, 2007.

[12] M. Taniguchi, H. Kobayashi, K. Kiyama, and Y. Shimogori, "Comparison of flame propagation properties of petroleum coke and coals of different rank," *Fuel*, vol. 88, no. 8, pp. 1478–1484, 2009.

[13] S. Peta, "Ignition Characteristics of Low Volatile Quality High Ash Coal," University of the Witwatersrand, 2014.

[14] S. Peta, C. Du Toit, R. Naidoo, W. Schmitz, and L. Jestin, "Investigations of operation problems at a 200 MW e PF boiler," *Chem. Process Eng. - Inz. Chem. i Proces.*, vol. 36, no. 3, 2015.

[15] M. Taniguchi, H. Kobayashi, K. Kiyama, and Y. Shimogori, "Comparison of flame propagation properties of petroleum coke," *Fuel*, vol. 88, pp. 1478–1484, 2009.

[16] R. Falcon and A. J. Ham, "The characteristics of Southern African coals *," *J. South African Inst. Min. Metall.*, vol. 88, no. 5, pp. 145–161, 1988.

[17] K. M. Czajka, N. Modliński, A. M. Kisiela-Czajka, R. Naidoo, S. Peta, and B. Nyangwa, "Volatile matter release from coal at different heating rates –experimental study and kinetic modelling," *J. Anal. Appl. Pyrolysis*, vol. 139, 2019.

[18] H. Kobayashi, "Devolatilization of Pulverized Coal at High Temperatures," 1976.

[19] S. Badzioch and P. G. W. Hawksley, "Kinetics of Thermal Decomposition of Pulverized Coal Particles," *Ind. Eng. Chem. Process Des. Dev.*, vol. 9, no. 4, pp. 521–530, Oct. 1970.

[20] D. B. Anthony, J. B. Howard, H. C. Hottel, and H. P. Meissner, "Rapid devolatilization and hydrogasification of bituminous coal," *Fuel*, vol. 55, no. 2, pp. 121–128, 1976.

[21] N. Hashimoto, R. Kurose, and H. Shirai, "Numerical simulation of pulverized coal jet flame employing the TDP model," *Fuel*, vol. 97, pp. 277–287, 2012.

[22] Stephen Niksa, “PC Coal Lab Manual and Tutorial V4.3.” Niksa Energy Associates LLC, 2015.

[23] P. R. Solomon, D. G. Hamblen, R. M. Carangelo, M. A. Serio, and G. V. Deshpande, “General Model of Coal Devolatilization,” *Energy and Fuels*, vol. 2, no. 4, pp. 405–422, 1988.

[24] D. M. Grant, R. J. Pugmire, T. H. Fletcher, and A. R. Kerstein, “Chemical Model of Coal Devolatilization Using Percolation Lattice Statistics,” *Energy and Fuels*, vol. 3, no. 2, pp. 175–186, 1989.

[25] D. Smit, W. Schmitz, R. Naidoo, and S. Peta, “Low NOx coal burner temperature profile evaluation,” in *33rd Annual International Pittsburgh Coal Conference: Coal - Energy, Environment and Sustainable Development, PCC 2016*, 2016, vol. 2016-Augus.

[26] S. Niksa and A. R. Kerstein, “FLASHCHAIN Theory for Rapid Coal Devolatilization Kinetics. 1. Formulation,” *Energy and Fuels*, vol. 5, no. 5, pp. 647–665, 1991.

[27] S. Niksa, “FLASHCHAIN Theory for Rapid Coal Devolatilization Kinetics. 2. Impact of Operating Conditions,” *Energy and Fuels*, vol. 5, no. 5, pp. 665–673, 1991.

[28] S. Niksa, “FLASHCHAIN Theory for Rapid Coal Devolatilization Kinetics. 3. Modeling the Behavior of Various Coals,” *Energy and Fuels*, vol. 5, no. 5, pp. 673–683, 1991.

[29] J. C. Chen and S. Niksa, “Coal devolatilization during rapid transient heating. 1. Primary devolatilization,” *Energy & Fuels*, vol. 6, no. 3, pp. 254–264, 1992.

[30] N. Modlinski and T. Hardy, “Development of high-temperature corrosion risk monitoring system in pulverized coal boilers based on reducing conditions identification and CFD simulations,” *Appl. Energy*, no. x, 2017.

[31] A. Williams, M. Pourkashanian, and J. M. Jones, “The combustion of coal and some other solid fuels,” *Proc. Combust. Inst.*, vol. 28, no. 2, pp. 2141–2162, 2000.

[32] P. . J. Walker, F. J. Runsiko, and A. L.G., “Gas reactions of carbon,” *Adv. Catal.*, vol.

11, pp. 133–221, 1959.

[33] R. E. Mitchell, “Experimentally Determined Overall Burning Rates of Coal Chars,” *Combust. Sci. Technol.*, vol. 53, no. 2–3, pp. 165–186, 1987.

[34] R. H. Hurt and R. E. Mitchell, “On the Combustion Kinetics of Heterogeneous Char Particle Populations,” in *Twenty Fourth Symposium on Combustion*, 1992, pp. 1233–1241.

[35] M. M. Baum and P. J. Street, “Predicting the Combustion Behaviour of Coal Particles,” *Combust. Sci. Technol.*, vol. 3, no. 5, pp. 231–243, 1971.

[36] C. M. Mitchell RE, Kee RJ, Glarborg P, “The effect of conversion in the boundary layer surrounding pulverized-col char particles,” in *The Twenty-third symposium on combustion, The Combustion Institute*, 1990, pp. 1169–76.

[37] ANSYS, “ANSYS Fluent Theory Guide.” 2015.

[38] Siemens, “Siemens Sim Centre Star CCM+ V14 User Manual.” 2020.

[39] G. P. Smith *et al.*, “GRI-Mech 3.0,” 2017. [Online]. Available: http://www.me.berkeley.edu/gri_mech/. [Accessed: 12-Feb-2017].

[40] D. J. Hautman, F. L. Dryer, K. P. Schug, and I. Glassman, “A Multiple-step Overall Kinetic Mechanism for the Oxidation of Hydrocarbons,” *Combust. Sci. Technol.*, vol. 25, no. 5–6, 1981.

[41] D. Shaw, X. Zhu, M. Misra, and R. H. Essenhigh, “Tar reactions for Hautman Model,” in *Twenty third sympsosium (international) on Combustion: The combustion Institute*, 1990, pp. 1155–62.

[42] W. P. Jones and R. P. Lindstedt, “Global Reaction Schemes for Hydrocarbon Combustion,” *Combust. Flame*, vol. 9, no. 73, pp. 233–249, 1988.

[43] D. Förtsch, F. Kluger, U. Schnell, H. Spliethoff, and K. R. G. Hein, “A kinetic model for the prediction of no emissions from staged combustion of pulverized coal,” *Symp. Combust.*, vol. 27, no. 2, pp. 3037–3044, 1998.

[44] T. Gronaz, “Modeling of Particle-Radiation-Interaction for the Numerical Simulation of Coal Combustion,” 2017.

[45] R. Laubscher and P. Rousseau, “Numerical investigation on the impact of variable particle radiation properties on the heat transfer in high ash pulverized coal boiler through co-simulation,” *Energy*, vol. 195, p. 117006, 2020.

[46] C. Yin, “On gas and particle radiation in pulverized fuel combustion furnaces,” *Appl. Energy*, vol. 157, pp. 554–561, 2015.

[47] F. C. Lockwood, S. M. . Rizvi, and N. G. Shah, “Comparative predictive experience of coal firing,” *Proc Inst Mech Engrs*, vol. 200, no. C2, 1986.

[48] R. Laubscher, “Coal Particle Emmissivity and Scattring Facter UDF.” 2019.

[49] L. L. Baxter, R. E. Mitchell, T. H. Fletcher, and R. H. Hurt, “Nitrogen release during coal combustion,” *Energy and Fuels*, vol. 10, no. 1, pp. 188–196, 1996.

[50] H. Y. Cai, A. J. Güell, D. R. Dugwell, and R. Kandiyoti, “Heteroatom distribution in pyrolysis products as a function of heating rate and pressure,” *Fuel*, vol. 72, no. 3, pp. 321–327, 1993.

[51] L. Smoot and P. J. Smith, *Coal Combustion and Gasification*, 1st ed. Plenum Press, New York and London, 1985.

[52] K. Ochi, K. Kiyama, H. Yoshizako, H. Okazaki, and M. Taniguchi, “Latest Low-NOx Combustion Technology for Pulverized-coal-fired Boilers,” *Hitachi Rev.*, vol. 58, no. 5, pp. 187–193, 2009.

[53] T. Abbas, P. Costen, and F. C. Lockwood, “The Influence of Near Burner Region Aerodynamics on the Formation and Emission of Nitrogen Oxides in a Pulverized Coal-Fired Furnace,” vol. 363, no. 1991, pp. 346–363, 1992.

[54] The Babcock & Wilcox Company, *Steam - Its Generation and Use*. 2015.

[55] R. H. Essenhigh, “Combustion and Flame Propagation in Coal Systems: A review.”

[56] D. Smit, “Low NOx Coal Burner Temperature Profile Evaluation,” University of the

Witwatersrand, 2016.

[57] S. Niksa and R. Naidoo, “Correspondence with Stephen Niksa,” p. 1, 2021.

[58] A. F. Peters and R. Weber, “Mathematical Modeling of a 2.4 MW Swirling Pulverized Coal Flame,” *Combust. Sci. Technol.*, vol. 122, no. 1–6, pp. 131–182, Apr. 1997.

[59] B. . Waters, R. G. Squires, N. M. Laurendeau, and R. E. Mitchell, “Evidence of Formation of CO2, in the Vicinity of Burning Pulverized Carbon Particles.,” *Combust. Flame*, vol. 74, p. 91, 1988.

[60] P. Rajoo, “The Application of Pilot Scale Coal Evaluation to Full Scale Boilers,” University of the Witwatersrand, 2010.

[61] Verref, “VR60 Furnace Refratory Material Specification,” 2010.

[62] B. Nyangwa and P. Rajoo, “DTF and Pilot Scale Combustion Tests of Reference Coal,” 2014.

[63] OEM, “200MW Boiler C Schedule and Boiler Schematics.”

[64] P. Rajoo, “200 MW Boiler Test Campaign,” 2014.

[65] R. Govindsamy, “200 MW Boiler Process Data,” 2014.

[66] R. Naidoo and W. Schmitz, “200 MW Boiler Burner and Windbox CFD Simulations,” 2011.

[67] VDI, *Heat Atlas*, 6th ed. VDI Society for Chemical and Process Engineering, 1993.

[68] Eskom, “200 MWe Boiler C- Schedule,” 2010.

[69] R. Govindsamy, “200 MW Boiler Combustion Reliability Improvement Project,” 2012.

Appendix A : Devolatilisation Wall Temperature Profile UDF

```
#include "udf.h"
DEFINE_PROFILE(Wall_Temp_1400C,t,i)
{
        real pos[ND_ND];
        real z;
        face_t f;

        begin_f_loop(f,t)
          {
                F_CENTROID(pos,f,t);
                z=pos[2];
                F_PROFILE(f,t,i) =    ((4795.0)*pow(z,3)) - ((4237.9)*pow(z,2)) +(1303.1*z) +
1534.8;
          }
        end_f_loop(f,t)
}
```

Appendix B : Char Combustion Wall Temperature Profile UDF

```
#include "udf.h"

DEFINE_PROFILE(Wall_Temp_Char,t,i)

{

        real pos[ND_ND];

        real z;

        face_t f;

        begin_f_loop(f,t)

          {

                F_CENTROID(pos,f,t);

                z=pos[2];

                F_PROFILE(f,t,i) =  253.16*pow(z,5) - 1185.80*pow(z,4) + 1952.60*pow(z,3) -
1621.60*pow(z,2) + 642.26*z + 1595;

          }

        end_f_loop(f,t)

}
```

Appendix C : One and Two Step Reaction Chemistry Calculation

The following is provided by ANSYS [37]

Introduction:

Detailed calculations done by ANSYS FLUENT 14.0 while setting up material properties using coal calculator are demonstrated in this document.

Nomenclatures:

Latent_H_2O	Latent Heat of Liquid Water
MW_C	Molecular Weight of C
MW_H	Molecular Weight of H
MW_N	Molecular Weight of N
MW_S	Molecular Weight of S
MW_O	Molecular Weight of O
MW_H_2O	Molecular Weight of H_2O
Formation_Enthalpy_CO_2	Formation Enthalpy of CO_2
Formation_Enthalpy_H_2O	Formation Enthalpy of H_2O
Formation_Enthalpy_SO_2	Formation Enthalpy of SO_2
Formation_Enthalpy_Volatile	Formation Enthalpy of Volatile
Ash_Weight	Input Ash Mass Fraction in the Proximate Analysis
Volatile_Weight	Input Volatile Mass Fraction in the Proximate Analysis
Fixed_Carbon	Input Fixed Carbon Mass Fraction in the Proximate Analysis
Moisture	Input Moisture Mass Fraction in the Proximate Analysis
High_Temp_Volatile_Yield	High Temperature Volatile Yield
Volatile_Weight_daf	DAF (Dry Ash Free) Volatile Mass Fraction
Fixed_Carbon_daf	DAF (Dry Ash Free) Fixed Carbon Mass Fraction
M_C	Input Mass Fraction of C in the Ultimate Analysis (DAF)
M_H	Input Mass Fraction of H in the Ultimate Analysis (DAF)
M_N	Input Mass Fraction of N in the Ultimate Analysis (DAF)
M_S	Input Mass Fraction of S in the Ultimate Analysis (DAF)
M_O	Input Mass Fraction of O in the Ultimate Analysis (DAF)
H_ar	Mass Fraction of H in the Proximate Analysis
mf_C	DAF Mass Fraction of C in the Coal
mf_H	DAF Mass Fraction of H in the Coal
mf_N	DAF Mass Fraction of N in the Coal
mf_S	DAF Mass Fraction of S in the Coal
mf_O	DAF Mass Fraction of O in the Coal

mo_C	DAF Mole Fraction of C in the Coal
mo_H	DAF Mole Fraction of H in the Coal
mo_N	DAF Mole Fraction of N in the Coal
mo_S	DAF Mole Fraction of S in the Coal
mf_O	DAF Mole Fraction of O in the Coal
m	m in Volatile $C_mH_nO_xN_yS_z$
n	n in Volatile $C_mH_nO_xN_yS_z$
x	x in Volatile $C_mH_nO_xN_yS_z$
y	y in Volatile $C_mH_nO_xN_yS_z$
z	z in Volatile $C_mH_nO_xN_yS_z$
mo_sum	Intermediate Variable
weight_sum	Intermediate Variable
molar_sum	Intermediate Variable
Coal_HCV_ar	Input Coal High Heating Value As-Received
Coal_LCV_ar	Coal Lower Heating Value As-Received
Coal_LCV_daf	Coal Lower Heating Value DAF
a_1	Stoichiometric Coefficient of O_2 in the one-step reaction
a_2	Stoichiometric Coefficient of CO_2 in the one-step reaction
a_3	Stoichiometric Coefficient of H_2O in the one-step reaction
a_4	Stoichiometric Coefficient of N_2 in the one-step reaction
a_5	Stoichiometric Coefficient of SO_2 in the one-step reaction
b_1	Stoichiometric Coefficient of O_2 in the two-step reaction
b_2	Stoichiometric Coefficient of CO_2 in the two-step reaction
b_3	Stoichiometric Coefficient of CO in the two-step reaction
b_4	Stoichiometric Coefficient of H_2O in the two-step reaction
b_5	Stoichiometric Coefficient of N_2 in the two-step reaction
b_6	Stoichiometric Coefficient of SO_2 in the two-step reaction
Split_CO_CO₂	CO/CO_2 Split in reaction-1 products in the two-step reaction

Constants:

Following constants are used for the latent heat of water, formation enthalpy and the molecular weight of different species during the calculations

Latent_H₂O	2263073 (*J/kg*)
MW_C	12.01115 (*kg/kmol*)
MW_H	1.00797 (*kg/kmol*)
MW_N	14.0067 (*kg/kmol*)
MW_S	32.064 (*kg/kmol*)
MW_O	15.9994 (*kg/kmol*)
MW_H₂O	18.01534 (*kg/kmol*)

Formation_Enthalpy_CO_2	-3.935324E8 (*J/kmol*)
Formation_Enthalpy_H_2O	-2.418379E8 (*J/kmol*)
Formation_Enthalpy_SO_2	-2.968612E8 (*J/kmol*)
Char_LCV_daf	3.2789E7 (*J/kg*)

Calculation Procedure:

1. **Calculation of Formation enthalpy of Volatile**

The inputs of *Ash_Weight, Volatile_Weight, Fixed_Carbon, Moisture* and *F_C, F_H, F_O, F_N, F_S* will be normalized at the beginning of the calculations

Mass fractions of *C, H, N, S, O* in the volatile are calculated as

$$mf_C = \frac{F_C - Fixed_Carbon_daf}{Volitile_Weight_daf}$$

$$mf_H = \frac{F_H}{Volitile_Weight_daf}$$

$$mf_N = \frac{F_N}{Volitile_Weight_daf}$$

$$mf_S = \frac{F_S}{Volitile_Weight_daf}$$

$$mf_O = \frac{F_O}{Volitile_Weight_daf}$$

where

$$Volatile_Weight_daf = \frac{High_Temp_Volatile_Yield \times Volatile_Weight}{(1{,}0 - Ash_Weight - Moisture)}$$

$$Fixed_Carbon_daf = 1.0 - Volatile_Weight_daf$$

The corresponding mole fractions are calculated as

$$mo_sum = \frac{mf_C}{MW_C} + \frac{mf_H}{MW_H} + \frac{mf_N}{MW_N} + \frac{mf_S}{MW_S} + \frac{mf_O}{MW_O}$$

and

$$weight_sum = mo_C \cdot MW_C + mo_H \cdot MW_H + mo_N \cdot MW_N + mo_S \cdot MW_S + mo_O \cdot MW_O$$

$$molar_sum = \frac{MW_Volatile}{weight_sum}$$

and

$$m = mo_C \cdot molar_sum$$
$$n = mo_H \cdot molar_sum$$
$$x = mo_N \cdot molar_sum$$
$$y = mo_S \cdot molar_sum$$
$$z = mo_O \cdot molar_sum$$

The formation enthalpy of the volatile can be calculated as

$$\begin{aligned} &Formation_Enthalpy_Volatile \\ &= m\,.\ Formation_Enthalpy_CO_2 + \frac{1}{2}\,.Formation_Enthalpy_H_2O \\ &+ z\,.\ Formation_Enthalpy_SO_2 \\ &+ \frac{coal_LCV_daf - char_LCV_daf \times Fixed_carbon_daf}{Volatile_Weight_daf}\,.\ MW_Volatile \end{aligned}$$

where the Coal Low Heating Value DAF (*coal_LCV_daf*) is derived from the input Coal High Heating Value As-Received (*coal_HCV_ar*) as

$$coal_LCV_daf = \frac{coal_LCV_ar}{(1 - Ash_Weight - Moisture)}$$

$$coal_LCV_ar = coal_HCV_ar - \left(Moisture + \frac{H_ar \times MW_H_2O}{2{,}0\ .\ MW_H}\right) \times Latent_H_2O$$

with

$$H_ar = F_H \cdot (1.0 - Ash_Weight - Moisture)$$

2. **Calculation of Stoichiometric Coefficients of the Reactions**

a. One-step Reaction (with SO_2)

$$C_mH_nO_xN_yS_z + a_1\ O_2 \rightarrow a_2\ CO_2 + a_3\ H_2O + a_4\ N_2 + a_5\ SO_2$$

b. One-step Reaction (without SO_2)

$$C_mH_nO_xN_y + a_1\ O_2 \rightarrow a_2\ CO_2 + a_3\ H_2O + a_4\ N_2$$

c. Two-step Reaction (with SO_2)

$$C_mH_nO_xN_yS_z + b_1\ O_2 \rightarrow b_2\ CO_2 + b_3\ CO + b_4\ H_2O + b_5\ N_2 + b_6\ SO_2$$

$$CO + 0.5\ O_2 \rightarrow CO_2$$

d. Two-step Reaction (without SO_2)

$$C_mH_nO_xN_y + b_1\ O_2 \rightarrow b_2\ CO_2 + b_3\ CO + b_4\ H_2O + b_5\ N_2$$

$$CO + 0.5\ O_2 \rightarrow CO_2$$

The stoichiometric coefficients are calculated as

$$a_1 = \frac{1}{2}\left(2m + \frac{1}{2}n + 2z - x\right)$$

$$a_2 = m$$

$$a_3 = \frac{1}{2}n$$

$$a_4 = \frac{1}{2}y$$

$$a_5 = z$$

$$b_1 = \frac{1}{2}\left(m(2 - Split_CO_CO_2) + \frac{1}{2}n + 2z - x\right)$$

$$b_2 = m(1 - Split_CO_CO_2)$$

$$b_3 = m \times Split_CO_CO_2$$

$$b_4 = \frac{1}{2}n$$

$$b_5 = \frac{1}{2}y$$

$$b_6 = z$$

Appendix D : Five Step Reaction Chemistry Calculation

Basic Units

$(n\ \ Nm\ \ C\ \ sec\ \ kJ\ \ MPa) \equiv (1\ \ 1\ \ 1\ \ 1\ \ 1\ \ 1)$

$(mm\ \ hr\ \ MW\ \ ton\ \ MJ\ \ J) \equiv \left(10^{-3}\ \ 3600\ \ 1000\ \ 1000\ \ 1000\ \ 10^{-3}\right)$

$\left(kg\ \ kg_{coal}\ \ kg_{tar}\ \ kg_{gas}\ \ kg_{d}\ \ kg_{daf}\ \ kg_{v}\ \ kg_{C}\ \ kg_{H}\ \ kg_{O}\right) \equiv (1\ \ 1\ \ 1\ \ 1\ \ 1\ \ 1\ \ 1\ \ 1\ \ 1\ \ 1)$

$\left(kg_{N}\ \ kg_{CO}\ \ kg_{CH4}\ \ kg_{H2}\ \ kg_{CxHy}\ \ kg_{air}\right) \equiv (1\ \ 1\ \ 1\ \ 1\ \ 1\ \ 1)$

$\left(kmol\ \ kmol_{v}\ \ kmol_{gas}\ \ kmol_{tar}\ \ kmol_{C}\ \ kmol_{H}\ \ kmol_{O}\ \ kmol_{N}\ \ kmol_{CxHy}\right) \equiv (1\ \ 1\ \ 1\ \ 1\ \ 1\ \ 1\ \ 1\ \ 1\ \ 1)$

Atomic and Particle Masses (Fluent Database)

$W_C \equiv 12.0115$

$W_H \equiv 1.00797$

$W_O \equiv 15.9994$

$W_N \equiv 14.0067$

$W_S \equiv 32.064$

$W_{O2} \equiv 2.W_O$

$W_{N2} \equiv 2.\cdot W_N$

$W_{H2O} \equiv 2.W_H + W_O$

$W_{CO} \equiv W_C + W_O$

$W_{CH4} \equiv 4.W_H + W_C$

$W_{H2} \equiv 2\cdot W_H$

$$W_{CO2} \equiv W_C + 2.W_O$$
$$W_{C2H4} \equiv 2 \cdot W_C + 4W_H$$
$$W_{C2H6} \equiv 2.W_C + 6.W_H$$
$$W_{C3H8} \equiv 3.W_C + 8W_H$$
$$W_{C3H6} \equiv 3 \cdot W_C + 6 \cdot W_H$$
$$W_{HCN} \equiv W_H + W_C + W_N$$
$$W_{H2S} \equiv 2 \cdot W_H + W_S$$
$$W_{NO} \equiv W_N + W_O$$
$$W_{NO2} \equiv W_N + 2.W_O$$
$$W_{urea} \equiv 60.5$$
$$W_{SO2} \equiv W_S + 2W_O$$
$$W_{H2O} \equiv 2 \cdot W_H + W_O$$

Air Density Calculation

$$N2 := 0.7899$$
$$O2 := 0.2101$$
$$\rho_{air273} := \frac{101325.}{8314 \cdot 273 \cdot \frac{1}{N2 \cdot W_{N2} + O2 \cdot W_{O2}}} = 1.288 \cdot \frac{kg}{Nm^3}$$

Based on Mole Fraction

Based on Mass Fraction

$mN2 := 0.767$

$mO2 := 0.233$

$$\rho_{air273} := \frac{101325}{8314 \cdot 273 \cdot \left(\frac{mN2}{W_{N2}} + \frac{mO2}{W_{O2}} \right)} = 1.288 \cdot \frac{kg}{Nm^3}$$

Standard State Enthalpy (kJ/kmol) (Fluent Database)

$$\left(hf_{O2} \quad hf_{N2} \quad hf_{H2} \quad hf_{CH4} \quad hf_{C2H6} \right) \equiv \left(0.0 \quad 0.0 \quad -1.881377 \quad -7.489518 \cdot 10^4 \quad -8.386329 \cdot 10^4 \right) \frac{kJ}{kmol}$$

$$\left(hf_{C3H8} \quad hf_{C_s} \quad hf_{CO2} \quad hf_{CO} \quad hf_{H2O} \right) \equiv \left(-1.038602 \cdot 10^5 \quad -0.101268 \quad -3.935324 \cdot 10^5 \quad -1.105396 \cdot 10^5 \quad -2.418379 \cdot 10^5 \right)$$

Heat of Reaction [kJ/kg]

C<s>+O2-->CO2

$$Q_C \equiv \left| \frac{hf_{CO2} - hf_{C_s}}{W_C} \right| = 3.276 \times 10^4$$

CO+1/2O2-->CO2

$$Q_{CO} \equiv \left| \frac{hf_{CO2} - hf_{CO}}{W_{CO}} \right| = 1.01 \times 10^4$$

C3H8+5O2-->3CO2+4H2O

$$Q_{C3H8} \equiv \left| \frac{3hf_{CO2} + 4hf_{H2O} - hf_{C3H8}}{W_{C3H8}} \right| = 4.635 \times 10^4$$

C2H6+3.5O2-->2CO2+3H2O

$$Q_{C2H6} \equiv \left| \frac{2hf_{CO2} + 3hf_{H2O} - hf_{C2H6}}{W_{C2H6}} \right| = 4.751 \times 10^4$$

C<s>+1/2O2-->CO

$$Q_{C_CO} \equiv \left| \frac{hf_{CO} - hf_{C_s}}{W_C} \right| = 9.203 \times 10^3$$

CH4+2O2 --> CO2+2H2O

$$Q_{CH4} \equiv \left| \frac{hf_{CO2} + 2hf_{H2O} - hf_{CH4}}{W_{CH4}} \right| = 5.001 \times 10^4$$

H2+1/2O2 -->H2O

$$Q_{H2} \equiv \left| \frac{hf_{H2O} - hf_{H2}}{W_{H2}} \right| = 1.2 \times 10^5$$

Dry and Moist Air Density in Function of Temperature

$$\rho_{air}(T) \equiv \frac{101325}{8314.T\left(\frac{0.767}{W_{N2}} + \frac{0.233}{W_{O2}}\right)}$$

Dry Air

$$\rho_{wet_air}(T, m_{O2}, m_{H2O}) \equiv \frac{101325}{8314.T\left(\frac{1 - m_{O2} - m_{H2O}}{W_{N2}} + \frac{m_{O2}}{W_{O2}} + \frac{m_{H2O}}{W_{H2O}}\right)}$$

Moist Air

$m_{o2} := 0.233$

$m_{h2o} := 0.0$

Calculate the Mass Fraction of Moist Air:

T - Inlet Temperature

vel - Velocity

Area - Cross sectional flow area

mcoal - Dry fuel flow to the furnace

Wd - Moisture converted per 1kg of dry fuel

$\rho_{wet_air}(T, m_{o2}, m_{h2o}) \cdot vel \cdot area \cdot m_{h2o} = m_{coal} \cdot W_d$

Given

$$\frac{m_{o2}}{1 - m_{o2} - m_{h2o}} = \frac{0.233}{0.767}$$

$FindMassFraction(T, vel, area, m_{coal}, W_d) := Find(m_{o2}, m_{h2o})$

Custom rounding function for vectors

m - number of digits after the decimal point

$$\begin{aligned}&\mathbf{ROUND}(v, m) := \left|\begin{array}{l}\mathbf{isvector} \leftarrow \mathbf{if}(\mathbf{cols}(v) = 1, 1, 0)\\ v \leftarrow v^{T} \ \ \mathbf{if} \ \ \mathbf{isvector} = 0\\ (n \ \ i1 \ \ i2) \leftarrow (\mathbf{length}(v) \ \ \mathbf{length}(v) - \mathbf{last}(v) + 1 \ \ \mathbf{last}(v))\\ \mathbf{for} \ \ i \in i1 .. i2\\ \quad a_i \leftarrow \mathbf{round}(v_i, m)\\ a \leftarrow a^{T} \ \ \mathbf{if} \ \ \mathbf{isvector} = 0\\ a\end{array}\right.\end{aligned}$$

Coal Input Data

Coal Data must be input on an air-dry basis

$$Q_{coal_r} := 18.401\,MJ \cdot kg^{-1}$$

$$Vol_r := 20.5\%$$

CHECK-->

$$(W_r \ \ A_r \ \ C_r \ \ H_r \ \ O_r \ \ N_r \ \ S_r) := (3.3\% \ \ 29.1\% \ \ 55.5\% \ \ 2.86\% \ \ 6.75\% \ \ 1.27\% \ \ 1.22\%)$$

$$\sum (W_r \ \ A_r \ \ C_r \ \ H_r \ \ O_r \ \ N_r \ \ S_r) \cdot 100 = 100$$

$$Fuel_r := \left(W_r \;\; A_r \;\; C_r \;\; H_r \;\; O_r \;\; N_r \;\; S_r \;\; 0.9\right)$$

Fuel Vector Definition

$$\rho_{fg}(\lambda, T) := \frac{101325}{8314 \cdot T \cdot \left(\frac{1}{rCO2(\lambda, Fuel_r) \cdot W_{CO2} + rH2O(\lambda, Fuel_r) \cdot W_{H2O} + rN2(\lambda, Fuel_r) \cdot W_{N2} + rO2(\lambda, Fuel_r) \cdot W_{O2} + rSO2(\lambda, Fuel_r) \cdot W_{SO2}} \right)}$$

Flue Gas Density

Coal Data - Conversion to d.a.f.

$$\left(C_{daf} \;\; H_{daf} \;\; O_{daf} \;\; N_{daf} \;\; S_{daf}\right) := \left(C_r \;\; H_r \;\; O_r \;\; N_r \;\; S_r\right) \cdot \left(1 - W_r - A_r\right)^{-1}$$

Coal Elemental Analysis d.a.f.

$C_{daf} := round(C_{daf}, 4)$
$H_{daf} := round(H_{daf}, 4)$
$O_{daf} := round(O_{daf}, 4)$
$N_{daf} := round(N_{daf}, 4)$
$S_{daf} := round(S_{daf}, 4)$
$\left(C_{daf} \;\; H_{daf} \;\; O_{daf} \;\; N_{daf} \;\; S_{daf}\right) = (82.1 \;\; 4.23 \;\; 9.99 \;\; 1.88 \;\; 1.8) \cdot \%$
$\sum \left(C_{daf} \;\; H_{daf} \;\; O_{daf} \;\; N_{daf} \;\; S_{daf}\right) = 1$

Theoretical Air Demand for Coal d.a.f.

$$Air_{daf} := \frac{1}{0.233}\cdot\left(W_{O2}\cdot W_C^{-1}\cdot C_{daf} + W_O\cdot W_{H2}^{-1}\cdot H_{daf} + W_{O2}\cdot W_S^{-1}\cdot S_{daf} - O_{daf}\right) = 10.476\cdot kg_{air}\cdot kg_{daf}^{-1}$$

Calorific Value of Coal d.a.f

$$Q_{coal_daf} := Q_{coal_r}\cdot\left(1 - W_r - A_r\right)^{-1} = 27.22\cdot\frac{MJ}{kg_{daf}}$$

$$Q_C = 32.763\cdot\frac{MJ}{kg_C}$$

Comparison with pure coke

According to VDI calc from Kruczek

$$Q_{wr} := \left[339.15\cdot C_r + 1214.2\cdot\left(H_r - \frac{O_r}{8}\right) + 104.7\cdot S_r - 25.1\cdot W_r\right]\cdot 100 = 21.316\cdot\frac{MJ}{kg}$$

$$Q_{coal_r} = 18.401\cdot\frac{MJ}{kg}$$

Development of Coal Coke and Volatile Production via PC Coal Lab

$Y_{gas} := 15.3$
$Y_{CO2} := 2.4$
$Y_{CO} := 2.9$
$Y_{HCN} := 0.29$
$Y_{CH4} := 0.8$
$Y_{C2H4} := 0.29$
$Y_{H2} := 1.52$

$$Correction := 1$$

$$Y_{H2} := Y_{H2} - Correction = 0.52$$

$$Y_{CO} := Y_{CO} + \frac{Correction}{2} = 3.4$$

$$Y_{CO2} := Y_{CO2} + \frac{Correction}{2} = 2.9$$

$$Y_{C2H6} := 0.05$$

$$Y_{C3H6} := 0.22$$

$$Y_{C3H8} := 0.0$$

$$Y_{H2S} := 1.54$$

$$Y_{H2O} := 5.3$$

$$Y_{CO2} + Y_{CO} + Y_{HCN} + Y_{CH4} + Y_{C2H4} + Y_{C2H6} + Y_{C3H6} + Y_{C3H8} + Y_{H2} + Y_{H2S} + Y_{H2O} = 15.31$$

$$Y_{gasC} := Y_{HCN} \cdot \frac{W_C}{W_{HCN}} + Y_{CH4} \cdot \frac{W_C}{W_{CH4}} + Y_{C2H4} \cdot 2 \cdot \frac{W_C}{W_{C2H4}} + Y_{C2H6} \cdot 2 \cdot \frac{W_C}{W_{C2H6}} + Y_{C3H6} \cdot 3 \cdot \frac{W_C}{W_{C3H6}} + Y_{C3H8} \cdot 3 \cdot \frac{W_C}{W_{C3H8}} = 1.204$$

$$Y_{gasH} := Y_{HCN} \cdot \frac{W_H}{W_{HCN}} + Y_{CH4} \cdot 4 \cdot \frac{W_H}{W_{CH4}} + Y_{C2H4} \cdot 4 \cdot \frac{W_H}{W_{C2H4}} + Y_{C2H6} \cdot 6 \cdot \frac{W_H}{W_{C2H6}} + Y_{C3H6} \cdot 6 \cdot \frac{W_H}{W_{C3H6}} + Y_{C3H8} \cdot 8 \cdot \frac{W_H}{W_{C3H8}} + Y_{H2} \cdot 2 \cdot \frac{W_H}{W_H} + Y_{H2S} \cdot 2 \frac{W_H}{W_{H2S}} = 1.426$$

$$Y_{gasO} := 0$$

$$Y_{gasN} := Y_{HCN} \cdot \frac{W_N}{W_{HCN}} = 0.15$$

$$Y_{gasS} := Y_{H2S} \cdot \frac{W_S}{W_{H2S}} = 1.449$$

$$Y_{gasSum} := Y_{gasC} + Y_{gasH} + Y_{gasO} + Y_{gasN} + Y_{gasS} = 4.23$$

$$Y_{gasC\%} := \frac{Y_{gasC}}{Y_{gasSum}} \cdot 100 = 28.475$$

$$Y_{gasH\%} := \frac{Y_{gasH}}{Y_{gasSum}} \cdot 100 = 33.719$$

$$Y_{gasO\%} := \frac{Y_{gasO}}{Y_{gasSum}} \cdot 100 = 0$$

$$Y_{gasN\%} := \frac{Y_{gasN}}{Y_{gasSum}} \cdot 100 = 3.553$$

$$Y_{gasS\%} := \frac{Y_{gasS}}{Y_{gasSum}} \cdot 100 = 34.253$$

$$Y_{gas\%sum} := Y_{gasC\%} + Y_{gasH\%} + Y_{gasO\%} + Y_{gasN\%} + Y_{gasS\%} = 100$$

$$Y_{gasC\%norm} := \frac{Y_{gasC\%}}{Y_{gas\%sum}} \cdot 100 = 28.475$$

$$Y_{gasH\%norm} := \frac{Y_{gasH\%}}{Y_{gas\%sum}} \cdot 100 = 33.719$$

$$Y_{gasO\%norm} := \frac{Y_{gasO\%}}{Y_{gas\%sum}} \cdot 100 = 0$$

$$Y_{gasN\%norm} := \frac{Y_{gasN\%}}{Y_{gas\%sum}} \cdot 100 = 3.553$$

$$Y_{gasS\%norm} := \frac{Y_{gasS\%}}{Y_{gas\%sum}} \cdot 100 = 34.253$$

$$Y_{gas\%norm_sum} := Y_{gasC\%norm} + Y_{gasH\%norm} + Y_{gasO\%norm} + Y_{gasN\%norm} + Y_{gasS\%norm} = 100$$

Setting up the tables for further processing:

f - mass fraction of pyrolysis components from 1kg of coal d.a.f. - $kg_{species}/kg_{coal_daf}$

char, tar, gas - elemental composition of pyrolysis components from 1kg of coal d.a.f. - $kg_{atom}/kg_{species}$

CHAR, TAR,GAS - distribution of component atoms in 1 kg of coal d.a.f - $kg_{atom}/kg_{coal\ daf}$

1 - C; 2 - H; 3 - O; 4 - N; 5 - S - Indices of the elements in the arrays

$ORIGIN := 1$

This sets the start point of of the array index

Proportion of the volatile products in kg of coal d.a.f.

$$\begin{pmatrix} f_{char} \\ f_{tar} \\ f_{gas} \end{pmatrix} := \begin{pmatrix} 55.7 \\ 29.0 \\ 15.3 \end{pmatrix} \%$$

$$\sum \begin{pmatrix} f_{char} \\ f_{tar} \\ f_{gas} \end{pmatrix} = 100 \cdot \%$$

This is input data from the flashchain run

This is input data from the flashchain run

However the gas elemental breakdown requires analysis of the hydrocarbon gases predicted by flashchain

Elemental compostion of each of the volatile products

$$\mathbf{char} := \begin{pmatrix} 97.5 \\ 0.4 \\ 0 \\ 2.1 \\ 0 \end{pmatrix} \%$$

$$\mathbf{tar} := \begin{pmatrix} 84.9 \\ 5.2 \\ 6.7 \\ 2.0 \\ 1.2 \end{pmatrix} \%$$

$$\mathbf{gas} := \begin{pmatrix} \frac{\mathbf{Y_{gasC\%norm}}}{100} \\ \frac{\mathbf{Y_{gasH\%norm}}}{100} \\ \frac{\mathbf{Y_{gasO\%norm}}}{100} \\ \frac{\mathbf{Y_{gasN\%norm}}}{100} \\ \frac{\mathbf{Y_{gasS\%norm}}}{100} \end{pmatrix} = \begin{pmatrix} 28.475 \\ 33.719 \\ 0 \\ 3.553 \\ 34.253 \end{pmatrix} \cdot \%$$

$$\begin{pmatrix} \mathbf{C} \\ \mathbf{H} \\ \mathbf{O} \\ \mathbf{N} \\ \mathbf{S} \end{pmatrix}$$

$$\sum \mathbf{char} = 100 \cdot \%$$

$$\sum \mathbf{gas} = 100 \cdot \%$$

$$\sum \mathbf{tar} = 100 \cdot \%$$

$$f_{gas} = 15.3 \cdot \%$$

$$Y_{H2O} = 5.3$$

$$f_{gas} := f_{gas} - \frac{Y_{H2O}}{100} - \frac{Y_{CO}}{100} - \frac{Y_{CO2}}{100} = 3.7 \cdot \%$$

$$\mathbf{CHAR} := f_{char} \cdot \mathbf{char}$$

$$\mathbf{TAR} := f_{tar} \cdot \mathbf{tar}$$

$$\mathbf{GAS} := f_{gas} \cdot \mathbf{gas}$$

Distribution of the elements in 1 kg of coal

$$\mathbf{CHAR} = \begin{pmatrix} 54.3075 \\ 0.2228 \\ 0 \\ 1.1697 \\ 0 \end{pmatrix} \cdot \%$$

$$\mathbf{TAR} = \begin{pmatrix} 24.621 \\ 1.508 \\ 1.943 \\ 0.58 \\ 0.348 \end{pmatrix} \cdot \%$$

$$GAS = \begin{pmatrix} 1.05357 \\ 1.2476 \\ 0 \\ 0.13147 \\ 1.26736 \end{pmatrix} \cdot \%$$

$$norm := \sum (CHAR + TAR + GAS) = 88.4 \cdot \%$$

$$CHAR := \frac{CHAR}{\frac{norm}{100}} = \begin{pmatrix} 61.434 \\ 0.252 \\ 0 \\ 1.323 \\ 0 \end{pmatrix}$$

$$TAR := \frac{TAR}{\frac{norm}{100}} = \begin{pmatrix} 27.852 \\ 1.706 \\ 2.198 \\ 0.656 \\ 0.394 \end{pmatrix}$$

$$GAS := \frac{GAS}{\frac{norm}{100}} = \begin{pmatrix} 1.192 \\ 1.411 \\ 0 \\ 0.149 \\ 1.434 \end{pmatrix}$$

$$\sum (CHAR + TAR + GAS) = 100$$

Simplification of the combustion reactions

(Sulfur. We eliminate sulfur from coke, tar and light hydrocarbons, converting it into a carbon element. The conversion we dock in accordance with the reactions: C + O2 = CO2, S + O2 = SO2)

$$CHAR_1 := CHAR_1 + CHAR_5 \cdot \frac{W_C}{W_S} = 61.434$$

$$CHAR_5 := 0$$

$$TAR_1 := TAR_1 + TAR_5 \cdot \frac{W_C}{W_S} = 27.999$$

$$TAR_5 := 0$$

$$GAS_1 := GAS_1 + GAS_5 \cdot \frac{W_C}{W_S} = 1.729$$

$$GAS_5 := 0$$

(Hydrogen. We eliminate hydrogen from the coke by transferring it to the tar)

$$TAR_2 := TAR_2 + CHAR_2$$

$$CHAR_2 := 0$$

(*Nitrogen. We eliminate nitrogen from components)*

$$CHAR_4 := 0$$

$$TAR_4 := 0$$

$$GAS_4 := 0$$

(Normalization of the distribution of pyrolysis products in coal)

$$sum := \sum (CHAR + TAR + GAS)$$

$$CHAR := \frac{CHAR}{sum}$$

$$TAR := \frac{TAR}{sum}$$

$$GAS := \frac{GAS}{sum}$$

Pyrolysis vectors after initial conditioning:

$$CHAR = \begin{pmatrix} 63.5111531 \\ 0 \\ 0 \\ 0 \\ 0 \end{pmatrix} \cdot \%$$

$$TAR = \begin{pmatrix} 28.9460515 \\ 2.0241238 \\ 2.272286 \\ 0 \\ 0 \end{pmatrix} \cdot \%$$

$$GAS = \begin{pmatrix} 1.7873505 \\ 1.4590351 \\ 0 \\ 0 \\ 0 \end{pmatrix} \cdot \%$$

Detailed formulation of coal pyrolysis products

The global chemical formula of tar $C_xH_yO_z$ Conversion of mass shares into moles. It was assumed that the main tar component is C_7 hydrocarbons

$$x := \frac{TAR_1}{W_C} = 0.0240986$$

$$y := \frac{TAR_2}{W_H} = 0.0200812$$

$$z := \frac{TAR_3}{W_O} = 0.0014202$$

$$norm := \frac{x}{7}$$

Based on the assumption that tar is a C_7 hydrocarbon

$$x := \frac{x}{norm} = 7$$

$$y := \frac{y}{norm} = 5.8330463$$

$$z := \frac{z}{norm} = 0.4125392$$

The global chemical formula of C_mH_n light hydrocarbons

Flashchain specifies among light hydrocarbons detailed mass proportions of such components as: H2O, CO, CO2

$$f_{H2O} := \frac{Y_{H2O}}{100} = 0.053$$

$$f_{co} := \frac{Y_{CO}}{100} = 0.034$$

$$f_{co2} := \frac{Y_{CO2}}{100} = 0.029$$

The inclusion of the above components in volatile parts requires reduction of the share of light hydrocarbons. After slight correction of the above values, light hydrocarbons will not contain oxygen.

Hence the new mass fraction of light hydrocarbons is given by:

Elemental composition of light hydrocarbons

$$C := GAS_1 = 1.7873505 \cdot \%$$

$$H := GAS_2 = 1.4590351 \cdot \%$$

$$O := GAS_3 = 0 \cdot \%$$

Thus, the global formula of light hydrocarbons

$$m := C \cdot W_C^{-1}$$

$$n := H \cdot W_H^{-1}$$

$$norm := m$$

$$m := \frac{m}{norm} = 1$$

$$n := \frac{n}{norm} = 9.728$$

Pyrolysis components - summary

$x = 7$

$y = 5.8330463$

$z = 0.4125392$

$f_{char} = 55.7 \cdot \%$

$C_xH_yO_z$

$f_{tar} = 29 \cdot \%$

C_mH_n

$m = 1$

$n = 9.7275992$

$f_{gas} = 3.7 \cdot \%$

$f_{H2O} = 5.3 \cdot \%$

$f_{co} = 3.4 \cdot \%$

$f_{co2} = 2.9 \cdot \%$

$f_{volatile} := f_{tar} + f_{gas} + f_{H2O} + f_{co} + f_{co2} = 0.443$

$f_{char} + f_{volatile} = 100 \cdot \%$

$Q_{coal_daf} = 27.2204142 \cdot \frac{MJ}{kg}$

$Q_C = 32.7629604 \cdot \frac{MJ}{kg}$

Volatile Definition

$(y_{tar} \quad y_{gas} \quad y_{H2O} \quad y_{co} \quad y_{co2}) := (f_{tar} \quad f_{gas} \quad f_{H2O} \quad f_{co} \quad f_{co2}) \cdot f_{volatile}^{-1}$

Mass fractions of volatile components

$$\sum\left(y_{tar}\ \ y_{gas}\ \ y_{H2O}\ \ y_{co}\ \ y_{co2}\right) = 1$$

$$W_{tar} := \text{round}\left(x \cdot W_C + y \cdot W_H + z \cdot W_O, 5\right) = 96.56042$$

Molar mass of tar and light hydrocarbons

$$W_{gas} := \text{round}\left(m \cdot W_C + n \cdot W_H, 5\right) = 21.81663$$

$$W_{volatile} := \text{round}\left[\left[\sum\left(\frac{y_{tar}}{W_{tar}}\ \ \frac{y_{gas}}{W_{gas}}\ \ \frac{y_{H2O}}{W_{H2O}}\ \ \frac{y_{co}}{W_{CO}}\ \ \frac{y_{co2}}{W_{CO2}}\right)\right]^{-1}, 5\right] = 46.56324$$

Molar mass of a mixture of hydrocarbons

Mole fractions of volatile components:

$$s_{tar} := \text{round}\left(\frac{y_{tar}}{W_{tar}}, 5\right) \cdot W_{volatile} = 0.3156988$$

$$s_{gas} := \text{round}\left(\frac{y_{gas}}{W_{gas}}, 5\right) \cdot W_{volatile} = 0.1783372$$

$$s_{H2O} := \text{round}\left(\frac{y_{H2O}}{W_{H2O}}, 5\right) \cdot W_{volatile} = 0.3091799$$

$$s_{co} := \text{round}\left(\frac{y_{co}}{W_{CO}}, 5\right) \cdot W_{volatile} = 0.1275833$$

$$s_{co2} := \text{round}\left(\frac{y_{co2}}{W_{CO2}}, 5\right) \cdot W_{volatile} = 0.0693792$$

$$\sum\left(s_{tar}\ \ s_{gas}\ \ s_{H2O}\ \ s_{co}\ \ s_{co2}\right) = 1$$

Reaction Chemistry

Determination of the stoichiometric coefficients of the reactions

reaction-1

1kmol **volatile ---> s_{tar} tar** + **s_{gas} gas** + **s_{co} co** + **s_{h2o} h2o** + **s_{co2} co2**

$$\mathbf{LHS} := 1 \cdot \mathbf{W_{volatile}} = 46.56324 \cdot \mathbf{kg}$$

Confirm Mass Conservation

$$\mathbf{RHS} := \mathbf{s_{tar}} \cdot \mathbf{W_{tar}} + \mathbf{s_{gas}} \cdot \mathbf{W_{gas}} + \mathbf{s_{co}} \cdot \mathbf{W_{CO}} + \mathbf{s_{H2O}} \cdot \mathbf{W_{H2O}} + \mathbf{s_{co2}} \cdot \mathbf{W_{CO2}} = 46.5718268$$

reaction-2

1kmol **tar** + **s_{21} o2** ---> **s_{22} co** + **s_{23} h2**

$$\mathbf{s_{22}} := \mathbf{x} = 7$$

$$\mathbf{s_{21}} := \frac{\mathbf{x}}{2} - \frac{\mathbf{z}}{2} = 3.29373$$

$$\mathbf{s_{23}} := \frac{\mathbf{y}}{2} = 2.9165231$$

$$\mathbf{s_{21}} := \mathbf{round}\left(\mathbf{s_{21}}, 5\right) = 3.294$$

$$\mathbf{s_{22}} := \mathbf{round}\left(\mathbf{s_{22}}, 5\right) = 7$$

$$\mathbf{s_{23}} := \mathbf{round}\left(\mathbf{s_{23}}, 5\right) = 2.917$$

$$\mathbf{LHS} := 1 \cdot \mathbf{W_{tar}} + \mathbf{s_{21}} \cdot \mathbf{W_{O2}} = 201.956$$

Confirm Mass Conservation

$RHS := s_{22} \cdot W_{CO} + s_{23} \cdot W_{H2} = 201.956$

reaction-3

1kmol **gas** + s_{31} **o2** ---> s_{32} **co** + s_{33} **h2o**

$s_{31} := \frac{m}{2} + \frac{n}{4} = 2.9319$

$s_{32} := m = 1$

$s_{33} := \frac{n}{2} = 4.8638$

$s_{31} := round(s_{31}, 5) = 2.932$

$s_{32} := round(s_{32}, 5) = 1$

$s_{33} := round(s_{33}, 5) = 4.864$

$LHS := 1.W_{gas} + s_{31} W_{O2} = 115.634$

Confirm Mass Conservation

$RHS := s_{32} \cdot W_{CO} + s_{33} \cdot W_{H2O} = 115.634$

reaction-4

1kmol **co** + 0.5 **o2** ---> 1 **co2**

reaction-5

1kmol **h2** + 0.5 **o2** ---> 1 **h2o**

Calculation of Enthalpy of Formation

f_{char} , f_{tar} , f_{gas} , f_{h2o} , f_{co} , f_{co2} **Mass fraction in daf coal**

$f_{volatile}$ ($f_{volatile}$+ f_{char} = 1) **Mass fraction of volatile parts in daf coal**

y_{tar} , y_{gas} , y_{h2o} , y_{co} , y_{co2} **Mass fraction of volatile components kg/kg$_{volatile}$**

s_{tar} , s_{gas} ,s_{h2o} , s_{co}, s_{co2} **Molar fraction of volatile components kmol/kmol$_{volatile}$**

Calorific value of volatile parts

$$Q_C \cdot f_{char} + Q_{volatile} \cdot f_{volatile} = Q_{coal_daf}$$

$$Q_{volatile} := \frac{Q_{coal_daf} - Q_C \cdot f_{char}}{f_{volatile}} = 20.2515694 \cdot \frac{MJ}{kg_v}$$

The calorific value of light hydrocarbons is assume to be the same as methane:

$$Q_{gas} := 50 \frac{MJ}{kg_{gas}}$$

The calorific value value of tar is based on the disintegration reaction #1:

$$Q_{volatile} = y_{tar} \cdot Q_{tar} + y_{gas} \cdot Q_{gas} + y_{co} \cdot Q_{CO}$$

$$Q_{tar} := \frac{Q_{volatile} - (y_{gas} \cdot Q_{gas} + y_{co} \cdot Q_{CO})}{y_{tar}} = 23.3722237 \cdot \frac{MJ}{kg_{tar}}$$

Enthalpy of formation light hydrocarbons (gas).

The reaction of complete combustion of light hydrocarbons:

1kmol **gas** + s_{31} **o2 --->** s_{32} **co** + s_{33} **h2o** R-3

+

1kmol **co** + 0.5 **o2 --->** 1 **co2** / * s_{32} R-4

1kmol **gas** + (s_{31} + 0.5 s_{32}) **o2 --->** s_{33} **h2o** + s_{32} **co2**

$$\mathbf{hf_{gas} - \left(s_{33} \cdot hf_{H2O} + s_{32} \cdot hf_{CO2}\right) = Q_{gas} \cdot W_{gas}}$$

$$\mathbf{hf_{gas} := s_{33} \cdot hf_{H2O} + s_{32} \cdot hf_{CO2} + Q_{gas} \cdot W_{gas}} = -4.7895208 \times 10^{5} \cdot \frac{\mathbf{kJ}}{\mathbf{kmol_{gas}}}$$

$$\mathbf{hf_{gas} := round\left(hf_{gas}, -1\right)} = -4.79 \times 10^{5} \cdot \frac{\mathbf{kJ}}{\mathbf{kmol_{gas}}}$$

Enthalpy of formation for tar

The reaction of complete tar combustion :

1kmol **tar** + s_{21} **o2 --->** s_{22} **co** + s_{23} **h2** R-2

1kmol **co** + 0.5 **o2** ---> 1 **co2** / *s_{22} R-4

1kmol **h2** + 0.5 **o2** ---> 1 **h2o** / * s_{23} R-5

1kmol **tar** + (s_{21} + 0.5 s_{22} + 0.5 s_{23}) **o2** ---> s_{22} **co2** + s_{23} **h2o**

$$hf_{tar} - \left(s_{22} \cdot hf_{CO2} + s_{23} \cdot hf_{H2O}\right) = Q_{tar} \cdot W_{tar}$$

$$hf_{tar} := s_{22} \cdot hf_{CO2} + s_{23} \cdot hf_{H2O} + Q_{tar} \cdot W_{tar} = -1.203 \times 10^{6} \cdot \frac{kJ}{kmol_{tar}}$$

$$hf_{tar} := round\left(hf_{tar}, -1\right) = -1.203 \times 10^{6} \cdot \frac{kJ}{kmol_{tar}}$$

Enthalpy of formation for volatile parts. Decomposition reaction - zero reaction heat:

1kmol **volatile** ---> s_{tar} **tar** + s_{gas} **gas** + s_{co} **co** + s_{h2o} **h2o** + s_{co2} **co2**

$$hf_{volatile} - \left(s_{tar} \cdot hf_{tar} + s_{gas} \cdot hf_{gas} + s_{co} \cdot hf_{CO} + s_{H2O} \cdot hf_{H2O} + s_{co2} \cdot hf_{CO2}\right) = 0$$

$$hf_{volatile} := s_{tar} \cdot hf_{tar} + s_{gas} \cdot hf_{gas} + s_{co} \cdot hf_{CO} + s_{H2O} \cdot hf_{H2O} + s_{co2} \cdot hf_{CO2} = -5.8144708 \times 10^{5} \cdot \frac{kJ}{kmol_{v}}$$

$$hf_{volatile} := round\left(hf_{volatile}, -1\right) = -5.814 \times 10^{5} \cdot \frac{kJ}{kmol_{v}}$$

TEST : Enthalpy of Formation

Reaction Heat:

1kmol **tar** + s_{21} **o2** ---> s_{22} **co** + s_{23} **h2** R-2

1kmol **gas** + s_{31} **o2** ---> s_{32} **co** + s_{33} **h2o** R-3

1kmol **co** + 0.5 **o2** ---> 1 **co2** R-4

1kmol **h2** + 0.5 **o2** ---> 1 **h2o** R-5

$$q2 := hf_{tar} - \left(s_{22} \cdot hf_{CO} + s_{23} \cdot hf_{H2}\right) = -4.2943731 \times 10^{5}$$

$$q3 := hf_{gas} - \left(s_{33} \cdot hf_{H2O} + s_{32} \cdot hf_{CO}\right) = 8.0784078 \times 10^{5}$$

$$q4 := hf_{CO} - hf_{CO2} = 2.829928 \times 10^{5}$$

$$q5 := hf_{H2} - hf_{H2O} = 2.4183602 \times 10^{5}$$

$$q_{tar} := s_{tar} \cdot \left(q2 + s_{22} \cdot q4 + s_{23} \cdot q5\right) = 7.125 \times 10^{5}$$

heat from tar:

$$q_{gas} := s_{gas} \cdot \left(q3 + s_{32} \cdot q4\right) = 1.945 \times 10^{5}$$

heat from gas

heat from co

$$q_{co} := s_{co} \cdot q4 = 3.611 \times 10^{4}$$

$$\frac{q_{tar} + q_{gas} + q_{co}}{W_{volatile}} = 2.0255 \times 10^{4} \cdot \frac{kJ}{kg_{v}}$$

Calculation of the Air Demand

1kmol **volatile** ---> s_{tar} **tar** + s_{gas} **gas** + s_{co} **co** + s_{h2o} **h2o** + s_{co2} **co2**

1kmol **tar** + s_{21} **o2** ---> s_{22} **co** + s_{23} **h2** R-2

1kmol **gas** + s_{31} **o2** ---> s_{32} **co** + s_{33} **h2o** R-3

1kmol **co** + 0.5 **o2** ---> 1 **co2** R-4

1kmol **h2** + 0.5 **o2** ---> 1 **h2o** R-5

1 kg_C + BurnoutStoichiometricRatio kg_{O2} ----> (1+ BurnoutStoichiometricRatio) kg_{CO}

$$\mathbf{BurnoutStoichiometricRatio} := \frac{W_{O2}}{2.W_C} = 1.3320068$$

Demand for O_2 kmols per 1 kmol tar:

$s_{21} + 0.5 \cdot s_{22} + 0.5 \cdot s_{23} = 8.252$

$s_{31} = 2.932$

$s_{32} = 1$

Demand for O_2 kmols per 1 kmol gas:

$s_{31} + 0.5 \cdot s_{32} = 3.432$

Demand for O_2 kmols per 1 kmol co:

0.5

Demand for O_2 kmols per 1 kmol H2:

0.5

Demand for O_2 kmols per 1 kmol volatile:

$$s_{tar}\cdot\left(s_{21}+0.5\cdot s_{22}+0.5\cdot s_{23}\right)+s_{gas}\cdot\left(s_{31}+0.5\cdot s_{32}\right)+s_{co}\cdot 0.5=3.281$$

Required kg of air per kg of volatile:

$$m_{air_v}:=\left[s_{tar}\cdot\left(s_{21}+0.5\cdot s_{22}+0.5\cdot s_{23}\right)+s_{gas}\cdot\left(s_{31}+0.5\cdot s_{32}\right)+s_{co}\cdot 0.5\right]\cdot\frac{W_{O2}}{W_{volatile}}\cdot\frac{1}{0.233}=9.677$$

Required kg of air per kg of C:

$$m_{air_c}:=2\cdot BurnoutStoichiometricRatio\cdot\frac{1}{0.233}=11.434$$

Required kg of air per kg of coal d.a.f

$$m_{air_daf_coal}:=f_{volatile}\cdot m_{air_v}+f_{char}\cdot m_{air_c}=10.655$$
$$Air_{daf}=10.476$$

Dry Conditions

Coal is fed to the burners in a dry state

$$A_d := A_r \cdot \left(\frac{1}{1 - W_r} \right) = 30.093 \cdot \%$$

$$A_r = 29.1 \cdot \%$$

Ash

Moisture entering the combustion chamber i.e. inherent moisture

Moisture

$$W_d := W_r \cdot \left(\frac{1}{1 - W_r} \right) = 3.413 \cdot \%$$

$$Q_{coal_d} := Q_{coal_daf} \cdot \frac{1. - A_d}{1} = 1.903 \times 10^4 \cdot kJ \cdot kg_d^{-1}$$

Calorific Value

Volatile Component

$$V_d := f_{volatile} \cdot \frac{1 - A_d}{1} = 30.969 \cdot \%$$

$$f_{volatile} = 0.443$$

Char Component

$$CHAR_d := f_{char} \cdot \frac{1. - A_d}{1} = 38.938 \cdot \%$$

$$A_d + V_d + CHAR_d = 1$$

Fluent Material Input Data

- Combusting particle

Volatile := V_d = 30.9688·%

Combustible := $CHAR_d$ = 38.9382·%

BurnoutStoichiometricRatio := 1.3320456

Devolatilizing Species : mv-vol

Oxiding Species: o2

Appendix E : Heat Exchanger Pressure Loss Calculation

The pressure loss characteristics of the various heat exchangers are described in this section.

Primary Superheater:

	Velocity [m/s]	1	5	10	15	20
S_T	[m]	0.1286	0.1286	0.1286	0.1286	0.1286
S_L	[m]	0.1016	0.1016	0.1016	0.1016	0.1016
d	[m]	0.0635	0.0635	0.0635	0.0635	0.0635
N_R	[]	10.0000	10.0000	10.0000	10.0000	10.0000
w_f	[m/s]	1.0000	5.0000	10.0000	15.0000	20.0000
a	[]	2.0250	2.0250	2.0250	2.0250	2.0250
b	[]	1.6000	1.6000	1.6000	1.6000	1.6000
w	[m/s]	1.9756	9.8780	19.7561	29.6341	39.5122
T	[K]	298.1500	298.1500	298.1500	298.1500	298.1500
p	[Pa]	101325.0000	101325.0000	101325.0000	101325.0000	101325.0000
rho	[kg/m^3]	1.1841	1.1841	1.1841	1.1841	1.1841
eta	[kg/ms]	1.85E-05	1.85E-05	1.85E-05	1.85E-05	1.85E-05
Re	[]	8047.168	40235.842	80471.685	120707.527	160943.369
$f_{a,t,f}$	[]	0.386	0.235	0.235	0.235	0.235
$zeta_t$	[]	0.190	0.102	0.096	0.093	0.091
$f_{a,l,f}$	[]	34.538	34.538	34.538	34.538	34.538
$zeta_l$	[]	0.004	0.001	0.000	0.000	0.000
zeta	[]	0.188	0.103	0.097	0.094	0.091
ΔP	[Pa]	4.351	59.272	223.568	486.494	844.838
		A	B	C		
		1.9973	2.3471	0.0000		

Secondary Superheater

	Velocity [m/s]	1	5	10	15	20
S_T	[m]	0.1312	0.1312	0.1312	0.1312	0.1312
S_L	[m]	0.2572	0.2572	0.2572	0.2572	0.2572
d	[m]	0.0635	0.0635	0.0635	0.0635	0.0635
N_R	[]	4.0000	4.0000	4.0000	4.0000	4.0000
w_f	[m/s]	1.0000	5.0000	10.0000	15.0000	20.0000
a	[]	2.0667	2.0667	2.0667	2.0667	2.0667
b	[]	4.0500	4.0500	4.0500	4.0500	4.0500
w	[m/s]	1.9375	9.6875	19.3750	29.0625	38.7500
T	[K]	298.1500	298.1500	298.1500	298.1500	298.1500
p	[Pa]	101325.0000	101325.0000	101325.0000	101325.0000	101325.0000
rho	[kg/m^3]	1.1841	1.1841	1.1841	1.1841	1.1841
eta	[kg/ms]	1.85E-05	1.85E-05	1.85E-05	1.85E-05	1.85E-05
Re	[]	7891.938	39459.688	78919.376	118379.064	157838.752
$f_{a,t,f}$	[]	1.765	1.571	1.571	1.571	1.571
$zeta_t$	[]	0.304	0.197	0.172	0.159	0.150
$f_{a,l,f}$	[]	24.913	24.913	24.913	24.913	24.913
$zeta_l$	[]	0.003	0.001	0.000	0.000	0.000
zeta	[]	0.298	0.198	0.173	0.159	0.151
ΔP	[Pa]	2.645	44.016	153.491	318.814	535.566
		A	B	C		
		1.1588	3.6815	0.0000		

Economiser

	Velocity [m/s]	1	5	10	15	20
S_T	[m]	0.1270	0.1270	0.1270	0.1270	0.1270
S_L	[m]	0.1312	0.1312	0.1312	0.1312	0.1312
d	[m]	0.0635	0.0635	0.0635	0.0635	0.0635
N_R	[]	8.0000	8.0000	8.0000	8.0000	8.0000
w_f	[m/s]	1.0000	5.0000	10.0000	15.0000	20.0000
a	[]	2.0000	2.0000	2.0000	2.0000	2.0000
b	[]	2.0667	2.0667	2.0667	2.0667	2.0667
w	[m/s]	2.0000	10.0000	20.0000	30.0000	40.0000
T	[K]	298.1500	298.1500	298.1500	298.1500	298.1500
p	[Pa]	101325.0000	101325.0000	101325.0000	101325.0000	101325.0000
rho	[kg/m^3]	1.1841	1.1841	1.1841	1.1841	1.1841
eta	[kg/ms]	1.85E-05	1.85E-05	1.85E-05	1.85E-05	1.85E-05
Re	[]	8146.516	40732.581	81465.162	122197.743	162930.324
$f_{a,t,f}$	[]	0.584	0.388	0.388	0.388	0.388
$zeta_t$	[]	0.230	0.129	0.121	0.116	0.112
$f_{a,l,f}$	[]	31.453	31.453	31.453	31.453	31.453
$zeta_l$	[]	0.004	0.001	0.000	0.000	0.000
zeta	[]	0.228	0.130	0.121	0.116	0.112
ΔP	[Pa]	4.317	61.696	229.097	493.836	851.786
		A	B	C		
		1.9803	3.0509	0.0000		

Appendix F : Additional PSCTF Postprocessing

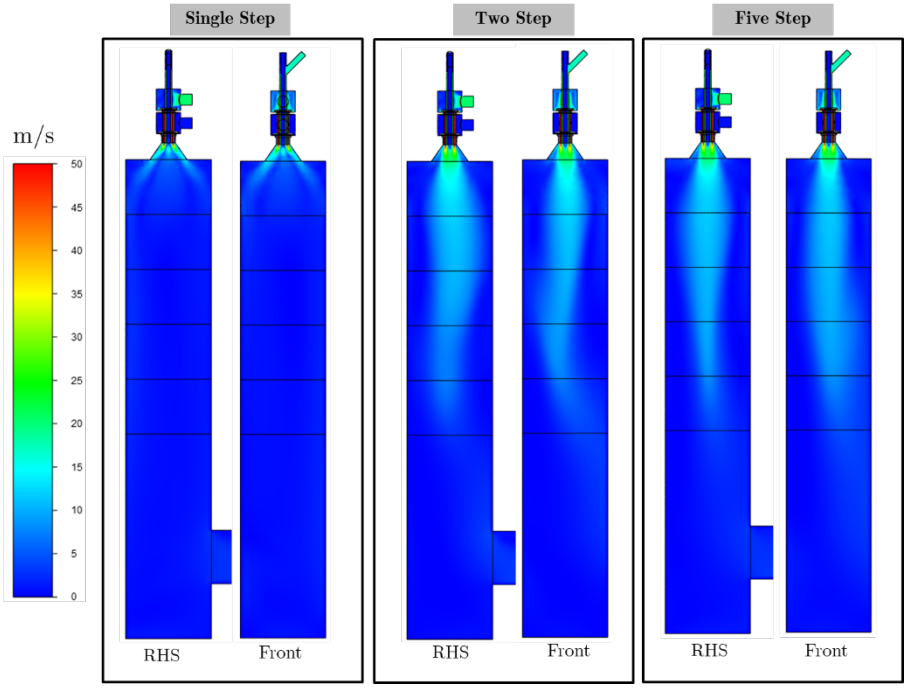

Figure F 1: Velocity Contours for Three Different Gas Phase Combustion Mechanisms

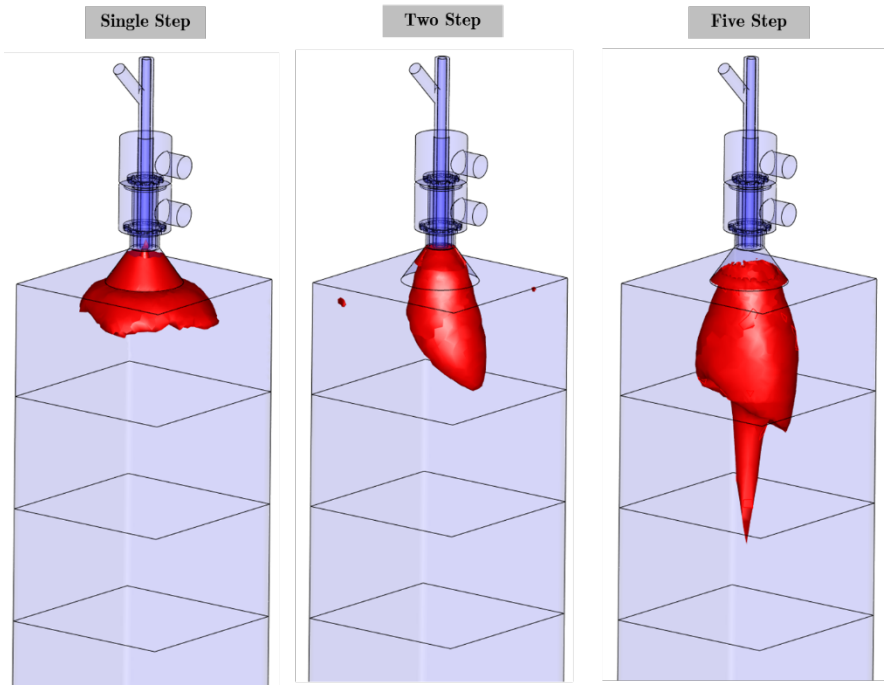

Figure F 2: 1400°C Iso Surface for Three Different Gas Phase Combustion Mechanisms

Appendix G : PSCTF Experimental Temperature Profiles

The following figures show the temperature profiles for port 10 and port D on the PSCTF. The portion of the test data that is used to gauge the average temperature values is shown in Figure G 2. It indicates that a steady state has been achieved and the maximum span of temperatures during the evaluation periods 16°C.

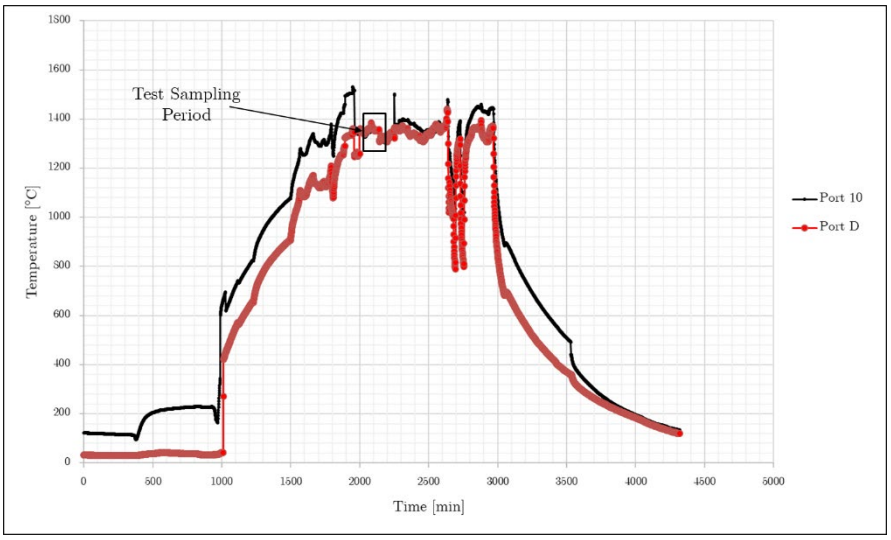

Figure G 1: Complete Temperature History for Port 10 and Port D Measurement Obtained from Reference PSCTF Test

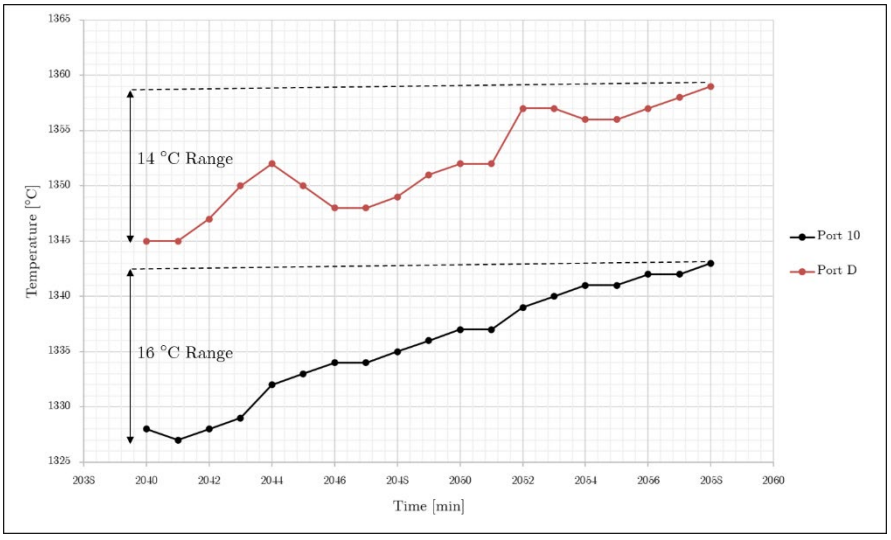

Figure G 2: Temperature Variation During Sampling Period for Port 10 and Port D

Appendix H : Additional Full Scale Boiler Post Processing

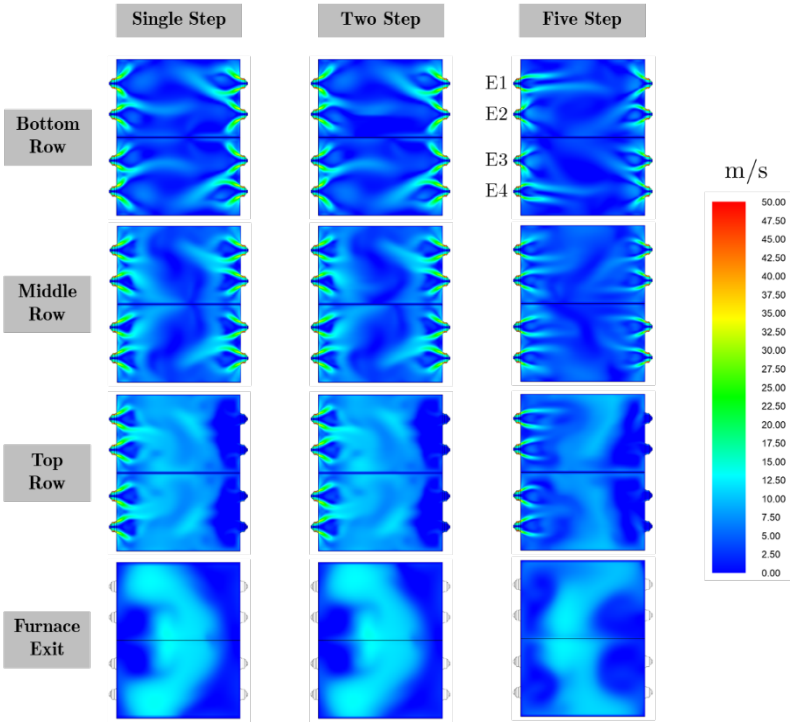

Figure H 1: Velocity Contours on Horizontal Section Planes through the Centrelines of the Burner Rows

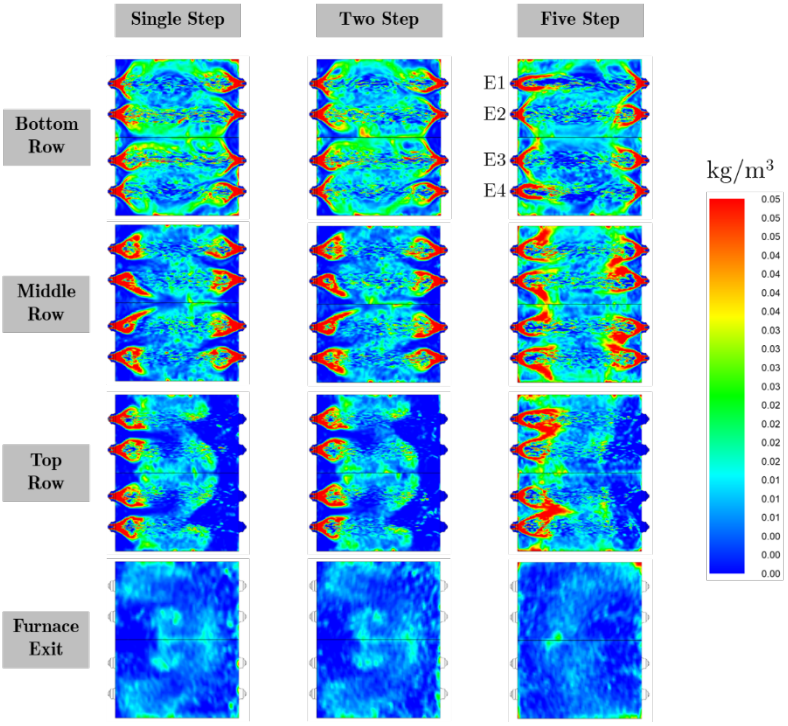

Figure H 2: Particle Concentration on Horizontal Section Planes through the Centrelines of the Burner Rows

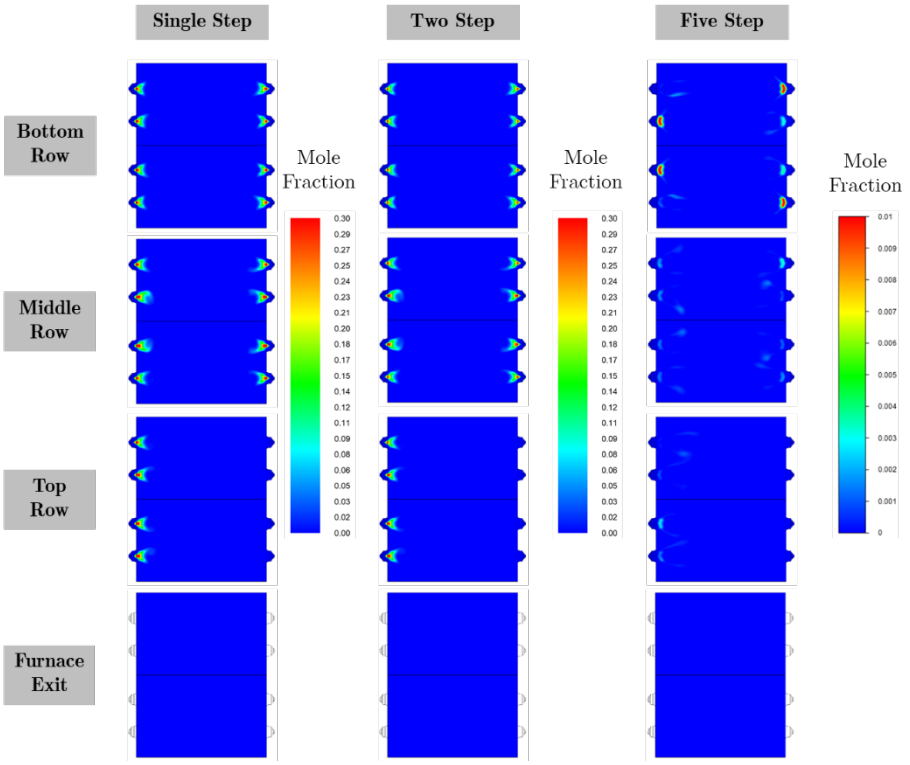

Figure H 3: Initial Volatile Concentration on Horizontal Section Planes through the Centrelines of the Burner Rows

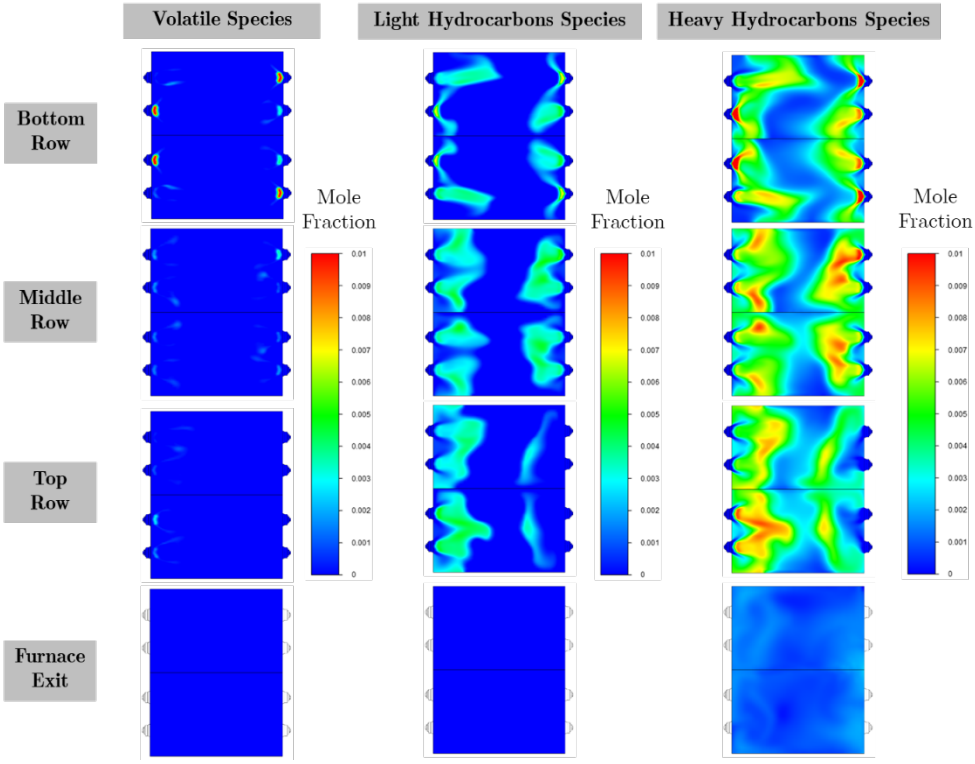

Figure H 4: Volatile Evolution on Horizontal Section Planes through the Centrelines of the Burner Rows (Five-Step Mechanism)

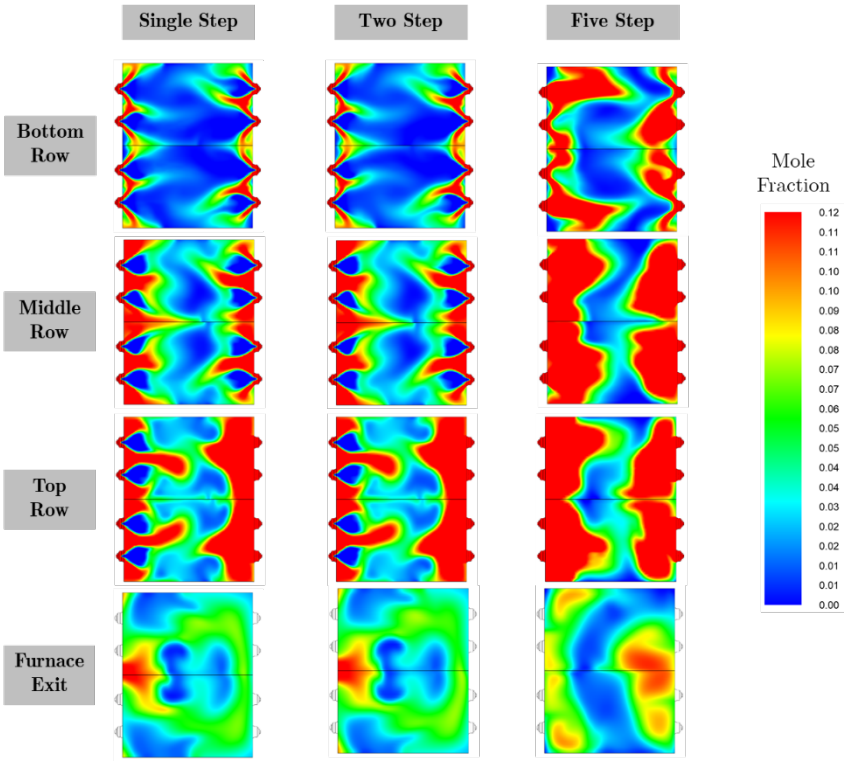

Figure H 5: Oxygen Concentration on Horizontal Section Planes through the Centrelines of the Burner Rows

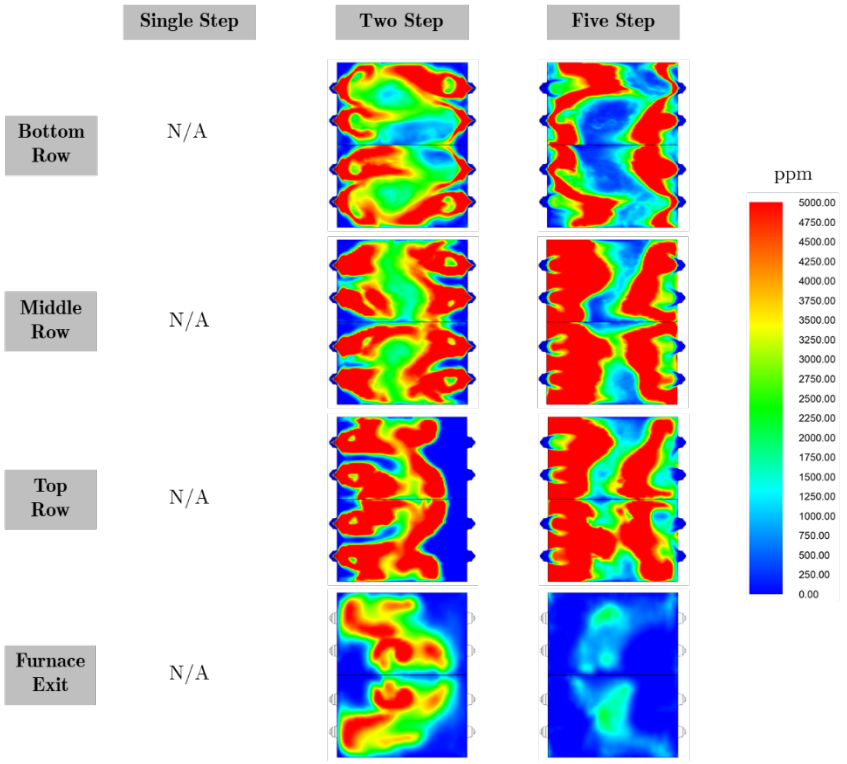

Figure H 6: Carbon Monoxide Concentration on Horizontal Section Planes through the Centrelines of the Burner Rows

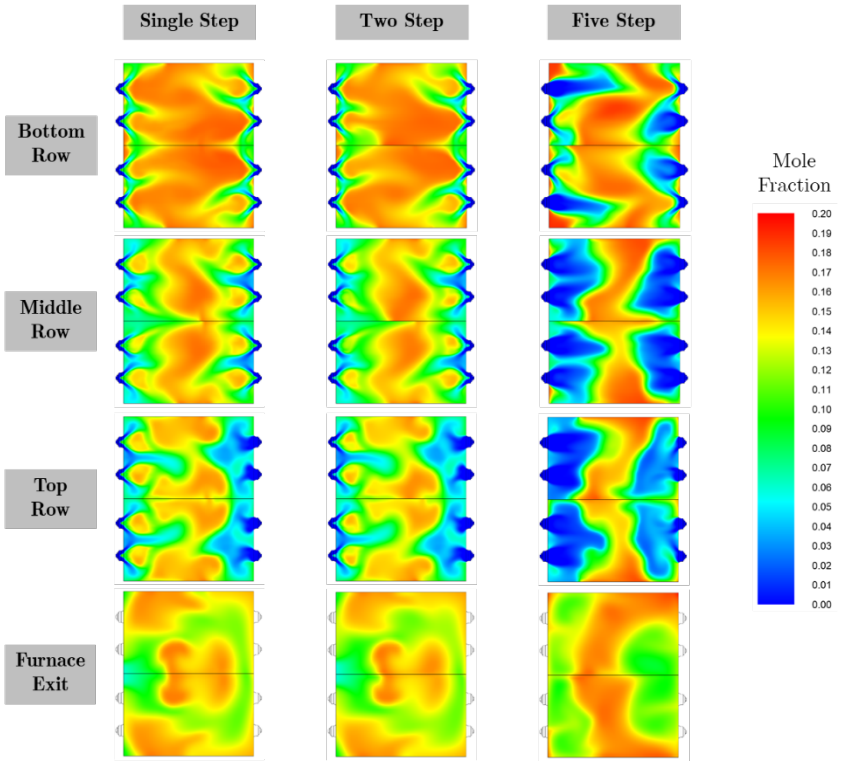

Figure H 7: Carbon Dioxide Concentration on Horizontal Section Planes through the Centrelines of the Burner Rows

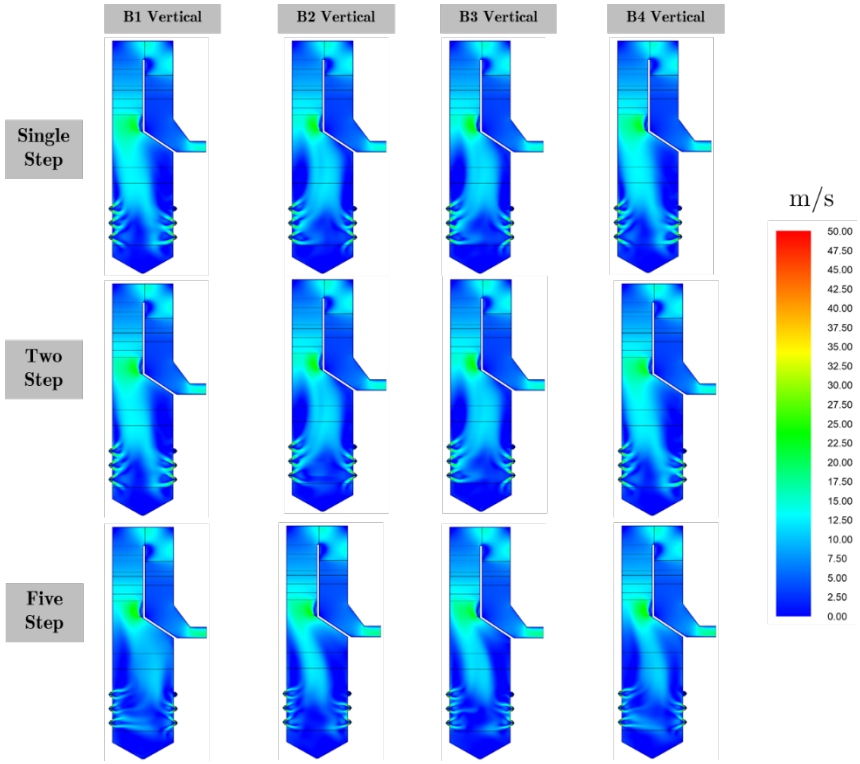

Figure H 8: Velocity Contours on Vertical Section Planes through the Centrelines of the Burner Rows

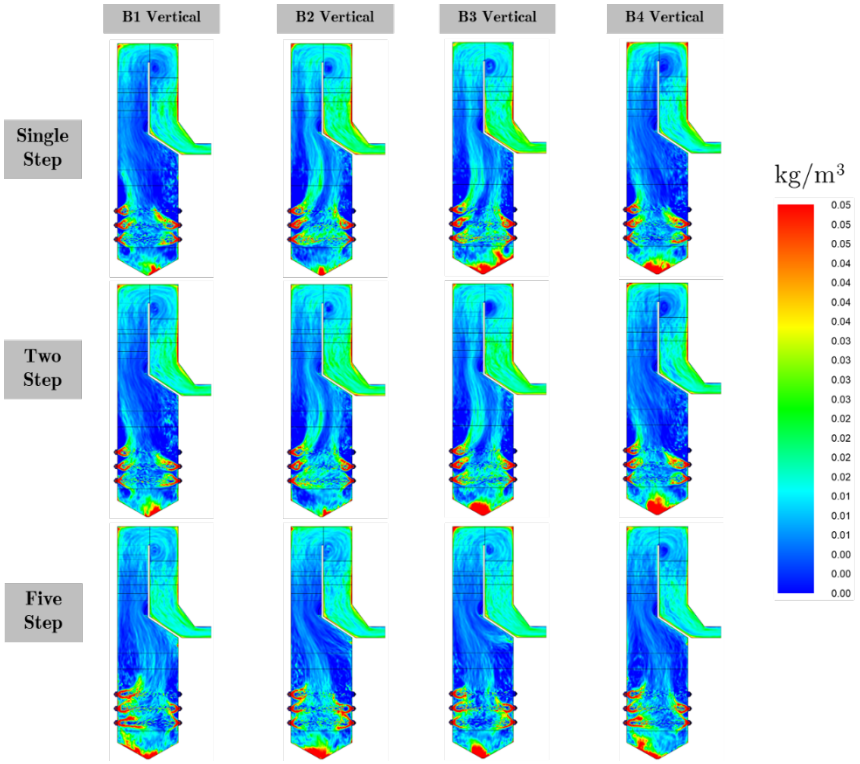

Figure H 9: Particle Concentration on Vertical Section Planes through the Centrelines of the Burner Rows

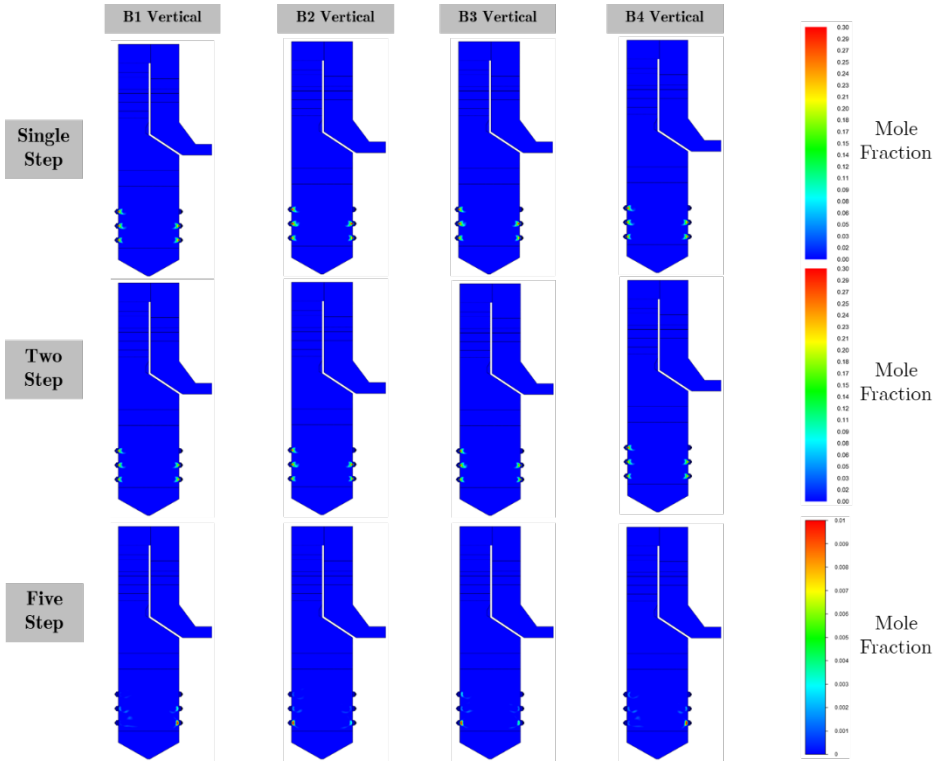

Figure H 10: Initial Volatile Concentration on Vertical Section Planes through the Centrelines of the Burner Rows

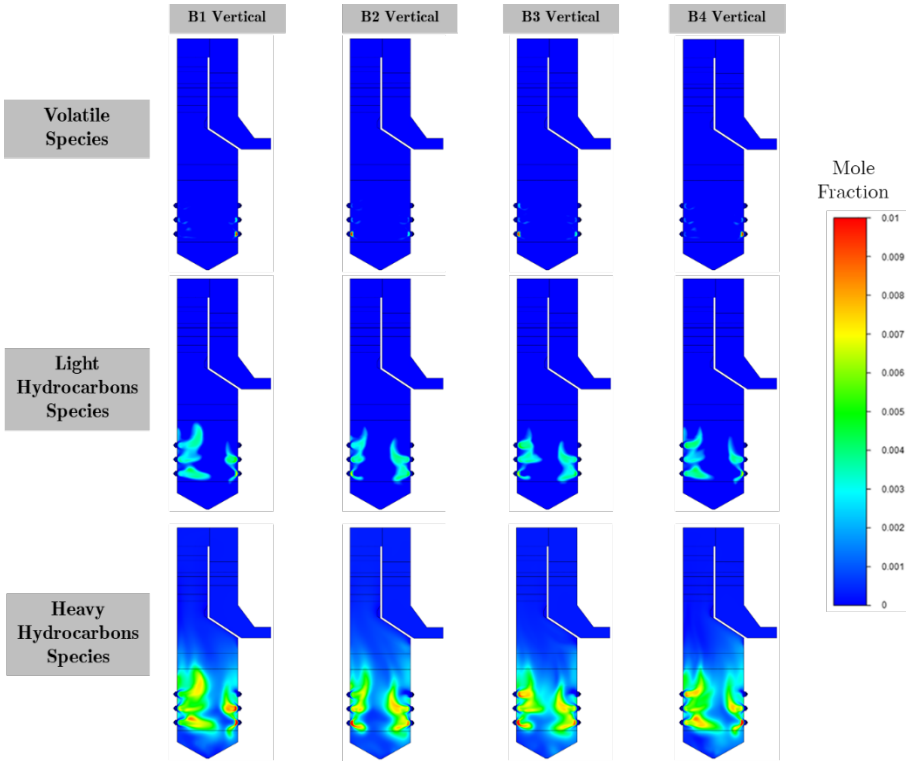

Figure H 11: Volatile Evolution on Vertical Section Planes through the Centrelines of the Burner Rows (Five-Step Mechanism)

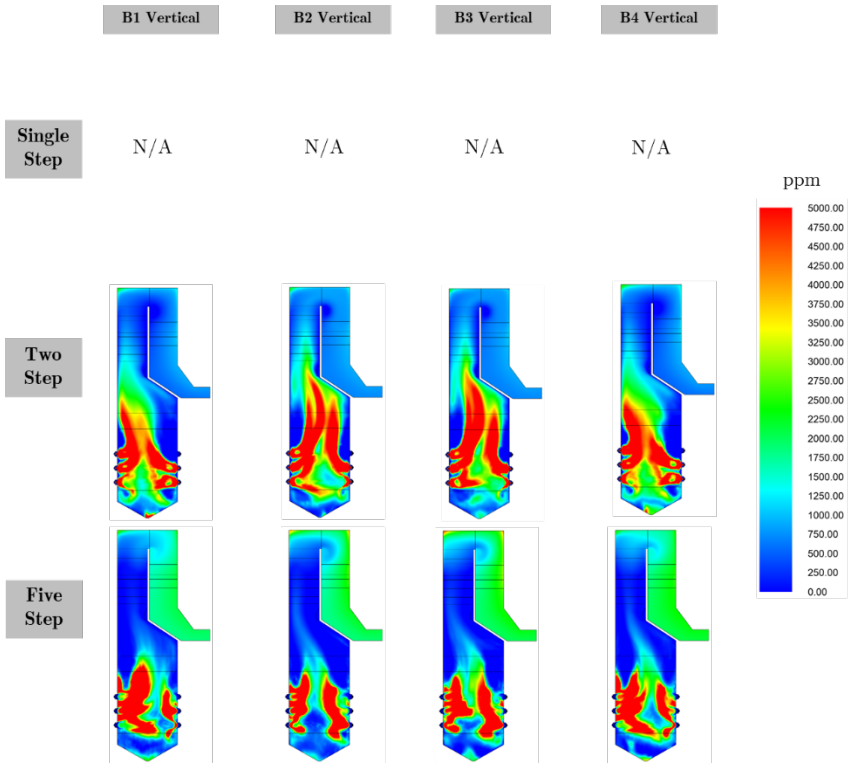

Figure H 12: Carbon Monoxide Concentration on Vertical Section Planes through the Centrelines of the Burner Rows

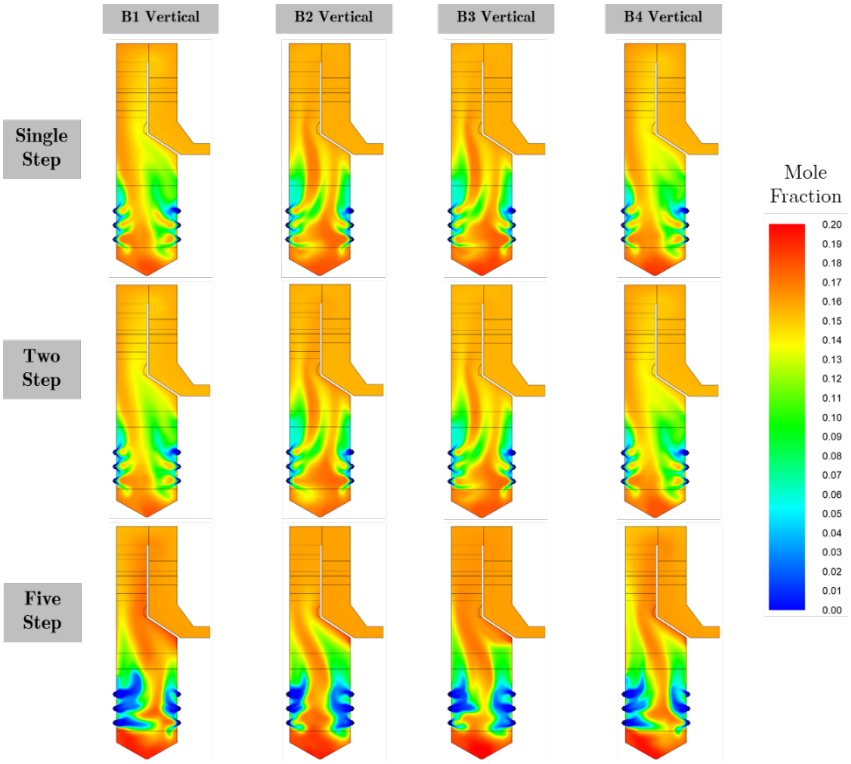

Figure H 13: Carbon Dioxide Concentration on Vertical Section Planes through the Centrelines of the Burner Rows